Technische Universität München
Fakultät für Chemie
Lehrstuhl für Biotechnologie

University of Illinois at Urbana-Champaign
Department of Cell and Developmental
Biology

Molecular Chaperones Modulate Chromatin and Transcription Events

Zlata Gvozdenov

Vollständiger Abdruck der von der Fakultät für Chemie der Technischen Universität München zur Erlangung des akademischen Grades eines Doktors der Naturwissenschaften genehmigten Dissertation.

Vorsitzende(r)	Univ.-Prof. Dr. rer. nat. Sevil Weinkauf
Prüfer der Dissertation	1. Univ.-Prof. Dr. rer. nat. Johannes Buchner
	2. Prof. Brian C. Freeman, Ph.D.

Die Dissertation wurde am 06.06.2018 bei der Technischen Universität München eingereicht und durch die Fakultät für Chemie am 08.06.2018 angenommen.

Technische Universität München
Fakultät für Chemie
Lehrstuhl für Biotechnologie

University of Illinois at Urbana-Champaign
Department of Cell and Developmental Biology

Molecular Chaperones Modulate Chromatin and Transcription Events

Zlata Gvozdenov

May, 2018

Contents

1. Introduction

1.1. Literature Review: Historical Overview of Molecular Chaperones in the Nucleus

1.1.1. Molecular Chaperones

Molecular chaperones are group of proteins that aid protein folding, oligomeric complex assembly or protein maturation through stabilization of the metastable states (Ellis 1987). They are connected to degradation pathways for effective removal of permanently denatured proteins (Baker 1984, Hayes 1996). Under adverse conditions, typically higher temperatures, cellular levels of molecular chaperones rapidly increase to prevent stress-induced protein malformations (Lindquist 1988, Morimoto 1993). Protein aggregates formed due to impaired protein homeostasis can lead to inexorable diseases such as Parkinson's, Alzheimer's and Huntington's (Dobson 1999, Ebrahimi-Fakhari 2011, Gammazza 2016, Reis 2017). Molecular chaperones are hence central proteostatic regulators and important targets for design of therapeutics strategies. Three main conserved and essential chaperones, CCT (TRiC), Hsp90 and Hsp70, are known. Since their identification and classification, about three decades ago (Ellis 1987, Hemmingsen 1988, McAlister 1979, Bardwell 1984), molecular chaperones have been viewed as cytosolic machineries. While it is true that initial protein genesis requires considerable folding assistance, post-synthetic constant monitoring of the overall protein structural and hence functional states is of great importance for the heathy proteome (Balchin 2016). Any cellular compartment can be equally affected by aberrations in protein quality control system. Biopsies of the patients affected by the above mentioned disease have shown that nuclear protein aggregates are common (Metuzals 1988, Hackam 1999). However,

very little attention has been devoted to molecular chaperones-mediated proteostasis in the nucleus.

1.1.2. CCT

CCT (chaperoning containing TCP1) or TRiC (TCP1-ring complex) is a 1 MDa complex comprised of two identical 8-subunit rings stacked onto each other to form a hollow sphere (Frydman 1992, Gao 1992, Rommelaere 1993). Paralogous subunits contain an equatorial ATP binding domain and apical substrate recognition domain (Kim 1994, Spiess 2004). ATP-driven closure of the apical domain facilitates encapsulation of the substrate, whose proper folding is mediated inside the chamber (Reissmann 2007, Bigotti 2008). The most famous CCT clients are polymeric complexes such as actin filaments and microtubules (Frydman 1992, Yaffe 1992, Gao 1992). Bacterial CCT homolog, 14-subunit GroEL complex, does not have a built-in lid but separate subunit GroES, which is together with ATP required for GroEL-mediated folding (Martin 1991, Xue 1997, Horwich 2007). Three to two decades ago, GroEL/ES used to be dominant model in protein folding/chaperone field, which rendered it to be best characterized system.

From the discovery of GroEL/ES to chaperone definition.
Hsp60 chaperonins were discovered during the attempts to identify host factors that supported the life cycle of bacteriophages. *GroE* gene was needed for the correct phage morphogenetic protein cleavage and head assembly, and hence, bacteria devoid of *groE* gene were not supportive of bacteriophage ʎ infection (Sternberg 1973, Georgopoulos 1973). In the case of T5 phages, the effect of *groE* gene was exerted on the tail assembly (Zweig 1973). Furthermore, another smaller gene with the same ʎ phage head phenotype was discovered and the two genes were renamed *groEL* (65 kDa) and *groES* (15 kDa) (Tilly 1981). At the time, it was unclear whether the two proteins, essential for *Escherichia coli* viability (Fayet 1989), were part of the same complex or the proteins work on different

steps of the same pathway during phage morphogenesis. Yet, already these initial studies anticipated pivotal roles of GroEL/ES in protein complex assembly (Sternberg 1973, Georgopoulos 1973, Zweig 1973). Similarly, Rubisco binding protein, plant GroEL homolog, was later shown to assist the assembly of the Rubisco enzyme (Barraclough 1980, Hemmingsen 1988), the most abundant protein complex on earth (Ellis 1979). GroEL/ES and Rubisco binding protein were proposed to be classified and re-named 'chaperonins' (Hemmingsen 1988), given their properties that were by large in agreement with what was defined for molecular chaperones: ubiquitous cellular proteins preventing aggregation and supporting folding or assembly of other proteins without being a constituent of the final protein structure or complex (Laskey 1978, Pelham 1986, Ellis 1987). Diminutive form in the name 'chaperonin', with respect to the 'chaperone', stems from the fact that the complexes displayed greater evolutionary, as well as structural and functional, ties to the endosymbiotic complexes (Hemmingsen 1988).

Early findings connect GroEL/ES to DNA processes.

Some of the earliest GroEL/ES findings suggested a strong involvement in DNA processes such as transcription and replication. At about the same time when *groE* gene was being discovered and analyzed within the context of ʎ phage, ATPase enzyme co-purifying with bacterial RNA polymerase was isolated and characterized (Ishihama 1976). It was not directly woven to the GroEL/ES, yet analysis of the biochemical properties and electron micrographs from the current perspective unequivocally show that the ATPase was GroEL. Furthermore, utilization of the temperature sensitive GroES strain revealed that bacterial DNA and RNA synthesis were defective at non-permissive temperature (Wada 1983). In an unrelated study by Takeda and Hirota (1982), a DNA fragment whose expression can suppress bacterial *dnaA*(Ts) gene mutation – a product essential for DNA replication – was further characterized to be g*roEL* gene (Jenkins 1986). Similarly, GroEL/ES was shown to be able to both protect RNA polymerase from heat inactivation and to reconstitute the activity of heat-inactivated RNA polymerase (Ziemienowicz 1993). Moreover, ω-less RNA polymerase, which renders bacterial cells less viable with slow growth phenotype, was more prone to GroEL association (Mukherjee 1999). Absence of

both ω and GroEL led to irreversible RNA polymerase defects – RNAP could not associate with σ[70], RNAP initiation factor, to form a functional holoenzyme.

Identification of tailless locus led to the discovery of TCP1 (eukaryotic GroEL).

Discovery of eukaryotic GroEL/ES followed a different route. 'T complex polypeptide 1' (TCP1), conserved between mouse, human, fruit fly and essential in budding yeast (Willison 1986, Willison 1987, Ursic 1988, Ursic 1991) was proposed to be the mammalian equivalent of the bacterial GroEL (Ellis 1990, Gupta 1990). The 'T' stems from the experiments in 1927 by Dobrovolskaia-Zavadskaia, where a 'tailless' phenotype resulted from deletions on the murine chromosome 17, regarded as one of the first known mammalian developmental mutations (Artzt 2012). The studies on taillessness complexities were further dissected by Dunn and Glueckshon-Schoenheimer (1939-1963), yet, it took about 6 decades to clone and analyze the 't complex' location – referred to the region of about 100 gene loci at the time (Herman 1987, Lyon 1988, Herman 1990). *Tcp1* gene within the t complex was identified during analysis of murine testicular polypeptides as it was shown that its expression was tightly associated with spermatogenesis (Silver 1979, Silver 1986). T complex in general contained a number of genes whose function was not known (Willison 1986, Rappold 1987, Schimenti 1988). However, given that the location was known for the expression of a few testis specific genes that caused transmission ratio disorder (TRD), which is the preferential transmission of a specific allele to the offspring of heterozygotes, the role of *Tcp1* in TRD was postulated (Silver 1981, Lyon 1984, Lyon 1986). Positing its more generalized roles, indirect immunofluorescence staining revealed the presence of the Tcp1 protein in all cell types tested (Willison 1989). Moreover, Tcp1 was reported to be spread through the cytosol in the form of 1 MDa hetero-oligomeric particle (Lewis 1992). Numerous studies followed up in parallel providing structural and mechanistic properties of the salient Tcp1 model – Tcp1 ring complex (TRiC) or chaperonin containing TCP1 (CCT) – the chaperonin renamed after its shape and origin.

TCP1 or CCT chaperonin structural and client-oriented characterization.

Similar to yet distinct from Hsp60 chaperone protein complex, it was elucidated that TCP1 complex is composed of related subunits organized into a ring and stacked onto each other to form a double toroid structure (Frydman 1992, Yaffe 1992, Gao 1992, Horwich 1993, Rommelaere 1993). Assortment of distinct subunits to form a substrate-recognizing cavity was proposed to be necessary for the recognition of diverse clients (reviewed in Dunn 2001). CCT was initially shown to mediate proper folding and maturation of actin and tubulin (Frydman 1992, Yaffe 1992, Gao 1992, Horwich 1993, Rommelaere 1993) and commonly held belief was that CCT chaperonin mostly supported maturation of cytoskeletal proteins. Furthermore, luciferase (Frydman 1992), G α-transducing, a protein important for retinal photo-transduction (Farr 1997), other cytoskeletal proteins such as myosin (Srikakulam 1999) and VHL tumor suppressor protein (Feldman 1999) were all revealed as structurally and functionally dependent on CCT. It was shown that many polypeptides are assisted by CCT cotranslationally (McCallum 2000) and the client repertoire of CCT was assessed to be ~9-15 % of the mammalian proteome (Thulasiraman 1999).

CCT's nuclear presence was mentioned.

The earliest reported CCT immunofluorescent staining might have indicated its presence in the nucleus (Lewis 1992), even though this was not pursued. CCT nuclear localizations were later mentioned in different contexts. Related proteins to TCP1, TRiC-P5 in Raji cells and hNMP238 in human leukocytes, were reported to be present in the nuclear matrix (Joly 1994, Gerner 1999) as well as certain subunits of the CCT complex (α and γ) according to a study in P19 embryonal carcinoma cell lines (Roobol 1998). TCP1 isoforms accumulated in the nuclear matrix during apoptotic chromatin condensation in HeLa (Gerner 2002) and CCT associated with both constitutive and facultative heterochromatin as observed during murine spermatogenesis (Soues 2003). Despite these observations, the mechanistic insights of CCT within a nuclear realm were scarce.

First links between CCT and nuclear macromolecular complexes – histone deacetylases.

The functional link between CCT chaperonin and nuclear proteins started with studies characterizing subunit compositions of chromatin regulators. Histone deacetylases, Set3 complex (Set3C) and Rpd3 Large complex (Rpd3L), were the first to be mentioned. Pijnappel 2001 found via tandem affinity purification that CCT associates with Set3C through the Hos2 subunit. The combination of mass spectrometry and tandem affinity purification was confirmative with these studies – Hos2 subunit pulled down seven of eight chaperonin subunits (Shevchenko 2002). Similarly, while characterizing the composition of the Rpd3 Small (Rpd3S) and Rdp3L histone deacetylases, all eight members of the CCT ring complex were detected via another mass spectrometric preparations, multidimensional protein identification technology (MudPIT) (Carrozza 2005). Further redefinition of the extended histone deacetylase complex Rpd3L, that included both Set3C and Hos2, and CCT's prominent co-occurrence among the complex subunits, lead to anticipation of the specific activity of the chaperonin in relation to the deacetylases (Shevchenko 2008). However, it was unclear whether the interactions were limited to cytosol and mirrored classical chaperone post-translational folding needs, or whether they happened in the nucleus to meet more specialized requirements. It was shown that priming of human histone deacetylase 3 (HDAC3), a Set3C yeast homolog, with CCT was essential for HDAC3 proper folding and activation (Guenther 2002), but again, the process was not compartmentalized. Perhaps functions of CCT, as a chaperone that assembles protein complexes rather than mediating immature protein folding, could be extended into modulation of defined protein complex activities in the nucleus.

Current CCT's nuclear interactome rooster encompasses crucial chromatin regulators.

In the past decade, the high throughput mass spectrometric studies on *Saccharomyces cerevisiae* proteome were further extending the CCT client roster and gene ontology tools allowed for associations of the annotated genes within the term nucleus. It was suggested that CCT interacts with transcriptionally important components, such as TAF5, a subunit of TFIID general transcription factor, members of CCR4-NOT

transcriptional complex, and pertinent SAGA histone acetyltransferase complex (Ho 2002). Finally, the known CCT physical and genetic interaction networks encompassed numerous chromatin regulators such as SWR1, SWI/SNF, Set1 methyltransferase complex (Set1C), type II histone deacetylase complex (HDAC) and ASTRA (Dekker 2008, Shevchenko 2008). On the whole, the yeast data base currently records 377 physical and genetic hits of the CCT complex, 48 % of which are located within the nucleus. They involve crucial chromatin regulators, yet the roles of CCT within chromatin field remain unexplored.

Summary.

The discovery of bacterial GroEL/ES is tied to the ʎ phage life cycle studies, in which its essentiality in bacteriophage head assembly was identified. The plant homolog was shown to assist assembly of rubisco, the most abundant protein on earth. The characteristics of GroEL/ES-like complexes were in agreement with what was defined under molecular chaperones, protein folding machineries, and their classification "chaperonins" was proposed. Identification of the CCT's subunit gene, TCP1, stems from the studies motivated to characterize the locus that rendered tailless animals. After several postulations about TCP1's specific roles, it was elucidated that CCT or TRiC, bacterial GroEL/ES homolog, is a barrel-shaped molecular chaperone spread throughout the cytosol in various cell types. Traditionally, CCT is known as cytosolic chaperonin which mediates assembly of oligomeric complexes, amongst which actin and tubulin are prominent clients. CCT was observed in nucleus in various cell lines but this did not receive much attention. Drawing a parallel line to bacteria, early observations indicated that GroEL/ES associated with bacterial RNA polymerase and it was essential for bacterial DNA replication. Current CCT interactome map suggests strong ties between CCT and nuclear events, but this field remains largely understudied.

1.1.3. Hsp90

Hsp90 molecular chaperones was named after its molecular weight (Aushburner 1979). Hsp90 is a homodimer with protomers connected via C-terminal domains to form a V shape (Nemoto 1995, Prodromou 1997), in which ATP binding domains are located within N-termini (Prodromou 1997). ATP is coupled to the closure of the protomers' N-termini and concomitant hydrolysis reinforces conformational changes that are communicated over to the rest of the chaperone, likely to mediate folding of certain substrates (Prodromou 2000, Wegele 2004, Richter 2006, Wandinger 2008). Hsp90 clamp-like open/close cycle and substrate choice are dynamically regulated by numerous co-chaperones (Buchner 1999, Hartl 2011, Li 2012). Hsp90 is needed downstream in the folding pathway to assist protein maturation and activation (Nathan 1995, Nathan 1997). It interacts with about 10% of the proteome, as estimated from the genome wide studies in *Saccharomyces cerevisiae* (Zhao 2005). Some of its most prominent clients are signal transducers, which are via Hsp90 kept in an activatable state (Pratt 1997, Picard 1990).

Hsp90 was identified as a cytosolic heat shock protein with mitigated nuclear connections.

The discovery of Hsp90 roots back to the use of a heat shock as a model to study environmentally triggered gene expression controls. Distinctive puffing of salivary gland chromosomes in *Drosophila* was microscopically trackable upon heat shock and structural changes were suspected to lead to synthetic changes to coordinate the adaptation (Ritossa 1962, Gross 1957, Pellin 1959). Heat-induced appearance of puffs was correlated with protein and RNA synthesis as distinctive protein pools, as well as localized RNA synthesis, were observed (Tissieres 1974). Pointing out Hsp90 in fruit fly at this stage was missed, but in similar budding yeast experiments that explored the alteration of protein patterns at elevated temperatures, Hsp90 was brought up for the first time as a drastically upregulated protein (McAlister 1979). It was speculated that products generated under stress conditions were meant to ease adaptation to the change. Due to Hsp90's pronounced co-occurrence with DNA-binding pool *in vitro*, tested via DNA-

cellulose assay – an introduced tool to investigate the potential of proteins to associate with DNA (Alberts 1968), its regulatory function was anticipated to be tied to DNA (McAlister 1979). Hsp90's heat-shock-triggered nuclear localization was acknowledged in series of cell lines such as chicken embryo fibroblasts, mouse neuroblastoma and fibroblasts, rat hepatoma, human cervical carcinoma cells and gingival fibroblasts (Collier 1986, van Bergen 1987, Berbers 1988, Akner 1992). Hsp90 was associated with both hetero- and euchromatin (van Bergen 1987). However, because Hsp90 was viewed as an abundant cytosolic, stress-associated protein, its nuclear roles under regular conditions might have been neglected.

The discovery of Hsp90 within hormone receptor field.

A branch independent of heat shock, studies exploring physiology of hormone stimuli, demonstrate that Hsp90 was in hands for discovery for quite some time, but it remained a 'hidden' constituent of the undefined hormone receptor complex. Inadvertently, Hsp90 was at one point suspected to be a transcription factor itself. In retrospect, it was appreciated earlier that hormones in sera co-exist with proteins (Haussler 1936). Further investigations quantified that two thirds of estrogen in blood, cells or sera are complexed with proteins to form so called 'estro-proteins' (Szego 1946, Roberts 1946) and attempts were made to isolate a soluble factor, meanwhile denoted 'receptor', that binds hormone estradiol (Jensen 1962, Toft 1966). Concealed Hsp90 came across in two ways: molecular weight (MW) estimated for the hormone receptor was larger than what is known today, and upon increase of the hormone concentration, density gradient (in terms of S) of the receptor complex would decline – nowadays equivalent to the release of the receptor from Hsp90. Similarly, chemical crosslinking of the progesterone receptor complex revealed constituents comprising higher molecular weight receptor complex (Birnbaumer 1978). Closer inspections of the results from today's perspective suggests that one of the contributing components in the crosslinked product was Hsp90. In general, varying density gradients in the course of characterizing biochemical properties of the hormone receptors were an intricate topic and it was alluded that numerous structural states existed. Within further advances in purification and characterization of the progesterone receptor, 90 kDa phosphoprotein was avidly detected in molybdate-

stabilized 8S progesterone receptor complex, which corresponded to hormone-binding fractions (Puri 1982, Renoir 1982). It was believed that higher molecular weight receptor complex, including 90 kDa protein, resembled a hormone binding form found in the crude cytosol. Postulations about 90 kDa protein's hormone-binding abilities were in conflict with an observation that incubation of the receptor complex with progesterone prior to affinity column led to the loss of the 90 kDa component (Baulieu 1983). In subsequent reports, 90 kDa protein was finally shown to be non-progesterone binding subunit of the hormone-receptor complex (Joab 1984, Renoir 1984), and also common structural constituent of numerous non-transformed hormone-receptors' complexes (Joab 1984). Studies in the following year identified 90 kDa protein to actually be Hsp90 associating with the steroid receptor prior to its transformation (Sanchez 1985, Catelli 1985), as well as intermediate subunit of the non-transformed Rous sarcoma virus complex (Schuh 1985). Interaction of the receptors with Hsp90 has been substantiated as essential to poise receptor for ligand binding (Pratt 1997, Picard 1990). It has been believed that Hsp90 release from the ligand-bound receptor complex allowed for the receptor binding to its response element and thus optimized transcriptional activity. However, another study proposed that Hsp90-progesterone receptor were in a steady state assembly/disassembly circuit regardless of the ligand (Smith 1993). With ligand binding, Hsp90 occluded progesterone receptor from interacting with other chaperones and allowed for the activation pathway (Smith 1993).

Hsp90 was postulated to affect hormone receptors in the nucleus as well.

Early attempts to define locations of the non-transformed hormone-receptor complex (complex that includes Hsp90, which is 8S for progesterone receptor and 9.5S for estrogen receptor) could not exclude its nuclear presence (Gorski 1968, Mester 1977). However, the picture about formation and residence of the receptor complex in the cytoplasm was adopted over the years. Calling for the revision of this model, 90 kDa non-progesterone-binding component of the progesterone receptor complex was found both in cytoplasm and nucleus according to the immunohistological data of chicken oviducts (Gasc 1984). The nuclear localization of the untransformed hetero-oligomeric form of steroid hormone receptor was confirmed via immunological detection in rabbit uterus cells

as well (Gasc 1990). However, not all nuclear Hsp90 was to be assigned to the 8S progesterone complex, as revealed by the substantial Hsp90 amounts in the nuclear extracts from the animal cells not treated with progesterone. Besides conventional steroid receptors, dioxin receptor, structurally and functional similar to steroid receptors, was in an 8S form, which likewise involves Hsp90 association, detected in nuclear extracts (Wilhelmsson 1990). Furthermore, it was posited that 8S receptor complexes themselves were also in part contributing to the nuclear localization of Hsp90. Human glucocorticoid receptor (GR) devoid of nuclear localization signal (NLS) was still detectable in the nucleus in the presence of Hsp90 carrying NLS, exemplifying thereby Hsp90's transport in the nucleus in the form of 8S complex (Kang 1994).

Hsp90 regulates hormone receptors' DNA binding, release and re-activation.

Hsp90 was shown to release ligand-bound dioxin receptor complex for its succeeding DNA interaction, similarly as in the case of progesterone receptor (Wilhelmsson 1990). It could be interpreted that remotely Hsp90 pre-prepared receptors for their DNA binding. In subsequent studies, Hsp90's capacity to modulate receptors' DNA binding was raised on a more elaborated level – it was shown that Hsp90 affected liganded receptor after its DNA interaction. Hsp90 was able to specifically dissociate ER from its cognate DNA and did not simply reform Hsp90-ER complex as a result of inherent ER-DNA off-rate (Sabbah 1996). Importantly, such ER was able to rebind the cognate DNA sequence. Similarly, increase of Hsp90/GR ratio in the nucleus, after priming the receptor with ligand, led to the decreased GR-DNA interaction (Kang 1999). The authors mentioned the possibility about competition between Hsp90 and DNA over the receptor, however, Hsp90 rebound GR only after hormone levels were saturated and GR was in its DNA-activated form. Furthermore, as both binding of the hormone to the unliganded GR and release of GR from the chromatin were inhibited by geldanamycin, an Hsp90 inhibitor, the role of Hsp90 in chromatin recycling was proposed (Liu 1999). In corroboration, Hsp90 was shown to physically associate with GR-containing regulatory complex at the GR genomic response element with an ability to disassemble the complex, and thereby affect transcriptional response (Freeman 2002). Thus, Hsp90 was pronounced to modify the hormone receptor and associated transcription in a more intricate way than just initial poising of the receptor.

Nuclear Hsp90 in *Drosophila melanogaster*: colocalization with ribonucleoproteins (RNP) movements.

In fly experiments, blocked splicing of mRNA transcripts at elevated temperature was rescued by the pre-made heat shock proteins, linking thereby RNA processing to the chaperones (Yost 1986). Localization-wise, Hsp90 was observed within extra- and perichromosomal ribonucleoprotein (RNP) fibrils, besides at the periphery of compact chromatin and in the nucleolus (Carabajal 1990, Vasquez-Nin 1992). Hsp90's presence was especially prominent in heat shock-induced puffs of flies' salivary glands chromosomes, specifically puff 93D (Morcillo 1993), which is an 'RNA-rich' puff. The general inhibition of transcription and not protein synthesis repressed Hsp90's co-occurrence within the chromosome sites 93D, indicating a tie between RNA genesis and Hsp90. 93D heat-shock or *hsrω* locus' importance was familiar from earlier as its depletion led to lethality – only 20% of the sterile embryos made it to the pupal stage (Mohler 1984). Combination of heterozygosity for *hsp83* locus and nullosomy for *hsrω* locus was further detrimental, rendering no viable pupae, suggesting a strong physiological connection between 93D and Hsp90 (Lakhotia 1996b). 93D heat-shock puff was described to be different compared to other puffs as it led to accumulation of various unpolyadenylated RNA transcripts that stem from the same non-coding locus (hsrω transcripts) (Spradling 1977, Garbe 1986, Fini 1989, Lakhotia 1996a). The prominence of both non-coding hsrω transcripts and Hsp90 within the puff anticipated a functional link (Lakhotia 1996b). Hsrω transcripts have an essential role in controlling organization and migration of heterogeneous nuclear ribonucleoproteins (hnRNP) (Prasanth 2000), and a parallel co-occurrence of Hsp90's can be observed. Namely, omega speckles, small gatherings of hsrω transcripts and hnRNP proximal to numerous chromosomal locations, were after a brief heat shock organized into larger and fewer speckles, which after longer heat shock (40 min) eventually all migrated into 93D puff (Prasanth 2000). Similarly, Hsp90 showed weaker nuclear associated with perichromatin RNP fibrils, and following heat shock, it relocalized to 93D resembling puffing pattern, with maximum signal about 30 min after the temperature shift (Morcillo 1993, Carabajal 1990, Vazguez-Nin 1992). Mobilization of hnRNP within a puff could be viewed as a protective phase under adverse

conditions and it is not clear whether Hsp90 could be involved in hsrω-dependent dynamic movement of hnRNP to the puff, or Hsp90 solely supports the puff milieu from the protein folding perspective – Hsp90 was already shown to support biogenesis of RNP (Boulon 2008). Alternatively, *hsrω* has genetic connection with Ras and JNK signaling pathways (Ray 1998, Mallik 2009), both of which are prominent Hsp90 targets. All in all, Hsp90 seemed to be both physically and genetically tied to the coding and non-coding RNA transcript.

Hsp90 controls chromatin regulators and chromatin status locally and globally.

Hsp90's link to DNA events ascended beyond hormone receptor clients. A clearer overview of Hsp90's potential functional domains in the nucleus was attained from high-throughput approaches that revealed numerous Hsp90 interactors involved in crucial chromatin processes. Perhaps the most prominent example was discovery of two novel Hsp90 cofactors Tah1 and Pih1, which simultaneously co-purified Rvb1 and Rvb2 helicases in stoichiometric amounts in yeast (Zhao 2005). Since Rvb1/2 are constitutive subunits of Ino80 and SWR-C chromatin remodeling complexes, a direct link between Hsp90 and chromatin physiology was provided. Additionally, Hsp90's interactors were also transcription factors, chromatin modifiers, components of mediator complex, and other regulators of gene expression (Zhao 2005). Follow-up studies substantiated that Hsp90 intervened in transcriptional and chromatin events via affecting target chromatin regulators. In fruit fly, inhibition of Hsp90 lead to depletion of chromatin regulator Trithorax from its homeotic gene response elements resulting in the inactivation of the transcriptional state (Tariq 2009). Another histone modifier in colorectal carcinoma cells, SMYD3, required Hsp90 for its histone methyltransferase activities at the subset of genes to control their expression (Hamamoto 2004). In general, Hsp90 was reported to colocalize with regulatory genomic regions close to transcription start site in fruit fly (Sawarkar 2012), the most important DNA element in terms of transcriptional regulation, and it is likely that many more promoter-specific, Hsp90-dependent targets will be identified. Unifying transcriptional and chromatin changes, *GAL1* promoter nucleosome removal in yeast was delayed in strains with compromised Hsp90, which was followed by impaired transcriptional activation (Floer 2008) – the same site was subject to increased

hypersensitivity upon short Hsp90 depletion (Echtenkamp 2016). Taking a look at other promoters, 63% of the yeast 5' regions (≥150 bp within the start codon) correlated with chromatin changes upon Hsp90 inactivation (Echtenkamp 2016). A mechanism was proposed that by directly impeding excessive RSC chromatin remodeling action, Hsp90 prevented creation of intrusive open chromatin regions genome-wide. In summary, Hsp90 affected functionalities of the proteins specialized for DNA processes on multiple levels, delivering differential chromatin states.

Hsp90 regulates reverse transcriptases and reverse transcriptase-derived DNA elements.

Among the enzymes directly acting on nucleic acids, reverse transcriptases were presented to have direct functional dependencies on Hsp90. Hsp90 was shown to facilitate hepatitis B viral RNP formation, as reverse transcriptase priming to the RNA pregenome for productive viral DNA synthesis was impaired in the absence of Hsp90 in rabbit reticulocytes (Hu 1996). The fact that Hsp90 was needed to maintain this functional state, and that it remained encapsulated within virus, postulated its potential need for the polymerase operation post viral assembly (Hu 1997, Hu 2000). Similarly in eukaryotes, Hsp90 associated with active telomerase, reverse transcriptase specialized for extension of chromosome ends, and supported assembly of telomerase components – reverse transcriptase catalytic core and RNA template (Holt 1999). Hsp90 was further shown to be needed for telomerase-DNA association and telomere extension, as well as for the efficient transition between telomere extending and precluding complexes (Toogun 2008, DeZwaan 2009). Thus, Hsp90 was shown to be an essential regulator of telomere genesis and homeostasis. Taking a further look on genomic elements that result from the reverse transcription, retrotransposons, a correlation with Hsp90-dependent chromatin changes can be seen. Retrotransposons are genomic sequences that, due to self-replicating potential, can reverse transcribe themselves using RNP intermediate and insert back into the genome (Baltimore 1970). More than 50% of known yeast retrotransposon (retrieved from Saccharomyces genome data base) are located within regions that experienced chromatin changes upon Hsp90 depletion (Echtenkamp 2016). It could be anticipated that Hsp90 has strong regulatory ties to the reverse transcriptase-

derived, fortuitous DNA sequences, either during their initial formation or throughout their maintenance. In support of this notion, Hsp90's ability to repress transcription of transposable elements, moving DNA sequences, was demonstrated in fruit fly and mouse (Specchia 2010, Hummel 2017). In these instances, Hsp90 activity was required for the genesis of the silencing machinery, comprised of piwi-interacting RNAs, or for recruitment of the chromatin repressive machinery – histone modifiers (Specchia 2010, Hummel 2017). In the later work, an evolutionary role of Hsp90 in buffering physical manifestations was extended to the regulation of non-coding DNA elements, in addition to previously described protein-coding genes (Rutherford 1988, Hummel 2017).

Hsp90 has DNA repair roles.

The presence of dsDNA was prerequisite for Hsp90 phosphorylation induced by various animal extracts (Walker 1985). The phosphorylation was shown to be catalyzed by DNA-activatable protein kinases (Lees-Miller 1989), an important DNA repair protein. This discovery can be viewed as an opening clue for Hsp90 importance in the process of DNA repair. It is known nowadays that phosphorylated Hsp90 accumulates within DNA double strand breaks foci to maintain repair kinetics – compromised Hsp90 activity led to defective repair (Quanz 2012). It was observed in tumorigenic cell lines that implementation of 17-AAG Hsp90 inhibitor correlated with reduce levels of the repair proteins engaged at the site of radiation-induced DNA damage (Russel 2003). Because detected factors were Hsp90 clients, the role of Hsp90 in radiation-response was proposed and inhibition of Hsp90 was further confirmed to lead to elevated radiosensitivity in array of different tumor cell lines (Bull 2004, Matsumoto 2005, Dote 2006). Currently, the contributing pathways and concomitant mechanistic insights of double strand break repair in relation to Hsp90 in mammalian cells are under intense examination. In yeast, Hsp90 could connect to the DNA repair process via Ssl2, a DNA helicase which is a part of RNA polymerase holoenzyme and an important incision factor for nucleotide excision repair (Flom 2005). Mutant alleles in *SSL2* combined with mutant alleles in *HSP82* and *HSC82* were shown to lead to synthetic growth defects. Deletion of *STI1*, an Hsp90 co-chaperone, or strains with either Hsp90 mutant alleles behaved similarly to *SSL2* deletion mutant – they displayed sensitivity to UV radiation. Furthermore, Ssl2 co-

immunoprecipitated with Hsp90 and Sti1, suggesting that they are part of the same complex.

Bacterial Hsp90 homolog, HtpG, connects to DnaA replication factor.

Unlike CCT and Hsp70, Hsp90's bacterial homolog, HtpG, is not essential (Bardwell 1988) and its importance within DNA processes is poorly examined. Interaction between HtpG and DnaA, an initiator of bacterial chromosomal DNA replication, has been identified in bacterial two-hybrid assay, and then confirmed with in vitro pull-down assays and chemical cross-linking (Grudniak 2015). The extent to which HtpG is able to intervene within DNA replication or sole DnaA stabilization *in vivo* is not known. However, it was noted that HtpG is far less abundant than DnaA *in vivo* and its overexpression, which physiologically happens only under stress conditions, was necessary to detect DnaA-HtpG interaction.

Summary.

Hsp90, named after its molecular weight, was identified as an abundant cytosolic protein whose levels significantly increased upon heat shock. Independently of these experiments, Hsp90 was shown to be a constituent of the cytosolic version of the hormone receptor complex. The elucidation of the Hsp90-regulated hormone receptor's functional cycle revealed the necessity for Hsp90's in the nucleus. Hsp90 was needed both before receptor-ligand binding for transactivation, and after receptor's DNA interaction – these findings led to the first proposals of homeostatic-like role of Hsp90 in the nuclear recycling. In retrospect, even though the earliest Hsp90's immunostainings pointed out its presence in the nucleus, this was not brought into the foreground. Nowadays, Hsp90 is known to control the activities of numerous local and global chromatin regulators and concomitant chromatin and transcriptional changes. Hsp90 readily colocalizes with RNPs, directly regulates reverse transcriptases in a conserved fashion and has an important role in DNA repair. Despite still being biased to cytosolic realms, Hsp90 is overall an important nuclear regulator.

1.1.4. P23

P23 molecular chaperone was named after its molecular weight (~ 24 kDa) or more precisely, after its electrophoretic mobility (~ 23 kDa) (Smith 2000). This small chaperone is traditionally viewed as Hsp90 co-chaperone due to its ability to stabilize the nucleotide-bound state of complex Hsp90 ATPase functional cycle (Sullivan 2002). It reinforces maturation of Hsp90 client proteins (Felts 2003). However, p23 is known to display chaperoning activities in the absence of Hsp90 (Bose 1996, Freeman 1996). P23 consists of globular β-sandwich domain and flexible C-terminal tail (Weaver 2000) important for its chaperoning functions (Weikl 1999). Similarly to Hsp90, p23 is associated with the regulation of hormone receptors (Felts 2003).

P23 was identified within hormone receptor field.

P23 was detected for the first time as a 23 kDa protein band co-immunopurifying with progesterone receptor (Smith 1990), similarly to Hsp90. As p23 was released from the receptor upon hormone addition, and hence receptor activation, the initial postulations about condition-specific p23 roles related to the intracellular hormone receptor function were proposed. P23 was further shown to be an important precursor for proper maturation of the progesterone receptor (Johnson 1994).

P23 targeted chromatin regulators, mostly transcription factors, in a highly selective manner.

Unlike for the other chaperones, the nuclear implications of p23 were straightforward, as it was elucidated to directly modulate transcriptional response. P23 exhibited enhancing or inhibiting effects on different steroid receptors transcription activation activities (Knoblauch 1999, Freeman 2000). Furthermore, p23-dependent modulation was observed not only to be receptor selective but also context specific. Since p23-receptor interaction was altered in the presence of a response element or agonist, it was speculated that allosteric or contextual situation changed p23 preference to target the

receptors (Freeman 2000). The concept was raised that p23 was able to distinguish 'experienced' versus naive receptors. This appealing concept was applied on a model outside steroid hormone physiology – it was shown that both HSF1 and GCN5 existed in at least two functional settings – one of which was not affected by p23 (Zelin 2012). Namely, it was shown that correct sequence of events, such as p23-dictated release of transcription factor HSF1 from its heat shock response element (HSE) followed by HSF1 acetylation by the prominent GCN5 histone acetyltransferase, was imperative for non-fortuitous transcriptional response. GCN5 acetylation itself was inhibited by p23 as pre-incubation with p23 without HSF1-HSE abolished its acetylation abilities. However, prerequisite for HSF1 acetylation by GCN5 to maintain hyperacetylated and DNA-free HSF1, was p23-dependent dissociation of HSF1 from its HSE. Hence, in this scenario p23 might have not affected acetylated HSF1 and acetylation-competent GCN5, in favor of proposed model.

P23 globally modulated chromatin landscape.

On the scale of global chromatin changes, it was shown that p23 deletion led to increased chromosome instability (Ouspensky 1999), suggesting that p23 effector functions could span larger chromosomal fragments. The magnitude of intracellular receptor transactivation control could potentially contribute to this effect, especially since p23 alone was able to disengage DNA association of entire receptor-mediated transcriptional regulatory complex (Freeman 2002), what likely affected local chromatin directly or indirectly. However, p23 interactome map revealed numerous other crucial chromatin regulators (Echtenkamp 2011) that could account for more pronounced chromatin changes. A generalized picture about chromatin status upon p23 depletion was acquired using DNase I high throughput sequencing (DNaseI-Seq) (Zelin 2012). DNaseI cleavage density delivered information about local chromatin openness (Crawford 2006, Boyle 2008, John 2011). While the genome in *sba1Δ* strain did experience some loss of open locations compared to the wild type, the average increase of chromatin openness was more conspicuous (Zelin 2012). Importantly, implementation of DNaseI-Seq in conjunction with digital genomic footprinting in yeast allowed for global monitoring of transcription factor occupancy at the single nucleotide resolution level (Hesselberth 2009,

Zelin 2012). Increase of the open chromatin was correlated with the surge of detected transcription factors binding sites. In corroboration, p23 did foster the off rate of transcription factor such as Mcm1 *in vitro* (Zelin 2011). On the whole, the data confirmed p23's potential to disengage DNA-protein binding abilities that thereby likely contributed to altered hypersensitive sites. For the first time it was shown that a molecular chaperone is able to globally affect chromatin status and transcription factor-DNA occupancy.

P23 as a hallmark of nuclear homeostasis.

Transcription factors alone are good candidates for DNA-binding proteins that nucleate chromatin changes and many well-studied and representative p23 clients are transcription factors. More pronounced chromatin perturbations are carried out by chromatin remodelers, such as RSC, which is able to alter nucleosomal structure and positioning, controlling the openness of underlying DNA (Clapier 2009). P23 was shown to interact with RSC according to the high-throughput map (Echtenkamp 2011). Functionally, p23 was shown to be able to disengage 1 MDa chromatin remodeler RSC both from DNA and nucleosome, whereby in the later case it also fostered completion of the remodeling reaction (Echtenkamp 2016). The findings here did not only explain prior excessively altered chromatin upon p23 depletion, but they also raised the awareness about nuclear proteostasis. The hypothesis was posited earlier that molecular chaperone are able to mediate recycling of the steroid hormone receptors in the nucleus (Knoblauch 1999, Liu 1999, Freeman 2000, DeFranco 2000, Freeman 2001), influencing thereby the functional protein pools. In conjunction with p23-dependent chromatin changes, it was shown that p23 readily controlled nuclear homeostasis both by fostering kinetics of the chromatin changes, as well as the availability of the functional proteins that modulate such changes (Echtenkamp 2016).

Summary.

P23, initially viewed as an Hsp90 co-chaperone, was identified in the context of steroid hormone receptors. Very soon after its discovery, p23 was shown to render complex yet rather specific modulatory effects on diverse steroid receptors, interfering in the transcriptional outcome. P23 has been the first chaperone shown to actively modulate

chromatin landscape, both through interfering with DNA-transcription factor occupancy, as well as chromatin remodeler-DNA or -nucleosome occupancy and remodeling. On the example of p23, it was sown that molecular chaperones elevate functionality of nuclear proteins, mediating thereby nuclear protein homeostasis.

1.1.5. Hsp70

Hsp70 molecular chaperone was named after its molecular weight, comparable to Hsp90 (Aushburner 1979). It consists of N-terminal ATPase, middle substrate binding region and C-terminal flexible lid that, upon ATP hydrolysis (N-terminally bound ADP), stabilizes the substrate to the middle domain (Flaherty 1990, Zhu 1996, Mayer 2010). ATP-driven conformational switches of Hsp70 convert misfolded substrate into unfolded intermediate and with the nucleotide exchange, substrate is released to refold spontaneously or it re-binds to Hsp70 (Sharma 2010). Hsp70 is famous for its association with the ribosome nascent chain and *de novo* protein folding assistance (Nelson 1992, Frydman 1994). Before entire polypeptide is synthesized and correctly folded, shorts segments emerging from the ribosome are endangered by potential aggregation. Hsp70 dynamically associates and protects these domains, mediates complete folding or it passes proteins to downstream CCT or Hsp90 machineries for further folding optimization (Hartl 2011).

DnaK, bacterial Hsp70, was discovered to be crucial regulator of bacteriophage DNA replication initiation.

The discovery of DnaK, bacterial Hsp70 homolog, parallels with the screens identifying GroEL/ES. It stems from the motivations to map the genes in *Escherichia coli* strains whose mutation inhibited bacteriophage λ DNA replication and thereby interfered with the λ life cycle progression. While some of the mutations fell within location of nowadays known *dnaB* gene, bacterial DNA helicase, others were within the region of *dnaK* gene (Georgopoulos 1971, Georgopoulos 1977, Saito 1978, Yochem 1978). Mutations in *dnaK* were not only detrimental for λ phage DNA replication but also affected host DNA metabolism, positing additional host dependencies on this protein. Utilization of the temperature sensitive *dnaK* mutant further revealed that both bacterial DNA replication and transcription were defective under the conditions of compromised DnaK activity (Itikawa 1979). At first, even though it could not be demonstrated that DnaK had DNA binding abilities *per se*, it was postulated that all enzymatic activities including ATP

hydrolysis and DNA replication resided in DnaK, as shown via *in vitro* ⋏ replication system (Zylicz 1984). In the following years, DnaK was shown to be required for the initiation of ⋏ DNA replication – it was one of the six pertinent proteins engaged at ⋏ origin of replication *ori⋏* (Dodson 1986). This macromolecular complex in the presence of ATP caused local unwinding of DNA to form a prepriming initiation state, as noticed by the existence of a different nucleoprotein structure at *ori⋏*, according to the electron micrographs. The studies on the complex in conjunction with previous extensive reports about *ori⋏* mechanisms clarified sequential association and dissociation stages of the involved components prior to productive DNA replication. The first stages encompassed preprimosomal complex formation – bacteriophage-encoded protein ⋏ O recognized unique *ori⋏* and through its interaction with ⋏ P, which associated with host DnaB, localize DnaB to the *ori⋏* (LeBowitz 1985, Dodson 1985). DnaK together with DnaJ (Hsp40) and Ssb (single stranded DNA-binding protein) were needed at later steps to release high affinity ⋏ P protein from the preprimosome and allow for restoration of DnaB helicase activity (Liberek 1988, Dodson 1989). Hence, DnaK was a constituent of the final, rate-limiting step of bacteriophage DNA replicon.

DnaK was augmented for effective chromosomal DNA replication under adverse conditions.

Regarding bacterial origin of replication *oriC*, chromosomal DNA replication initiation was also affected in the DnaK temperature sensitive strain at elevated temperature (Sakakibara 1987, Ohki 1989). Furthermore, *in vitro* systems augmented that bacterial DNA synthesis was considerably reduced when using extracts isolated from the strains mutated in *dnaK* gene, and it was recovered once purified DnaA or DnaK were supplemented (Malki 1991). At elevated temperatures, the residual replication potential was completely obliterated, emphasizing the replication role of DnaK under the stress conditions, particularly higher temperatures. DnaK was shown to restore DnaA replication activity in ATP-dependent manner by releasing it from phospholipids (Hwang 1990).

DnaK regulated transcription of heat shock genes via modulating $E\sigma^{32}$ holoenzyme formation.

It was known from earlier that the synthesis of DnaK increased at higher temperatures (Pedersen 1978, Herendeen 1979), and mutations in DnaK rendered bacteria thermosensitive (Paek 1987, Bukau 1989). DnaK and Hsp70 were shown to be homologous in 1984 (Bardwell 1984), which substantiated that DnaK was a heat shock protein. Further connecting heat shock and DNA processes, DnaK was revealed to play an important role in modulating bacterial transcription of heat shock genes. It was initially observed that purified bacterial RNA polymerase preparations contained DnaK (Skelly 1988), and further studies presented DnaK's ability to protect RNAP from the heat, as well as to reactivate heat-inactivated RNAP in an ATP-dependent manner (Skowyra 1990). Similarly to the phage replication findings, it was speculated that DnaK aided RNAP to transition between active and inactive states (Skowyra 1990). However, other lines of evidences proposed different aspects, nowadays foundations of DnaK-mediated regulation. Bacterial strain with *dnaK* mutations failed to efficiently discontinue the heat shock response upon cessation of adverse temperature conditions, which was also correlated with high levels of, at the time uncharacterized product of the *htpR* gene, σ^{32} (Tilly 1983). Thus, DnaK was proposed to be direct or indirect negative regulator of the heat shock response. The crucial role of DnaK and other chaperones, such as DnaJ and GrpE, in controlling heat shock response was further shown to be their ability to maintain stability and synthesis of σ^{32} (Straus 1990). DnaK physically interacted with σ^{32} preventing its association with RNAP to form $E\sigma^{32}$ holoenzyme complex at the promoters of heat shock genes and to initiate transcription (Liberek 1992, Gamer 1992). As all DnaK, DnaJ and GrpE were shown to associate with σ^{32}, individual contribution of the chaperones were further dissected. Three chaperones conveyed an ATP-dependent binding/release cycle that controls σ^{32} activity – DnaJ and then DnaK associated with σ^{32} independently to form a ternary complex, and GrpE came in further to yield quaternary complex, after which DnaK and DnaJ release activated σ^{32} (Gamer 1996). Hence, dnaK was, is an important constituent in a negative feedback loop within a homeostatic equilibrium that regulated heat shock gene expression.

DnaK is involved in various DNA repair processes.

Apart from DnaK's involvement in replication and transcription, DnaK mutants were observed to exert higher sensitivity to UV irradiation (Zou 1988). In the same work, the authors have proposed the role of DnaK in stabilizing UvrA, a component of nucleotide excision repair exonuclease, enhancing thereby the catalytic incision activity. Further linking DnaK to the lesions, DnaK recovered DNA binding ability of UmuC, a SOS-induced gene product and a subunit of DNA Pol V, which is the bacterial DNA repair polymerase (Petit 1994). Moreover, DnaK and RecA, an important bacterial DNA repair protein, were shown to have a synergistic effects on cell viability and replication inhibition (Goldfless 2006). DnaK was also assigned a RecA-independent role in misalignments during replication-coupled genetic rearrangements, and it was shown to be epistatic to DNA Pol III in terms of deletion recovery. Overall, DnaK demonstrated series of contributions in maintaining DNA repair fidelity. It maybe generally supported stability of DNA repair components or it was directly woven to the repair processes by remodeling DNA replication fork for efficient DNA repair (Goldfless 2006).

Hsp70 was discovered as a heat shock protein with minor, heat-induced nuclear presence.

Similarly to Hsp90, eukaryotic Hsp70's discovery was associated with heat-shock induced puffing in *Drosophila melanogaster* salivary gland chromosomes and observed changes in protein and RNA synthesis. Upon exposing larvae to elevated temperatures and incubating salivary glands with [^{3}H]uridine, one of the most prevalently changed puffs pointed out was 87B on the chromosome arm 3R (Tissieres 1974) – nowadays known site of HSP70 transcription and HSF1 binding. In corroboration, gel electrophoresis and autoradiography revealed 70 kDa band as one of the most prominent proteins in *Drosophila* after the heat shock (McKenzie 1975). As several other heat-shock associated polypeptides of different molecular weights were conspicuous, the proteins were arbitrary renamed heat shock proteins (HSPs) (Aushburn 1979), the name they hold today as well. Hsp70 was shown to be highly conserved protein – anti-Hsp70 antibodies raised in chicken cross-reacted with Hsp70 in human, hamster and fruit fly cells (Kelley 1981). While studying Hsp70's localization in insect and mammalian cells, it was observed that

substantial amounts of Hsp70 were detected in nuclei after the heat-shock (Arrigo 1980, Velazquez 1984). Once temperature declined, a general shift of HSPs to the cytoplasm was observed. Nuclear Hsp70 was proposed to hold a classical chaperoning role, just like in the cytoplasm, in that it assisted in coping with environmental stresses (Velazquez 1984, Pelhalm 1984). Hsp70 was prominently detected in nucleoli, RNP-enriched sites, and it was shown to interact with RNPs to promote their assembly (Kloetzel 1983, Welch 1984, Pelhalm 1984). Serving as a negative regulator of the heat shock response, Hsp70 was also associated with and modulated DNA binding of Hsf1 transcription factor (Abravaya 1992), much like σ^{32}-RNA Pol association was DnaK-dependent.

Nuclear Hsp70 roles under non-stress conditions are limited to DNA repair findings.

Small quantities of Hsp70 were still localized in the nucleus regardless of stresses and they associated with decondensed chromatin (Lindquist, unpublished, cited in Velazquez 1984). The nuclear roles of Hsp70 under non-stress conditions are poorly explored. *Δssa1* and *Δssa2* deletion strains displayed reduced transcriptional activation at *GAL1* promoter, likely due to delayed promoter nucleosome removal, which would connect Hsp70 to the modulatory chromatin processes (Floer 2008). Majority of the present literature about nuclear Hsp70 strongly points towards DNA repair, which is, however, still not mutually exclusive to the Hsp70's contributions under adverse conditions. As the physical interaction of Hsp70 with human apurinic/apyrimidinic endonuclease HAP1 was observed, the functional role of Hsp70 was demonstrated as well – Hsp70 enhanced the catalytic HAP1 activity, demonstrating an input in base excision repair (BER) (Kenny 2001). Following base removal, Hsp70 stimulated DNA polymerase β DNA gap-filling (Mendez 2003). In agreement with this model and as its application, radiated leukemia cells accompanied by higher exogenous Hsp70 levels displayed enhanced BER activity (Bases 2006). Apart from BER, Hsp70 seemed to be woven to repair mechanisms and genomic events globally. Murine embryonic fibroblasts deficient for Hsp70 demonstrated elevated genomic instability, reflected by the presence of micronuclei and high ratio of normochromatic to polychromatic erythrocytes (Hunt 2004). With heat shock, the effects were detrimental given the phenotypes in which

telomerase activity was reduced, end-to-end chromosomal joining was increased, and S-phase chromosomal aberrations surged. Several studies showed that Hsp70 colocalized with and bound to repair proteins in nucleus, and it helped mitigate radiation or hydrogen peroxide-induced DNA damage, as well as progression past DNA damage check points (Gilbert 2003, Doulias 2007, Kabakov 2006, Kotoglou 2009). The mechanisms by which Hsp70 aids repair processes or genomic maintenance in general have not been fully delineated, but it is strongly anticipated that Hsp70 structurally supports or remodels the DNA repair protein complexes, akin to its prokaryotic homolog.

Hsp70 is involved in viral DNA replication.

Similarly to Hsp90 and p23, Hsp70 was shown to be a eukaryotic host chaperone taking part in viral DNA replication (Hu 1997). As tested with cell-free systems, Hsp70 was required for the reverse transcriptase priming reaction to form hepatitis B viral RNP. Unlike p23, Hsp70 could not be co-immunoprecipitated with the reverse transcriptase, suggesting that its association was very short-lived. Likewise, Hsp70 promoted binding of human papilloma virus initiator to the respective origin and stimulated replication (Liu 1998).

Summary.

Motivations to characterize heat-shock induced puffing of flies' salivary gland chromosomes greatly contributed to the identification of heat shock proteins. One of the most pronouncedly increased puffs contained actively transcribed HSP70 locus – electrophoretic analysis confirmed dominant 70 kDa protein. Decades of studies have shown that Hsp70's roles can be roughly divided in two classes: chaperone association with ribosome nascent chain to assist *de novo* protein folding and stress protein whose levels increase under adverse conditions for the protein rescue. Early findings mentioned heat-shock-triggered surge of Hsp70's in the nucleus, which was naturally linked to the stress-related response. Under non-stress conditions, Hsp70's nuclear connections are currently restricted to the DNA repair field. Unlike prominent stress roles in eukaryotes, bacterial Hsp70 homolog, DnaK, was since its early discovery shown essential for DNA events. It is an important constituent of both bacteriophage and bacterial chromosomal

DNA replication initiation. DnaK is also transcriptionally central figure as it modulates formation of bacterial holoenzyme to control transcription of the heat shock genes. Similarly to its eukaryotic homolog, DnaK has strong ties to several DNA repair processes.

1.2. DNA Events

1.2.1. Chromatin Organization

Basic unit of chromatin fiber is a nucleosome.

Since discovery of the DNA structure in 1953 and appreciation of the DNA length, the packing of total DNA within the nuclei was an intriguing topic. Chromatin was observed to consist of two biochemically distinct categories – free DNA sensitive to DNase digestion and compacted DNA elements resistant to DNase, yet sensitive to tryptic digestion (Rill 1973, Sahasrabuddhe 1974). It was thereby resolved that DNase sensitivity was not restricted to enhanced DNA supercoiling, but involvement of proteins in aiding DNA packing was introduced (van Holde 1974). Using small angle x-ray scattering, DNA was characterized to be intermittent helically packed, "beads on a string" structure or nu (v) bodies (Olins 1973). Since several reports excluded the possibility that the bead species are ribonucleoproteins, it was alluded that they corresponded to nucleoproteins (cited in Olins 1973). DNA associated with proteins or chromatin, as denoted by Walther Flemming (Flemming 1882), was further proposed to be organized in repeating units consisting of eight histone molecules – four different histones being present in duplicates – and less than 200 bp DNA (Kornberg 1974, Noll 1974). The basic chromatin units, DNA wrapped around histones, were defined to be nucleosomes (Kornberg 1974, Kornberg 1977). The name stems from nuclear body (*soma*=body) or nu (v) body, according to the first denotation for the "beads" on strings (Olins 1973). Nucleosomes were further shown to be arranged circularly to form a toroid-like shape (Varshavsky 1975), also known as solenoid or 30 nm fiber, and solenoids loop-wise condense radially to supercoils (Bak 1977, Pienta 1984). Series of early models led to conclusions that overall chromatin fiber was comprised of flexibly jointed chains which allow for coiling to form a higher order structures up to chromosomes (Elgin 1975, Worcel 1977, Schwarzacher 1977, Pienta 1984). These models offered solution for the organization of long DNA (2-3 m) within the small nuclei (several microns).

Chromatin was divided in euchromatin and heterochromatin.

Distributions of nucleosomes across the genomes is not uniform – both in terms of linear nucleosome spacing and further coiling of higher order structures (Leuba 1994). For interphase nuclei, which is the resting phase with no engagement of division-specific processes, it was observed that chromatin can be highly condensed (heterochromatin) or moderately to highly dispersed (euchromatin) (Heitz 1928, Ris 1970). Centromeres, key genomic locations that organize chromosomes during cell division, and telomeres, chromosomal ends, represent some of the first examples of heterochromatin with constitutively condensed elements regardless of the cell cycle stage (Heitz 1928). The term euchromatin was at first used for all chromatin fiber regions that have undergone uncoiling within the telophase (Heitz 1928) – the final stage of the cell division in which chromosomes are separated to two opposite ends to constitute two nuclei. The concepts of heterochromatin and euchromatin were slowly linked to the ability to synthesize RNA off the given DNA template (Berlowitz 1965). It was clear that histone-enriched DNA could hamper RNA production and there were disputable models that the species of histones present within the DNA elements controlled these event (Allfrey 1963, Barr 1963, Comings 1967). The final purpose of DNA structurally occlusive characteristics in heterochromatin or exposed in euchromatin would be to control the activities of specific genes (Stedman 1951). It was, however, observed that the borders between the hetero- and euchromatin were loose as heterochromatin was not completely genetically inert (Hsu 1962). Distinction between constitutive and facultative heterochromatin was introduced – whereas constitutive heterochromatin would be permanently repressed, facultative only under certain cellular circumstances (Brown 1966).

Euchromatin and heterochromatin in modern terms.

In modern terms, specific features are assigned to either chromatin class and transitions between the classes are not necessarily irreversible. Euchromatin is unequivocally regarded to be transcriptionally active region and (facultative) heterochromatin is viewed as a form of conditionally inactivated chromatin state (Henikoff 2000). Heterochromatin is low in gene density, enriched in repetitive sequences, and it

displays low sensitivity to nucleases (reviewed in Henikoff 2000). With arise of epigenetics field, it became evident that distinct post-translational modifications of histone proteins contributed to different chromatin conditions (Braunstein 1996). Euchromatin was shown to be enriched in histone 3 and histone 4 acetylation marks, as well as methylations for the conserved lysine 4 on the histone 3 (Braunstein 1996, Noma 2001). Heterochromatin, on the other hand, is hypermethylated for histone 3 lysine residue 9, and cytosine DNA methylation (Richards 2002). In the literature, eukaryotic heterochromatin is sometimes also referred to intergenic regions (Xue 2015) – elements between the open reading frames (ORFs). Heterochromatin was proposed to functionally regulate euchromatin spread (Weiler 1995). Perhaps the best example for this phenomenon is position effect variegation (PEV) in which, due to gene position alterations, heterochromatin exerted differential effects on euchromatin in *Drosophila melanogaster*, resulting in different eye color phenotypes (Lewis 1950).

1.2.2. Canonical Transcription

Defining transcription process.

Transcription field, which encompasses all entities that enable or are connected to synthesis of RNA using the DNA template, boosted with successful identification and characterization of three distinct eukaryotic DNA-dependent RNA polymerases (Roeder 1969), denoted RNA polymerase I, II and III (Young 1991). Defining RNA polymerase activities was proposed to be a valuable instrument in understanding the mechanisms of gene expression (Roeder 1970). It was mapped earlier in prokaryotes that transcription initiates at selective DNA sequences, termed promoters (Jacob 1964) and terminates at other DNA elements, named terminators (Reznikoff 1972), which together comprise a transcriptional unit. Transcription process was correspondingly divided in three different stages: assembly of RNA polymerase complex, extension of RNA (elongation) and release of the RNA product (termination) (Ossipow 1995). Transcription initiation was

shown to require a cooperative assembly of a multi-subunit complex at the promoter region, named RNA polymerase holoenzyme complex (Chamberlin 1974).

Transcription initiation.

In eukaryotes, RNA polymerase holoenzyme complex was identified to consist of RNA polymerase and several basal or general transcription factors (GTFs) with each having distinct roles within transcription initiation (Zawel 1993). Studies on RNA polymerase II initiation cycle provided explanations of transcriptional regulation that became a keystone model. TFIID is the first GTF to recognize conserved TATA promoter sequences and this interaction is stabilized by TFIIA, after which TFIIB and TFIIF help assemble the RNA polymerase complex (reviewed in Zawel 1993). TFIIE then recruits TFIIH (Maxon 1994), an ATP-dependent helicase that separates DNA double strand (Schaeffer 1993). TFIIH greatly contributes to promoter clearance, which is detachment of most of the GTFs subunits with exception of TFIID, and preparation for elongation (Goodrich 1994, Maxon 1994).

Transcription elongation is coupled to chromatin marking and RNA processing.

A motif of the largest RNA polymerase II subunit Rpb1, heptapeptide repeat on the C-terminal domain (CTD) is subject to posttranslational modifications that are crucial for transition into productive elongation (Phatnani 2006). In particular, phosphorylation of serine 5 on CTD catalyzed by Kin28 (yeast TFIIH) recruits mRNA capping enzymes (Rodriguez 2000). Capping of mRNA allows for splicing (Edery 1985), which is excision of introns or non-coding transcribed RNA sequences (Sharp 2005), and it serves as a recognition mark for later protein synthesis (Sonenberg 1993). Transcription elongation factors Spt4/5 in *Saccharomyces cerevisiae* are also associated with RNA polymerase II after CTD serine 5 phosphorylation to stimulate recruitment of polymerase association factor (PAF1) (Qiu 2006). PAF1 allows for binding of CTD phosphorylated serine 5 target factors, such as H2B ubiquitination machinery Rad6/Bre2, Set1 methyltransferase and early termination complex (Wood 2003, Krogan 2003, Buratowski 2009). H2B ubiquitination is a mark required for active elongation and it forms a platform for both

Set1-mediated H3K4 methylation, 5' specific mark corresponding to active genes, and H3K79 trimethylation, mark for actively transcribed ORFs (Ng 2003, Weake 2008, Pokholok 2005). H3K4 trimethylation is recognized by the early termination complex Nrd1-Nab3-Sen1 (Terzi 2011). Several transcription termination pathways are to be distinguished – Nrd1-Nab3-Sen1 ceases production of cryptic transcripts (Terzi 2011). The most dominant transcription termination employed by the RNA polymerase II is associated with polyadenylation signal, usually past stop codon and engagement of termination components (Kuehner 2011). Overall, the step-wise progression from early into productive transcription elongation is tightly regulated process that safeguards consistency and memory of just passed RNA polymerase, and it prepares the transcript for the downstream events.

Different RNA polymerases transcribe specific gene groups.

Whereas majority of the RNA polymerases' subunits are structurally and functionally conserved, RNA polymerase I and III have subunits not present in RNA polymerase II, which though are still related to TFIIE, TFIIF and TFIIB (Vannini 2012). This was proposed to contribute to different target gene specificities, as RNA polymerases alone are not capable of independent recognition (Liu 2013). RNA Polymerase II transcribes majority of the genome. It is particularly known for transcription of protein coding genes generating mRNAs and also some small nuclear RNA (snRNA) (Koch 2008, Kuhlman 1999), components involved in cellular RNA processing. RNA polymerase III synthesizes 5S ribosomal RNA (rRNA) and transfer RNA (tRNA) (Turowski 2016), which is an adaptor molecule between mRNA and amino acids (Sharp 1985). RNA polymerase I is engaged at loci to synthesize other than 5S rRNAs (Goodfellow 2013).

Removal of transcriptional barriers is mediated by chromatin regulators.

The passage of RNA polymerase is negatively impacted by the presence of the nucleosomes. Nucleosome occupancy in the course of translational elongation is modulated by histone chaperones, post-translational modifications, chromatin remodeling machineries, histone variants and transcription factors (Workman 2006). Histone removal and deposition are actively facilitated by histone chaperones (Schwabish 2004, Kim

2007). Via interaction with elongation subunits, FACT for instance travels with elongating RNA polymerase II to destabilize nucleosomes by removing H2A-H2B dimers (Mason 2003, Belotserkovskaya 2004). In addition to this, FACT reinforces nucleosomal integrity by depositing histones onto DNA (Belotserkovskaya 2003). It is of note that, besides being barriers, nucleosomes are required for proper transcriptional activation as well (Santisteban 1997). Whereas nucleosomal modification marks *per se* have no power to exert considerable structural chromatin changes, they are usually strong tethering points recognized by remodeling machineries that complete this work. Such proteins contain bromodomains or chromodomains – domains that specifically anchor to acetylated or methylated residues (Josling 2012, Murawska 2011). Subunit Rsc4 of the RSC, chromatin remodeler with an ability to perturb chromatin structure (Cairns 1996), has bromodomain that recognizes lysine 14 residue on the histone H3 (Kasten 2004). Mutation of this residue led to impaired RSC-modulated target genes activation (Kasten 2004). Finally, in addition to the chromatin regulators, histone variants are correlated with RNA polymerase activities. H2A.Z, H2A histone variant, colocalizes with the promoters of active genes (+1 nucleosome) (Zhang 2005). It acts as a transcriptional activator via posing for transcription initiation, facilitating elongation, or it serves as a susceptible nucleosome that creates transcriptionally conducive, open region (Zhang 2005, Adam 2001, Santisteban 2011).

Transcription factors regulate transcription.

Besides GTFs that form a part of the RNA polymerase pre-initiation complex (PIC), other transcription factors with no direct physical connections to RNA polymerase serve as important transcriptional regulators. It was observed earlier that genes with comparable patterns of regulation contain similar DNA sequences in their regulatory regions, which were detected to be bound by identical transcription factors (Latchman 1997). For instance, HSF1 recognizes heat shock elements (HSE) and controls the induction of heat shock genes, and hormone receptors bound to glucocorticoid response elements (GRE) comparably induce transcription of hormone-regulated genes (Latchman 1995, Latchman 1997). Hormone receptors are special group of transcription factors superfamily that serve both as cytosolic aporeceptors and nuclear transcription factors

(Yamamoto 1985). Typically, transcription factors can bind numerous unrelated genomic loci and they are classified in families according to their DNA binding domains – helix-loop-helix, leucine zipper, zinc finger or cluster, and other classes (Pabo 1992). Myc proto-oncogene and cell differentiation factors, and Ino2/Ino4 heterodimers that regulate phospholipid biosynthesis, are examples of basic helix-loop-helix transcription factors (Blackwood 1991). Zinc cluster can be found in transcription factors Rsc3 and Rsc30, subunits of RSC chromatin remodeler, and Gal4, a galactose responsive transcription factor (Kraulis 1992, Angus-Hill 2001). To positively or negatively affect transcriptional outcome, transcription factors are believed to contain effector domains that allow for recruitment of downstream transcriptional regulators (Hahn 2011). Whereas such domains are well studied for the transcription factors that directly connect to the basal transcription machinery (Frietze 2011), they have not been well identified for other factors. Transcription factors are in competition with nucleosome positioning or occupancy (Workman 1992, Morse 2003, Ganapathi 2011, Afek 2011), yet sometimes they cooperate to form open chromatin. Reb1 binding is hypothesized to mediate nucleosome depleted regions by recruitment of RSC chromatin remodeler (Hartley 2009). Overall, transcription factors are engaged genome-wide to modulate transcriptional outcomes.

1.2.3. Chromatin Remodeling

Repositioning of nucleosomes, nucleosome removal or modifications of nucleosomes can change the accessibility of DNA elements. Members of the of multi-subunit ATP-dependent helicases superfamily carry out dynamic chromatin remodeling processes for the purpose of controlling chromatin state (Singleton 2007). Four different chromatin remodeler classes with conserved ATPase domain are classified according to their structural traits, chromatin remodeling capabilities and biological context (Clapier 2009). The most abundant class of chromatin remodeling complexes represents SWI/SNF (Sucrose Nonfermenting) family, where also RSC (Remodel the Structure of Chromatin), remodeler essential for viability, belongs (Mohrmann 2005). These molecular

machineries comprised of 8-17 subunits were demonstrated to be very effective in nucleosomal sliding and ejection genome-wide (Cairns 2007). RSC is structurally and in terms of remodeling activities very similar to SWI/SNF, yet the complexes are not identical (Tang 2010). SWI/SNF is known for its ability to activate transcription of numerous genes through relieving chromatin structure (Burns 1997). RSC is more implicated in regulation of the nucleosomes within coding regions (Spain 2014).

INO80 15-subunit complex from the INO80/SWR-C family is the most versatile in terms of its nucleosomal regulation: it can remodel nucleosome to regulate spacing, facilitate ejection and catalyze specific H2A.Z removal (Gerhold 2014). It has roles in transcription, DNA repair, replication and chromosome segregation (Morrison 2009). Related SWR-C chromatin remodeler is specialized for deposition of H2A.Z histone variant (Krogan 2003, Mizuguchi 2004, Kobor 2004), hence, reverse reaction to INO80. ISWI (Imitation Switch), a family of remodelers comprised of 2-4 subunits, and Chd1 monomer and the only member of the family, have the capability to regulate the nucleosomal arrays by sliding octamers (Längst 2001).

1.2.4. Histone Code

It has been established that specific post-translational modifications of the histone protein have the potential to determine the chromatin status (Allfrey 1964). Conserved modification marks are found sequentially or in combination to form so called histone code (Strahl 2000). Despite successful assignment of a mark to a state, discordances occur and it is still not entire clear how histone code models chromatin within the complex regulatory nuclear network. Some examples of the histone code allowed for generalization.

H3 and H4 acetylations.

Acetylation marks are known to changes nucleosomal structure into more open configuration (Norton 1989). Passage of replication fork is also known to leave behind enrichment of histones H3 and H4 acetylated residues (Peterson 2004) – global H3 and H4 acetylations are a hallmark of actively transcribed chromatin. The highest degree of histone H3 and H4 acetylation is to be found after the ATG start codon, within the first 500 bp of the ORF (Roh 2004). Whereas SAGA multi-subunit histone acetyltransferase complexes is mostly in charge of H3 tail residues acetylation, another smaller acetyltransferase NuA4 acetylates H4 tails (Tse 1998, Roh 2004, Allard 1999). The antagonistic removal of acetylated residues is carried out by Hda1 and Rpd3L, which includes Set3C, histone deacetylases (Wu 2001, Kadosh 1998, Wang 2002).

SAGA.

SAGA is 2 MDa conserved HAT comprised of about five modules: acetylation module Gcn5-Ada2-Ada3, which is also known to function independently of the SAGA complex (Grant 1997), module Tra1 that recruits the complex to the DNA (Grant 1998), Spt module (Koutelou 2010), deubiquitinase module (Henry 2003, Ingvarsdottir 2005), and other structural subunits (Sterner 1999). Spt module positively regulates TATA-binding protein (TBP) recruitment (Dudley 1999), which is a constituent of TFIID, RNA polymerase II preinitiation complex (Li 2000). SAGA also contains deubiquitinase activities due to Ubp8 enzyme (Henry 2003), even though it is classified to be a histone acetyltransferase. Both ubiquitination and deubiquitination are sequentially needed for effective transcriptional induction (Henry 2003). Structural integrity of SAGA complex is aided by several subunits, some of which are Spt20 and Ada1 (Wu 2002).

H3 acetylation.

SAGA/GCN5 acetylate H3 at conserved residues H3K9, H3K18, H3K14, H3K27, H3K36, and also H4K8 (Kuo 1996, Grant 1999, Vogelauer 2000, Suka 2001, Bian 2011, Morris 2007). H3K9 acetylation peaks at the promoters and transcription start site of active genes and together with H3K14 correlates with the transcription rate genome-wide – both of the modifications are catalyzed by Gcn5 (Robert 2004, Pokholok 2005,

Karmodiya 2012, Bonnet 2014). Loss of the acetyltransferase SAGA subunit, GCN5, in human cells was shown to cause enormous reduction in the H3 acetylation levels, as expected (Roh 2004). However, impairment of SAGA HAT activities led to both loss of acetylation levels for some genes and gain of acetylation for others (Roh 2004). This suggests involvement of compensatory mechanisms that replenished for the GCN5-mediated loss of H3 acetylation and existence of the complex regulatory network.

NuA4 and H4 acetylations.

Esa1, catalytic subunit associated with the only essential NuA4 acetyltransferase complex, acetylates all four H4 tail residues: H4 at K5, K8, K12 and K16 (Smith 1998, Allard 1999, Clarke 1999, Vogelauer 2000). Esa1 was shown to hyperacetylate H4 lysine resides at the transcription start site of active genes, which modestly correlated with transcription rates (Pokholok 2005). H4K16 was proposed to be the most frequently monoacetylated H4 site of all the other H4 sites (80 %) (Smith 2003). Genome-wide analysis of mutated single and combined H4 lysine residues revealed that H4K16 acetylation perturbations displayed unique consequences for the gene expression, whereas H4K5, K8 and K12 accounted for the cumulative effect with little functional differences (Dion 2005). Of note, H4K12 acetylation mark can also signal gene repression (Turner 1992). It was shown that Esa1 recruitment prevails at the ribosomal protein genes, which colocalized with the general transcription factors such as Rap1 and Abf1 (Reid 2000). It is speculated that NuA4 and INO80/SWR1 work together to promote remodeling changes necessary at the lesion sites, similarly to mammalian TIP60 complex that possesses both HAT and ATPase activities (Attikum 2005).

Rpd3/Set3C histone deacetylases.

Rpd3L expanded histone deacetylase complex involves Rpd3 small (Rpd3S), Rpd3 large (Rpd3L) and Set3 complexes (Set3C) (Shevchenko 2008) – each of which are differentiated according to the shared modules. Targeted recruitment of Rpd3 histone deacetylase complex was shown to facilitate deacetylation (Kadosh 1998). Both Rpd3 and Hos2 subunits deacetylate H4 at K5, K8 and K12, and only Hos2 is necessary for deacetylation of H4K16 (Wang 2002). Rpd3 has been usually described as a repressor

(Kadosh 1997, Robyr 2002), yet there is a subset of genes whose transcription is downregulated upon RPD3 mutation (Robyr 2002).

Hda1 deacetylase.

Hda1 histone deacetylase complex contains another two related subunits, Hda2 and Hda3, both of which are necessary for Hda1 catalytic activity (Wu 2001). Hda1 deacetylates histones H3 and H2B at 2-3 nucleosomes adjacent to the upstream regulatory sequence (URS) to repress the gene activity (Wu 2001). Hda1 suppresses so called Hda1-affected-subtelomeric-regions (HAST) – domains 10-25 kb from the telomeres that are hyperacetylated upon *Δhda1* (Robyr 2002). The HAST domains encode genes that function primarily under the stressful conditions and the transcript levels of these genes are kept low under regular conditions (Robyr 2002). Increase of H3K9 acetylation, as well as transcription rate, was observed in *Δhda1* histone deacetylase knockouts in yeast (Robyr 2002), as expected. However, another acetylation mark H3K18 was reduced in *Δhda1*, suggesting alternative regulatory pathways (Robyr 2002).

Set1 and H3K4 methylation.

H3K4 methylation, catalyzed by Set1 methyltransferase, is a prominent mark usually connected to the 5' region of actively transcribed genes (Bernstein 2002, Briggs 2001, Krogan 2003, Ng 2003, Santos-Rosa 2002, Pokholok 2005). Set1 has been directly linked to the transcription initiation – its recruitment was shown to necessitate both TFIIH and PAF1 elongation machinery (Ng 2003). H3K4 methylation marks were shown to establish a continuous profile along the ORFs – H3K4 trimethylation peaks at the transcription start site of the actively transcribed genes and correlates with the transcription rate, H3K4 dimethylated histones are mostly enriched within transcribed regions, in the middle of the genes, and H3K4 monomethylation peaks at the 3' or at the end of the active genes (Pokholok 2005).

Set2 and H3K36 methylation.

H3K36 trimethylation is catalyzed by Set2 methyltransferase (Strahl 2002), which is believed to be recruited by the elongating form of Pol II (phosphorylated serine 2 of CTD) (Li 2003). Unlike the H3K4 trimethylation pattern that colocalizes at the 5' of the active genes, H3K36 trimethylation peaks throughout the coding region towards the 3' of the active transcription unit and is in correspondence with transcription rates (Pokholok 2005). H3K36 methylation recruits Rpd3 histone deacetylase complex to suppress transcription initiation from 3' (Keogh 2005).

Dot1 and H3K79 methylation.

H3K79 (mono-, di- and tri-) methylation is one of the few modifications that occurs at the core of the histones. It is catalyzed by the Dot1 (disruptor of telomere silencing) (Feng 2002, Ng 2002). H3K79 methylation is estimated to occur in the 90% of all histones and it is proposed to control telomere silencing in yeast (Ng 2003). H3K79 methylation mark genome-wide studies in *Drosophila m.* proposed that the mark associates with active transcription (Schubeler 2004). In other studies it was found that, whereas H3K79 methylation is enriched within the transcribed regions of the genes, there is very little correlation between H3K79 methylation and transcriptional activity (Pokholok 2005). Interestingly, a link between H3K79 methylation by Dot1 DNA damage response was brought up (Wood 2018). Overall, the functionality of this conserved and abundant modification mark is poorly defined.

1.2.5. Aberrant Transcription

Cryptic transcription cases.

The ability of RNA polymerase complex to distinguish transcription start and transcription end, as well as 5' to 3' transcription directionality, has been the founding transcription rule. However, RNA polymerase does not always initiate transcription from the start site till the terminator, nor does it happen in the right direction. Well-studied

example proposed that terminator or 3' in general can be used as a transcription start site under the conditions of impaired chromatin regulators (Carrozza 2005, Churchman 2011). Set2 methyltransferase methylates H3K36 towards the end of the ORF, which then recruits RPD3 histone deacetylase complex to remove 3' acetylations (Krogan 2003, Li 2003). Defective chromatin modifiers from Set2-Rpd3S pathway failed to remove transcriptionally conducive chromatin environment, which allowed for RNA polymerase re-firing and generation of antisense cryptic transcripts originating in the vicinity of the terminator (Carrozza 2005, Churchman 2011). Besides terminators, it was observed that ORF contains numerous cryptic promoters. Here, importance of chromatin remodelers Iswi1, Iswi2 and Chd1, and their nucleosome positioning roles to cover genic cryptic initiation sites was pronounced (Whitehouse 2007, Tirosh 2010, Quan 2010, Henning 2012). Similarly, depletion of histone chaperones such as Spt6 was shown to cause hypersensitivity to micrococcal nuclease and increased transcription initiation from cryptic genic promoters, as well as undermined transcriptional accuracy in general (Kaplan 2003, DeGennaro 2013). Furthermore, transcription past the termination was observed in the absence of a functional termination complex (Steinmetz 2001). Overall, the causes for the aberrant transcription events were explained by defective chromatin regulator in combination with sequence elements within specific chromatin context.

Bidirectional transcription from canonical promoters.

Considering majority of known cryptic transcription events, the least understood yet the most common phenomenon is bidirectional transcription from the canonical promoter. It was observed that active promotes are enriched for short, divergent non-coding transcripts, suggesting that RNA polymerase fires in both directions from the same promoter (Seila 2008). In corroboration, the genome-wide mapping of aberrant transcription confirmed that considerable weight of divergent transcripts is generated within nucleosome free regions associated with promoters of protein-coding genes, which proposed that promoters are intrinsically bidirectional (Xu 2009, Neil 2009). It is not clear what impairs RNA polymerase balance to cause pervasive bidirectionality. While the sole dominance of the underlying sequence *per se*, such as bidirectional promoter nature that fosters bidirectional transcription, has been highlighted (Jin 2017), some contributions of

the chromatin regulators have been underscored as well. For instance, MINC (Mot1, INO80, NC2) complex was reported to operate between eu- and heterochromatin boundary elements to prevent pervasive intergenic transcription (Xue 2017). The question remains whether certain multi-subunit complexes affect transcriptional directionality. It could be assumed that they interact with and modulate RNA polymerase complex – INO80 was shown to facilitate release of RNA polymerase II from the chromatin (Lafon 2015). On the other hand, RNA polymerase holoenzyme is a multi-subunit complex itself comprised of numerous subunits whose function is not fully elucidated. It could be that some of them have specialized, to be discovered roles, depending on the context of available chromatin regulators. In general, the links between chromatin regulating complexes and polymerase, as well as contributions of many of their subunits, are unexplored area within promoter-specific bidirectional transcription field.

2. Objective and Significance

Molecular chaperones are traditionally viewed as cytosolic stress proteins that aid in nascent polypeptide folding, protein maturation and oligomeric protein complex assembly. Many inexorable afflictions correlate with a breakdown in protein homeostasis including neurodegeneration, diabetes and hearts diseases. Notably, molecular chaperone network is inextricably woven to this process. While protein homeostasis is usually only viewed from a cytosolic perspective, patient biopsies have shown that protein aggregates readily occur in the nuclei, indicating an importance for the chaperoning of proteins in the nucleus. Nuclear proteins have one crucial characteristic that differentiates them from cytosolic proteins – they are directly or indirectly challenged by a ligand DNA. Nuclear proteins thus modulate chromatin structure and transcriptional response. Molecular chaperones contributions are, however, less well explored within DNA realms. Whereas molecular chaperones p23 and to some extent Hsp90 were shown to have a few nuclear functions, CCT has been regarded to be solely a cytosolic chaperone. This work will hence address nuclear functions of molecular chaperones CCT, Hsp90 and p23.

In this PhD thesis, the global roles of molecular chaperones in the nucleus, particularly within chromatin under physiological, non-stressful conditions will be examined. Firstly, in-depth historical overview of molecular chaperones CCT, Hsp90, p23 and Hsp70 rooting from their identification to their contemporary stand is delineated. Here, the neglected or less well pronounced examples of molecular chaperones' nuclear functions are described. Secondly, CCT's global nuclear contributions have been examined by utilizing several high-throughput approaches suitable for *de novo* nuclear protein characterization. The results undermine the traditional CCT cytosolic ramifications and present it to be crucial for many nuclear pathways including chromatin and transcription across the genome. Since CCT is found to have a strong effect on bidirectional transcription events, numerous pathways linked to the field of cryptic transcription have been interrogated for CCT's mechanistic influence. The targets are mostly histone modifying complexes, their concomitant histone codes contributions and

involvement at the affected regulatory regions, as well as RNA polymerase complex. Thirdly, Hsp90 system is discovered to lead to global alterations of the chromatin status that will be divided in two independent categories – dynamic chromatin changes tied to active chromatin remodeling where a single chromatin remodeler has been utilized as a model, and chromatin changes dependent on transcription factor stability with evolutionary and oncological applications. In addition, Hsp90's effects on the aberrant transcriptome phenotype will reveal parallels to CCT. P23 has also been explored within the active chromatin remodeling pathway, with a bit of general transcription factor-DNA occupancy. All the mentioned subtleties will be addressed experimentally by implementing an array of chromatin related *in vivo* and *in vitro* assays in conjunction with chaperones and bioinformatics.

The findings of this work are entirely novel and suggest a new insight of molecular chaperones in the nucleus under steady-state conditions, in which they act as highly specific yet global chromatin regulators, either aiding the change of the chromatin status or controlling the transcriptome identity. This work will merge together the fields of chromatin remodeling and transcription with chaperone biology.

Objective and Significance (German)

Molekulare Chaperone werden traditionell als zytosolische Stressproteine angesehen, die bei der Polypeptidfaltung, der Proteinreifung und der Zusammenlagerung von oligomerem Protein helfen. Viele schwere Erkrankungen, wie beispeilsweise Neurodegeneration, Diabetes und Herzerkrankungen, gehen mit einem Zusammenbruch der Proteinhomöostase einher. Die molekularen Chaperon-Netzwerke sind in diese Prozesse involviert. Obwohl die Proteinhomöostase normalerweise im Zytoplasma lokalisiert wird, haben Patientenbiopsien im Zellkern vorkommende Proteinaggregate gezeigt, was auf die Wichtigkeit von Chaperonen in den Zellkernen hinweist. Kernproteine haben eine entscheidende Eigenschaft, die sie von cytosolischen Proteinen unterscheidet – sie werden direkt oder indirekt durch eine Liganden-DNA herausgefordert. Kernproteine modulieren somit Chromatinstruktur und Transkriptionsantwort. Die Beiträge der molekularen Chaperone sind jedoch innerhalb der DNA-Bereiche weniger gut erforscht. Es wurde jedoch gezeigt, dass die molekularen Chaperone p23 und teilweise Hsp90 einige nukleare Funktionen aufweisen, während CCT als ausschließlich cytosolisches Chaperon angesehen wird. In dieser Arbeit werden die Kernfunktionen der molekularen Chaperone CCT, Hsp90 und p23 erforscht.

In dieser Dissertation werden die globalen Rollen molekularer Chaperone im Zellkern, insbesondere bezogen auf das Chromatin unter physiologischen, stressfreien Bedingungen untersucht. Zunächst wird ein detaillierter historischer Überblick über die molekularen Chaperone CCT, Hsp90, p23 und Hsp70, die von ihrer Identifizierung zu ihrem gegenwärtigen Stand führen, gegeben. Es werden die vernachlässigten oder weniger gut ausgeprägten Beispiele der Kernfunktionen molekularer Chaperone beschrieben. Zudem wurden die globalen Kernbeiträge von CCT untersucht, durch Verwendung von mehreren Hochdurchsatz-Ansätzen, die für die *de novo* Kernproteincharakterisierung geeignet sind. Die Ergebnisse unterstreichen die traditionellen CCT-zytosolischen Rollen und präsentieren CCT als entscheidend für viele nukleare Wege, einschließlich Chromatin und Transkription im gesamten Genom. Da

CCT eine starke Wirkung auf die bidirektionalen Transkriptionsereignisse hat, wurden zahlreiche mit dem Gebiet der kryptischen Transkription verbundene Wege auf den mechanistischen Einfluss von CCT untersucht. Die Targets sind hauptsächlich Histon-modifizierende Komplexe, ihre begleitenden Histon-Code-Beiträge und die Beteiligung an den betroffenen regulatorischen Regionen, sowie RNA-Polymerase-Komplex. Dannach werden die Entdeckungen beschrieben, wie das Hsp90-System zu globalen Veränderungen des Chromatinstatus führt. Diese werden in zwei unabhängige Kategorien unterteilt: (i) dynamische Chromatinveränderungen, die mit aktivem Chromatin-Remodeling verbunden sind, wobei ein Chromatin-Remodeler als Modell verwendet wurde; (ii) und Chromatinänderungen in Abhängigkeit von der Transkriptionsfaktorstabilität, mit evolutionären und onkologischen Anwendungen. Darüber hinaus zeigen die Auswirkungen von Hsp90 auf aberrante Transkriptom-Phänotyp Parallelen zu CCT. P23 wurde auch innerhalb des aktiven Chromatin-Remodelling-Wegs mit allgemeiner Transkriptionsfaktor-DNA-Belegung untersucht. Alle genannten Phänomene wurden experimentell untersucht, indem eine Reihe von Chromatin-bezogenen *in vivo* und *in vitro* Assays in Verbindung mit Chaperonen und Bioinformatik durchgeführt wird.

Die Ergebnisse dieser Arbeit sind völlig neu und deuten auf eine neue Erkenntnis von molekularen Chaperonen im Kern unter stationären Bedingungen hin, in denen sie als hochspezifische, aber globale Chromatinregulatoren fungieren, die entweder die Veränderung des Chromatinstatus oder die Kontrolle der Transkriptomidentität unterstützen . Diese Arbeit wird die Bereiche Chromatin Remodelling und Transkription mit Chaperon-Biologie zusammenführen.

3. Protocols

3.1. PCR Reactions

PCR reactions were performed using commercial Taq Polymerase, Phusion Polymerase or Q5 Polymerase (NEB) in 25 µl or 50 µl reaction volume. The reaction was assembled on ice. dNTPs were supplied to 400 nM final concentration for each nucleotide. Primer concentration was 0.5 µM each when using Taq Polymerase, and 0.2 µM for Phusion and Q5 Polymerases. Primers were usually designed to meet the annealing temperature of 60 ˚C. 2.5 µM $MgCl_2$ was supplied for Taq Polymerase PCR reaction and it was omitted for Phusion and Q5 Polymerases PCRs. 50 ng genomic DNA or pg-ng plasmid was used as a template. 1:100 of the commercial polymerase was added to the reaction, after which samples were promptly placed in hot-started thermal cycler (BioRad iCycler or Applied Biosystems Pro-Felx 3x32 well PCR System).

3.2. Cloning

PCR product to be cloned was purified with QIAGEN kit directly or gel excised prior to QIAGEN purification. Restriction digestion reactions were prepared on ice with enzyme(s) being added the last. The restriction enzymes and corresponding buffers were combined according to NEB manufacturer's instructions. PCR product was digested in 40 µl reaction volume and ~ 2 µg plasmid was digested in 20 µl reaction volume – both were digested overnight in 37 ˚C room. Before proceeding with ligation, plasmid was additionally treated with CIP for half an hour (0.25-0.5 µl of the CIP enzyme stock was added to the digested plasmid directly). Both plasmid and PCR product were purified directly with QIAGEN column or gel excised prior to purification. 0, 1, 2 and 4 µl of the insert were combined with 1 µl vector, together with T4 Ligase buffer and T4 ligase (0.25

µl T4 Ligase) in 10 µl reaction volume on ice. Ligation reaction were incubated overnight in 16 ˚C incubator. Samples were briefly spun down to collect droplets, kept on ice and transformed with XL1 blue strains. Following day, colony PCR for the insert was done. Positive clones were grown in LB with appropriate antibiotic, and plasmids were mini-prepped and restriction digested to verify correct insertion.

3.3. Bacterial Mini-prep

Colonies were inoculated in 1.5 or 2-ml microcentrifuge tubes containing LB media with appropriate antibiotic. The tubes were closed with membrane lids (Eppendorf) and placed in a mini shaker (IKA Vibrax VXR basic, Ika-Werke Type VX2E) and bacteria were grown at 500-1000 rpm for 3-4 h at 37 ˚C. The membrane lids were recycled, the tubes were closed and bacteria were spun down at 4000 rpm for 5 min. Media was discarded and bacterial pellet was resuspended in 200 µl P1 buffer (50 mM Tris·HCl (pH 8), 10 mM EDTA·NaOH (pH 8), 100 µg/ml RNase A). 200 µl P2 buffer (1% SDS, 0.2 N NaOH) was added and cells were lysed by inverting tubes couple of times. Then, 200 µl P3 buffer (3 M potassium acetate, 11.5% glacial acetic acid) was added, tubes were mixed by inversion couple of times and incubated on ice for 10 min. The cells were spun down at 13000 rom for 10 min and 600 µl were transferred to a new, clean tube, to which 700 µl isopropanol was added. Tubes were inverted couple of times and centrifuged at 14000 rpm for 20 min to precipitate DNA. Supernatant was decanted and pellet was washed with 500 µl 70% ethanol. Thereby, DNA pellets were incubated for 1 min in 70% ethanol, centrifuged for 5 min at maximum speed and supernatant was discarded. DNA pellet was dried using speed vacuum and resuspended in 40-50 µl sterile water.

3.4. Preparation of Chemically Competent Cells

Chemically competent cells were streaked out on LB plates (containing 12 µg/µl tetracycline for XL1 strain) and incubated overnight in 37 ˚C room. Cells were inoculated in 50 ml LB (with 12 µg/µl tetracycline) and overnight culture was grown at 30 ˚C, usually in VWR DS-500E Orbital Shaker set at 16500 rpm, placed in the incubator (BioCold Environmental). Following day, 10-20 ml of the overnight culture was inoculated into 1 L LB media at OD(600)=0.25. Cells were grown at room temperature to OD(600)=0.4-0.5 (in the Labline Orbit Shaker 3590 (Labline Instruments) at the setting 6) and then centrifuged down for 5 min at 3700 rpm in Sorvall RC 3CPlus at 4 ˚C. The bacteria were resuspended in 150 ml ice cold MS buffer (10 mM MOPS·HCl (pH 6.7), 15 mM $CaCl_2$, 250 mM KCl, 55mM $MnCl_2 \cdot 4H_2O$) and incubated on ice for 10 min. The cells were centrifuged down at 3700 rpm for 5 min at 4 ˚C and resuspended in 18.6 ml ice cold MS buffer, after which 1.4 ml cold DMSO was added. The bacterial cells were incubated for 10 min on ice, aliquoted in pre-cooled 1.5 ml microcentrifuge tubes and flash frozen in dry-ice and methanol.

3.5. Bacterial Transformation

Stocks of chemically competent cells (from the -80 ˚C store) were thawed on ice. 50-100 µl cells were added to the tubes containing 1 ng – 1 µg plasmid DNA and kept on ice for additional 30-60 min. The bacterial were heat-shoked in 42 ˚C water bath (Isotemp 215 Fisher Scientific) for 90 s and recovered on ice for 20-60 min. 400-1000 µl LB media was added to the bacterial and the microcentrifuge tubes containing bacteria were placed in a 500-ml flask. The flask was attached via shaker flask flip holder to the 37 ˚C-room shaker (Gio Girotory shaker, New Brunswick Scientific) set to 210-230 rpm and shook for 1-2 h. The cells were plated on 15-25 ml LB-agar plates containing appropriate antibiotic (Table 3.5.1.) and incubated overnight in 37 ˚C room.

Table.3.5.1. Antibiotics and concentrations used.

	Working stock	Final concentration	Dissolved in
Ampicillin	200 mg/ml	200 µg/ml	water
Kanamycin	50 mg/ml	50 µg/ml	water
Chloramphenicol	25 mg/ml	25 µg/ml	100% ethanol
Streptamycin	50 mg/ml	50, 500 µg/ml	water

3.6. Yeast Transformation

The protocol for the yeast transformation was modified from Gietz 2008. For the final transformation with 8 different target DNAs, 10 ml YPD in 50-ml test tube was inoculated with the yeast. For the slower growing strains, half of the loop tip was inoculated and for the faster growing strains, only a small dot was taken. The yeast were inoculated from the plates with well grown yeast (the sterilized and cooled down loop was passed over several colonies prior to inoculation), not older than 1 week, preferable 3 days recovered after restreaking from -80 ˚C glycerol storage. The cells were grown overnight in roller drum (New Brunswick Scientific Tc-7 Roller Drum) set at 7 and placed in 30 ˚C incubator (BioCold Environmental). Following day, overnight yeast cultures were inoculated in 50 ml YPD to OD(595)=0.25 and grown to OD(595)=1 at 16500 rpm on VWR DS-500E Orbital Shaker placed in the incubator (BioCold Environmental) set at 30 ˚C. The cell culture was harvested in 50 ml conical tube at 2500 rpm for 5 min in Sorvall Legend RT. The cells were washed with 25 ml sterile water, resuspended in 1 ml 100 mM lithium acetate and transferred in 1.5 ml microcentrifuge tube. Cells were pelleted for 10 s at top speed and lithium acetate was removed with P1000. The cells were gently resuspended to a final volume of 500 µl and 50 µl was added to the basic transformation mix consisting of: 240 µl PEG (50% w/v), 36 µl 1M lithium acetate, 5 µl freshly boiled and cooled down salmon sperm DNA, 0-20 µl DNA, 14 µl sterile water. The samples were vortexed quickly and vigorously for up to 1 min and incubated for 40 min at 42 ˚C (Isotemp 215 Fisher Scientific). Temperature sensitive strain were incubated 30 min at 30 ˚C (Isotemp 210

Fisher Scientific) followed by 20 min incubation at 37-42 °C, or transformation mix was left overnight at the bench. The samples were centrifuged at 6000 rpm for 10-15 s and the supernatant was removed using P1000. Pellet was gently resuspended in 100-200 µl sterile water and plated on the plates with appropriate selection markers (2% dextrose, 6.7 g/l nitrogen base without amino acids, commercial amino acid drop-out mix). The cells were incubated 2-3 days at 30 °C (BioCold Environmental), or until healthy colonies were to be seen. If G148 selection marker was used, transformed yeast were plated on YPD plates and the following day replica plated on G148-containing YPD plates (400 µg/µl). Yeast transformants verification was performed using PCR and Western Blot.

3.7. Yeast Viability/Contamination Assay

For the fast contamination check-up of the yeast in the liquid media, 250-1000 µl yeast were spun down in a 1.5 ml microcentrifuge tubes for 3-5 min at 2500 rpm. The yeast pelleted down at this speed and the supernatant appeared clear if the culture was free of contamination. Provided there was a turbid cloud in the supernatant after the centrifugation, samples were contaminated with bacteria.

Another yeast contamination assay involved usage of the light microscope at 20-40x magnification. 10 µl of logarithmically dense yeast or briefly centrifugation-concentrated yeasts were pipetted on the previously 70% ethanol washed and dried slides and covered with sterilized cover slips. Alternatively for more volume, a chamber was created with heat-block-melted parafilm pieces organized on the sterile slide to create a cubic well, over which a cover slip was 3-sidedly sealed – the final side was sealed after filling the chambers with the cells. Yeast cells were circular or budding, sometimes slightly oval and significantly different in shape than smaller bacterial rod-shaped, spiral or spherical species.

3.8. Colony PCR for Bacteria and Yeast

Small amount of colony was inoculated in 25 µl 20 mM NaOH and vortexed at maximum setting for 10 s. The samples were incubated on heat block (95 ˚C) for 10 min, cooled on ice for 2 min, and then centrifuged at maximum speed for 5 min at 4 ˚C. 2 µl of this supernatant was used for 50 µl colony PCR reaction. The PCR reaction was modification of the standard PCR reaction where Taq Polymerase was applied at 1:250 and primers were supplied to 100 nM final concentration each. Check primer pairs were designed to verify correct insertion both upstream and downstream of the target location (~100-500 bp up- or downstream). Thereby, upstream check primer pair included the gene or plasmid specific sequence upstream of the insertion as a forward primer, whereas a reverse primer was reverse complement of the insert specific sequence. Downstream check primer pair contained the insert specific sequence as a forward primer and reverse complement of the gene or plasmid specific sequence downstream from the insert location as a reverse primer. Positive control (primers used for the initial generation of the insert) and negative control (primers applied on non-specific DNA) were used as well.

3.9. Yeast Genomic DNA Isolation

The protocol was modified from CSH Protocols (Amberg 2005). 10 ml YPD (or selective) medium was inoculated with appropriate yeast culture and incubated on roller drum (New Brunswick Scientific Tc-7 Roller Drum) placed in 30 ˚C incubator (BioCold Environmental) overnight to saturation. The cells were transferred in 15 ml conical tubes and centrifuged at 2500 rpm for 5 min in Sorvall Legend RT. Supernatant was decanted and the cells were resuspended in 500 ml sterile water and transferred in 2 ml microcentrifuge tubes. The cells were briefly spun down (by bringing the centrifuge to the maximum speed), supernatant was removed and the pellet was resuspended in 200 µl SDS-Triton lysis buffer (10 mM Tris·HCl (pH 8), 2% (v/v) Triton X-100, 1% (w/v) SDS, 100 mM NaCl, 1 mM EDTA·NaOH (pH 8)), following addition of 200 µl

phenol:chloroform:isoamyl alcohol and 0.3 g acid-washed glass beads. The cells were vortexed horizontally at the maximum speed setting on the micro vortexer (Fisher Scientific) for 5 min, after which 200 µl of TE was added and the lysate was clarified for 10 min at 14000 rpm. The aqueous layer was transferred into a new tube and nucleic acids were precipitated with 100% ethanol. Thereby, 1 ml 100% ethanol was added to the separated aqueous phase and the tubes were mixed by inversion. For a better yield, samples were incubated at -20 ˚C for 1h to overnight prior to centrifugation at 14000 rpm for 10 min. Supernatant was removed and 400 µl TE containing 75 µg/µl RNase A were added to the pellet. The pellet was resuspended only by gently tapping the tubes. The samples were incubated for 1 h at 37 ˚C to digest RNA, and then precipitated with 10 µl 4 M ammonium acetate and 1 ml 100% ethanol (mixed by inversion, centrifuged for 10 min at 14000 rpm). The pellet was dried using speedvac concentrator (Eppendorf Vacufuge 5301 Vacuum Centrifuge Concentrator) and resuspended in 50 µl sterile water.

3.10. Yeast Cell Extract Preparation for Western Blot

10 ml YPD overnight culture was collected and supernatant was discarded. 500 µl TE (100 mM Tris·HCl (pH 8), 10 mM EDTA·NaOH (pH 8)) was added to the cell pellet, which was resuspended and the volume was recorded using P1000. The solution was transferred into 2-ml flat bottom tubes, centrifuged for 10 s or enough to bring the centrifuge to maximum speed and the supernatant was decanted. Pellet was resuspended in 3x pellet volumes of cold Western blot lysis buffer (20 mM Tris·HCl (pH 6.9), 1 mM EDTA·NaOH (pH 8), 100 mM NaCl, 0.1% Triton-X100, 1mM PMSF, 1 mM DTT, 1x protease inhibitor cocktail). Cold glass beads were added to ~1mm below the liquid volume in the tube. The tubes were put in the beat beating machine (Thermomixer R, Eppendorf) programmed to 37 min with alternating beating cycles (1 min beating, 2 min rest) at 4 ˚C. Two duplicate sets of fresh tubes were prepared by poking a hole with a push pin on the bottom of the first tube and placing it over the second tube. The beaten

solution was transferred into the first tube attached to the second tube by holding both openings tightly together and flicking the wrist hard to transfer the beads. It was made sure that the second new tube under the hole of the first tube does not slip away, since some of the liquid started to drain through the hole. Two new tubes were placed in the 4 °C-room centrifuge (Eppendorf 5417C) and pulsed to 5000 rpm without the lid to push the cell extract in the second tube, retaining the beads in the first tube. The first tube was discarded and the cell extract was clarified for 10 min at 7000 rpm at 4 °C. Supernatant was preserved (~ 200 μl) and the pellet was discarded. Concentration was determined using BCA assay.

3.11. BCA Assay for Protein Concentration

For determining total protein content of the crude extracts, Pierce BCA Protein Assay Kit was used (Thermo Fisher Scientific). A standard regression curve was generated using bovine serum albumin (BSA) concentration gradient and unknown concentrations of the samples to be tested were extrapolated from the curve. Thereby, albumin standard from the kit ampule (2 mg/ml) was added to the tubes containing 10 μl water to create following gradient: 0, 1, 3, 5, 10, 15 and 20 μg/μl BSA. Samples to be tested were prepared similarly as standards, usually adding 1 and 2 μl of the prepared crude extract to the tubes (each in duplicates), or using higher dilutions if concentrated purified proteins were to be measured. Buffer A and buffer B from the kit were mixed in in 50:1 ratio and 1 ml AB mix was added to each tube containing protein standard and samples to be tested. The tubes were incubated at 37 °C (Isotemp 215 Fisher Scientific) for 30 min and the absorbance was measured at 562 nm using spectrophotometer (Amersham Biosciences Ultrospec 3100 Pro).

3.12. Agarose Gels

Agarose (1-2%) was dissolved in 1x TAE buffer (40 mM Tris, 20 mM acetic acid, 1 mM EDTA) by brief boiling and intermittent mixing. Ethidium bromide was added to the melted agarose at 0.5 µg/ml final concentration, which was then cast on the gel tray tightened into gel caster to solidify, together with the comb of appropriate size (BioRad). Agarose gels were ran on horizontal electrophoretic systems (BioRad) using 1x TAE running buffer, usually at 120 V for 20-30 min. Separated DNA fronts within agarose gel were visualized with BioRad Gel Doc System using ethidium bromide filters.

3.13. Native Gradient Gels

A gradient maker (Hoefer SG Series Gradient Makers: 15 and 50) was set up with the chamber A containing 4% acrylamide gel (4% from 40% 37.5:1 acrylamide, 89 mM Tris, 28.5 mM Taurine, 0.5mM 0.1% APS, 0.01% TEMED) and chamber B containing 15% acrylamide gel (15% from 40% 37.5:1 acrylamide, 89 mM Tris, 28.5 mM Taurine, 0.5mM 0.1% APS, 0.01% TEMED). The stopcock between the chambers was closed, as well as the tube outlet from the chamber B (a mixing chamber with a stir bar) leading to the spacer- and short-glass plates cassette with 8 cm (L) x 0.75 mm (W) x 7.3 cm (H), tightened on the casting stand via casting frames (Mini-Protean Tetra Cell Casting Stand with Clamp Kit, BioRad). After adding APS and TEMED to both gels in chamber A and B, pressure was applied to the chamber A and the stopcock between the chambers was opened. The tube outlet from the chamber B was opened as well and the pressure was applied to the chamber B until the gel solution started to drain and finally was dispensed. If the flow rate from the chamber A was slow as displayed by lower chamber B volume, additional pressure was applied to the chamber A. Alternatively for smaller gradient makers (Hoefer SG 15), all stopcock and outlet were opened at once and pressure applied firstly to the chamber A and then to the chamber B. After solidifying, stacking gel was cast (3.2% from 40% 37.5:1 acrylamide, 89 mM Tris, 28.5 mM Taurine, 0.5mM 0.1%

APS, 0.01% TEMED) and the gel was ran at 150 V for at least 1 h at room temperature or 4 ˚C (Mini-Protean 3 Cell and PowerPac 300/Basic, BioRad) in 1 x GTG buffer (89 mM Tris, 28.5 mM Taurine, 0.5mM).

3.14. SDS-PAGE Gels

SDS-PAGE buffers were prepared as described in or modified from Lab Ref (Roskams and Rodgers 2002, CSH). Resolving gel (0.375 M Tris·HCl (pH 8.8), 10-15% from 30% 37.5:1 acrylamide, 0.1% SDS, 0.05% APS, 0.01% TEMED) was cast first in Mini-Protean system glass plates (BioRad), on top of which stacking gel (0.125 M Tris·HCl (pH 6.8), 4% 37.5:1 acrylamide, 0.1% SDS, 0.05% APS, 0.024% TEMED) was added together with 8- or 15-well combs. Protein samples were resuspended with 5x Laemmli (0.312 M Tris·HCl (pH 6.8), 10% SDS, 25% β-mercaptoethanol, 0.05% bromophenol blue, 25% glycerol) and cooked on 95 ˚C heat block before loading; Precision Plus Protein Dual Color Standard (BioRad) was included as a marker. SDS denaturing gels were run in 1x SDS running buffer (25 mM Tris, 192 mM glycine, 0.1% SDS) using Mini-Protean 3 Cell and PowerPac 300/Basic (BioRad) at 240 V for 30 min (10% gel) or 40 min (15% gel). For protein visualization, gels were stained in Coomassie Brilliant Blue staining (45% methanol (methanol:H_2O 1:1 v/v), 10% glacial acetic acid, 0.25% Coomassie Brilliant Blue) and destained in water by bringing it to the boiling point and letting it cold down. For more sensitive visualization, Sypro Ruby Protein Gel Stain (Thermo Scientific) was used. Thereby, a gel was fixed in 100 ml fixation solution (50% methanol, 7% glacial acetic acid) nutating for 30 min at room temperature. The fixation step was repeated in another clean 100 ml of fixation solution, after which it was stained in Sypro Ruby Protein Gel Stain nutating overnight at room temperature. The gel was washed in wash solution (10% methanol, 7% acetic acid) nutating for 30 min, then washed in deionized water for 5 min and visualized with BioRad Gel Doc System using ethidium bromide filters (UV light source).

3.15. Western Blot

Wester blot buffers were prepared as described in or modified from Lab Ref (Roskams and Rodgers 2002, CSH). After size separating proteins on the SDS gel via Mini-Protean electrophoretic setup, the gel was incubated for a minute, together with nitrocellulose membrane (6 cm x 9 cm) (GE Healthcare Amersham Hybond Membrane), in Western blot transfer buffer (192 mM glycine, 25 mM Tris, 0.037% SDS, 20% methanol). Two pieces of Whatman paper (6 cm x 9 cm) were soaked in the same buffer, placed on a support frame of a Trans-Blot SD Semi-Dry Transfer Cell (BioRad) and any bubbles were removed with a roller. Soaked membrane was gently put on the Whatman papers, after which gel was placed together with additional two pre-soaked Whatman paper pieces on the top. The final "sandwich" was rolled out to remove air bubble and the lid of the setup was closed. The transfer proceeded at 22 V for 30 min for 1 gel (and up to 40 min for 4 gels). The membrane was blocked in PBS (137 mM NaCl, 2.7 mM KCl, 8 mM Na_2HPO_4, 2 mM KH_2PO_4) containing 4% milk for 10 min nutating, washed in PBS containing 0.02% Tween three times for 10 min (each wash) and incubated in primary antibody solution (PBS with 5% BSA, 0.02% sodium azide and appropriate diluted antibodies) overnight at 4 °C. The membrane was washed in PBS with 0.02% Tween three times for 10 min and then incubated with secondary antibodies (ECL Anti-rabbit (or mouse) IgG Horseradish Peroxidase linked fragment $F(ab')_2$ from donkey, Amersham) in PBS with 4% milk for 1 h nutating at room temperature. The membrane was washed in PBS with 0.02% Tween three times for 10 min and the chemiluminescence reaction via secondary antibodies was started with Pierce ECL Western Blotting Substrate reagents (Thermo Scientific) that were pipetted on the membrane. The Saran wrapped membrane was placed in a hypercassette (Amersham), exposed in the dark room with autoradiography films (HiBlot CL Autoradiography films, Denville), and developed (Futura 2000 K automatic x-ray film processor).

3.16. Electrophoretic Mobility Shift Assay

20 bp double-stranded DNA probe or PCR-amplified DNA fragment was phosphorylated with radioactive ^{32}P via ATP[γ-^{32}P] (Perkin Elmer, MP Biomedicals). For the preparation of a 20 bp oligo, 50 µl labeling reaction was set up, consisting of 2 µM forward primer, T4 Polynucleotide Kinase (T4 PNK) Buffer (NEB), 10 µU T4 PNK (NEB) and 10 µCi ATP[γ-^{32}P] at 3000 Ci/mmol. The reaction was incubated for 1 h in 37 ˚C water bath. For longer, to be amplified DNA fragments, primers were labeled similarly as oligos, except 10 µM forward and reverse primer, and 20 µCi ATP[γ-^{32}P] were used. After incubation, sample were spun down to collect all droplets and purified using prepared sepharose-packed spin columns (Micro Bio-Spin 6 Column, BioRad). The mini spin columns were equilibrated by inverting the content several times, breaking the bottom snap-off tip and uncapping the tube top to allow the storage solution to drain by gravity. Residual storage solution was removed by centrifugation at 5000 rpm for 3 min at 4 ˚C (Sorvall Biofuge Fresco). The mini spin columns were placed in fresh 1.5 ml microcentrifuge tubes, radiolabeled samples were pipetted on the resin and eluted by centrifugation at 5000 rpm for 5 min at 4 ˚C. For short oligo preparation, 20 bp forward labeled and purified oligo was annealed to excess of its unlabeled reverse primer in 40 µl reaction volume consisting of: 20 µl (1 µM) previously labeled forward primer, 2.5 µM cold reverse primer and annealing buffer (10 mM Tris·HCl (pH 7.58), 50 mM NaCl, 1 mM EDTA·NaOH (pH 8)). The sample was held for 3 min at 95 ˚C (Dry Bath Incubator, Fisher Scientific) and then allowed to cold down to room temperature together with the removable heat block. Regarding longer fragments, labeled purified primers were used at 0.5 µM for the PCR reaction and the PCR product was verified on 2% agarose gel. In binding reactions, labeled oligos were used at 20-50 nM final concertation and the PCR product at 50 nM. For decayed probes older than 2 weeks, concentration used were increased 1.5-3 fold.

SUMO-tag purified recombinant transcription factors (Abf1, Cbf1, Ino2, Ino4, Met31, Rap1 and Reb1) were incubated in transcription factor binding buffer (4 mM Tris·HCl

(pH8), 4mM MgCl$_2$, 4% glycerol 250 mM KCl or 50 mM KCl (250 mM for the protein preps with high nuclease contamination) and 1 mM DTT (Lopes 1991)) with increasing Hsp82 concentrations (0, 4, 12, 36 µM) and 20-50 nM oligos for 30 min at 37 °C, usually in 25 µl reaction volume. All binding buffers were prepared as 5x concentrates; buffer-oligo master mix was added to each reaction tube the first and proteins were always added the last. Reactions were prepared on ice quickly until all components were added.

Table 3.16.1. Optimized transcription factor concentrations and respective oligos sequences used.

Transcription factor	Final protein concentration	DNA oligo
Abf1	100 nM	GAAG ATCACTTCTAACC AAAG (PGK1)
Cbf1	1 nM	GCG CACGTGACTACAACTGTGG CTG (GSH1)
Ino2	1.25 µM	TTAATT CACATGG AGCAGA (INO1)
Ino4	1.25 µM	TGCGG CATGTGAAAA GTATT (INO1)
Ino2/4	300 nM	TGCGG CATGTGAAAA GTATT (INO1)
Met31	1 µM	GCG CACGTGACTACAACTGTGG CTG (GSH1)
Rap1	250 pM	CACACACCCACACACCACA
Reb1	113 nM	GGGGAA GCGGGTAA GCTGCC (ACT1)
Rsc3/30	70-200 nM	ACGCGCGCGCGGCCGGGCCA (ACC1_TIM23)

SUMO-tag purified Rsc3 (90 nM), Rsc30 (90 nM) and Rsc3/30 (90 nM) were incubated in nucleosome binding buffer (10 mM Tris·HCl (pH 7.4), 40 mM NaCl, 4% glycerol, 1 mM DTT and 50 µg/ml BSA) with 20-50 nM oligo (ACC1/TIM23) and Sba1 (4, 12, 32 µM) or Hsp82 (0, 4, 12, 36 µM) for 10 min at room temperature in 10 µl reaction volume. TAP-tag purified RSC (10 nM) was treated under the same conditions, except 100 bp PHO8 promoter nucleosome depleted region (forward primer: TACACCCCTCGTAAGGCGC, reverse primer: CCCTTTACTTTTCCTCTACGC) was used and sba1 or sba1Δ84 control titrated in the following range: 0, 2, 4, 8, 16, 32 µM.

Proteins were diluted in nucleosome binding buffer before usage and dilutions were not to be reused on the following day.

Native GTG gel (89 mM Tris, 28.5 mM Taurine, 0.5mM, 4% (40% 37.5:1 or 19:1) acrylamide, 0.04% APS, 0.01% TEMED) was cast between spacer-separated glass plates appropriate for Vertical Electrophoresis System 20x20 cm (Fisher Scientific) 1 h before samples were ready to run to allow the gel to polymerize. The gel was pre-run at 150 V (PowerPac 300/Basic, BioRad) in 1 x GTG buffer (89 mM Tris, 28.5 mM Taurine, 0.5mM) for 30 min prior to loading the samples. The samples were resolved for 1.5 h (oligo) and 2 h (DNA fragment) at 150 V and 4 ˚C. After the run, the glass plates were separated without disrupting the gel and fostering the gel to stay attached to one plate. The gel was transferred onto Whatman paper by placing the paper over the gel and lightly pressing. The gel was dried in the gel drier (Speed Gel SG210D, Savant) with Saran wrap over it. Dried gel was put in a storage phosphor cassette (Bas Cassette 3 2040, Fujifilm), with pre-bleached storage phosphor screen on top of it and developed using Storm 860 Molecular Imager (Molecular Dynamics).

3.17. Spot Test Assay

For each strain, the yeast culture inoculum was kept identical and in as small quantity of cells as possible. Tip of the loop containing respective strain was inoculated in 50 ml test tube containing 5 ml YPD or other indicated selective media. Yeasts were grown to the stationary phase on roller drum (New Brunswick Scientific Tc-7 Roller Drum) set at 7 for 2 days in 30 ˚C incubator. Pre-labeled 1cm^2 templates were attached to the YPD, YPGE (1% yeast extract, 2% peptone, 3% glycerol, 2% bacto agar and 9.5% ethanol) or selective media (2% dextrose, 6.7 g/l nitrogen base without amino acids, commercial amino acid drop-out mix) plate bottom. 100 and 10 μl multichannel pipettes were used to generate serial dilution of the yeast culture in sterile 96-well plates. 5 μl yeast was pipetted for each determined spot, starting from the first dilution (cells directly from the 5-ml culture

were omitted in the case of YPD media) up to the sixth dilution. As soon as the spots dried, plates were parafilmed and incubated at 30 °C (control) and 34 °C (lethal temperature for *cct1-2* and G170D) for 2 days, after which images were taken with BioRad Gel Doc System (plates were placed on transilluminator with no filter chosen, hence open camera) and Quantity One software. For 2-hybrid assay, 5-fold serial dilution was spotted onto the plates (onto indicated Leu-, His-, Trp- media) without omitting the first culture with the cells grown to saturation (2 days).

3.18. Cycloheximide Treatment

WT and ts G170D strains with select transcription factors genomically fused to TAP-tag were subject to cycloheximide treatment. Fresh stock of cycloheximide solution was prepared at 10 or 50 mg/ml in 100% ethanol. WT/G170D cultures (50-100 ml) were grown in YPD under non-permissive temperature (37 °C) for 6 h. After taking 10 ml control (0 time point), cycloheximide was added at 50 µg/ml. 10 ml of the cells were taken at indicated time points: 15 min, 1 h, 2.5 h, 4 h and 6 h; after which cells were clarified and flash frozen. Once all pellets were collected, yeast were lysed and the concentrations of the crude extracts were measure using BCA assay. Relative total levels of the target transcription factors were determined by Western blotting with αTAP-tag antibodies.

3.19. Limited tryptic digestion

For Western blotting partially cleaved proteins, reactions were prepared similarly as for EMSA except about 10x higher protein concentration was used. All components were gathered on ice. Freshly made trypsin stock (200 ng/µl) in trypsin reaction buffer (40 mM HEPES pH 7.6, 8 mM Mq Acetate, 0.3 mM EDTA, 20 mM NaCl, 20 mM KCl, 2 mM DTT) (Liberek 1991) was applied last up to 50 ng final concentration (20 ng/µl was usually optimal) and the reactions were incubated at room temperature for 10 min. 5x Laemmli

buffer was added, the samples were ran on SDS-PAGE and Western blotted for anti-Rsc3 or anti-Rsc30 antibodies (Cairns' lab). For limited tryptic digestion in conjunction with EMSA, 200 ng/µl trypsin stock dissolved in water was diluted to 20 ng/µl using nucleosome binding buffer, and applied to 4 ng final concentration (2.5 µl from 20 ng/µl diluted trypsin was added to 10 µl reaction). Sba1 and 4 ng were added to the pre-incubated reaction at the 7th or 8th min (see 'Electrophoretic Mobility Shift Assay'), which were then incubated for another 5-6 min. The samples were resolved via EMSA and phosphor-imaged.

3.20. Yeast DNaseI Hypersensitivity Mapping for the High-Throughput Sequencing

DNaseI hypersensitivity protocol was modified from the versions available in Hesselberth 2009 and Zelin 2012. 50-100 ml YPD overnight culture was grown for about 12-18 h at 30 ˚C. 500 ml YPD media was inoculated with the overnight cultures to OD(595)=0.25 and the cells were grown till OD(595)=0.7 at 30 ˚C and 1650 rpm shaking at VWR DS-500E Orbital Shaker placed in BioCold Environmental incubator. If the yeast were grown under non-permissive temperature (37 ˚C), overnight cultures were incubated 10 min in 37˚C water bath (Isotemp 215 Fisher Scientific) and added to preheated (38.5 ˚C) 500 ml YPD media to respective OD(595) values that will allow the cells to grow till OD(595)=0.7 while shook in 37 ˚C incubator (HT Infors Multitron Standard) at 230 rpm. Starting ODs for the non-permissive temperature condition were strain-dependent: Hsp82 WT=0.25, G170D=0.37, CCT WT=0.22, *cct1-2*=0.41, Ssa1 WT=0.26 , *ssa1-45*=0.46. Hsp82 WT/G170D pair was grown at the non-permissive temperature for 6 h, CCT WT/*cct1-2* 4-5 h and Ssa1 WT/*ssa1-45* 5 h. For the 15-min non-permissive temperature treatment, yeasts were inoculated to OD Hsp82 WT=0.22 and G170D=0.27 and grown at 30˚C to OD(595)=0.65 in HT Infors Multitron Standard at 230 rpm. Cells were collected using 1 L Millipore Stericup/Steritop vacuum driven sterile filters, rapidly resuspended with 10 ml pre-heated YPD media (38.5 ˚C) and transferred to 500 ml pre-heated YPD.

The remaining cells on Steritop filter unit were collected with additional 10 ml preheated media. Cells were shook for additional 10 min in 37 ˚C incubator. The total time from starting the resuspension of the cells in preheated media till the collection of the cells in the centrifuge at 4 ˚C was 17 min. The cells were collected using 750 ml centrifuge tubes for 7 min at 5000 rpm in Sorvall RC 3CPlus precooled to 4 ˚C. The cells were resuspended with 10-20 ml cold sterile water, transferred in 50 ml conical tubes and spun down at 2500 rpm in Sorvall Legend RT for 5 min at 4 ˚C. The yeasts were washed additional two times with spheroplasting buffer (1 M sorbitol, 50 mM K-phosphate (pH 6.5), 0.018% β-mercaptoethanol) with freshly added β-mercaptoethanol. Cells were resuspended with warmed (30 ˚C) spheroplasting buffer containing freshly added 90U Zymolyase 20T and incubated at 30 ˚C for 45 min with continuous gentle shaking (at 500 rpm on VWR DS-500E Orbital Shaker). Spheroplasts were pelleted at 2500 rpm for 5 min, washed once with 5 ml cold spheroplasting buffer and resuspended in 25 ml lysis buffer (18% ficoll 400, 20 mM K-phosphate (6.8), 1 mM $CaCl_2$, 0.5 mM EDTA·NaOH (pH 8), 3 mM DTT, 1 mM PMSF, 1x protease inhibitor cocktail), with DTT, PI and PMSF added freshly. Cells were mechanically lyzed on ice with 20 strokes of pre-chilled Dounce homogenizer using pestle type A. The sample was clarified at 2000 rpm for 10 min in Sorvall Legend RT. Supernatant was collected in a new 50 ml conical tube without transferring the viscous pellet, and clarified at 3700 rpm for 10 min. The supernatant was collected and finally spun down at 13000 rpm using Sorvall SS34 rotor for 30 min at 4 ˚C. Supernatant was discarded and pellet (nuclei) resuspended with 2.2 ml buffer A (15 mM Tris·HCl (pH 8), 15 mM NaCl, 60 mM KCl, 1 mM EDTA·NaOH (pH 8), 0.5 mM EGTA·NaOH (pH 8), 0.5 mM spermidine, 11% sucrose) using P1000 pipette. The suspended nuclei were divided into ten 250 μl aliquots using 2-ml tubes and allowed to warm to room temperature. 250 μl of the reaction buffer B (buffer A with 12 mM $CaCl_2$ and 150 mM NaCl) supplemented with DNaseI was added. For testing the optimal DNaseI concentration, DNaseI titration was done in the following range: 0, 0.1, 0.2, 0.5, 1, 2, 5 and 20 U/ml DNaseI. DNaseI was diluted using reaction buffer (buffer B). For the Hsp82 WT/G170D strain 2 U/ml were used; for the CCT WT 4-5 U/ml and *cct1-2* 2-3 U/ml; for Ssa1 WT 6 U/ml and *ssa1-45* 2 U/ml. The reaction was incubated 5 min at room temperature and terminated by adding 500 μl stop buffer (50 mM Tris·HCl (pH 8), 100 mM NaCl, 0.1% SDS, 100 mM

EDTA·NaOH (pH 8), 1 mM spermidine, 0.3 mM spermine, 10 µg/µl ribonuclease A). 20 mg proteinase K (1000x) was dissolved in 1 ml proteinase K buffer (25 mM Tris·HCl (pH 8), 10 mM CaCl$_2$, 50% glycerol), sterile filtered and aliquoted. 20 µg proteinase K was added to each tube and the samples were incubated overnight (for at least 12 h) at 55 ˚C. To verify whether the samples were correctly digested, 10 µl of the reaction was resolved on 1% agarose gel (BioRad Mini-Sub Cell GT and BioRad PowerPac 300/Basic). The samples were isopropanol precipitated by using 100 µl 3 M sodium acetate and 880 µl 100% isopropanol and centrifuged 20 min at 14000 rpm (room temperature). Supernatant was decanted and the pellet was washed with 500 µl 70% ethanol. Pellets were resuspended in 75 µl 25 mM Tris pH 9 (only by very gently tapping the tubes) and incubated at 55 ˚C overnight to reconstitute the DHS fragments. The volume of each tube was reduced to 40 µl using the speedvac concentrator (Eppendorf Vacufuge 5301 Vacuum Centrifuge Concentrator) and the content from all 10 tubes was unified (400 µl total). 100 µl 5x loading dye (Qiagen GelPilot DNA Loading Dye) was added, the samples were loaded on 1% agarose gel and TEA buffer was filled only till the top of the agarose edge. The samples were resolved by starting at 75 V (BioRad Sub Cell Gi and BioRad PowerPac 300/Basic) and once the samples have entered the gel (~30 min), TAE buffer was refilled and the gel was run for additional 1 h at 200 V. Area of the gel corresponding to size 100-650 bp was cut out based on the dye fronts – area slightly above blue dye all the way down to orange, touching only the top of the orange. DNA was isolated using only one Qiagen column (QIAprep Spin Miniprep Columns) with vacuum manifold (Promega) and eluted with 50 µl water.

3.21. Yeast RNA Isolation for High-Throughput Sequencing

Yeast RNA isolation protocol was performed according to the modified version described in RiboPure Yeast kit. 50 ml of the YPD culture grown from OD(595)=0.25 to OD(595)=0.7 (or for non-permissive temperature conditions, see 'Yeast DNaseI

Hypersensitivity Mapping for the High-Throughput Sequencing') was spun down at 2500 rpm in Sorvall Legend RT at 4 °C and flash frozen. Preferably, an aliquot from the same culture grown for DNase I hypersensitivity mapping was taken. Next day, cells were briefly thawed on ice and it was proceeded with RNA isolation using RiboPure Yeast kit buffers and consumables. To the thawed cells, following components were added: 480 µl lysis buffer, 48 µl 10% SDS, 480 µl phenol:chloroform:isoamyl alcohol. The cells were vortexed for 10 s on the micro vortexer (Fisher Scientific) and transferred into screw cap tubes containing ~2.5 cm zirconia beads. To lyse the cells, the samples were vortexed 10 min vertically at the maximum speed setting on the mini vortexer and then centrifuged for 10 min at 14000 rpm using the benchtop centrifuge. The watery phase (supernatant) was transferred into 15 ml conical tubes that contained 1.9 ml pre-chilled binding buffer and mixed thoroughly with P1000, after which 1.25 ml 100% cold ethanol was added. Sample was passed through the filter cartridge in 700-µl steps by only bringing the centrifuge to the maximum – enough to pass the liquid through the filter. The final centrifugation step was 1 min at 14000 rpm, as well as all the following washes: one wash with 700 µl wash buffer 1 and two washes with 500 µl wash buffer 2. An additional centrifugation steps of the empty tubes was performed to remove residual wash buffers and the cartridge filters were transferred into new clean tubes. The elution solution was pre-heated for 5-10 min at 100 °C heat block (Dry Bath Incubator, Fisher Scientific), 50 µl was added to the filter cartridges and the samples were rapidly spun down. The elution was repeated with additional 25 µl elution buffer. 3 µl of the RNA sample was preserved for the later genomic DNA contamination comparison and the remaining 72 µl were digested with RiboPure Yeast DNaseI enzyme from the kit using 15 µl DNaseI buffer, 6 µl DNaseI (8U) and 27 µl DNase-free water. The samples were incubated 30 min at 37 °C and reaction was stopped using 15 µl DNase inactivation reagent (thoroughly vortexed before usage). Reaction was incubated 5 min at room temperature with occasional tapping of the tube to redistribute inactivation buffer solid materials and the sample was spun down at 14000 rpm for 3 min. 100 µl was taken out by carefully not disturbing the white pellet from the inactivation reagent and placed on ice. 5 µl was ran on the 1% agarose gel together with the previously preserved undigested 3 µl to compare for the effective genomic DNA removal, as well as possible RNase contamination causing smearing of the RNA bands. The RNA

concentration was measured using spectrophotometer (Amersham Biosciences Ultrospec 3100 Pro) with 700x dilution in TE buffer and quartz cuvettes, and by using Nanodrop. For the maximum purity the expected R value was between 2-2.2. The samples were stored at -80 ˚C.

3.22. Histone Isolation for Histone Mass Spectrometry

The nuclei isolation and acid histone extraction protocol was modified from Neil Kelleher and Craig Mizzen laboratories. Overnight cultures (50 ml, 30 ˚C) prepared for WT and *cct1-2* strains were used to inoculate 500 ml pre-heated media (38.5 ˚C). Cultures were grown 4-5h to OD(595)=0.7. Cells were spun down at 5000 rpm in Sorvall RC 3CPlus for 7 min at 4 ˚C, transferred in 50 ml conical tubes and washed with sterile water. Pellets were resuspended in 10 ml cold Nuclei Isolation Buffer, NIB (15 mM Tris·HCl (pH 7.5), 60 mM KCl, 15 mM NaCl, 5 mM $MgCl_2$, 1 mM $CaCl_2$, 250 mM Sucrose, 1 mM DTT, 2 mM sodium vanadate, 1x protease inhibitor mix, 10 mM sodium butyrate) containing 0.3% NP-40, and incubated on ice for 5 min. Pellets were spun down at 600 g in Sorvall Legend RT for 5 min at 4 ˚C and washed with 10 ml NIB (without NP-40). Cell pellets were resuspended in another 10 ml NB buffer and aliquoted in five 2-ml tubes per sample. The cells were spun down at 2300 rpm for 5 min (in the cold room table centrifuge), supernatant was decanted and 1 ml 0.8 N H_2SO_4 was added. The samples were nutated overnight in the cold room. Following day, the samples were spun down at maximum speed (14000 rpm) for 2 min at 4 ˚C. 1 ml supernatants were taken out with P1000 and the samples were precipitated with 250 µl 100% TCA (added to all five tubes per sample, hence 10 total). The samples were nutated 4-5 h at 4˚C, spun down at maximum speed for 20 min at 4 ˚C and supernatant was discarded. 1 ml 0.1% HCl in 100% acetone (kept at -20 ˚C) was added, samples were vortexed vigorously, spun down and washed additional two times with 100% acetone (-20 ˚C), spinning each time at maximum speed for 20 min at 4 ˚C. Lastly, the pellets from the four tube were unified with acetone (-20 ˚C)

by resuspending with pipette as much as possible (also washing off everything from the tube walls), whereas the sample from the fifth tube was used for gel verification and protein concentration measurement. The samples were spun down at maximum speed for 20 min at 4 °C, supernatant was discarded with P1000 and the pellet was dried in speed vacuum. The pellet from the fifth tube was resuspended in 50 µl water (not everything could be dissolved). 1 and 5 µl were used for protein concertation measurements and for resolving on 15% SDS-acrylamide protein gel. Histones sent for mass spectrometry were estimated to sum up to total of 200-300 µg.

3.23. Chromatin Immunoprecipitation

Chromatin immunoprecipitation protocol was modified from Kuras 1999. Cultures grown under appropriate conditions to OD(595)=0.7 were crosslinked to 1% formaldyhyde (10.8 ml for 400 ml culture) for 15 min at room temperature nutating. The cultures were neutralized with 25 ml 2.5 M glycine for 15 min at room temperature nutating. Clarified cells were washed with sterile water, centrifuged and resuspended in another 4 ml sterile water. Cells were divided in 4-8 2-ml microcentrifuge tubes, briefly spun down to maximum speed and flash frozen. Following day, the cell pellet thawing on ice was resuspended with 1 ml ice cold FA lysis buffer (50 mM HEPES·KCl (pH 7.5), 150 mM NaCl, 1mM EDTA·NaOH (pH 8), 1% triton X-100, 0.1% Na-deoxycholate, 0.1% SDS, 2 mM PMSF), after which cold glass beads were added. The samples were beat beaten for 37 min (1 min beating, 2 min rest) in the cold room (4 °C) using Thermomixer R (Eppendorf). Lysate was recovered by transferring sample to an Eppendorf tube with a hole on the bottom and centrifugation into a fresh tube. Samples were centrifuged at maximum speed for 15 min at 4 °C, supernatant was discarded and another 1 ml of fresh FA lysis buffer was added. Samples were sonicated with double stepped microtip (Branson Digital Sonifier) for 30 s at 20% power output (amplitude) 4 times. Samples were centrifuged 30 min at maximum speed at 4 °C and supernatant was transfer to a 15-ml conical tube containing 4 ml fresh FA lysis buffer. 800 µl from this chromatin solution was

incubated with 20 µl Protein A/G plus (Santa Cruz) with company suggested antibody dilution or 20-50 µl 50% IgG Sepharose G Fast Flow (GE Healthcare) in TBS on an end-over-end rotator for 90 min at room temperature. Prior to adding them to the samples, IgG Sepharose G Fast Flow beads were washed at least 3 times with TBS (for 500 µl beads, 10 ml TBS was used for each wash step), centrifuged no faster than 700 rpm in Sorvall Legend RT. After incubation, samples were centrifuged at 3000 rpm for 1 min at room temperature and supernatant was discarded without disrupting the beads. Beads were resuspended with 700 µl fresh FA lysis buffer and transferred to a Spin X centrifuge filter (Costar, 0.45 µm cellulose acetate in 2-ml polypropylene tube). The Spin X centrifuge filters with samples were rotated for 3 min on a rotator, spun 1 min at 3000 rpm and the liquid at the bottom (flow through) was discard. Beads were washed identically with another 700 µl of fresh FA lysis buffer. 3-min wash on a rotator followed by 1 min centrifugation to discard the flow through was repeated with 700 µl FA lysis buffer containing 500 mM NaCl, ChIP wash buffer (10 mM Tris·HCl (pH 8), 0.25 M LiCl, 1 mM EDTA·NaOH (pH 8), 0.5% Nonidet P40, 0.5% Na-deoxycholate) and TE (10 mM Tris·HCl (pH 7.5), 1 mM EDTA·NaOH (pH 8)). After the final spin, filters were placed in a fresh tube and 100 µl ChIP elution buffer (50 mM Tris·HCl (pH 7.5), 10 mM EDTA·NaOH (pH 8), 1% SDS) was used to resuspend the beads, that were further incubated 10 min in 65 ˚C water bath. Samples were centrifuged for 3 min at 3000 rpm, filters with beads were discarded and 80 µl TE and 20 µl Proteinase K (20 mg/ml) were added to the eluate. Samples were incubated 2 h at 42 ˚C, then 6 h at 65 ˚C. DNA was purified using Qiagen PCR purification kit and finally dissolved in 50-80 µl water. 2 µl were used for quantitative PCR, performed on StepOnePlus Real-Time PCR System (Applied Biosystems)), with total reaction volume of 25 µl using iTaq Universal SYBR Green Supermix (BioRad).

3.24. Indirect Yeast Immunofluorescence for Calculating Nuclear Hsp90 Concentration

50 ml SD BY4741 culture were grown from OD(595)=0.25 to OD(595)=0.7. The cells were collected 5 min at 2500 rpm in Sorvall Legend RT at 4 °C and fixed with 5 ml methanol for 1 h at -20 °C. Fixed cells were washed two times with 5 ml spheroplasting buffer (1 M sorbitol, 50 mM K-phosphate (pH 6.5), 0.018% β-mercaptoethanol), resuspended in 2 ml spheroplasting buffer and divided in two 2-ml tubes (one tube was kept as a non-spheroplasted control). 0.5 mg Zymolyase 20T was added to one tube and cell suspension was incubated at 30 °C for 45 min with continuous gentle shaking (at 500 rpm on VWR DS-500E Orbital Shaker). While spheroplasting samples, 10-well Teflon-coated slides were prepared. Following part of the protocol was modification from the versions described in Molecular Cloning Laboratory Manual (Sambrook and Russell, 2001). 20 µl of poly-L-lysine was pipetted onto each well and incubated for 30 min at room temperature. The poly-L-lysine was aspirated, the wells were washed 3-4 times with autoclaved Milli-Q water (pipetting and aspirating) and air dried. After verifying successful spheroplasting under the light microscope (Eclipse E400, Nicon), spheroplasts were washed two times with 1 ml spheroplasting buffer (2500 rpm, 3 min, 4 °C) and resuspended in 200 µl spheroplasting buffer. Undigested yeast cells from another preserved tube were also spun down and resuspended in 200 µl spheroplasting buffer. Strains such as NDY05 with internally expressing GFP and/or RFP did not necessitate spheroplasting for the antibody treatment, and it was proceeded similarly as in the case of the control (unspheroplasted yeasts). 20 µl of cells/spheroplasts was added to each well and the slides were incubated 30 min at room temperature. The excessive cells were aspirated and the wells with attached cells/spheroplasts were washed 3-4 times with PBS containing 3% BSA. The slides were incubated 5 min at -20 °C in methanol (pre-chilled to -20 °C) and then 30 s in -20 °C acetone. The slides were air dried, rehydrated with PBS containing 3% BSA for 30 min at room temperature, and washed 2-3 times with PBS containing 3% BSA. 10 µl primary antibodies, 1:500 dilution of rabbit α-Hsp90 from S. Lindquist laboratory, were added to each well and the slides were incubated overnight at

4 ˚C in a dark moist chamber (pyrex dish with wet paper towels covered with alufoil). The wells were washed 3-4 times with PBS containing 3% BSA and 10 µl secondary antibodies were added – 1:100 FITC (α-rabbit AlexaFluor488-conjugated antibodies, Santa Cruz Biotechnology). The slides were incubated 4-6h at room temperature in a dark moist chamber. The wells were washed 3-4 times with PBS with 3% BSA and 10 µl 0.1 µg/µl DAPI (in PBS) was added. DAPI was allowed to incubate for 10-15 min at room temperature in dark and the wells were washed 3-4 times with PBS. 2 µl of mounting solution was added before the wells completely dried out and the cover slips were sealed using the nail polish. Controls without primary antibodies, secondary antibodies or DAPI were all included. Fluorescent microscopy data are acquired on Carl Zeiss Axio Observer.Z1 microscope with X-Cite Series 120Q (Lumen Dynamics) illumination and Vivatome mode camera using 63x oil immersion objective compounded with 1.6x, with a numerical aperture of 1.4. The system was supported by software Axiovision. Exposure levels were adjusted for each focus and channel. Multidimensional acquisition was preferred, and maximum and minimum z positions were determined manually with live camera. Due to bleaching effects, no more than 10 stacks were taken per selection and unused channels were deactivated.

To assess nuclear Hsp90 concentration, images were processed using ImageJ program. Thereby, the images with split channels were generated: blue channel (DAPI staining standing for nuclei) and green channel (standing for cellular Hsp90). The areas representing the nucleus were selected on the blue channel image using the oval selection tool and the selection was restored on the green channel image, hence selecting the nucleus within its cell to determine green nuclear signal intensity. Integrated density was determined using the 'measure' option from the 'analyze' menu for both nucleus and entire cell on the green channel image. Corrected fluorescence was calculated for each cell/nucleus pair as

corrected fluorescence = integrated density – (area of selected cell/nucleus x mean fluorescence of the background)

and % of the indirect nuclear fluorescence was used to generate the mean value. Nuclear to cellular corrected fluorescence was calculated to be 8.2%. Given that a yeast cell is

estimated to have 577000 Hsp82 and Hsc82 molecules (Ghaemmaghami 2003) and average volume of budding yeast is 42 fL (Jorgensen 2007), cellular Hsp90 is calculated to be 22.8 µM and nuclear 1.87 µM.

3.25. Hsp90 Purification

The pET28a-Hsp82 vector expressing recombinant yeast Hsp90 was transformed in chemically competent Rossetta cells and plated on LB plates containing kanamycin. Following day, 400 ml overnight LB culture (with kanamycin) was inoculated with the colonies from the plate and incubated in 30 ˚C shaker. Next morning, 6x1.5 L LB media (with kanamycin) in Fernbach flasks were inoculated with the overnight culture at OD(600)=0.25 and grown till OD(600)=1 at room temperature. The cultures were induced with 1 mM IPTG and protein expression proceeded for 6 to 8 h. Pre- and post-induction time points (600 and 200 µl) were taken, spun down, resuspended in 200 µl 1x Laemmli buffer, heated and 15 µl were resolved on 10% SDS-PAGE gel to verify the expression. The cultures were spun down at 5000 rpm (Sorvall RC Plus) for 7 min at 4 ˚C, washed with pre-chilled autoclaved water and unified. After the wash, the bacterial pellet was resuspended in 25 ml Talon binding buffer (50 mM NaH_2PO_4 (pH 7), mM 300 mM NaCl) and the volume was recorded with the pipette. The pellet was resuspended in 3x final volume of the Talon binding buffer (or 150 ml maximum for 9 L culture) including the initial 25 ml, and divided in 3x50 ml conical flasks. A tiny crumble of lysozyme was added on the lids of the conicals and transferred to the bacterial suspension. The tubes were closed and nutated for 20 min in the cold room. 1000x protease inhibitor (PI) mix was prepared by dissolving 25 mg aprotinin, 5 mg pepstatin and 5 mg leupeptin in 25 ml DMSO – the mix was aliquoted and stored at - 20˚C. 1-2xPI mix was added to the bacteria, which were then flash frozen for 20-30 min. Bacteria were then thawed in 37 ˚C water bath for 30-50 min, with occasional inverting by hands for better mixing and more efficient thawing. The freeze/thaw cycle was repeated three times total – after the fourth freeze, bacteria were stored at -80 ˚C, and thawed fourth time on the day of the purification. Following part of

the protocol refers to the purification of one third of the total bacteria prepared. Before complete thawing (ice chunks were still to be noticed), another batch of 1xPI mix was added and the sample was sonicated for 30 s at 70% aptitude with thick tapered microtip (Branson Digital Sonifier) for about four times or until the lysate was homogeneous. Between each sonication interval, lysate was kept on ice to cool down. The homogenous lysate was spun down at 16000 rpm in SS-34 or A27-8x50 rotor at 4 ˚C. Meanwhile, Talon beads (Gold Biotechnology or GE Healthcare) were prepared by washing ~ 10 ml slurry. Thereby, 10 ml slurry was transferred to 50 ml conical tube, spun down at 2500 rpm in Sorval Legends RT for 2-3 min at 4 ˚C, storage solution was decanted and the beads were resuspended in 25 ml Talon binding buffer by gently inverting the tube. The beads were spun down using the same setting, supernatant was discarded and the wash was repeated. Before applying the crude extract from the centrifugation to the beads, 2 µl was mixed with 58 µl 1xLaemmli buffer and preserved for SDS gel. Bacterial supernatant was added to the washed beads and the sample was nutated for 1 h in the cold room. The protein-enriched beads were spun down at 2500 rpm for 5 min and the crude extract after the bead incubation was preserved. Similarly, 2 µl of this crude extract was mixed with 58 µl 1xLaemmli buffer and preserved for SDS gel. The beads were washed twice with 25 ml Talon binding buffer by inverting the tube couple of times and spinning it down at 2500 rpm for 5 min. All supernatants were preserved due to the possibility of the protein loss at any of the washing steps. 2x25-ml wash was repeated with Talon binding buffer containing 1 M NaCl by nutating the sample for 10 min in the cold room and collecting the beads at 2500 rpm for 5 min. The beads were washed again two times with 25 ml Talon binding buffer (inverting the tube couple of time to resuspend beads) and two times with 25 ml Talon low salt buffer (Talon binding buffer with 25 mM NaCl). The protein was eluted with 12.5 ml imidazole elution buffer (20 mM Tris·HCl (pH 6.9), 50 mM NaCl, 100 mM imidazole) by nutating the sample for 15 min in the cold room, spinning it down at 2500 rpm for 5 min and preserving the supernatant (eluate). The residual proteins were re-eluted with another 12.5 ml elution buffer and the eluates were unified. The eluate was spun down couple of times to remove residual beads. 10 µl of eluate, as well as each wash, was resuspended with 5x Laemmli and, together with previously prepared crude extracts, ran on 10% SDS gel. FPLC was prepared by submerging the pumphead A in

TEN$_0$ buffer (20 mM Tris·HCl (pH 6.9), 1 mM EDTA·NaOH (pH 8)), pumphead B in TEN$_1$ buffer (20 mM Tris·HCl (pH 6.9), 1 mM EDTA·NaOH (pH 8), 1 M NaCl), and both pumps were washed before proceeding. ResourceQ (2 ml) anion exchange column (GE Healthcare) was attached to the system in a reverted way (top-down, bottom-up) and washed at 2 ml/min and 4 MPa with at least 6 column volumes of each TEN$_0$ (0% B), then with TEN$_1$ (100% B), and finally with 0% B. If UV signal indicated impurities as displayed by the peak size, 100-0% B cycles were repeated. The column was equilibrated with TEN$_0$, column orientation was switched (top-up, bottom-down) and the metal affinity eluate was injected via 50 ml loop at 1-2 ml/min. The flow through was collected and the column was washed with 6 column volumes 0-10% B. Once conductivity, pressure and UV were stable, protein was eluted with 6 column volumes to 50% B and collected in 0.75 ml fractions. All UV peak-containing fractions, as well as the flow through, were checked on SDS gel for the protein of interest. Correct fractions were unified and concentrated down using Amicon Utra Centrifugal Filters 10 K MWCO (Millipore) to ≥ 300 µl. Size exclusion column (Superdex 200, GE Healthcare) was equilibrated with HEN$_0$/HEN$_1$ buffer pair (the same composition as TEN$_0$/TEN$_1$, but instead of 20 mM Tris·HCl (pH 6.9), 20 mM HEPES·HCl (pH 7.2) was used) at 2.5 % B (50 mM NaCl) and 0.25 ml/min with 1.5 MPa alarm pressure. In general, TEN$_0$/TEN$_1$ buffers at 5%B were used for the sizing column as well. However, the subsequent column to be used was Heparin column for which all sample and column are required to be in HEN$_0$/HEN$_1$ buffer. 50 ml loop was replaced with 500 µl loop, which was, prior to loading the sample, washed with HEN$_0$ buffer via 3 ml needled syringe, not leaving air bubble in the system. Thereby, syringe was removed before all buffer was injected, further pressing the plunger while taking the syringe out. Once the conductivity stabilized (2-3 h of equilibration), the sample was injected via needled syringe in pre-washed 500 µl loop. The sample injection proceeded for 2 min at 0.25 ml/min, after which the system was switched to load (wash), and the fraction collector was started 26 min after the initial injection, with 0.6 ml fraction volume. All UV peak-containing fractions were checked on SDS gel – in the case of Hsp90, higher molecular weight fractions were of interest. The Hsp90-containing fractions were collected and unified in a bigger, washed loop (500 µl loop was replaced). Inverted heparin column was washed with, similarly to ResourseQ, 0-100-0% B cycles using

HEN$_0$/HEN$_1$ buffers at 0.5 ml/min flow rate with 0.15 MPa alarm pressure. Only during the sample injection, pressure was increased to 0.5 MPa, the column was otherwise always ran with 0.15 MPa upper pressure limit. The Hsp90 protein sample was passed over correctly oriented heparin column several times in the course of couple of days – each time the salt range was narrower, but resolution better (it was started with 2.5-50% B). The eluted fractions (0.5 ml fraction volume) were checked for nuclease activity by incubating 10 µl of the fraction with radiolabeled DNA (30 min at 37 ˚C in nucleosome binding buffer) and tracking degradation after phosphor imaging. The least nuclease-containing fractions were unified and concentrated down. Hsp90 concentration was determined both using BCA assay and densitometry. For densitometry, picture of SDS gel containing increasing Hsp90 concentration and known increasing BSA concentration was taken and analyzed with ImageJ. Thereby, lanes containing protein of interest were selected with Analyze > Gel > Select first lane, then Analyze > Gel > Select next lane. The lanes were plotted (Analyze > Gel > Plot lanes); with the drawing tool, the curve bottom was closed and the value for each curve was obtained via wand (tracing) tool. Based on the standard BSA curve and concomitant equation, Hsp90 concentrations were derived.

3.26. SUMO-Transcription Factors, Sumo-Hsp90 and Sumo-Sba1 Purification

SUMO tag was implemented for the recombinant purification of yeast transcription factors (Butt 2005). pET28a-SUMO-Ino2, -Ino4, Rsc3, Rsc30, -Abf1, -Met31, -Reb1, -Sth1, -Sfh1 vectors were transformed in Rosetta cells. Overnight culture was started following day in the early afternoon by inoculating almost entire transformation plate (bacteria were picked up with a cell scraper) in 500 ml LB containing kanamycin. The cells were grown at 30 ˚C for 2-3 h or until the overnight culture was lightly cloudy. The culture was shifted to 18 ˚C and grown overnight. Following day, pre-cooled (18 ˚C) 2x1.5 L LB media (per transcription factor) in Fernbach flasks were inoculated with the overnight

at OD(600)=0.25 and grown till OD(600)=0.6-1 at 18 °C, which usually took entire day. In the evening, cells were induced with 1 mM IPTG and protein expression proceeded overnight (12-18 h) at 18 °C. SUMO-Hsp82 and SUMO-Sba1 were expressed at room temperature or 37 °C. Further purification steps were performed similarly as for his-tagged Hsp90, with several exceptions. Transcription factors' buffers (not for chaperones), such as TEN buffers and Imidazole elution buffer, contained 10% glycerol (TEN buffers were hence denoted TEN_0G/TEN_1G), and in the case of Rsc30, 0.1% NP-40 was added. These buffers were used for the equilibration of the columns and all subsequent FPLC steps. ~ 1:1000 of the purified SUMO protease was added to the Talon bead eluate and SUMO tag was cleaved off by incubating the samples for 2 h at 16 °C lightly nutating (65 rpm). SUMO cleavage was omitted for Ino2 and Rsc30 as it would degrade them. Transcription factors were passed over ResQ (eluted to 50% B) and SEC columns, and no other column was needed.

3.27. Sumo Protease and TEV Protease Purification

Sumo protease was expressed from the pET28a-Sumo protease vector at room temperature. Crude extract preparation as well as metal affinity purification were performed similarly as described for Hsp90, except TEN_0G/TEN_1G buffers were used. Very low salt eluate (TEN_0-diluted metal affinity eluate) was passed over 12 ml ResQ column and eluted with 5-35 %B with 1.8 ml fraction volume. Correct fractions were unified and concentrated down. For TEV protease purification, metal affinity and SEC were sufficient as it bound very weakly on ResQ, and it was expressed substantially - elimination of impure fractions did not cause considerable loss.

3.28. Sba1 Purification - Large and Small Scale

Sba1 purification was performed according to the modified protocols described in Freeman 1996 and Toogun 2007. PET23-Sba1 vector was used to transform bacteria, express protein and prepare crude extracts similarly as for Hsp90, except $TEN_{0.1}$ buffer was used. Crude extract was loaded on 50 ml DEAE column at 5 ml/min (0.5 MPa) with $TEN_{0.1}$. Flow-through was collected in 4x 50 ml conical tubes (18&30 mm tubes, serpentine row, 30 mm tube type, 50 ml fraction size). After pressure and conductivity were stable, 10-40% B gradient was applied over 6 column volumes (60 min) and sample was collected in 8 ml fractions. Correct fractions were preserved, and since a lot of Sba1 was in X2 flow-through fraction, it was reapplied to DEAE. All Sba1-containing fractions were unified, diluted with TEN_0, passed over ResQ (12 ml column, 2 ml/min flow rate, 4 MPa pressure) and eluted with another 10-40% B gradient. Correct fractions were ran several times over 2 ml MonoQ column at 1 ml/min (4 MPa). Clean Sba1 fractions were preserved, while impure fractions were reapplied to MonoQ and eluted with narrower salt range. Fractions of interest were unified and finally passed over SEC.

Small scale Sba1 purification was optimized for photocrosslinkable Sba1 constructs (Sba1-F164BPA and Sba1-F198BPA) in plasmid pET23a (Appendix 7.3.). 50 ml culture with expressed protein was spun down and resuspended in 1.7 ml $TEN_{0.1}$ buffer. Couple of brief thaw and freeze cycles followed, after which the sample was sonicated with microtip for 3-4x for 15 s at 15% amplitude, with intermittent cooling on ice. The sample was spun down for 20 min at 16000 rpm using SS34 rotor at 4 ˚C. The sample was injected via 2 ml TEN_0-prewashed loop onto 5 ml pre-washed DEAE column at 0.5 ml/min and at 0%B for about 5 min. The small DEAE resin volume was set up in a 50-ml column and the maximal pressure and flow rate were 2 MPa and 5 ml/min (2 ml was used for washing). The loaded protein was washed with 2 column volumes of 0% B and 3 column volumes of 10% B. The sample was eluted with 6 column volumes to 50% B in 1 ml fraction size. Correct fractions were unified and shortly (5 min) treated with 10 mM DTT at 37 ˚C. The sample (7 ml) was diluted to 25 ml with TEN_0 and ran on 2 ml ResQ column

(at 1 ml/min, 4 MPa maximal pressure). Correct fractions were shortly treated with DTT and concentrated down to about ~300 µl and frozen. Concentrated Sba1 was injected via 500 µl loop onto MonoQ column (both loop and column were pre-washed) at 1 ml/min (4 MPa) for 2.5 min. The loaded sample was washed with 4 column volumes of 0% B and then with 6 column volumes of 10% B. The sample was eluted to 50% B over 12 min. Correct fractions were unified, concentrated down and passed over SEC. The photocrosslinkable constructs in pET28a-SUMO and pBAD-SUMO (Appendix 7.3.) were to be purified similarly to SUMO-tagged transcription factors, with volumes optimized as described here.

3.29. TAP-Tagged Protein Purification

TAP-tagged proteins were purified according to the protocol from Benjamin Manning (Craig Peterson's laboratory web page). 3 L cultures of the strain carrying appropriate TAP-tagged subunit of the protein complex or TAP-tagged protein to be purified were grown in Fernbach flasks to OD(595)~0.7-0.9. The cells were spun down, washed with water, transferred in 50 ml conical tubes, and the pellet was flash frozen and stored at -80 ˚C. Following purification steps were performed in the cold room (4 ˚C). The pellet was separated from the conical tube by wrapping the conical bottom (where the pellet was) with a paper towel and hammering it or breaking it to dislodge the pellet, which was transferred in dry ice pre-chilled coffee grinder. Dry pellet was ground together with about the same size or less of dry ice until powdery or dust-like mass was formed (20-40 s). The cell powder was transferred with spatula in SS-34 or A27-8x50 rotor tubes and 10 ml E buffer (20 mM HEPES·KOH (pH 7.5), 350 mM NaCl, 0.1% Tween 20, 10% glycerol) with 1xPI was added to it. The lysate was nutated in cold room for ~20-30 min or until or crumbles were dissolved in the buffer. The recovered lysate was centrifuged at 17000 rpm (A27-8x50, Thermo Scietific) for 15 min at 4 ˚C. Meanwhile, 400 µl IgG beads slurry was washed with 10 ml E buffer (with 1xPI). Thereby, the bead slurry was transferred in Poly-Prep Chromatography Columns (polypropylene columns, BioRad), allowing the

storage solution to drain off, after which buffer was pipetted against the walls of the column, slowly and circularly without disturbing the resin. The buffer was allowed to flow through by gravity. The bottom (and top) of the column were closed with provided lids from the kit right before all buffer eluted to prevent drying out of the resin. The supernatant of the centrifuged lysate was transferred in a clean 15 ml conical tube. 1 ml of the lysate was used to resuspend the washed IgG resin (with bottom of the column closed), which was transfer back to the lysate in the 15 ml conical tube. The rest of the resin in the column was washed off with additional 1 ml of the lysate, and the column was preserved. The conical tube containing the lysate and the beads was closed tightly and nutated for 2 h on an orbital shaker in the cold room. After incubation, the samples were spun down at 750 rpm in Sorvall Legend RT for 3 min at 4 °C. Supernatant was decanted without disturbing the beads collected at the bottom and also leaving behind ~200-500 µl supernatant. The beads were resuspended in this residual supernatant and transferred into the initial column in which the beads were washed. 1 ml E buffer with 1xPI mix was used to pick up residual beads from the bottom of the conical and transferred into the column to the rest of the beads. After settling, the resin was carefully washed with 10 ml E buffer containing 1xPI, then with another 10 ml E buffer supplemented with 1xPI and 1 mM DTT. At all times, buffer was pipetted against the walls of the column in a circular motion. The bottom of the column was closed shortly before all buffer eluted. Purified TEV protease (obtained as described under 'SUMO Protease and TEV Protease Purification') was diluted at 1x1000 in 4 ml E buffer (with 1xPI and 1 mM DTT), hence 4 µl of purified TEV protease was used per sample. Alternatively, 10 µl of commercial TEV protease (Promega) was used. E buffer with diluted TEV protease was added to the resin and the top of the column was closed as well. Both bottom and top of the column were thoroughly parafilmed and TEV cleaved proceeded overnight nutating samples at orbital shaker in the cold room. Following morning, eluate was collected into a clean 15 ml conical tube. The beads were washed with additional 1 ml E buffer (1xPI, 1mM DTT) and eluate was collected. This 1 ml was also used to wash residual resin from the cap and it was applied against the walls of the column picking up the remaining beads. $CaCl_2$ was added to the 5 ml eluate at 2 mM final concentration (10 µl from 1 M $CaCl_2$). 400 µl calmodulin resin was prepared in a new column similarly as IgG resin, yet washing the resin with 10 ml E

buffer (1xPI, 1mM DTT) containing 2 mM CaCl$_2$. The eluate was applied to the washed calmodulin resin (with closed bottom). After the top and the bottom of the column were tightly closed and parafilmed, the samples were placed on an orbital shaker and nutated 2-3 h in the cold room. After incubation, the flow through was allowed to drain off by gravity and the resin was washed with 20 ml E buffer (1xPI, 1mM DTT). 2 ml E buffer (1xPI, 1mM DTT) containing 10 mM EGTA was added to the sample (with closed column bottom), after which the top was closed as well, and the samples were nutated for 5 min before elution. The resin was collected in a 15 min conical tube or directly into a concentrator (Amicon Ultra-4 Centrifugal Filter units, Millipore). The column, the lids and the resin were washed off with additional 1 ml E buffer (1xPI, 1mM DTT) with 10 mM EGTA, which was unified to the previous 2 ml eluate. 3 ml sample was concentrated down in Sorvall Legend RT for 50 min at 4 ˚C. Another 2 ml of fresh E buffer (1xPI, 1mM DTT) were added to wash the sample, which was re-concentrated to ~ 100 µl, aliquoted and stored at -80 ˚C.

3.30. CCT Purification

The CCT4-TAP was purified according to the protocol described under 'TAP-Tagged Protein Purification'. CCT2-CBP construct was received from Dan Gestaut (Frydman laboratory) together with the protocol that was lightly modified. Since CCT2-CBP is encoded on the plasmid and CCT is essential, the cultures were grown in YPD similarly as in the case of regular TAP-tagged protein purifications. The flash frozen pellet (stemming from 6 L liquid culture) was ground with dry ice and recovered using 15 ml buffer A (200 mM NaCl, 50 mM HEPES·KCl (pH 7.4), 5 mM CaCl$_2$, 20% glycerol) supplemented with PI and PMSF, nutating in the cold room. Lysate was centrifuged at 17000 rpm (A27-8x50, Thermo Scietific) for 15 min at 4 ˚C. Meanwhile, 2x 1.5 ml calmodulin slurry (~800 µl beads) were equilibrated with 2x 20 ml buffer A in two BioRad columns. Beads were transferred in a 50-ml conical tube and lysate was applied to it. Samples were nutated in the cold room for 2.5-3 h, after which they were spun down at

500 rpm in Sorvall Legend RT for 3 min at 4 ˚C. The supernatant was discarded, the beads were transferred back into BioRad columns and washed with 20 ml buffer A, 40 ml buffer B (500 mM NaCl, 50 mM HEPES·KCl (pH 7.4), 2 mM $CaCl_2$, 20% glycerol) and 20 ml buffer A (all containing PI and PMSF). In the meantime, heparin column was equilibrated with CCT HEN_0 (50 mM HEPES·KCl (pH 7.4), 1 mM EDTA·NaOH (pH 8), 20% glycerol) and CCT HEN_1 buffers (1 M NaCl, 50 mM HEPES·KCl (pH 7.4), 1 mM EDTA·NaOH (pH 8), 20% glycerol). The sample was eluted form the calmodulin beads with total 16 ml elution buffer (100 mM NaCl, 50 mM HEPES·KCl (pH 7.4), 10 mM EDTA·NaOH (pH 8), 20% glycerol) with PI. Total elution volume includes final washing of the beads as well. The eluate was applied to the heparin column at 20% B (2 ml column at 0.5 ml/min and 0.5 MPa) and eluted to 50% B for 12 min. 1 mM ATP was added to the unified fractions that were concentrated down to ~250-300 µl and ran over SEC.

3.31. Fluorescence Anisotropy

Anisotropy measurements were performed on Ultra Evolution 384 plate reader (Tecan Inc.). Pre-programmed anisotropy settings involving measurement of fluorescence polarization were chosen (with fluorescein specific excitation and emission wavelengths). Only sample-containing plates were selected. 5 flashes per cycle were sufficient and kinetics was set to 5 cycles. For the first couple of adjustment measurements with buffer, water and fluorescent DNA, Z-position was calculated from the well, after which recorded well position was set to manual and kept constant. Reaction buffer was nucleosome binding buffer (10 mM Tris·HCl (pH 7.4), 40 mM NaCl, 4% glycerol, 1 mM DTT and 50 µg/ml BSA), prepared as 5x. Freshly made fluorescently labeled DNA (*ACC1_TIM23* probe) was added at 12.5 nM for the experiments mirroring EMSAs (protein bound to DNA is displaced by p23) or in excess using 125 nM DNA (for competitor reactions or titrations to verify maximum anisotropy changes). After reaction stabilized, as displayed by unaltered anisotropy, doors were open and Rsc3, Rsc30 or RSC were added at the concentrations similarly to EMSA or lower, depending on whether

immediate or gradual increases were tracked down. For gradual increase, Rsc3 and Rsc30 were added slowly in the range of 50 to 300 nM and Sba1 in the range of 2 to 20 µM, both diluted in 1x nucleosome biding buffer, comparably to the reaction itself. In both cases, measurements were restarted until no significant increase was observed, or the doors were open to add more protein, immediately after which new measurements were started. Measurements/addition steps were interchangeably repeated until plateau was reached. The total reaction including final additions did not exceed 15 µl. Measurements with Hsp90 were performed along similar lines, except the concentration range was 5-40 µM.

3.32. Nucleosome Reconstitution

Nucleosomes were reconstituted according to the protocol from Luger 1999 and Benjamin Manning (Craig Peterson's laboratory web page). Bacterial expression constructs encoding engineered *Xenopus* histones were obtained from Dr. Craig Peterson's laboratory: CP7171 (H2A), CP718 (H2B), CP719 (H3), CP720 (H4); as well as 601 plasmid containing nucleosome positioning sequence CP1024 (pGEM-3Z/601, Lowary 1998). The expression plasmids were transformed in Rosetta, BL21-CodonPlus (DE3)-RIPL or BL21-GroEL (H2A) and bacteria were recovered on LB ampicillin plates overnight. In the morning, 2x5 ml 2xYT media (1.6% tryptone, 1% yeast extract, 0.5% NaCl) with ampicillin was inoculated with several different colonies from the plate (for each histone separately) and the cultures were shaken at low setting in 37 ˚C room. In the evening, 1 ml of each culture were combined to the fresh 50 ml 2xYT with ampicillin (4 cultures for all 4 histones) and the cultures were incubated overnight in 37 ˚C room without shaking. Following day, the overnight cultures were resuspended and 10 ml overnight was used to inoculate 1 L 2xYT with ampicillin. The bacterial cultures were grown to about OD(600)=0.6 and induced with 0.2 mM IPTG for 2 h (H3 and H4) and 3 h (H2A and H2B) at 37 ˚C. The cultures were spun down for 7 min at 5000 rpm (Sorvall RC Plus) at room temperature, resuspended in 16.7 ml Histone Wash T (50 mM Tris·HCl (pH

7.4), 1 mM EDTA·NaOH (pH 8), 100 mM NaCl, 1xPI, 1 mM PMSF and 1 mM DTT) and flash frozen. Pre- and post-induction time points (600 and 200 µl) were taken, spun down, resuspended in 200 µl 1x Laemmli buffer, heated and 15 µl were resolved on 15% SDS-PAGE gel to verify expression. PI, DTT and PMSF were added to the pellets, which were further thawed in 30 ˚C water bath. Before complete thawing, pellets were transferred on ice and sonicated 6 times for 15 seconds at 60% amplitude with cooling in between (H4 was not sonicated in this step). The samples were spun down at 23000 g (SS-34 rotor) for 20 min at 4 ˚C. The supernatant was discarded and the inclusion body pellet was washed with 25 ml Histone Wash TW (Histone Wash T with 1% v/v Triton X-100) by pipetting up and down until the samples were resuspended as much as possible. Short sonification was repeated (~ 3x15 s at 60%), except in the case of H4 for which complete sonification (6x15 s at 60%) was done at this stage. The pellets were spun down at 23000 g (SS-34 rotor) for 20 min at 4 ˚C, supernatant discarded and washes repeated one more time with 25 ml Histone Wash TW and two more times with 25 ml Histone Wash T (with no or minimal sonification 1x10 s at 60%). The pellets were flash frozen in the centrifuge tubes (SS-34 type) or it was proceeded with the experiment. The pellets were thawed at room temperature, 350-700 µl DMSO was added to the pellets and the samples were incubated for 30-45 min. A small volume (~ 3 ml) of fresh unfolding buffer (20 mM Tris·HCl (pH 7.4), 7 M guanidine HCl, 10 mM DTT) was added and the pellets were minced as much as possible. 20 ml total unfolding buffer was added (counting initial small volume) together with a small stir bar and the samples were left stirring for 1-2 h at room temperature. The samples were centrifuged at 23000 g (SS-34 rotor) for 20 min at room temperature, supernatant was preserved and re-extraction was repeated with another 5 ml unfolding buffer, by mincing and 30 min of stirring, and final spin down. The supernatants were unified and dialyzed against two changes (4 h and overnight) of 2 L urea dialysis buffer (10 mM Tris·HCl (pH 8), 1 mM EDTA·NaOH (pH 8), 100 mM NaCl for H2A/H2B and 200 mM NaCl for H3/H4, 7 M urea, 1 mM PMSF and 5 mM β-mercaptoethanol) at 4 ˚C. The following day, the chromatography columns, ResourceQ (2 or 12 ml) anion exchange column (GE Healthcare) and SP Sepharose Fast Flow (12 or 25 ml) cation exchange column (Amersham Biosciences) were prepared by washing them with filtered MilliQ water, 2 M NaCl and again filtered MilliQ water. Pumphead A of

the chromatography apparatus was submerged in urea low buffer (10 mM Tris·HCl (pH 8), 1 mM EDTA·NaOH (pH 8), 7 M urea, 1 mM PMSF and 5 mM β-mercaptoethanol) and pumphead B in urea high buffer (10 mM Tris·HCl (pH 8), 1 mM EDTA·NaOH (pH 8), 1 M NaCl, 7 M urea, 1 mM PMSF and 5 mM β-mercaptoethanol). The columns were equilibrated at 10% B for H2A/H2B and 20% B for H3/H4. The dialyzed samples were spun down at 23000 g for 20 min at 4 ˚C to remove particles before loading them onto the columns. The samples were firstly passed over the anion exchanger and then over cation exchanger, at 2 ml/min flow rate (4 MPa max pressure). The samples were washed with 3-6 column volumes and eluted to 50% B over 6 column volumes. Correct fractions were inspected by UV and SDS-PAGE gel, unified and dialyzed against three or more changes of 3.5 L MilliQ water containing 1 mM PMSF and 5 mM β-mercaptoethanol at 4 ˚C. The columns were washed with numerous rounds of excess water, 2 M NaCl, water, and then 20% ethanol and water. After dialysis, histones concentrations were derived from the measured absorption at 275 nm (against last dialysis water), histone specific extinction coefficients and molecular weights (Table I, Luger 1999). For instance, H2A(0.43)=1.48 mg/ml=106 μM, H2B(0.23)=0.52 mg/ml=37.9 μM, H3(0.20)=0.76 mg/ml=49.5 μM, H4(0.23)=0.48 mg/ml=42.6 μM. The samples were concentrated down with centrifugal filter units (Millipore) as much as possible (~300 μl), aliquoted in microcentrifuge tubes (~3x100 μl), lyophilized using speed vacuum, flash frozen, and stored at -80 ˚C. An aliquot of each of the four histones was unfolded in fresh unfolding buffer, which was added such that final concentration of the protein was approximately 1 mg/ml (~ 250-800 μl). Samples were thoroughly resuspended with pipette and unfolding proceeded for 3 h at room temperature. The samples were spun down at 7000 rpm for 3 min to separate undissolved material and the supernatants were transferred into fresh tubes. The concentrations of histones were determined by measuring extinction at 275 nm, subtracting from that the reading at 320 nm and using the values from the Table I (Luger 1999) mentioned before (with unfolding buffer as a blank) (~0.2 μg/μl x total volume, divided by MW to derive moles). The histones were mixed into equimolar ratios (the lowest MW histone moles were multiplied by MW of other histones and divided by determined mg/ml concentration to obtain to be added volumes). The histones were dialyzed against three changes of 3.5 L octamer refolding buffer (10 mM Tris·HCl (pH

7.5), 1 mM EDTA·NaOH (pH 8), 2 M NaCl, 5 mM β-mercaptoethanol) at 4 ˚C, with the second or third dialysis step being overnight. The octamer was concentrated down to 300-600 µl and passed over size exclusion column (Superdex 200, GE Healthcare), which was previously equilibrated with octamer refolding buffer. The fractions containing all four histones in equimolar ratio were collected (three histone bands should be seen on 15% SDS-PAGE – one of which has double stronger intensity), concentrated down and further used for nucleosome reconstitution or stored in 50% glycerol (adjusted to final 1x octamer refolding buffer) at -20 ˚C. Provided stored in glycerol, octamer was dialyzed against octamer refolding buffer before nucleosome reconstitution. Octamer concentration was determined via equation A_{276}=0.45 for 1 mg/ml (taking cuvette dilution into account), and verified with densitometry and BCA assay. The PCR product containing 601 positioning fragment was amplified from CP1024 (pGEM-3Z/601) plasmid using primers listed in Manning 2014. To obtain enough DNA, about 50-100 50 µl PCR reactions were performed and the product was purified using QIAGEN columns or phenol:chloroform extraction. The product was radiolabeled as described under 'Electrophoretic Mobility Shift Assay' section (in short, initial primers were radiolabeled). Molecular weight of DNA fragment was calculated as 660 Daltons x bp length and molecular weight of the octamer was taken as 108000 Daltons. Nucleosome reconstitution was performed in 100 µl reaction volume and several reactions were started in parallel with varying octamer:DNA ratios, r= 0, 0.9, 1.1, 1.5. Thereby, DNA, BSA (100 µg/ml) and 2 M NaCl (excluding NaCl from the histones i.e. octamer) were mixed thoroughly before adding the octamer to the reaction. It was safer to use octamer refolding buffer adjusted to 1x for the entire reaction volume than just 2 M NaCl, and higher total octamer/DNA concentrations resulted in much better reconstitution efficiency (~3 µM octamer used). If necessary, the volume of DNA was additionally reduced in the speed vacuum. At all times, reactions containing octamers were kept on ice due to the danger of octamer disassembly. The assembled reactions for nucleosome reconstitution were transferred to the Slide-A-Lyzer Mini Dialysis Units, 3500 MWCO (thermos Scientific) equilibrated in the first dialysis buffer, which included TE containing 1 M NaCl at 4 ˚C. Deposition of octamer onto DNA included dialysis for 3-4 h in 3.5 L of the TE buffer with reducing salt concentration: 1 M, 0.8 M, 0.6 M and two times at 2.5 mM – one of which went overnight. After dialysis, the new chromatin volume was

recorded with pipette and chromatin concentration was measured by dividing starting mass with new volume (~ 100 µl volume increased to 120 µl, and the concentration of 3 µM chromatin was thereby reduced to 2.5 µM). Reconstitution efficiency was verified on 4% native GTG gel that was ran at 150 V for 1-2 h. Thereby, 5 nM, 200 nM and 2 µM chromatin of all octamer:DNA ratios were loaded on the gel (including 5 nM free DNA), with 200 nM sample being loaded in duplicates as one half of the gel was dried and exposed for phosphor-imaging (5 nM, 200 nM) and the other was stained with Coomassie blue (200 nM, 2 µM). Increasing nucleosome band intensity, and decreasing octamer intensities are expected with increasing DNA concentrations (Coomassie). Reconstitution efficiency was also verified on 1% agarose gel (5 nM and 200 nM of the chromatin was loaded) that was briefly stained with ethidium bromide in 1xTAE after the run. Increasing free DNA was expected, whereas for low DNA concentrations, all DNA disappeared into nucleosomal band. Chromatin was stored at 4 ˚C. For further reactions, nucleosomes were always diluted in TE containing 2.5 mM NaCl and 100 µl/mg BSA.

3.33. Acetylation Assay

Acetylation assay was optimized to test acetylation or deacetylation activities of purified TAP-tagged HAT or HDACs complexes (described under 'TAP-Tagged Protein Purification'), in the absence or presence of purified molecular chaperones (described here in previous sections). Commercial synthesized histone 3 and 4 tail peptides (Cayman Chemicals) or reconstituted nucleosome (described under 'Nucleosome Reconstitution') were used as substrates, and radiolabeled Acetyl[^{3}H]CoA as means of tracking the acetylated residue. The reaction conditions involved several different reaction buffers, usually prepared as 5x stocks. General HAT buffers for testing various HATs (SAGA, NuA4, Spt10) and HDACs (Hda1, Rpd3L, Set3C, Hst3/4) on short synthetic peptides as substrate consisted of 10 mM Tris·HCl (pH 8), 10% glycerol, 0.1 mM EDTA·NaOH (pH 8), 1 mM DTT. The reaction buffer involving nucleosomes was the same as nucleosome binding buffer for EMSAs (10 mM Tris·HCl (pH 7.4), 40 mM NaCl, 4%

glycerol, 1 mM DTT and 50 µg/ml BSA) and the reaction buffer involving CCT was modified to 20% glycerol. The reaction included following components assembled on ice: reaction buffer with water adjusted to 12.5 µl total volume, 125 nCi Acetyl[^{3}H]CoA (50 µCi/0.5 ml, with 8.6 Ci/mmol) (Perkin Elmer), 200 ng/µl short (1-21 amino acids) histone peptide (1 mg/ml stock) or 40 nM nucleosomes as a substrate (for initial titration pM to nM range was tested), purified HAT and HDACs in the range of 400 pM (depending on the prep, initial titration involved 1-1000 pM), 40 nM yeast or human recombinant CCT (or yeast Hsp90, Hsp70 and p23). Control samples consisting of reaction buffer, nucleosomes or histone peptides and Acetyl[^{3}H]CoA were included. For testing HDACs, equimolar HAT and HDAC counter partners were supplied. The reaction was incubated for 1 h at room temperature or in 30 ˚C water bath. After incubation, samples were briefly spun down, 2x5 µl of the reaction were spotted onto 2x1 cm^2 Whatman paper, allowed to dry for half a minute, transferred in 50-100 ml Na_2HPO_4 using forceps and gently nutated for 5 min. The liquid was exchanged with clean Na_2HPO_4 and the samples were washed four more times (5 min each wash). The Whatman paper containing samples was soaked in 50 ml acetone (30-60 s) and the squares were cut out and placed into scintillation vials containing 1 ml scintillation fluid (EcoLume, MP Biomedicals). The papers were incubated in the scintillation fluid for 1 h or overnight before being read in scintillation counter (LS6500 Multipurpose Scintillation Counter, Beckman Coulter). Thereby, the chosen program for 1-h incubated sample involved reading ^{3}H for 5 min per sample, whereas for the overnight incubation, 1 min ^{3}H reading per sample was sufficient.

3.34. Yeast Nuclear Extract Preparation

Yeast nuclear extract was prepared according to the protocol from Hahn laboratory. 4-6 L of the culture was grown to OD(595) ~0.7-0.9 at 30 ˚C or at non-permissive temperature 37 ˚C for obtaining extracts specific for temperature sensitive strains (G170D and *cct1-2*, with corresponding WTs). The cells were spun down at 5000 rpm (Sorvall RC Plus) for 7 min and unified with sterile water in a single 250 ml centrifuge flask, which was

then spun down at 4000 rpm using F14-6x250y rotor (Thermo Scientific) for 5 min. 10-20 g of the cells is expected per prep. The cells were resuspended in 35 ml of 50 mM Tris·HCl (pH 7.5) containing 30 mM DTT and incubated in 30 ˚C water bath for 15 min. The cells were spun down at 4000 rpm (F14-6x250y, Thermo Scientific) for 5 min at room temperature and resuspended in YPD/S (YPD with 1 M sorbitol), to which 15 ml 1 M sorbitol, 15 ml 50 mM Tris·HCl (pH 7.5) containing 180U zymolyase per 1 L cell culture (10 mg zymolyase 100T or 50 mg zymolyase 20T) and 2xPI mix were added. The cells were nutated in 30 ˚C incubator at 500 rpm or lower for 45 min or until 80% spheroplasts were formed (verified under the light microscope). Usually, 45 min was sufficient when using zymolyase 20T and ~1 h was needed for zymolyase 100T. 100 ml YPD/S was added to the spheroplasts, which were briefly resuspended by gentle circular nutating in hands, and the samples were spun down at 4000 rpm for 10 min at room temperature. After discarding supernatant, spheroplasts were resuspended in 20 ml YPD/S, to which another 230 ml YPD/S were added (250 ml YPD/S total), and recovered in 30 ˚C water bath for 30 min. The samples were spun down at 4000 rpm for 10 min and supernatant was decanted. From this step onwards, the samples were kept on ice and all buffers used were ice cold. The samples were firstly resuspended in 20 ml cold YPD/S, then filled to 200-250 ml cold YPD/S and briefly nutated by hand. The samples were spun down at 4000 rpm for 10 min at 4 ˚C, supernatant decanted, and another wash step with cold YPD/S was repeated. Similarly, the samples were resuspended with 20 ml cold 1 M sorbitol, which was then added to 200-250 ml total volume. The samples were briefly nutated by hand, spun down at 4000 rpm for 10 min and the supernatant was discarded. The samples were resuspended with 20 ml buffer A (18% Ficoll, 10 mM Tris·HCl (pH 7.5), 20 mM K acetate, 5 mM Mg acetate, 1 mM EDTA·NaOH (pH 8), 0.5 mM spermidine, 0.15 mM spermine, 3 mM DTT), to which another 20 ml of buffer A was added. The samples were passed through a pre-chilled Dounce homogenizer using pestle B – 3 times per load of 5-10 ml (for 15 ml homogenizer). The samples were divided in SS-34 or A27-8x50 (Thermo Scientific) rotor tubes such that not more than half of the tube was filled with the sample. The samples were spun down at 5000 rpm for 8 min at 4 ˚C and the supernatant was transferred into fresh tubes avoiding the transfer of the slimy pellet. This step was repeated one more time. The samples were spun down at 5000 rpm for 5 min at 4 ˚C and

supernatant was transferred into new tubes – this step was done one or two more times. The samples were finally spun down at 13000 rpm for 30 min at 4 °C, supernatant was drained off as much as possible and the pellet was resuspended using P1000 in up to 3-6 ml buffer B (100 mM Tris acetate (pH 7.9), 50 mM K acetate, 10 mM $MgSO_4$, 20% glycerol, 2 mM EDTA·NaOH (pH 8), 3 mM DTT). The sample was flash frozen and stored at -80 °C for further preparation. Nuclei were thawed on ice and 3 M ammonium sulfate was added to 0.5 M final concentration (~0.6-1.2 ml). Any lumps were broken with a glass rod and the samples were nutated for another 30 min in cold room. The samples were spun down at 34100 rpm with ultracentrifuge SW55Ti rotor for 50 min at 4 °C. The supernatant was transferred into a clean 15 ml conical tube, to which 0.35 g solid ammonium sulfate per ml of the sample were added (~1-2.5 g). The samples were nutated for 30 min in the cold room and spun down at 12200 rpm for 15 min at 4 °C (using ultracentrifuge SW55Ti rotor). Supernatant was discarded and the samples were re-spun at the same rpm for another 4 min. Supernatant was pipetted out with P200 and the pellet was resuspended in 200-500 µl cold buffer C (20 mM HEPES·KOH (pH 7.6), 10 mM $MgSO_4$, 1 mM EGTA·NaOH (pH 8), 20% glycerol, pH adjusted to 7.5 with KOH, 3 mM DTT and PI added freshly). The pellet was meshed with a glass rod to homogeneity and entire content was transferred into pre-wetted dialysis tubing. Nuclear extract was dialyzed against buffer C supplemented with 75 mM ammonium sulfate, with three changes of at least 2 L buffer (one dialysis step went overnight). After dialysis, the concentration of the nuclear extract was measured with BCA assay. The nuclear extract was stored in aliquots at -80 °C and recovered on ice right before usage.

3.35. *In Vitro* Transcription

All buffers were autoclaved and tubes and pipettes were kept RNase free. HEMG buffer was made as 1x (32.5 mM HEPES·KOH (pH 7.6), 50 mM KCl, 6.25 mM $MgCl_2$, 0.5 mM DTT, 0.05 mM EGTA, 5% (v/v) glycerol). The nucleotide mix was prepared separately in a reaction volume adjusted to 7.5 µl (the volume comprising at least one third of the

entire reaction mix) on ice; nucleotides were added to a HEPES solution (66.7 mM HEPES·KOH (pH 7.6)). The nucleotide concentrations here were 1.67 mM ATP, CTP, GTP, only 83.3 µM UTP, and 667 nCi/µl UTP[α-^{32}P] (0.5 µl from 3000 mCi/µmol (10 mCi/ml) UTP[α-^{32}P]). Following components were added to the reaction mix in this order (prepared on ice): water (to adjust reaction to 25 µl), 7.5 µl HEMG buffer, 30 ng/µl template DNA (PCRed product), 5 µg/µl nuclear extract and finally 7.5 µl prepared nucleotide mix (hence, final concentration for ATP/CTP/GTP were 0.5 mM, 0.25 µM UTP and 200 nCi/µl radiolabeled UTP[α-^{32}P]). Reaction was incubated at 25 ˚C for 30 min and stopped with 100 µl transcription stop buffer (20 mM EDTA·NaOH (pH 8), 0.2 M NaCl, 1% (w/v), SDS, 0.25 µg/µl glycogen), mixed by pipetting or tapping. 1 µl 20 mg/ml Proteinase K was added and the reaction was incubated for 3.5-5 min. Then, 200 µl 0.4 LiCl and 400 µl phenol-chloroform (1:1 v/v) were added. The tubes were vortexed vigorously and then centrifuged at maximum speed for 5 min. Aqueous layer was transferred to a clean tube to which 800 µl 100% ethanol were added. Samples were mixed by inversion and spun down at maximum speed for 15 min. Supernatant was discarded and the precipitate was washed with 800 µl 75% ethanol (sample was spun down for 5 min). The precipitate was dried in speed vacuum and resuspended in 6 µl formamide loading buffer (95% deionized formamide, 0.025% (w/v) bromophenol blue, 0.025% (w/v) xylene cyanol, 5 mM EDTA·NaOH (pH 8)). The samples were boiled for 3 min, and then immediately placed on ice. If the samples were not loaded and ran on the gel right away, they were preserved at -20 ˚C and before loading re-boiled and cooled on ice. A denaturing urea gel (8 M urea, 12% acrylamide (40% 19:1 or 37.5:1), 0.02% APS, 0.01% TEMED, and TBE (89 mM Tris·borate and 2 mM EDTA)) was cast between the spacer-separated glass plates suitable for aluminum-backed sequencers (Thermo Scientific) and allowed to polymerize for at least 2 h. The polymerized gel was soaked in 1x TBE and the comb was gently pulled up and down before completely removing it. The gel was pre-run at 3500 V, 300 mA and 50 W to heat up. The urea in the wells was cleaned couple of times with 1x TBE using a syringe with a needle before loading the samples. The gel was ran for about 1.5 h at 3500 V, 300 mA and 50 W or until the dye front reached two thirds of the entire gel. The gel was transferred onto Whatman paper, dried for 1 h (Speed Gel SG210D, Savant) exposed overnight in storage phosphor

cassette (Bas Cassette 3 2040, Fujifilm), with pre-bleached storage phosphor screen on top of it, and imaged with Storm 860 Molecular Imager (Molecular Dynamics).

3.36. DNaseI Footprinting with Nuclear Extract

For *in vitro* DNaseI footprinting, ~ 400-500 bp long DNA samples were used as binding and digestion templates. The DNA fragments were a mimic of genomic segments that were transcribed bidirectionally in *cct1-2*. The DNA fragment was amplified from genomic DNA such that promoter or TSS was followed by shorter upstream and longer downstream sequence. Radiolabeled DNA was generated using one radiolabeled primer and one non-labeled primer, as described under 'Electrophoretic Mobility Shift Assay'. Nuclear extract for WT and *cct1-2* were incubated at increasing concentrations (30-50 µg was a middle, optimal range) with 30-50 ng radiolabeled DNA in nucleosome binding buffer for 30 min at room temperature. Samples were digested with DNaseI (~ 100 U/ml was usually appropriate concentration) for 5 min at room temperature. Digestion was stopped with transcription stop buffer, DNA was extracted with phenol:chloroform and ethanol precipitation. Samples were run on a sequencing gel, as described under '*In Vitro* Transcription' and phosphor imaged.

3.37. Anchor Away – Triggered Nuclear Depletion

Anchor away method developed by Haruki 2008 was performed according to the protocol from Fan et al. 2011, using appropriate strain with FKBP12-tagged anchor protein (RPL13A), an fpr1 deletion and a Tor1-1 mutation (VDY1874 strain as described in Solis 2016, obtained from Euroscarf). FRB-tag was added on the C-terminus of the gene of interest, in this case H2A.Z, to enforce its nuclear loss upon rapamycin addition. Thereby, FRB was amplified from the vector pFA6a-FRB-KanMX6 (Haruki 2008, obtained from Euroscarf), using forward primer that contained 40 bp of gene specific sequence

upstream of the stop codon (without its inclusion) AGCATTATTATTGAAAGTGGAAAAAAAGGGAAGTAAGAAA, to which CGGATCCCCGGGTTAATTAA sequence was attached (pFA6a-FRB-KanMX6 forward specific), and using the reverse primer that contained reverse complement of the 40 bp downstream from the stop codon (stop codon was not included) AGGGAGAATTACGGGAAATGGGAAAGAAAAACTATTCTTC, to which GAATTCGAGCTCGTTTAAAC sequence was added (pFA6a-FRB-KanMX6 reverse specific). VDY1874 strains were transformed with the modified FRB PCR fragment at 1-10 ng concentration, recovered overnight on YPD plates and replica plated on YPD plates containing 400 µg/µl G418. Colonies were re-stroke and selected with colony PCR, then genomic DNA isolation and PCR verification of the correct insert (verification was performed both upstream and downstream of the target insert location).

For initial nuclear depletion experiment, overnights and media were prepared as described previously, accounting for the number of time points taken for negative control and treat, replicates, as well as extra media used to resuspend the cells after concentrating them down. VDY1874 strain with H2A.Z-FRB::KAN (~ 2 or 3x300 ml) was grown to logarithmic phase (OD(595)~0.5) and the cells applied to Stericup/top (Millipore) using vacuum to remove media. The cells were quickly resuspended in 1/5th volume of fresh media (2 or 3x60 ml) and 10 ml for each replicate was taken as a 0 time point (negative control). Cells were crosslinked, neutralized, spun down and flash frozen as described under 'Chromatin Immunoprecipitation'. The remaining cells were equally divided in two flask for each replicate – to one flask rapamycin was added at 1 µg/ml final concertation (25 µl since stock solution was at 1 mg/ml in 100% ethanol), and to the control flask, the same amount (25 µl) of ethanol without rapamycin was added. 10-ml samples were taken from treats and controls at various time points (15 min, 1 h, 2 h, 4 h), crosslinked, neutralized, spun down and flash frozen. Chromatin immunoprecipitation was performed using α-H2A.Z antibodies to monitor the loss of H2A.Z at the select locations listed in Appendix 7.5. The experiment was repeated for 2 h and 4 h rapamycin treatment including negative control, except the cells were not crosslinked but used for RNA isolation and further RNA high-throughput sequencing, as described in the section 'Yeast RNA Isolation for High-Throughput Sequencing'.

3.38. Tissue Culture

Mouse fibroblast cell lines, vSRC 3T3, 3T3 MET and MET 412480H, were received from Prof. Leonard Neckers. The cells were cultured in 10 ml Dulbecco's modification of Eagle's Medium with 4.5 g/L glucose, L-glutamine and sodium pyruvate supplemented with 10% heat-inactivated fetal bovine serum (HI FBS, Gibco). The cells were cultured in tissue culture dish 100 x 20 mm style and incubated in water jacketed CO_2 incubator (Forms Series II, Thermo Electron Corporation) at 37 $^\circ$C and 5% CO_2. When reaching 80% confluency, the cells were split by aspirating old medium, washing the cells with 10 ml 1xPBS (pipetting 1xPBS towards the edge, nutating the plate once and aspirating 1xPBS), and detaching the cells with 1 ml 0.05% trypsin, 0.53 mM EDTA, 1x [-] sodium bicarbonate with 2-min incubation at 37 $^\circ$C. The cells were resuspended in complete growth medium at appropriate dilution for further culturing, or in only 1 ml medium per plate for storage. 80% confluent cells were stored in the complete growth medium containing 10% DMSO in liquid nitrogen. For radicicol treatments, cells were diluted to 40% confluency in 6-well plates (2 ml per well). Following day, provided 70% of the confluency was reached, the medium was aspirated and the cells were briefly washed with 1xPBS. Medium containing DMSO control, and up to 10 µM radicicol were added to the cells, which were then incubated for 24 h. The medium was aspirated, the cells were washed with 1xPBS and detached from the surface using a cell scraper. The cells were collected with lysis buffer that contains 50 mM Tris·HCl (pH 7.5), 150 mM NaCl, 1.5 mM EDTA·NaOH (pH 8), 1% NP-40, 3% glycerol. The crude extract concentrations were determined with BCA assay. Control samples and radicicol-treated samples were ran on SDS gel at adjusted (equalized) concentrations. The gel was Western blotted with antibodies directed against various transcription factors, as well as against HSP90 control.

3.39. Bioinformatics

3.39.1.   Compressing and Uncompressing Files

Raw sequencing files (.fastq files) provided from the sequencing facility were downloaded using command

wget link_address

Directory was extracted

tar -xvf directory.tar.gz

and compressed

tar -cvf directory.tar.gz

whereas file was uncompressed

tar -zxvf file.tar.gz

and compressed with

tar -zcvf file.tar.gz

3.39.2.   DNaseI-Seq Pipeline

For quality control, FastQC (v0.10.1) (Andrews 2010) was used

./fastqc -o output_directory -f fastq

To map the reads to the reference genome (UCSC, April 2011), bowtie (0.12.8) (Langmead 2009) was used with following options

bowtie --threads 4 -m 1 -v 2 --sam --un output_directory

.sam files were converted to .bam files with samtools (Li 2009)

sam2bam.sh file.sam

and .bam files were converted to .bed files with bedtools (2.17.0) (Quianlan 2010)
bamToBed -i mapped_file.bam >mapped_file.bed

Index statistics was performed with samtools
samtools idxstats mapped_file.bam

.bam was converted to .wig via
bam2wig.py -i mapped_file.bam -o output_directory -s
/Genome_UCSC/Yeast/chrall_length -t 100000000

Wig was converted to bigwig using wigToBigWig (v4, UCSC)
wigToBigWig mapped_file.wig /Genome_UCSC/Yeast/chrall_length
mapped_file.bigWig

DNase hypersensitive sites were detected with hotspot (v4) (John 2011)
/hotspot-distr-v4/pipeline-scripts/runhotspot

after adjusting parameters in /hotspot-distr-v4/pipeline-scripts/runall.tokens.txt
(_FDRS_= 0.01, _TAGS_ mapped_file.bam, _OUTDIR_ and _RANDIR_
output_directory,)

As an alternative, F-seq (v3) was used as well to detect and compare DNase
hypersensitive sites
/F-seq/dist~/fseq/bin/./fseq -v -f 0 -of bed -d input_directory -o output_directort
file.bed

Footprints were detected with footprinting finder (v1.0) (Chen 2008)

footprinting_run.sh mapped_file.bed
/footprinting_finder/yeast.sacCer3.K100.unmappableBase.bed file_hotspot.bed
file_footprint.bed wig file_footprint.wig file_cleavage 1000000

Alternatively, other programs were used to detect footprints from the hotspot-computed DNaseI hypersensitivie sites.

3.39.3. pyDNase/Wellington

Hotspot generated DHSs were converted in a format acceptable for Wellington (Piper 2013), in which fourth column contained numerated DHSs, z score was shifted to the fifth column, and sixth column involved strandness information, i.e. directionality (+ or -)

```
awk
'BEGIN{num=1}{printf("%s\t%s\t%s\tDHS_%s\t%s\t+\n",$1,$2,$3,num,$4);num=num+1}' file_ hotspot.bed >file_hotspot_converted.bed
```

Wellington footprint computation required converted hotspot files and bowtie mapped files

```
.local/bin/./wellington_footprints.py file_hotspot_converted.bed
file_mapped.bam file_name -o directory_name
```

Wellington footprint computation was also run with modified parameters, which restricted footprint size from 8 to 30 bp (similarly to parameters from Hesselberth 2009), and overlapping footprints were not merged

```
.local/bin/./wellington_footprints.py -fp 8,30,2 -dm file_hotspot_converted.bed
file_mapped.bam file_name -o directory_name
```

Final footprint file required one more modification, performed via .vi to remove M

```
%s/\r//g
```

3.39.4.   DNase2TF

This program was published in Sung 2014. A compact .bed file was created from a bowtie mapped .bed file

```
awk '{if($6=="+") {printf("%s\t%s\t%s\tF\n",$1,$2+1,$3)} else
{printf("%s\t%s\t%s\tR\n",$1,$2+1,$3)}}' file.bed >compact_file.bed
```

compact_file.bed file was split by chromosomes, retaining suffix
```
awk '{print $0 >> $1".txt"}' compact_file.bed
```

Nucleotide frequency was calculated with below command, specifying the suffix of the compact_file_chr.txt
```
/dnase2tf/calcdft/./calcDFT /Genome_UCSC/Yeast/fasta
/directory_compact_files/compact_file
```

DNase2TF was ran in R with following commands, with Mapability_Map developed from http://archive.gersteinlab.org/proj/PeakSeq/Mappability_Map/Code
```
library ('dnase2tf')
hotspotfilename = 'hotspot_file.bed';
datafilepath = '/directory_compact_files/compact_file'
mapfiledir = '/Mappability_Map'
outputfilepath = '/file_dnase2tf_dft'
assemseqdir='/Genome_UCSC/Yeast/fasta'
dftfilename='/dinuc_freq_table_ac_file.txt'
    dnase2tf(datafilepath, hotspotfilename, mapfiledir, outputfilepath, maxw=30,
    minw=6, z_threshold =-2, numworker = 10, FDRs=c(0, 0.0000001, 0.000001,
    0.00001, 0.0001, 0.001, 0.01, 0.05, 0.1));
```

3.39.5.　RNA-Seq Pipeline

RNA-Seq reads were trimmed using

    java -classpath /usr/share/java/trimmomatic.jar
    org.usadellab.trimmomatic.TrimmomaticSE -threads 4 -phred33 -trimlog
    trimlog.txt file.fastq file_trimmed.fastq TRAILING:20 MINLEN:40
    (Bolger 2014)

The trimmed reads were aligned to the reference genome using tophat (2.0.9). The index was generated in fasta folder

    bowtie2-build <reference_in> <bt2_base>

inspected using

    bowite2-inspect

and aligned

    tophat /bowtie2-index/SacCer3 file_trimmed.fastq

The reads were also aligned using STAR (Dobin 2013), with firstly building index

    /STAR-2.5.2b/bin/Linux_x86_64/./STAR --runMode genomeGenerate --
    genomeDir /STAR --genomeFastaFiles /Genome_UCSC/Yeast/fasta/chr_all.fa --
    sjdbGTFfile UCSC_sgdGene.gtf

then aligning

    ./STAR --genomeDir /STAR --sjdbGTFfile /UCSC_sgdGene.gtf --readFilesIn
    file_trimmed.fastq --outFileNamePrefix file_star --quantMode TranscriptomeSAM
    GeneCounts --outFilterType BySJout --outFilterMultimapNmax 1 --alignIntronMin
    10 --alignIntronMax 2500 --alignMatesGapMax 2500 --alignSJDBoverhangMin 1
    --outSAMtype BAM Unsorted SortedByCoordinate --limitBAMsortRAM
    7160709711

STAR allowed for counting the number of read within defined genomic segments, hence, count of intergenic reads was possible as well, by firstly creating artificial intergenic.gtf annotation file, building an index, similarly as for UCSC_sgdGene.gtf, and then aligning by using intergenic index and intergenic.gtf.

Alternatively, the reads were also count with HTSeq (0.6.1), using tophat alignments
        htseq-count -f bam /tophat_out/accepted_hits.bam UCSC_sgdGene.gtf
    >htseq_tophat.txt

Differentially expressed genes were computed using GFold (V1.1.0) (Feng 2012)
        samtools view mapped_file.bam | /gfold.V1.1.0/./gfold count -ann
    /UCSC_sgdGene.gtf -tag stdin -o file.read_cnt
        /gfold.V1.1.0/./gfold diff -s1 file1 -s2 file2 -suf .read_cnt -o file1vsfile2.diff

The aligned reads were visually displayed with IGV (2.3.25 and 2.3.94), in collapsed or squished form, color-coding the read direction (reads aligned to the Watson strand were blue and to the Crick strand red).

3.39.6.   Chip-Seq

SRA files obtained from NCBI were converted to .fastq using fastq-dump.2.4.5 from sratoolkit.2.4.5-2-ubuntu64. Fastq files were aligned to the reference genome using bowtie (0.12.8)
        bowtie -m 1 -v 2 --threads 4 --sam
    /Genome_UCSC/Yeast/bowtie_index/SacCer3_nochrM file.fastq file.sam

For Chip-Seq peak calling MACS (1.4.2) was used

macs14 file.sam -c input_or_control.sam -g 12495682 -n file_name -w -S –
nomodel

A newer MACS version was used (2.1.0) as well, but I found that older one (1.4.0) would deliver information for the files with otherwise no peaks according to MACS 2.1.0.

macs2 callpeak -t file.sam -c input_or_control.sam -f SAM -g 12495682 -n file_name --outdir directory_name --nomodel

3.39.7.   .bed Files Comparison

The .bed files were overlapped using PeakAnnotator (version 1.4)

PeakAnnotator ODS file1.bed file2.bed output_file

which also automatically generates unique.bed files for both file1 and file2.

Output_file is a non-standard 7-column file with lines of overlapping coordinates for both files. To further use only overlapping coordinates of either file1 or file2, output_file was separated into two original .bed files and duplicate values were removed. This was done either using Microsoft Excel or using made program SplitterForPeakAnnotator.py (Appendix 7.9.1.). SplitterForPeakAnnotator.py splits PeakAnnotator generated file output_file into two original files, removing duplicate, returning the files in the right .bed format and thereby making them ready-to-use for another round of overlap analysis, finally naming the file with respect to the stem file and overlapping partner (e.g. file1_from_outputfile.bed).   Furthermore,   another   program   was   created UsingPeakAnnotator.py (Appendix 7.9.2.) that would perform the whole PeakAnnotator overlap of the pairwise partner files, splitting the output_file, and making the filtered, overlapping .bed files ready for another round of comparison, for endless number of files, provided the pairwise comparison partners are placed in two different directories. The program would preserve the initial output_files as well. It further required .bed files to

contain 4 columns and to be sorted after chromosome number, starting and ending position. Sorting was done in excel or using below command

sort -k1,1 -k2,2n -k3,3n file.bed > file_sorted.bed

3.39.8.   Consensus Motif Search

Footprints were extended for 10 bp in each direction

slopBed -i file_footprint.bed -g /Genome_UCSC/Yeast/chrall_length -b 10 >file_footprint_extend10bp.bed

For more stringent search, footprints extension was omitted. Footprint .bed files were converted to fasta

fastaFromBed -fi /Genome_UCSC/Yeast/fasta/chrall.fa -bed file_footprint.bed -fo -fo file_fooptprint.fa

For motif search, online available RSA-tool was used (van Helden 2000), located at http://rsat-tagc.univ-mrs.fr/rsat/matrix-scan-quick_form.cgi. Appropriate fasta files were uploaded from the server and frequency matrices from Jaspar (Sandelin 2004) were pasted into the indicated box. Following parameters were selected:

Background Markov order 0

Organism-specific: Saccharomyces cerevisiae

Sequence type: upstream-noorf

Scanning options   Sequence Origin: start

Return: sites+pval

Treshold: 0.0001

Output file was further open in excel and consensus motifs coordinates were corrected with respect to the original file .bed start sites. Consensus motif coordinates were used to create a .bed file for display in IGV (2.3.25 and 2.3.94), or the motif count was performed (using COUNTIF) to obtain number of consensus motifs for the given pool of footprints.

3.39.9. DHS Searcher for Genes/Intergenic

A python tool was developed for quick check-up whether a molecular chaperone affects chromatin around a gene of interest or its intergenic location (Appendix 7.9.3.). Before starting, all components have to be gathered in the same folder: the DHS_searcher program, the hotspot .bed files containing hypersensitive sites for mutant and respective WT (Hsp90 short and long-term inactivation, p23 depletion, CCT inactivation), as well as the intergenic .bed file, with fourth column specifying its name derived from contiguous genes (e.g. YAL049C_YAL048C). The program asks for the chaperone files first ('Enter a file name'). Single files are specified and followed by enter. It is always useful to specify pairs (mutant with its wild type). After blank enter ('Enter to quit'), systematic gene names are specified ('Enter a name to search'). Similarly to file names, single gene names are specified and followed by enter. After final blank enter, the program outputs genomic coordinates with scores of the hypersensitive sites associated for the input gene/intergenic and for the requested chaperones.

Figure 3.39.9.1. **Overview of DHS_searcher.** (Upper) Schematic overview. Given a region of interest, the DHS_searcher allows for quick checkup whether a chaperone might affect it. (Lower) Snapshot representing the standard input and output. Only one DHS pair (for WT and mutant) corresponds to the indicated intergenic region in upper panel, since it was a match for both left and right gene.
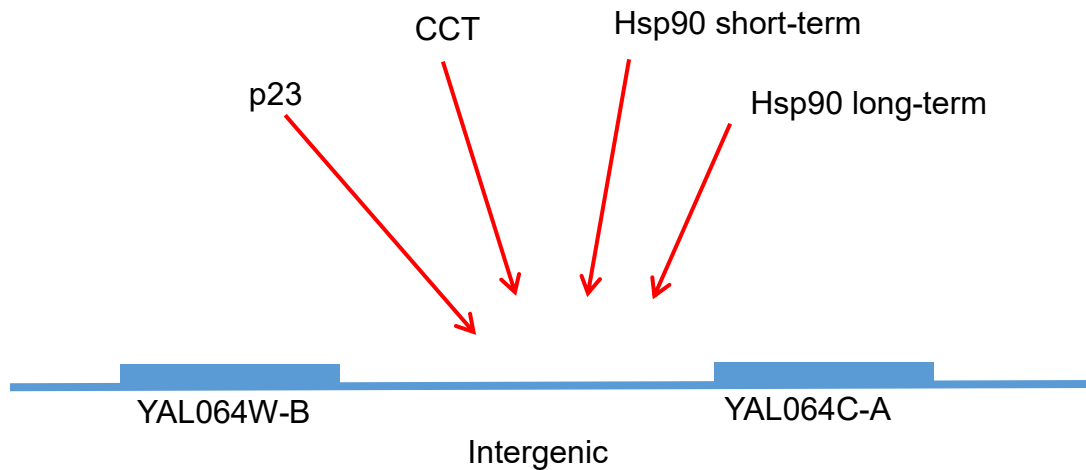

```
Enter a filename (or Enter to quit): CCT
Enter a filename (or Enter to quit): CCT12
Enter a filename (or Enter to quit):
Enter a name to search (or Enter to quit): YAL064W-B
File - CCT:    chrI, 12545, 12707, 4.855500
File - CCT12:    chrI, 12498, 12759, 8.731180
Enter a name to search (or Enter to quit): YAL064C-A
File - CCT:    chrI, 12545, 12707, 4.855500
File - CCT:    chrI, 18897, 19451, 13.828200
File - CCT:    chrI, 15460, 18038, 44.801000
File - CCT12:    chrI, 12498, 12759, 8.731180
File - CCT12:    chrI, 21042, 21411, 4.976010
File - CCT12:    chrI, 19016, 19322, 7.419130
File - CCT12:    chrI, 16628, 17846, 40.803400
File - CCT12:    chrI, 15487, 16461, 13.833600
Enter a name to search (or Enter to quit):
```

4. Results

4.1. CCT

With exceptions of several indirect observation, CCT is regarded to be a cytosolic chaperonin. The possibility that CCT is a nuclear protein are checked with quick and preliminary approaches that would offer initial idea about CCT's nuclear connections and relevance of studying its nuclear realms further.

To determine whether CCT is present in the nucleus, its cellular localization was assessed by indirect immunofluorescence staining using antibodies raised against several CCT subunits. The staining shows that CCT's nuclear signal intensity remains unabated compared to its cytoplasmic (Figure 4.1.1). The nuclear CCT signal intensity comprised ~13% of the entire cellular CCT signal, which based on the number of CCT molecules per cell and yeast cell volume (Kulak 2014, Jorgensen 2007) estimates its nuclear concentration to be ~ 0.1 μM. Another approach taken to explore the extent of CCT's nuclear implications was analysis of nuclear proteins that physically and genetically interact with CCT. Curated CCT interactors in SGD were extracted and using GO slim tool, the hits mapped in the nucleus were separated from the cytosolic. Strikingly, out of 377 known CCT interactors, half of them (181, 48%) exhibit nuclear features (Figure 4.1.2A). Many CCT nuclear interactors are subunits of macromolecular complexes including numerous canonical histone modifiers (SAGA, NuA4, Set3C, Rpd3S/L, Set1C, HDA1), chromatin remodelers (SWI/SNF, SWR-C), RNA polymerase, octamer components, and numerous other chromatin regulators (Figure 4.1.2B). Further classification reveals that there is an equal distribution of physical and genetic interactors (Figure 4.1.2C).
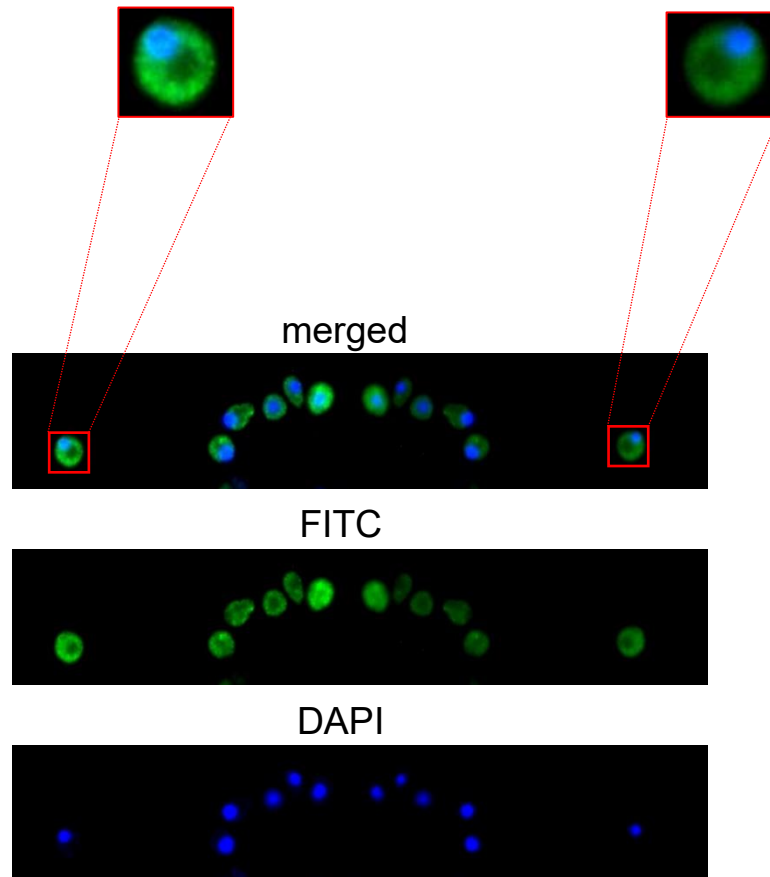
Figure 4.1.1. **CCT is not excluded from the nucleus.**
A. The cellular CCT localization was determined with immunostaining using antibodies directed against CCT subunits and α-rabbit AlexaFluor488-conjugated secondary antibodies. ImageJ was used to determine the percent area of each nuclei relative to the total cell area along with the relative CCT signal intensity. In conjunction with the established copy number of CCT molecules per cell (17166; Kulak 2014) and average volume of budding yeast (42 fL; Jorgensen 2007), the nuclear concentration of CCT was calculated to be 0.1 μM.
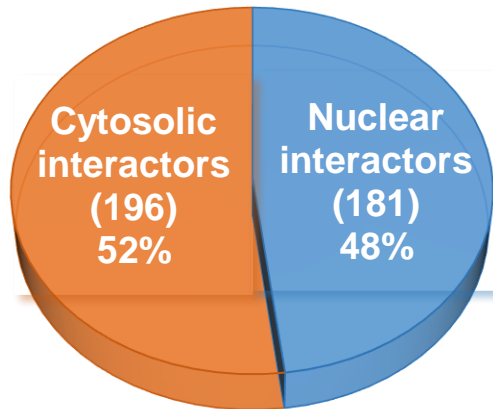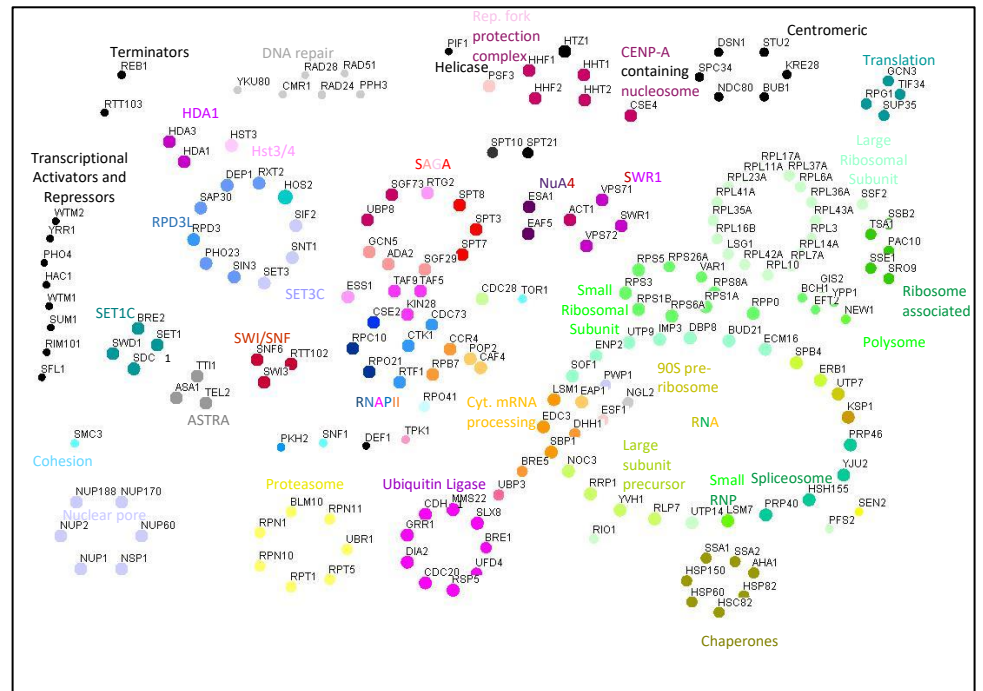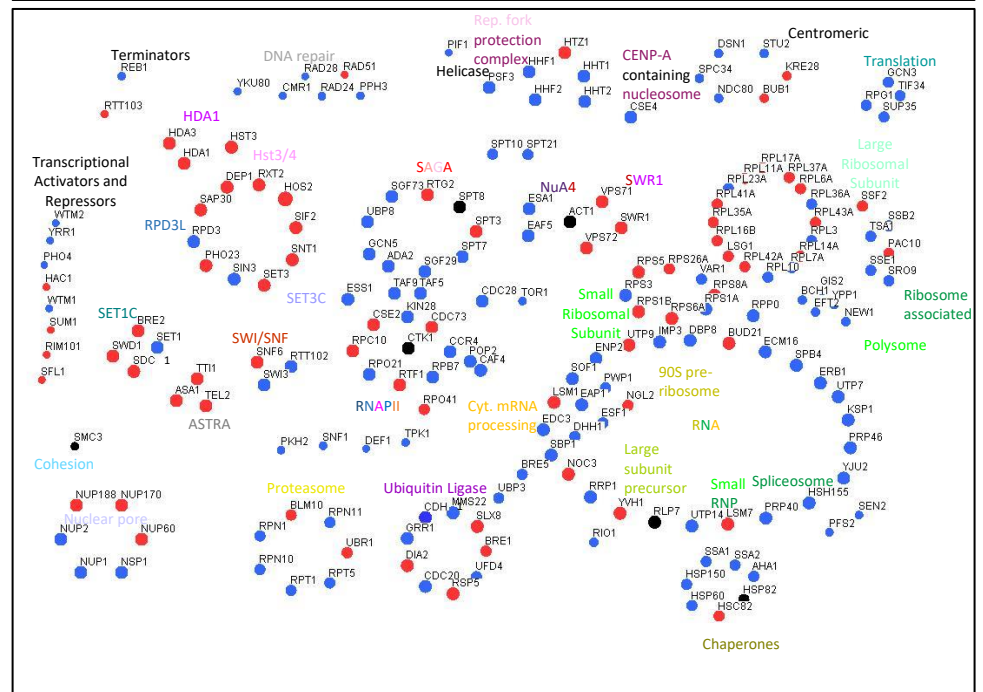
Figure 4.1.2. **CCT nuclear interactome.**
A. CCT nuclear and cytoplasmic interactors extracted from SGD. B. CCT nuclear interactors organized according to the macromolecular complexes (similarly as in Dekker 2008). C. Physical (blue), genetic (red) and both (black) CCT nuclear interactors as in B.

Hence, CCT does not seem to be excluded from the nucleus according to the immunofluorescence. The results of the interactome approach are to be considered with caution due to the limitations of the integrative data. Yet, CCT links to the overarching and crucial nuclear complexes and the interactome map parallels to other prominent chromatin-associated factors (Lambert 2010).

Based on the interactome data and effector roles of the prospective target chromatin regulators, further intention was to examine gene expression, post-translational modifications and structural chromatin dependencies on CCT. It was attempted to unravel CCT's nuclear roles with high-throughput techniques suitable for *de novo* nuclear protein characterization: RNA-Sequencing (RNA-Seq), histone mass spectrometry and DNaseI-Sequencing (DNaseI-Seq). The flow of the three approaches are summarized in the Figure 4.1.3. The techniques were utilized in conjunction with the temperature sensitive (ts) CCT strain, *cct1-2* (also *tcp1-2*, Ursic 1994), which circumvents the fact of CCT being essential.

WT and ts *cct1-2* were grown at non-permissive temperature

| RNA-Seq | Histone Mass Spec | DNaseI-Seq |

Total RNA isolation

Histone purification

Limited digestion of the nuclei to release short DNA sequences

Expression level changes

Post-translational modification quantification

Structural chromatin changes
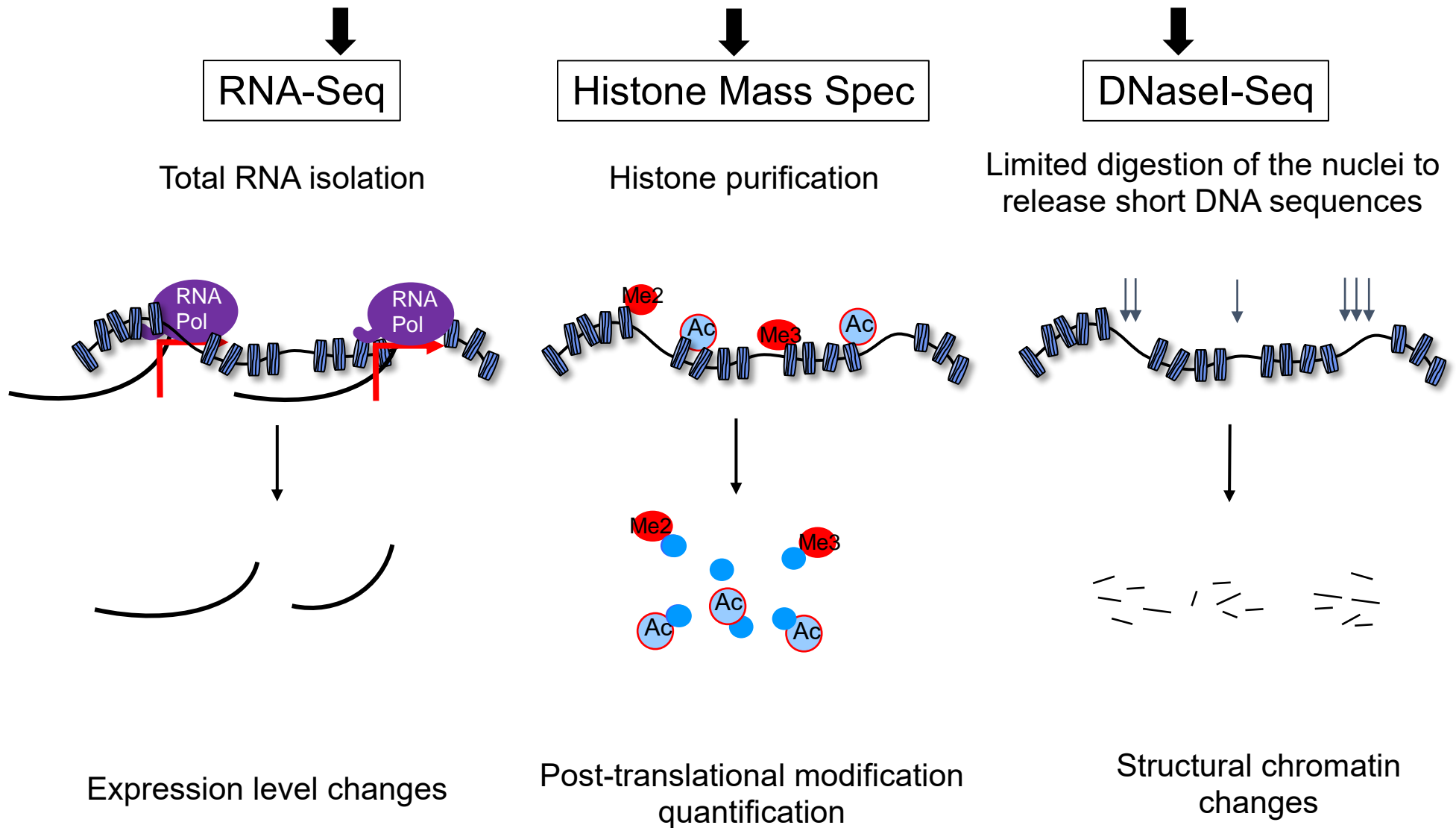
Figure 4.1.3. **Schematic overview of high-throughput approaches utilized for characterization of CCT's nuclear roles.**
WT and ts *cct1-2* were grown at non-permissive temperature and (left) total RNA isolated was subject to RNA-Seq to investigate expression level changes; (middle) histones were subject to mass spectrometry to examine post-translational modification changes; (right) isolated nuclei were subject to limited DNaseI digestion and high-throughput DNaseI-Seq to inspect for structural chromatin changes.

Cct1-2 strain, which allows for CCT inactivation (Ursic 1994), was implemented together with the wild type reference strain. When shifted to the non-permissive temperature of 37 ˚C, 99% *cct1-2* were reported to lose viability after 17 h (Ursic 1994). Because CCT is essential, termination of cell growth was equalized to CCT inactivation. Characterization of *cct1-2* strain revealed caseation of cell division 4-5 h after shifting the strains to 37 ˚C (Figure 4.1.4). Correspondingly, to investigate the influence of CCT on global expression changes and general RNA steady-state levels, RNA from wild type and ts *cct1-2* strains grown at non-permissive temperature 37 ˚C for 4 h was interrogated with RNA Sequencing (Figure 4.1.3). The differential gene expression revealed that, out of 6692 ORFs, the total number of 2-fold up- and downregulated genes was only 162 and 130 (Appendix 7.7.1). Select up- and downregulated genes were confirmed with qPCR (Figure 4.1.5). GO functional classification suggested that the upregulated genes were mainly heat shock proteins, and downregulated genes were linked to ribosome biogenesis. These genes were not tied to CCT-specific cellular response – it was observed that depletion of other chaperones led to similar outcome (see results in Hsp90 chapter). The list of genes also parallels to a general heat shock response (Wu 2008).
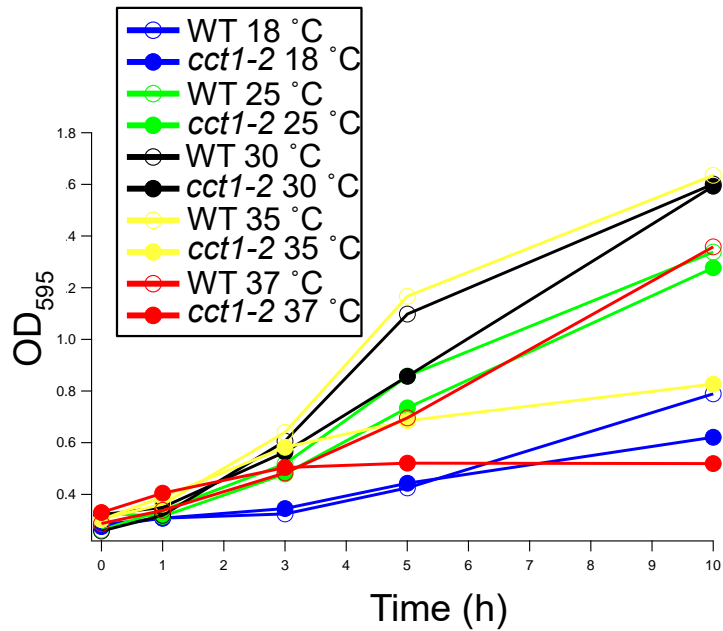
Figure 4.1.4. **Optimization of conditions for CCT inactivation.**
Growth of WT and *cct1-2* strains, tracked via optical density at 595 nm, was examined at different temperatures (18, 25, 30 and 37 ˚C) over time.

WT/*cct1-2* RNA-Seq
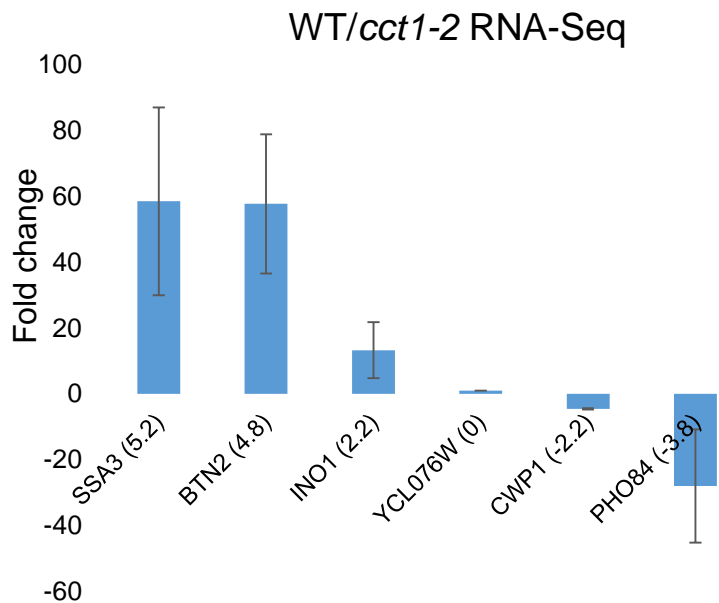
Figure 4.1.5. **Validation of RNA-Seq up- and downregulated genes.**
Select computed up- and downregulated genes according to the RNA-Seq were validated with qPCR. The numbers in brackets are computed Gfold (Feng 2012) expression changes.

Important observation from the RNA-Seq data is that CCT molecular chaperone inactivation led to aberrant intergenic transcription (Figure 4.1.6A). Canonical transcription is reflected by the directional transcripts, 100-bp reads (blue), within annotated ORFs (blue boxes), and absence of transcripts within intergenic location (spaces between annotated ORFs pointed out with green brackets), as represented for the wild type (Figure 4.1.6A). In *cct1-2*, there is an increase of aberrant intergenic transcripts with respect to the wild type (locations pointed out with green brackets) (Figure 4.1.6A). These intergenic transcripts have different directionality (100 bp red reads) from the canonical, ORF sense transcripts (blue). When an exemplary location is enlarged, it becomes apparent that the intergenic transcripts are not only running antisense from the downstream gene 5', but they are also extend into 5' region of an ORF (Figure 4.1.6B, left). Antisense transcripts are not affecting the upstream tandem gene pair and its terminator (Figure 4.1.6B, left). The phenotype on the whole suggests 5' bidirectional transcription from the same core promoter or its vicinity. Deducing from the read orientation and positions, 70% of all ORFs displayed 5' bidirectional transcription (Figure 4.1.6B, right). Furthermore, it was detected that ORFs in *cct1-2* displayed changed read directionality when compared to the wild type (Figure 4.1.7A). At least 2-fold total read directionality switch was observed for 4422 (62%) ORFs in *cct1-2* with respect to the wild type (Figure 4.1.7B). Thereby, only ~ 50 genes were transcribed completely in the antisense orientation (Appendix 7.6.) – these genes were usually located within subtelomeric and centromeric regions (Figure 4.1.7C). Most of the genes with switched directionality were classified above set threshold due to the 5' bidirectional transcription that tended to extend into the ORF (Figure 4.1.6B).
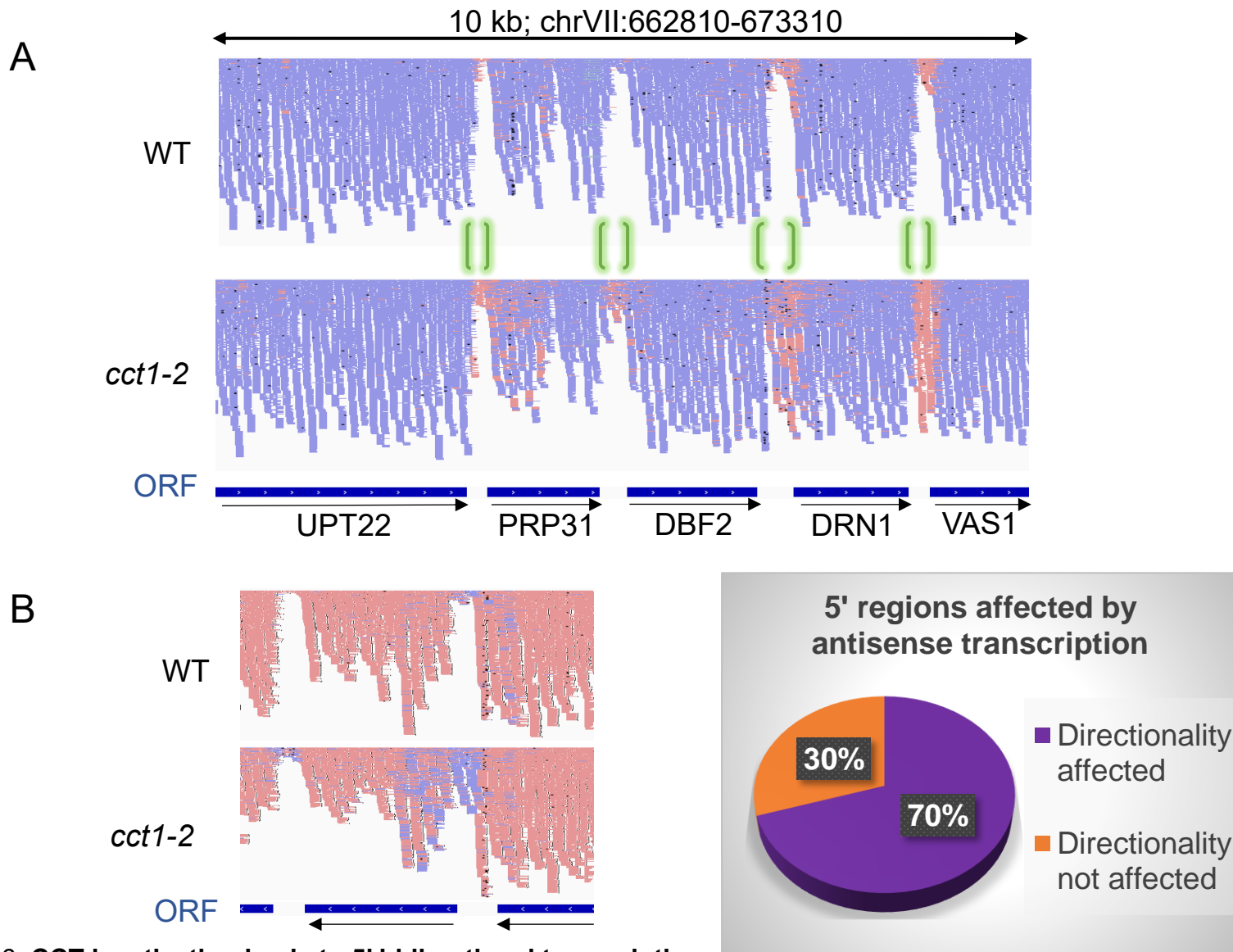
Figure 4.1.6. **CCT inactivation leads to 5' bidirectional transcription.**
RNA-Seq reads obtained via deep sequencing RNA isolated from WT and *cct1-2* strains grown at non-permissive temperature, aligned to the reference genome (UCSC, April 2011) with STAR (Dobin 2013) depicting A. global cryptic transcription in *cct1-2* as represented by the increase of antisense reads (red) within intergenic regions and at 5', compared to the sense ORF transcription (blue). B (left) zoomed in representative case of cryptic 5' bidirectional transcription as displayed by the increase of antisense reads (blue) compared to the sense reads (red) from the same 5' core promoter (or its vicinity). (right) The number of 5' locations affected by bidirectional transcription above 2-fold in *cct1-2* compared to the WT.
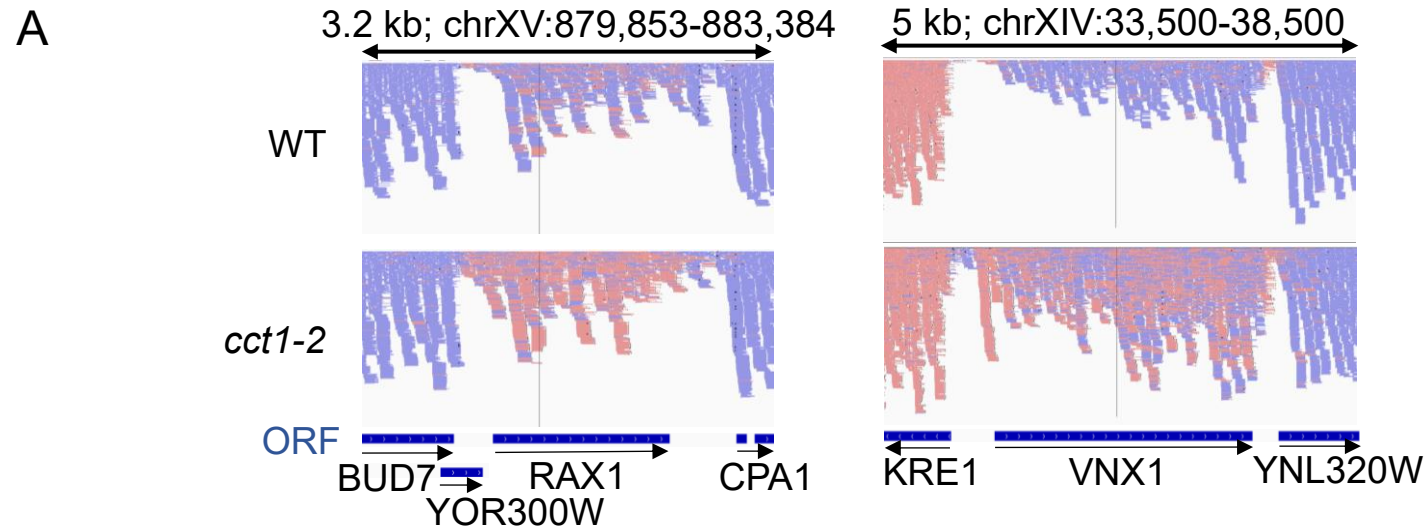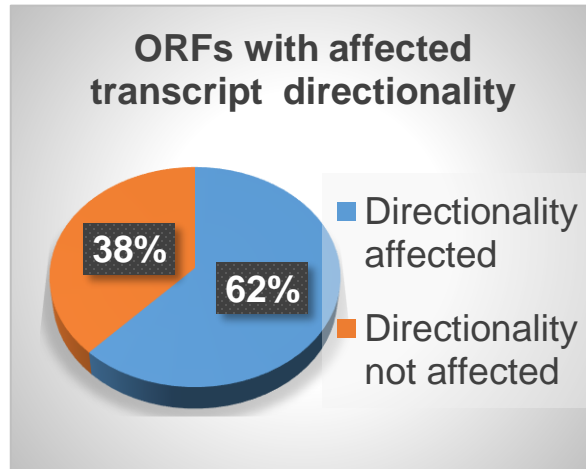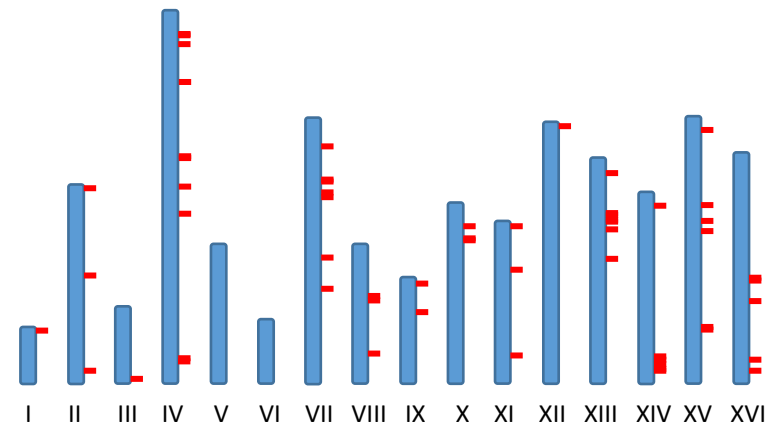
Figure 4.1.7. **CCT inactivation leads to antisense transcription of subsets of genes.**
A. RNA-Seq reads obtained via deep sequencing RNA isolated from WT and *cct1-2* strains grown at non-permissive temperature. The reads aligned to the reference genome at indicated locations demonstrate antisense transcription (red reads as opposed to sense reads that are blue) in *cct1-2* affecting entire VNX1 and RAX1 ORFs. B. The number of ORFs whose sense/antisense read ratio is >2. C. Chromosomal locations of the genes for which more than half of the total reads switched directionality in *cct1-2* (marked as red).

Initial RNA-Seq experiment were performed with Illumina HiSeq2000 that generated about 50 million high-quality reads. To confirm the transcript phenotype, RNA-Seq was repeated with improved HiSeq4000 generating 200 million reads for either strain (Figure 4.1.8A). Comparison of the two data sets for both strains revealed near identical profiles (Figure 4.1.8B). Up- and down regulated genes were similar between two data sets (not shown).

A

		HiSeq 2000		HiSeq 4000	
		WT	*cct1-2*	WT	*cct1-2*
Number of input reads		49,518,984	46762545	215152872	189183628
Uniquely mapped reads number		45536457	43340767	199142052	176192577
Uniquely mapped reads %		91.96%	92.68%	92.56%	93.13%
number of reads mapped to too many loci		3746931	2997553	14963773	11238902
% of reads mapped to too many loci		7.57%	6.41%	6.95%	5.94%
% of reads unmapped: too short		0.41%	0.82%	0.48%	0.91%
Total number of splices		283841	122365	1790113	703566
Number of annotated splices		273455	111338	1694824	640143
Number of non-canonical splices		2135	2818	6483	11948

B
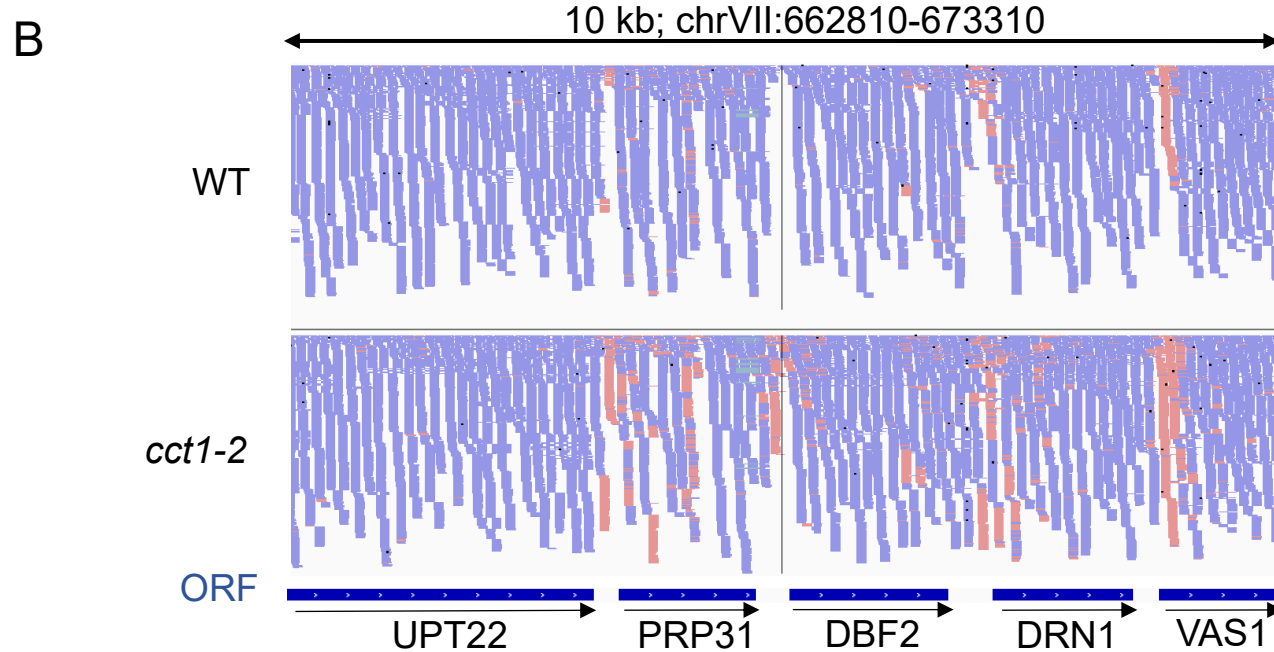
Figure 4.1.8. **Aberrant transcription phenotype in *cct1-2* is reproducible.**
A. WT and *cct1-2* RNA-Seq reads obtained with Illumina HiSeq 2000 and HiSeq 4000. Quality of the reads aligned to the sacCer3 reference genome with STAR. B. Illumina HiSeq 4000 RNA-Seq data showing read directionality and distribution in WT and *cct1-2*. For comparison, the data spans the same window as the data from the Figure 2A that was generated with Illumina HiSeq2000.

Since CCT interacts with numerous histone modifiers, it was speculated that depletion of the CCT molecular chaperonin might affect their function and lead to a change in the histone code. To address this, histone mass spectrometry (Pesavento 2006) was exploited on histones isolated from wild type and *cct1-2* strains grown under non-permissive temperature 37 ˚C for 4 h. The results of multi reaction monitoring are represented in the form of a relative abundance of the given modification mark from the relative total peptide pool (Figure 4.1.9). In this pool, a peptide is identified in all its forms within the histones. A mild decline of the H3 and H4 tail residues' acetylation is seen in histones from *cct1-2* compared to the wild type (H3K9, H3K14, H3K23, H4K5, H4K8 and H4K12) (Figure 4.1.9A), whereas no prominent changes can be observed for methylation levels (H3K4me1, H3K36me2/3 and H4K20me3) (Figure 4.1.9B).

H3K79me3 is the only modification notably increased in *cct1-2* (125% ± 8% SD) (Figure 4.1.9B). The total levels of H3K79me3 in wild type and *cct1-2* crude extracts validated the mass spectrometric results (Figure 4.1.10A). H3K79me3 demarcates actively transcribed regions such as ORFs – it is absent from intergenic and subtelomeric heterochromatin under regular conditions (Ng 2003, Pokholok 2005). H3K79me3 within intergenic regions was directly implicated in pervasive intergenic transcription (Xue 2015). The increase of intergenic transcripts within affected 5' locations in *cct1-2* could indicate H3K79me3 increase therein. To test this, chromatin immunoprecipitation was performed targeting H3K79me3 at the locations that are subject to increased intergenic transcription (Appendix 7.5.). Results suggest an average of 0.32 fold (± 0.14) increase of H3K79me3 (Figure 4.1.10B). Dot1 histone methyltransferase is the sole enzyme responsible for H3K79 mono-, di- and trimethylation (van Leeuwen 2002) – its DNA occupancy changes could not be detected (Figure 4.1.10C). However, a genetic connection between CCT and Dot1 was noticed using spot test assay (Figure 4.1.10D).
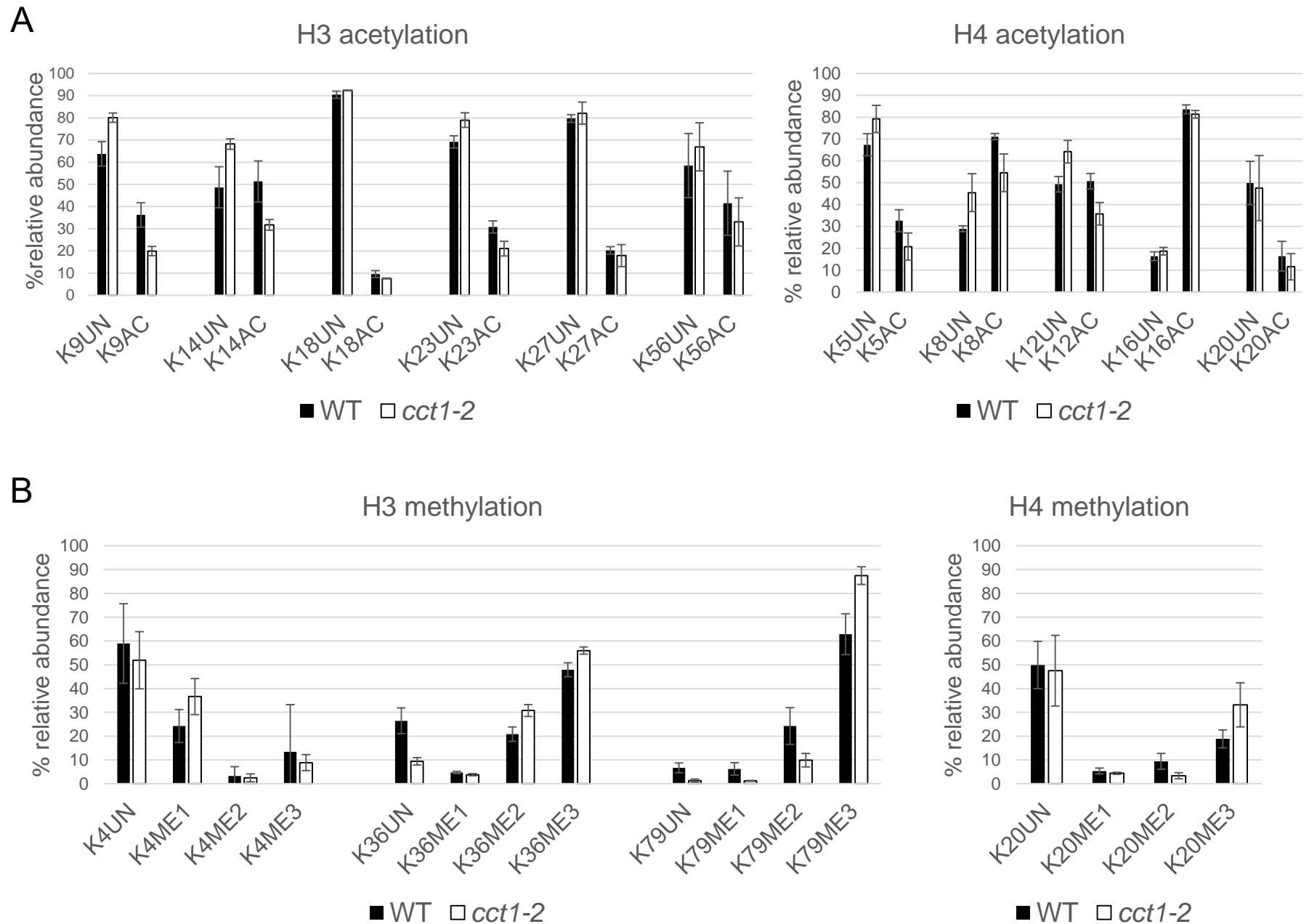
Figure 4.1.9. **Histone 3 and 4 mass spectrometry of WT and *cct1-2* strains' histones.**
Relative abundance of A. acetylated and B. methylated residues in WT and *cct1-2* histones. The histones were isolated from the strains grown at non-permissive temperature, and were subject to multi-reaction monitoring technology (Pesavento 2006).
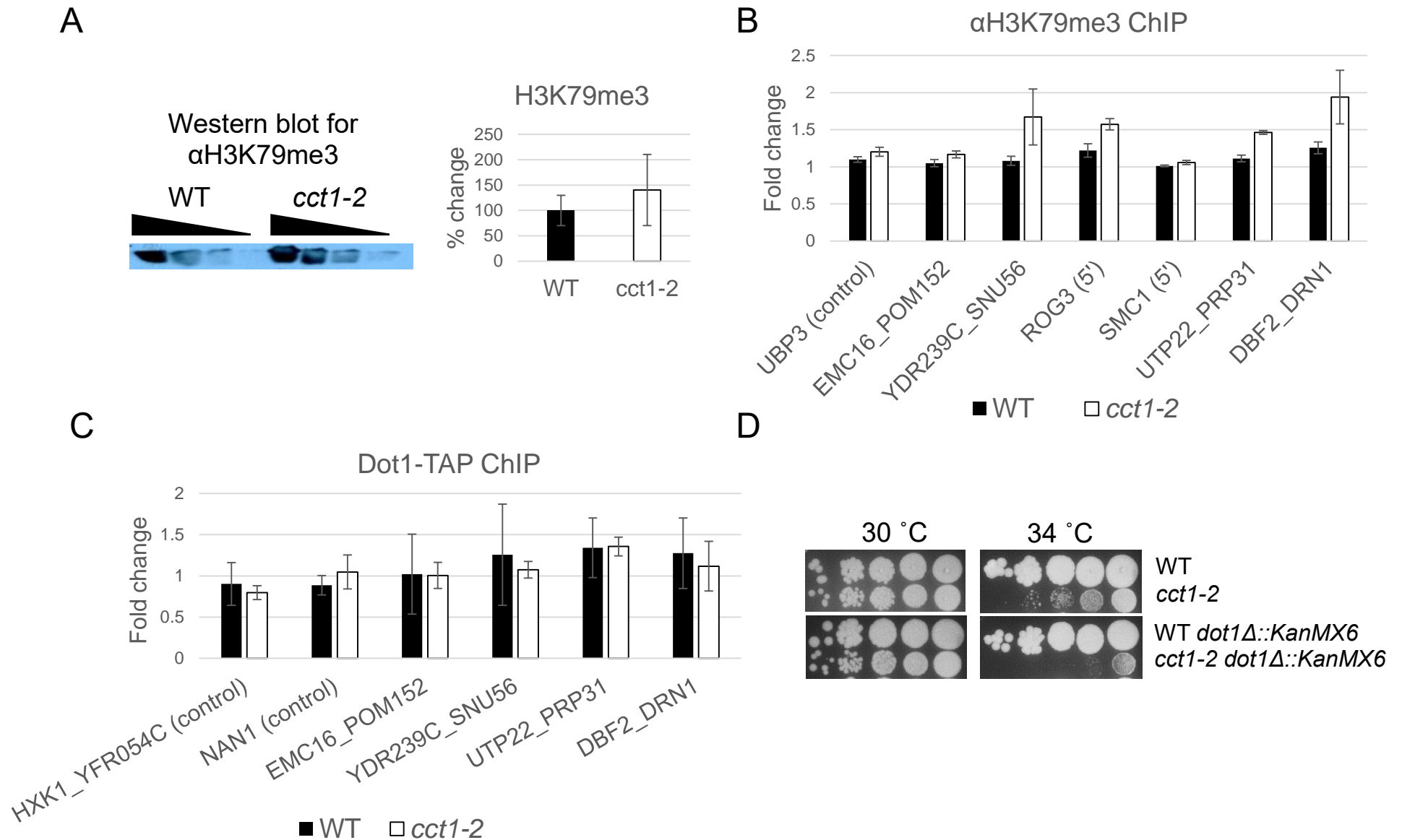
Figure 4.1.10. **H3K79me3 mildly increased in *cct1-2*.**
A. H3K79me3 total levels verified on WT and *cct1-2* crude extracts by Western blotting using αH3K79me3 antibodies. Crude extracts were obtain from the strains grown at non-permissive temperature. B. H3K79me3 and C. Dot1-TAP DNA occupancy measured in WT and *cct1-2* grown at non-permissive temperature via ChIP at the locations affected by 5' bidirectional/intergenic transcription. D. Spot test assay for WT *Δdot1* and *cct1-2 Δdot1* grown at control (30 ˚C) and lethal (34 ˚C) temperature.

PAF1 elongation complex was reported to be a prerequisite for H3K79 methylation in the course of transcription elongation (Nguyen 2011). It was tested whether PAF1 connects to the misregulated transcription and H3K79me3 increase. Using chromatin immunoprecipitation on *cct1-2* strain epitope-tagged for PAF1 subunit, the enrichment of the complex was investigated at the location affected by bidirectional transcription. The results show that PAF1 occupancy was not affected upon CCT inactivation (Figure 4.1.11).
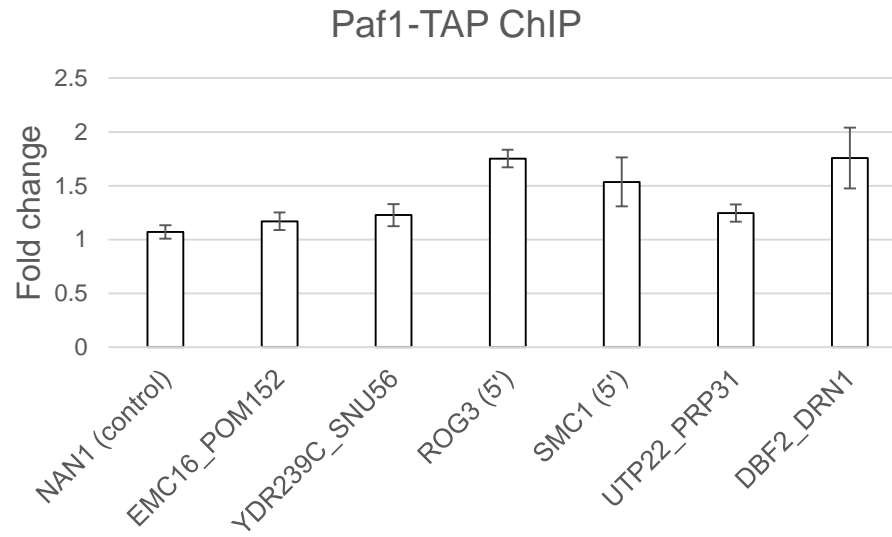
Figure 4.1.11. **PAF1 occupancy at the affected locations remains unaltered.**
PAF1 complex was interrogated for the DNA binding in *cct1-2* under non-permissive temperature (37 ˚C) with respect to control (30 ˚C) by utilizing chromatin immunoprecipitation against epitope tagged Paf1 subunit at the locations affected by 5' bidirectional transcription.

H3K79me3-containing nucleosomes are mutually exclusive with H2A.Z histone variant (Li 2005). H2A.Z is one of the heterochromatin boundary elements (Meneghini 2003, Zhou 2010), that is, it is found at the interface between transcribed ORFs and non-transcribed intergenic locations. It is believed to both activate and inhibit transcription (Zlatanova 2008). The involvement of H2A.Z was inspected at CCT-dependent 5' bidirectional transcription sites. H2A.Z nucleosomes colocalized very well with the 5' affected regions covering 78% of the reported H2A.Z locations according to the map by Zhang 2005 (Figure 4.1.12A). Surprisingly, H2A.Z DNA occupancy declined two fold at every location tested that displays 5' bidirectional transcription phenotype (Figure 4.1.12B and C). Yet, the expression levels for the coding regions of the affected genes stayed unaltered (data not shown).

Next it was tested whether Dot1-mediated H3K79me3 increase is connected to the H2A.Z loss upon CCT inactivation at the locations with aberrant intergenic transcription. Thereby, H2A.Z occupancy was measured in *cct1-2 Δdot1* strain by implementing ChIP. The results show that H2A.Z loss was not dependent on or influenced by H3K79me3 itself, as H2A.Z decline was observed upon temperature inactivated CCT in *cct1-2* strains with deleted DOT1 gene (Figure 4.1.13A). Additional verification experiment was performed to test whether H2A.Z nucleosomes indeed are negative for H3K79. Thereby, tandem purified H2A.Z nucleosomes from the wild type and *cct1-2* strains grown at non-permissive temperature were assessed for H3K79me3 mark via Western blotting (Figure 4.1.13B). TAP-purified H2A.Z did not contain H3K79me3 mark. The results show that observed increase of H3K79me3 mark is not prerequisite for H2A.Z loss at the sites affected by 5' bidirectional transcription.
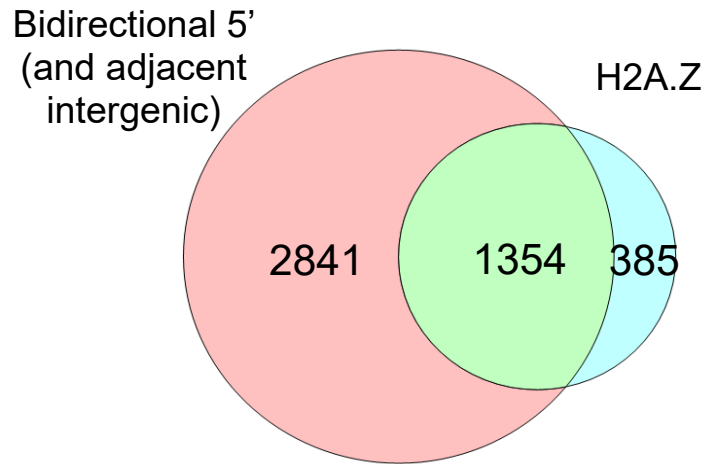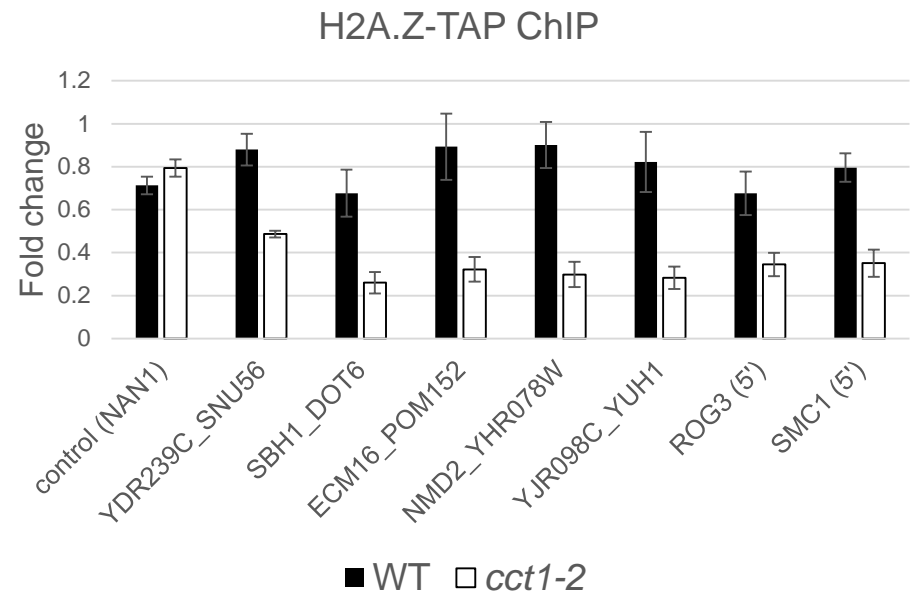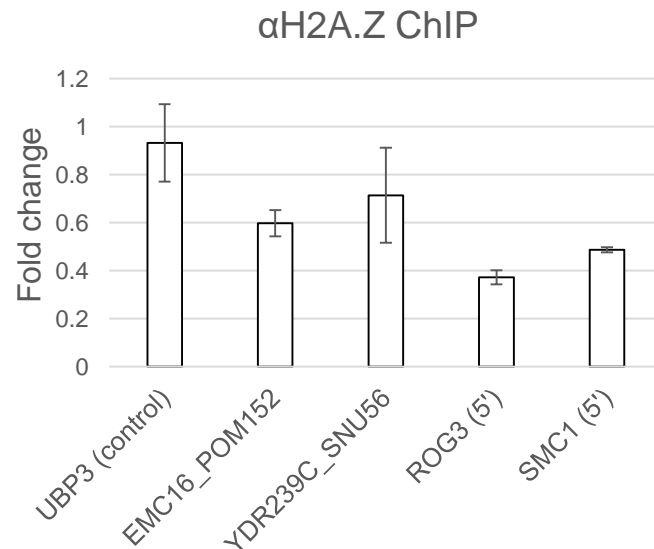
Figure 4.1.12. **CCT inactivation leads to H2A.Z loss at the sites affected by 5' bidirectional transcription.**
A. The number of reported H2A.Z locations (Zhang 2005) overlapping with regions affected by 5' bidirectional transcription in *cct1-2*.
B. H2A.Z DNA occupancy at the locations with increased 5' bidirectional transcription in WT and *cct1-2* grown at non-permissive temperature. C. H2A.Z DNA occupancy verified in *cct1-2* grown at 37 ˚C with antibodies raised against yeast H2A.Z.

124
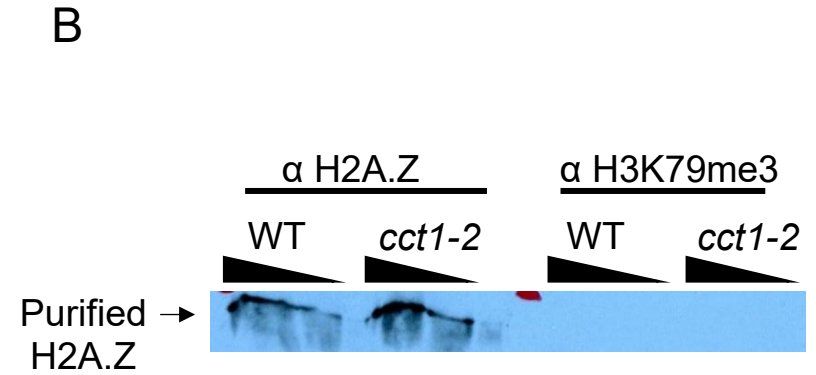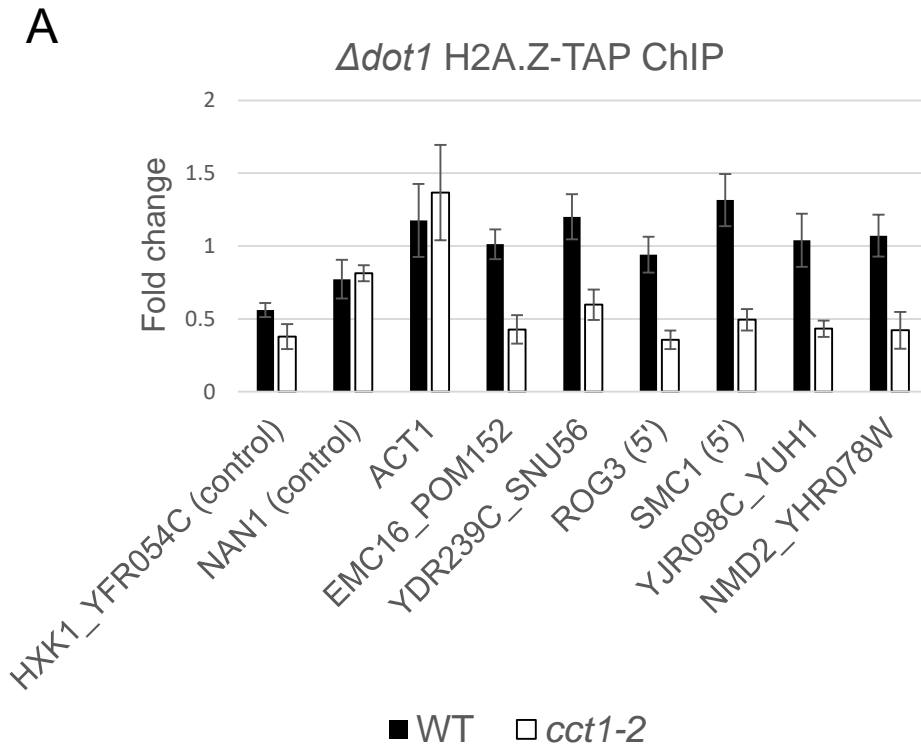
Figure 4.1.13. **H2A.Z loss is not linked to H3K79me3.**
A. H2A.Z occupancy in WT *Δdot1* and *cct1-2 Δdot1* strains grown at non-permissive temperature. B. H2A.Z obtained from WT and *cct1-2* grown at non-permissive temperature by tandem affinity purification and Western blotted for αHtz1 and αH3K79me3.

Besides at the 5' location, H2A.Z decline colocalized with subtelomeric genes that were transcribed in the antisense orientation upon CCT depletion (Figure 4.1.14A and B). H2A.Z was reported to occur in clusters in subtelomeric locations, where transcription activation is potentially altered upon its removal (Meneghini 2003, Guillemette 2005, Shia 2006). H2A.Z decline did not correlate with the differential expression but sole read directionality switch. In the case of several subtelomeric H2A.Z-containing genes, such as BIO4, the wild type gene was initially transcribed in reserve orientation and transcript directionality was switched in *cct1-2* (Figure 4.1.14C).
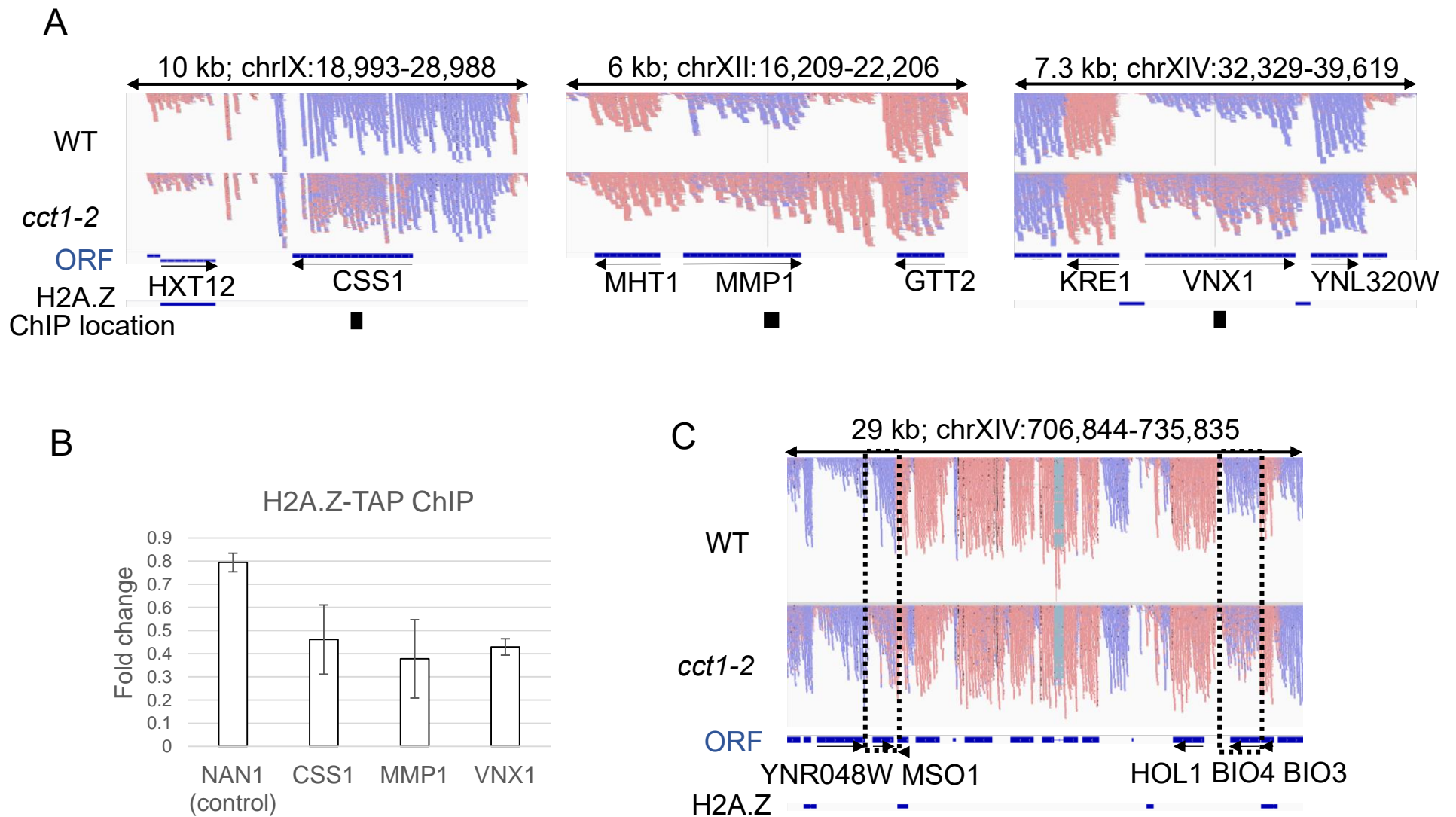
Figure 4.1.14. **H2A.Z loss correlates with antisense transcription in *cct1-2*.**
A. RNA-Seq reads obtained via deep sequencing RNA isolated from WT and *cct1-2* strains grown at non-permissive temperature. The reads aligned to the reference genome at indicated locations present antisense transcription for subtelomeric genes that colocalize with reported (Zhang 2005) or previously unidentified H2A.Z-containing regions. B. Decreased H2A.Z occupancy upon CCT inactivation for the genes in A. verified by ChIP in *cct1-2* grown at 37 ˚C. C. H2A.Z loss in *cct1-2* correlates with reads' directionality switch (boxes with dashed lines) with respect to WT.

Next, it was checked whether H2A.Z links to cryptic intergenic transcription. The findings that, upon CCT inactivation, H2A.Z is evicted from the locations with 5' bidirectional transcription, as well as subtelomeric antisense transcription, lead us to seek the mechanistic insight among the targets regulating H2A.Z. H2A.Z removal is catalyzed by INO80 chromatin remodeling complex (Papamichos-Chronachis 2011). INO80 was also reported to prevent euchromatin spread past the gene borders by competing with H3K79me3, and its depletion was associated with intergenic transcription (Xue 2015, Xue 2017). For these reasons, it was suspected that INO80 could be affected in the absence of functional CCT, which would contribute to H2A.Z loss and cryptic transcription. Since CCT is a chaperone capable of assembling polypeptides into an oligomeric complex (Frydman 1994), the subunit integrity of INO80 complex was examined in the absence of functional CCT. INO80 was purified from ts and wild type strains, which were previously grown under non-permissive temperature, by utilizing TAP-tagged Ino80 subunit. Analysis of SDS gel-resolved complex shows that no alterations were detected between the complexes obtained from the wild type and ts strain (Figure 4.1.15A). Furthermore, it was tested with ChIP whether inactivation of CCT affected INO80 chromatin binding at the cryptic transcription sites. Differential INO80 DNA binding at various 5' target locations, as well as at various time points after CCT depletion, was not identified (Figure 4.1.15A).

It was also asked whether the reverse reaction, that is, component mediating incorporation of H2A.Z variant, was dependent on CCT. Deposition of H2A.Z histone variant is catalyzed by SWR-C (Krogan 2003, Mizuguchi 2004, Kobor 2004). Similarly to INO80, investigating SWR-C subunit integrity via Swr1-TAP pull down from the wild type and *cct1-2*, as well as measuring DNA occupancy via ChIP, showed that neither the subunit integrity nor the DNA occupancy were altered in the absence of functional CCT (Figure 4.1.15B). Furthermore, Nap1 histone chaperone involved in H2A.Z nuclear transport and deposition (Straube 2010, Dronamraju 2017) did not show differential binding at the locations affected by 5' bidirectional transcription, nor changed total protein levels upon inactivating CCT (Figure 4.1.16). Overall, according to the utilized assays the components regulating H2A.Z occupancy were not dependent on CCT.
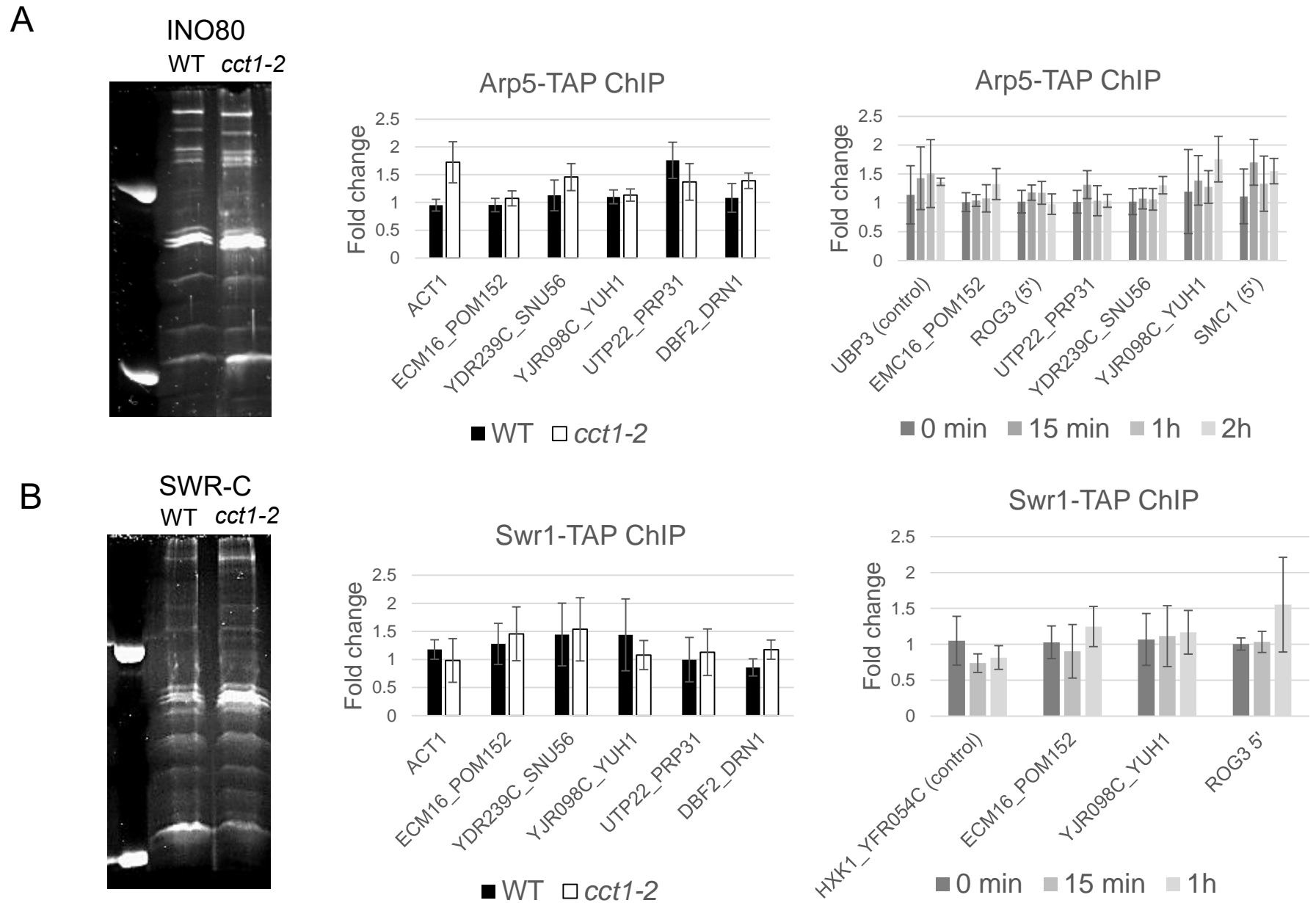
Figure 4.1.15. **H2A.Z loss and cryptic transcriptions are not due to INO80 and SWR-C.**
A. (left) INO80 complex purified from WT and *cct1-2* strains grown at non-permissive temperature stained with Sypro Ruby stain. (middle) INO80 occupancy in WT and *cct1-2* after 4 h at 37 ˚C, at the locations affected by 5' bidirectional transcription. (right) INO80 occupancy in *cct1-2* at 0, 15 min, 1 h and 2 h after shifting the cultures from 30 ˚C to 37 ˚C. B. SWR-C as in A.
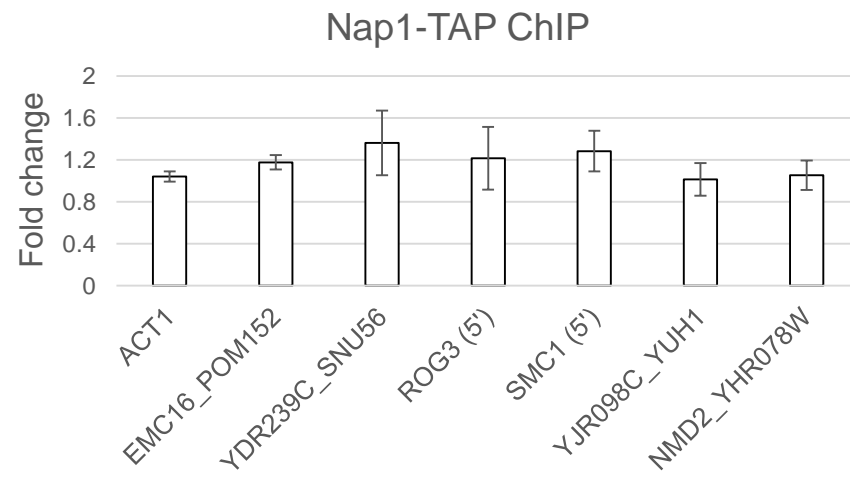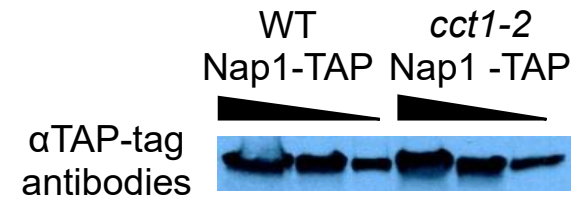
Figure 4.1.16. **H2A.Z loss and cryptic transcriptions are not due to Nap1.**
A. DNA occupancy of Nap1 histone chaperone in *cct1-2* grown at 37 ˚C at locations affected by 5' bidirectional transcription. B. Total Nap1-TAP levels in WT and *cct1-2* strains grown at 37 ˚C, detected by Western Blot with αTAP antibodies.

Given the results that canonical H2A.Z chromatin regulators were not involved in the H2A.Z maintenance, it was asked whether general histone chaperones-directed nucleosome turnover could be responsible for H2A.Z loss and bidirectional transcription. Earlier studies highlighted that nucleosome turnover is generally high within promoter regions (Dion 2007, Rufiange 2007). Newly incorporated histones are enriched for H3K56 acetylation mark that is catalyzed on soluble histones by Rtt109-Vps75 or Asf1 histone chaperones (Rufiange 2007, Tsubota 2007, Kaplan 2008). Since CCT did connect to Asf1 histone chaperone genetically (Figure 4.1.17A), it was intuitive to test whether histone chaperones and concomitant mark are altered upon CCT inactivation. According to the mass spectrometry, there was no global change in H3K56 acetylation (Figure 4.1.9A). These results were validated by measuring occupancy of H3K56 acetylation mark via ChIP at the sites affected for 5' bidirectional transcription (Figure 4.1.17B). Testing differential binding of epitope-tagged Rtt109 and Asf1 histone chaperones in *cct1-2* at the sites that were subject to 5' bidirectional transcription via ChIP also delivered negative results (Figure 4.1.17C). Hence, Rtt109, Asf1 and H3K65 acetylation were not altered in *cct1-2* according to the utilized assays.
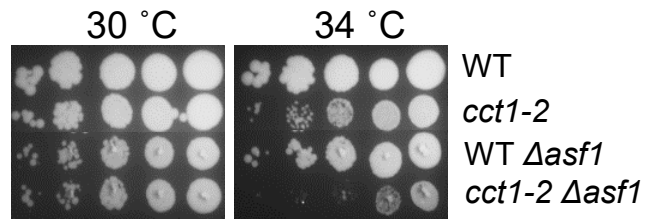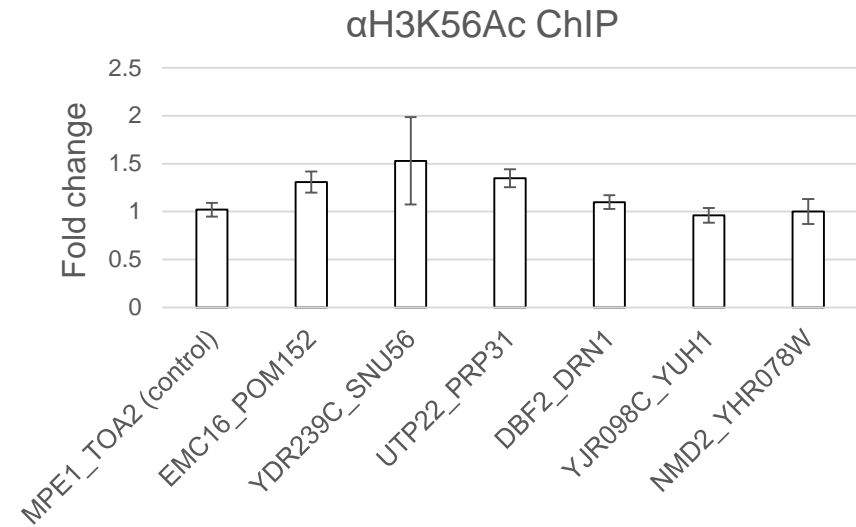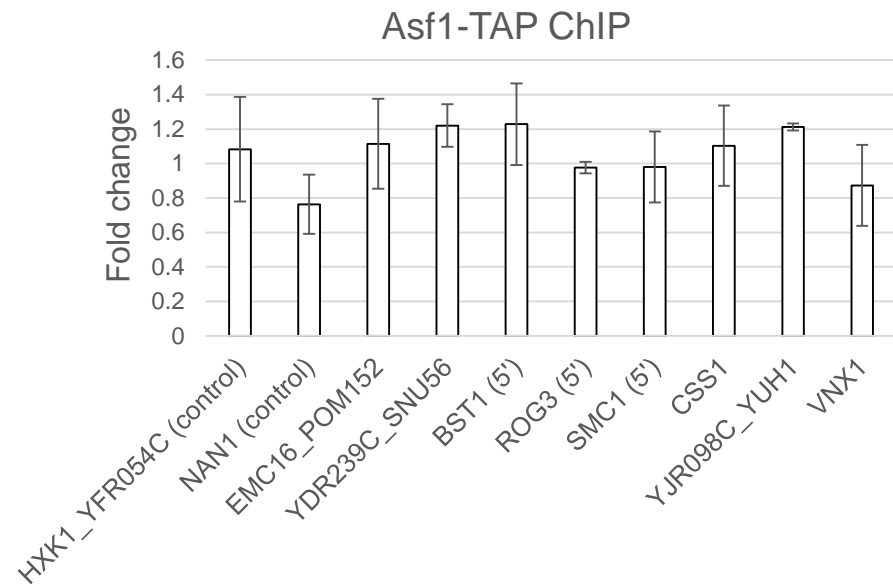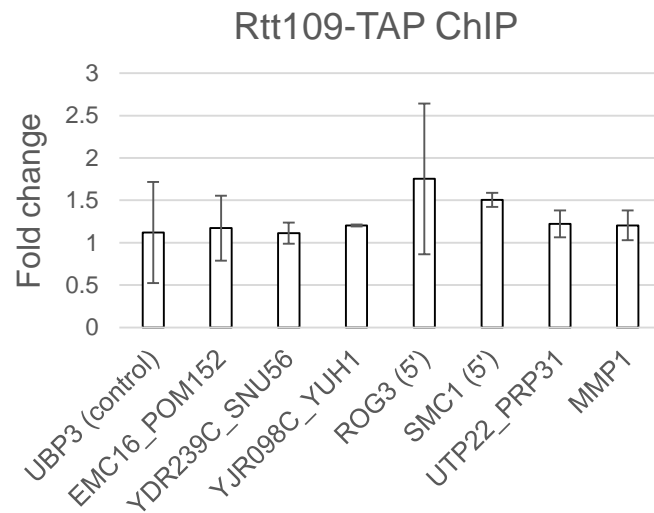
Figure 4.1.17. **H3K56Ac remains unaltered, as well as histone chaperones Rtt109 and Asf1.**
A. Spot test assay for WT *Δasf1* and *cct1-2 Δasft1* grown at control (30 ˚C) and lethal (34 ˚C) temperature. B. H3K56 acetylation in *cct1-2* grown at 37 ˚C verified by ChIP using αH3K56Ac antibodies at the locations affected by 5' bidirectional transcription. C. DNA occupancy of histone chaperones Rtt109-TAP and Asf1-TAP in *cct1-2* grown at 37 ˚C at the locations affected by 5' bidirectional transcription.

Another histone chaperone FACT affects nucleosome turnover, as well as RNA polymerase occupancy at promoter regions (Schwabish 2004). FACT associates with travelling RNA polymerase to support transcriptional fidelity as it is involved in proper histone deposition, and it prevents transcription initiation at cryptic promoters (Orphanides 1998, Belotserkovskaya 2003, Mason 2003, Schwabish 2004). Furthermore, depletion of FACT lead to the loss of H2A.Z histone variant from the 5' locations, which was followed by concomitant gain of mislocalized H2A.Z within genic regions together with cryptic transcription increase (Jeronimo 2015). For these reason, FACT occupancy was checked via ChIP by utilizing Spt16-TAP subunit in *cct1-2* strain at the affected locations. However, the results show that FACT DNA occupancy was not changed upon inactivation of CCT (Figure 4.1.18A). Finally, disruption of another chromatin chaperone, Chromatin Assembly Factor (CAF-I), was reported to cause genome-wide derepression of nascent divergent noncoding transcripts (Marquardt 2014). Although 82% of the reported promoters affected for cryptic transcription in the absence of CAF-I (Marquardt 2014) overlaid with our CCT affected 5' locations (Figure 4.1.18B), CAF-I did not seem altered (Figure 4.1.18C and D). Hence, the cause of 5' bidirectional transcription in *cct1-2* could not be explained by these histone chaperones.
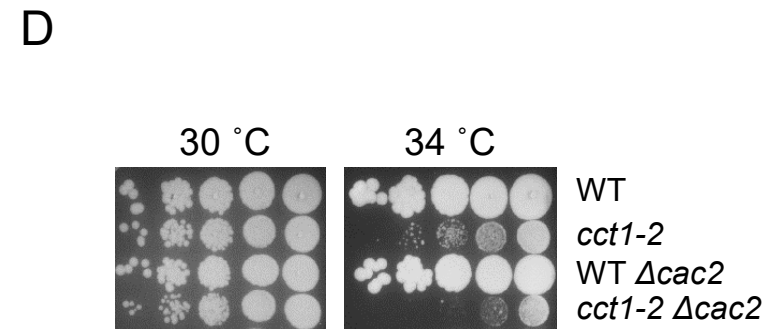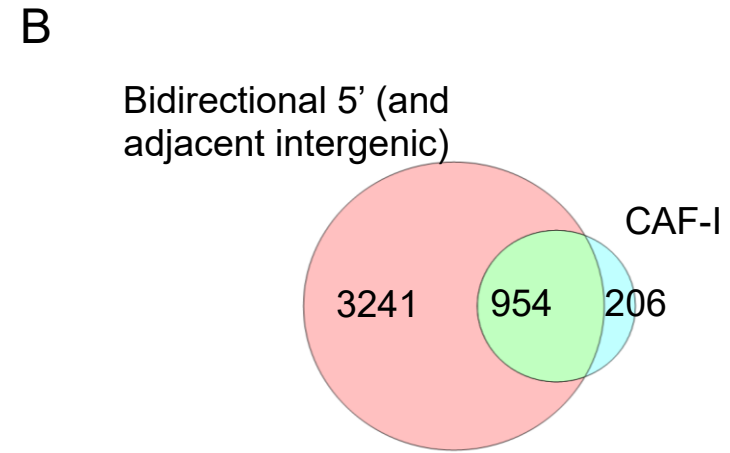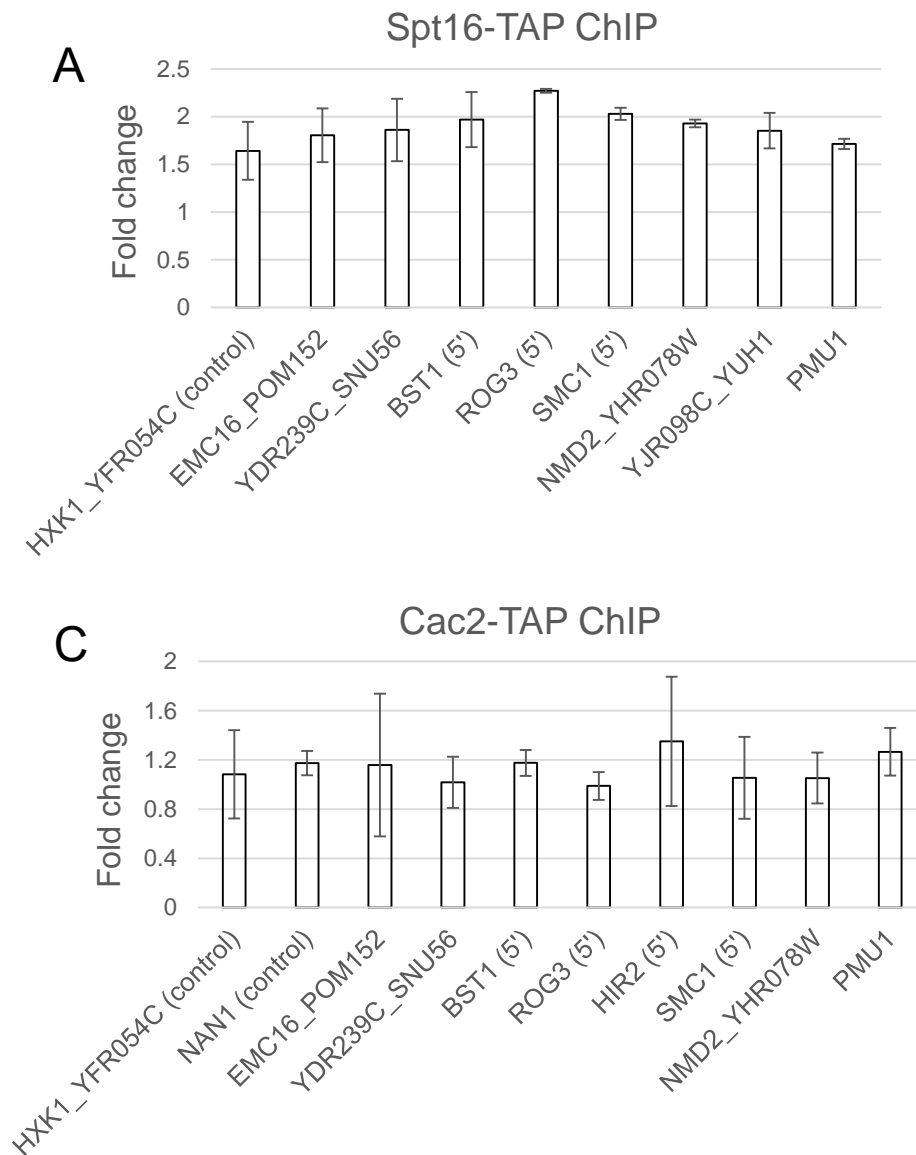
Figure 4.1.18. **FACT and CAF-I are not affected in *cct1-2*.**
A. DNA occupancy of histone chaperone Spt16-TAP in *cct1-2* grown at 37 ˚C at the locations affected by 5' bidirectional transcription.
B. The number of reported locations CAF-I-dependent on 5' cryptic transcription (Marquardt 2015) overlapping with *cct1-2* regions affected by 5' bidirectional transcription. C. CAF-I occupancy in *cct1-2* grown at 37 ˚C at the locations with increased 5' bidirectional transcription. D. Spot test assay of WT *Δcac2* and *cct1-2 Δcac2*, grown at control (30 ˚C) and lethal (34 ˚C) temperature.

H2A.Z eviction and likely cryptic transcription at 5' do not seem to take place due to defects of any of the known complexes involved in H2A.Z chromatin homeostasis, nor many other histone chaperones responsible for the nucleosomal dynamics. Based on about ~ 20 tested genic location, H2A.Z loss at 5' locations was not followed by subsequent misincorporation of H2A.Z elsewhere in the genome, or particularly genic locations, as reported before (data not shown) (Jeronimo 2015). However, H2A.Z was largely involved beyond changed occupancy. CCT and H2A.Z were shown to have a strong genetic connection in the spot test assay (Figure 4.1.19A). In addition, it was found that upon CCT inactivation, it took about 2.5 h for H2A.Z occupancy decline to reach plateau and thereby the total cellular H2A.Z levels decreased (Figure 4.1.19B and C). Given these results and previous strong correlations between H2A.Z and cryptic transcription events (Jeronimo 2015, Tramantano 2016), it was postulated that a sole H2A.Z transient depletion could lead to bidirectional transcription. To examine this, depletion of H2A.Z was triggered from the nucleus using anchor away method (Haruki 2008) (Figure 4.1.20A) and the strains were inspected for the transcriptional events. Thereby, the RNA samples from the H2A.Z-depleted strains together with non-depleted control were subject to RNA-Seq. According to the high-throughput RNA analysis, no cryptic transcripts were detected in the samples with induced H2A.Z loss with respect to the control (Figure 4.20B), suggesting that eviction of H2A.Z is a result of or simultaneous event to the 5' bidirectional transcription. Indeed, H3K79me3 transcriptionally concomitant mark was not altered upon induced H2A.Z loss (Figure 4.1.20C). In addition, ts *cct1-2* strain with inactivated CCT and devoid of HTZ1 gene still displayed light increase in H3K79me3, alluding upregulated intergenic transcription regardless of permanent H2A.Z loss (Figure 4.1.21A). However, since chaperonin such as CCT, affecting 9-15% of the proteome (Thulasiraman 1999) intervenes with numerous pathways, we wanted to make sure that no complementary mechanisms have taken over in *Δhtz1*, rendering thereby the same phenotype.
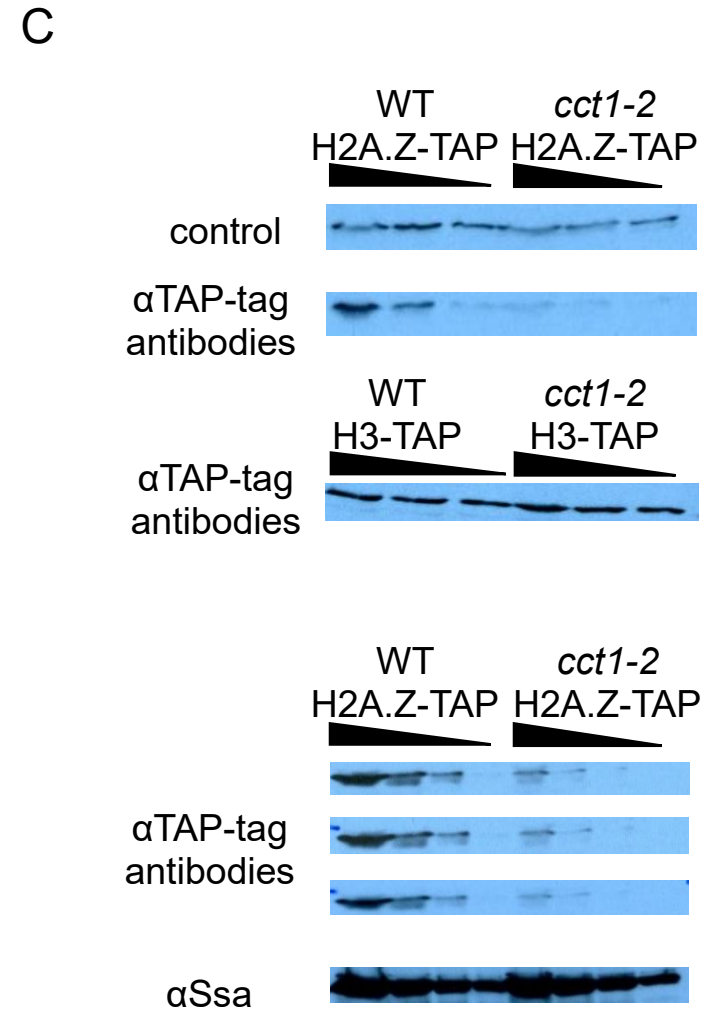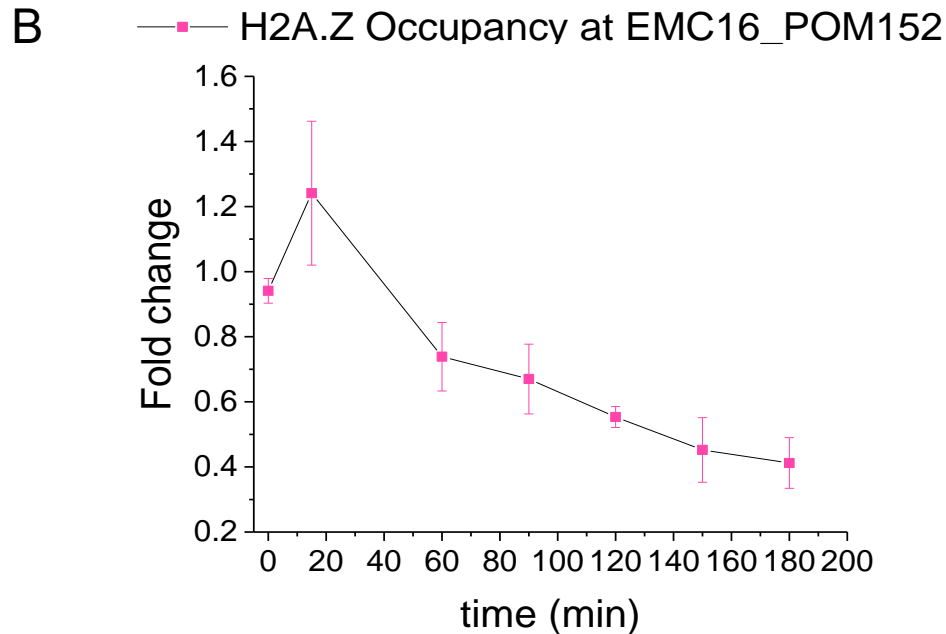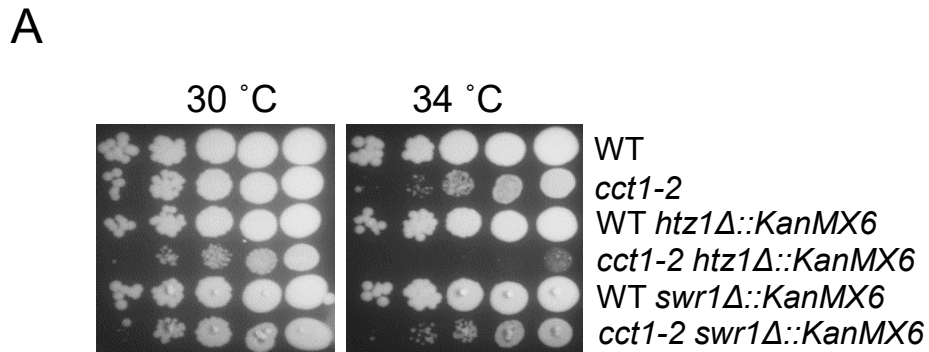
Figure 4.1.19. **H2A.Z total cellular levels decline upon CCT inactivation.**
A. Spot test assay for WT and *cct1-2* strains with indicated deletions, grown at control (30 ˚C) and lethal (34 ˚C) temperature. B. H2A.Z DNA occupancy decline over time after shifting *cct1-2* strains at 37 ˚C, at the location with increased 5' bidirectional transcription EMC16_POM152. C. Total H2A.Z levels in WT and *cct1-2* strains grown at 37 ˚C, detected by Western blot with αHtz1 antibodies.
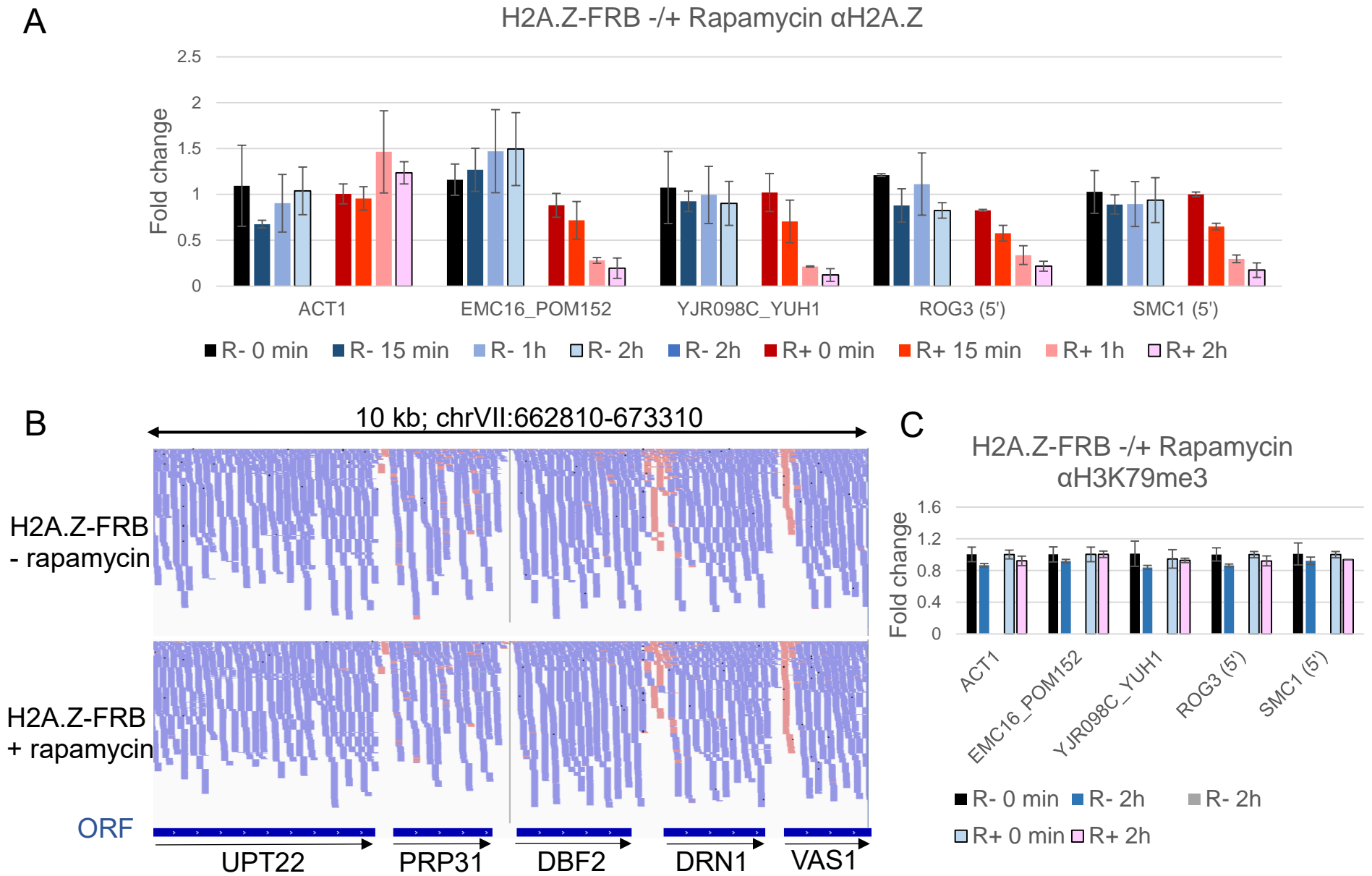
Figure 4.1.20. **Nuclear depletion of H2A.Z using anchor away does not lead to cryptic transcrition.**
A. H2A.Z-FRB occupancy over time in VDY1874 *H2A.Z-FRB::KanMX6* strain upon rapamycin addition (+), with respect to no treatment (-). B. RNA-Seq reads obtained via sequencing total RNA from VDY1874 *H2A.Z-FRB::KanMX6* without and with 4-h rapamycin exposure. C. Quantifying H3K79me3 of the +/- 2 h rapamycin samples from A. via ChIP using αH3K79me3 antibodies.

A Δhtz1 αH3K79me3 ChIP

B αH3K79me3 ChIP in WT::Δhtz1/WT

■ WT ☐ cct1-2
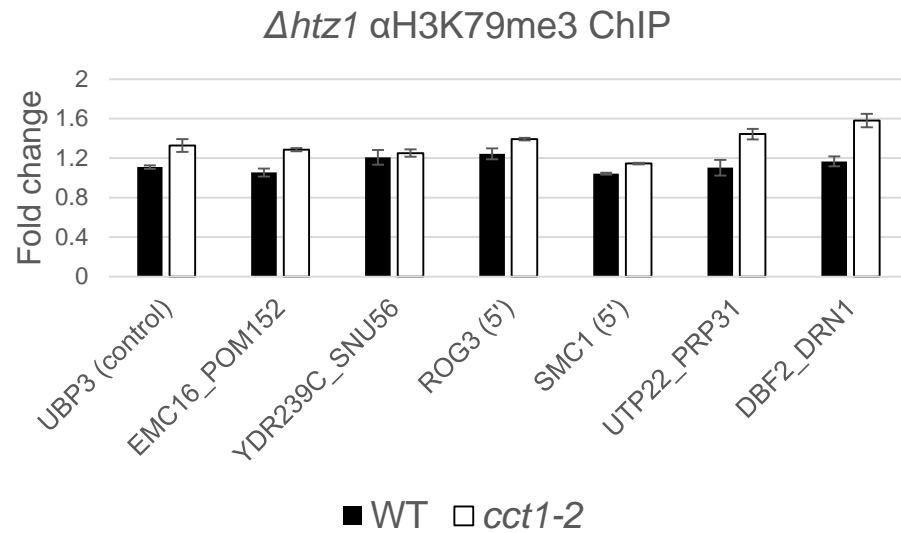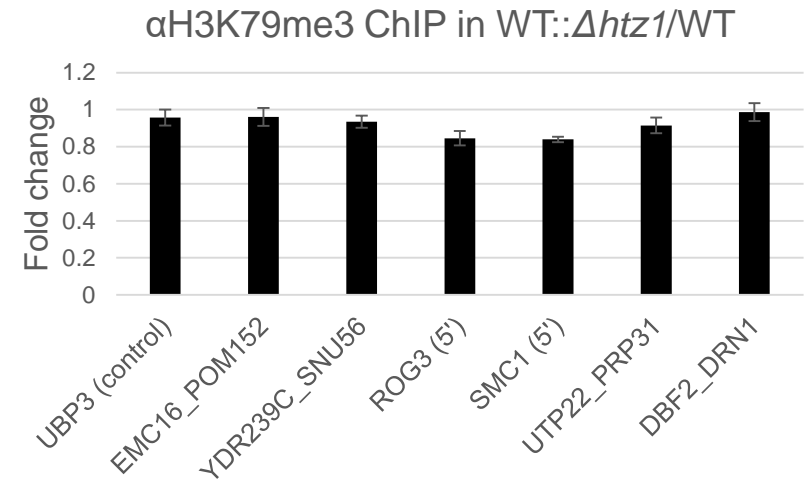
Figure 4.1.21. **Cct1-2 strains devoid of HTZ1 exhibits poor increase in H3K79me3.**
A. H3K79me3 DNA occupancy measured by ChIP with αH3K79me3 antibodies in A. WT Δhtz1 and cct1-2 Δhtz1 strains grown at 37 ˚C. B. WT Δhtz1 with respect to WT (both grown at 30 ˚C), in which, for comparison, no H3K79me3 changes are detected.

138

The focus was shifted on the histone modifiers that, in addition to interacting with CCT and some of the targets displaying a light histone code change, are well explored within the cryptic transcription field. Rpd3S histone deacetylase complex is recruited by Set2-mediated H3K36me3 mark in the coding and 3' regions to keep H3 and H4 hypoacetylated and prevent 3' antisense cryptic transcription (Krogan 2003, Keogh 2005, Carrozza 2005, Li 2009, Govind 2010, Churchman 2011). Both H3/4 acetylations and K36me2/3 are lightly altered in our data sets. To inspect whether Set2-RpdS3 pathway could be affected by CCT and therefore responsible for the observed phenotype, Set2-RpdS3 and our cryptic transcription data were compared. The high-throughput Net-Seq data from Churchman 2011 elucidated global increase of the cryptic transcripts antisense and upstream to an ORF in the presence of defective Set2-Rpd3S components, as shown on the select location (Figure 3A in Churchman 2011). Comparing the same select location to our data (Figure 4.1.6A), it is evident that CCT inactivation does not lead to the increase of 3' antisense transcription. As previously described, it is 5' cryptic transcription, leading to the increase of antisense intergenic transcripts initiated from the same core promoter or its vicinity. The possibility that Set2-Rpd3S mechanism could be involved were excluded and it was assumed that the light code change is rather an indirect consequence of other processes.

Similarly to Set2-Rpd3S pathway involvement at 3', Set1-Set3C histone methyltransferase and deacetylase pathway is known to be engaged at 5' and it was implicated in 5' cryptic transcription (Kim 2016). Set1-mediated H3K4me2/3 correlates with the 5' locations of active transcription (Ng 2003, Pokholok 2005) and H3K4me2/3 was proposed to recruit Set3C histone deacetylase to modulate acetylation status and transcription (Kim 2009, Kim 2012). An overlay of our locations affected by 5' bidirectional transcription with H3K4me3 ChIP-Seq data (Bonnet 2014) reveals that 84% 5' locations are enriched for this modification mark (Figure 4.1.22A). According to the histone mass spectrometry, however, there were no significant changes in the H3K4me2/3, when comparing total relative levels between WT and *cct1-2* ts mutant (Figure 4.1.9B). The unaffected H3K4me3 levels were confirmed with ChIP (Figure 4.1.22B). Furthermore, there was no alteration in Set1 or Set3 DNA occupancy either (Figure 4.1.22C). CCT does not have a genetic connection to Set1 (Figure 4.1.22C), but it still genetically interacts with certain Set3C and Rpd3L/S subunits (Figure 4.1.23), suggesting that the complexes are likely to operate within the parallel pathways. On the whole, it was concluded that the observed transcription phenotype in *cct1-2* is not due to affecting select roles of histone methyltransferases Set1 and Set2, and their concomitant histone deacetylases Set3C and Rpd3S.
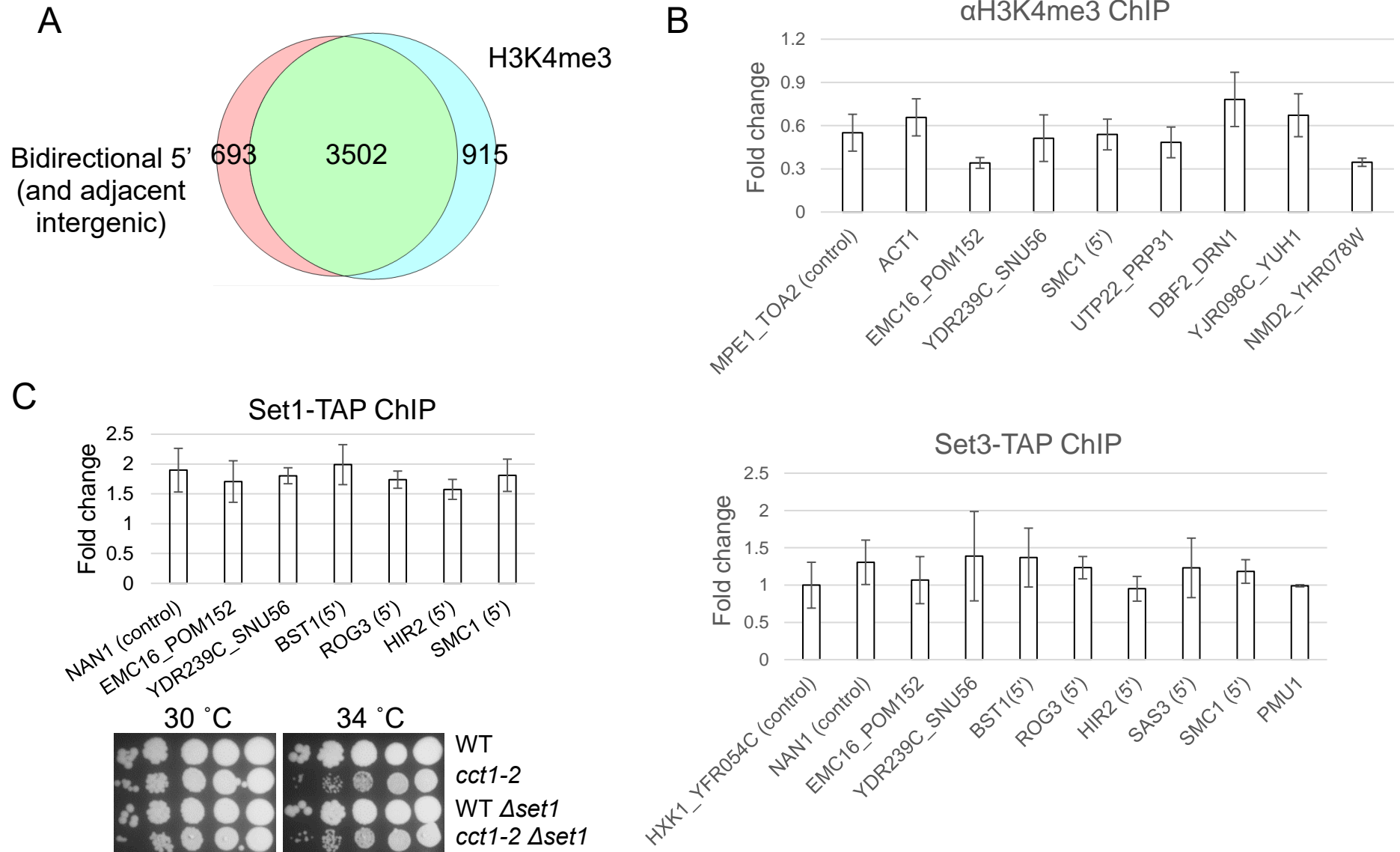
Figure 4.1.22. **Set1-Set3 pathway is not involved in cryptic transcription.**
A. Overlap between *cct1-2* locations affected by 5' bidirectional transcription and H3K4me3 (Bonnet 2014). B. ChIP in *cct1-2* grown at 37 ˚C using αH3K4me3 antibodies at the locations affected by 5' bidirectional transcription. C. DNA Occupancy of Set1-TAP and Set3-TAP in *cct1-2* grown at 37 ˚C at the affected locations, as well as spot test assay for WT *Δset1* and *cct1-2 Δset1* grown at control (30 ˚C) and lethal (34 ˚C) temperature.
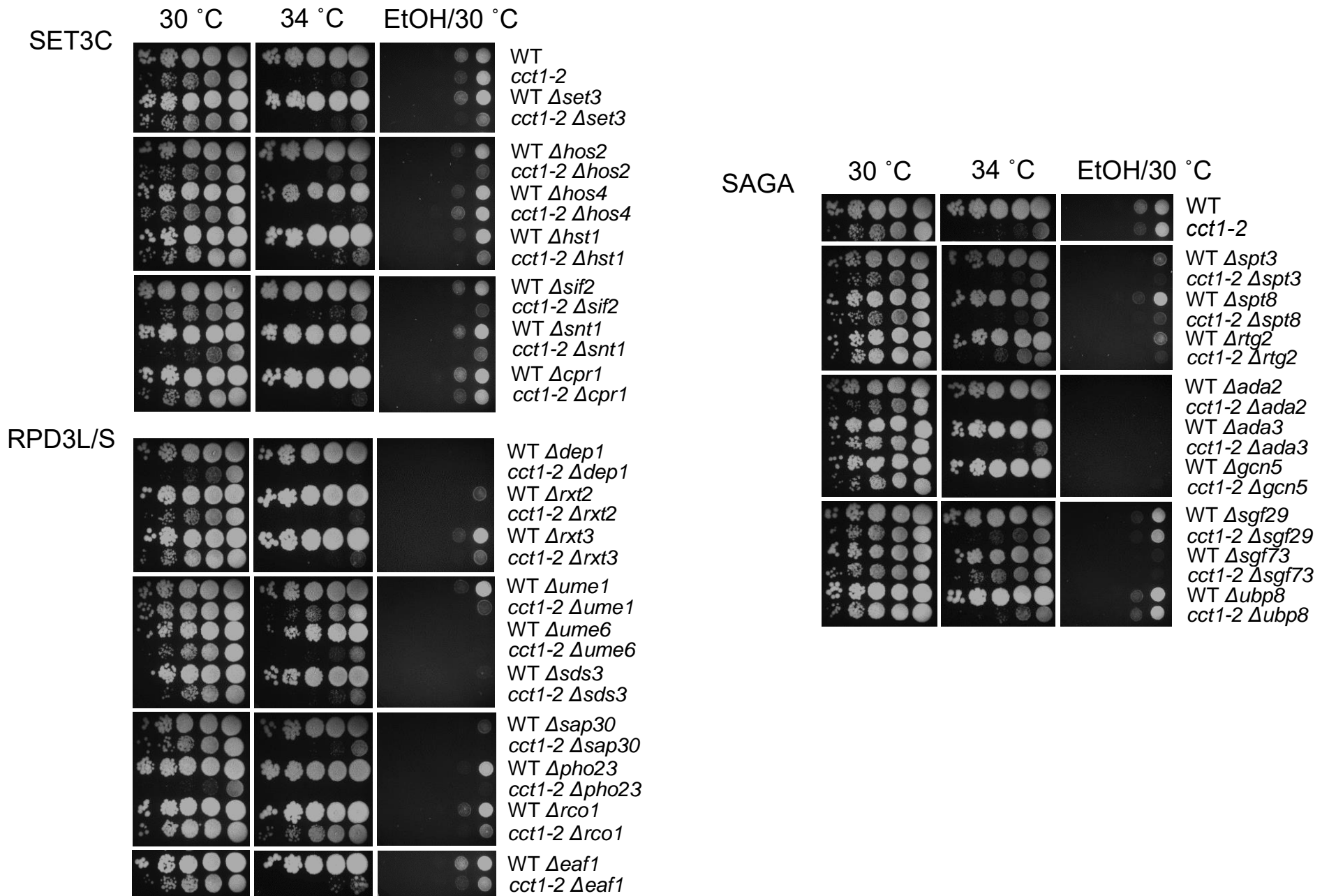
Figure 4.1.23. **CCT genetically connects to histone modifiers' subunits, especially to SAGA Gcn5-Ada module.**
Spot test assay for WT and *cct1-2* ts mutant knocked out for Set3, Rpd3L/S and SAGA complex subunits, grown at 30 ˚C and *cct1-2* lethal temperature 34 ˚C, on YPD and YPGE.

It was questioned whether the central histone acetyltransferases, SAGA and also NuA4, catalyzing H3 and H4 acetylation (Tse 1998, Roh 2004, Allard 1999), could be responsible for the phenotype, since CCT interacts with numerous subunits of these complexes. Given a strong genetic connection between CCT and catalytic Gcn5 module of SAGA histone acetyltransferase (Figure 4.1.23), and decline of H3 and H4 acetylation observed in the histone mass spectrometry (Figure 4.1.9A), it was examined whether CCT is able to modulate the enzymatic ability of SAGA or NuA4. Thereby, an *in vitro* acetylation assay with reconstituted nucleosomes as substrates and purified HATs, as well as purified recombinant CCT, was utilized. The nucleosome acetylation levels tracked via radiolabeled acetyl group show that acetylation was not dependent on CCT' presence (Figure 4.1.24A and 4.1.25A). As the modulation of catalytic traits was negative, the HAT complexes were inspected for the general subunit integrity, similarly as in the case of INO80/SWR-C. The results suggest that the complexes obtained from the wild type and the mutant appear identical (Figure 4.1.24B and 25B). Furthermore, DNA occupancy of the HATs did not change at the location affected by the 5' bidirectional transcription in *cct1-2* either (Figure 4.1.24C and 25C). It was therefore assumed that large HATs SAGA and NuA4 are not directly involved in the given phenotype. In addition, histone deacetylase HAT1, another CCT interactor and antagonist to HATs, was also shown to be negative for the differential binding at the affected locations in *cct1-2* (Figure 4.1.26).
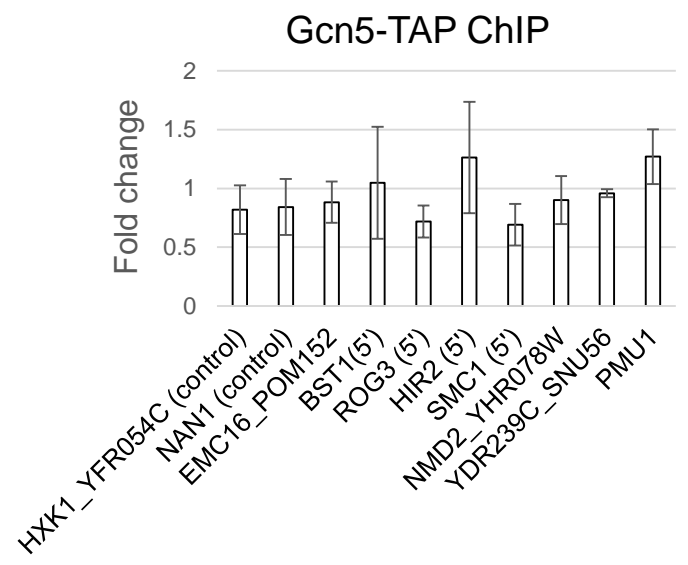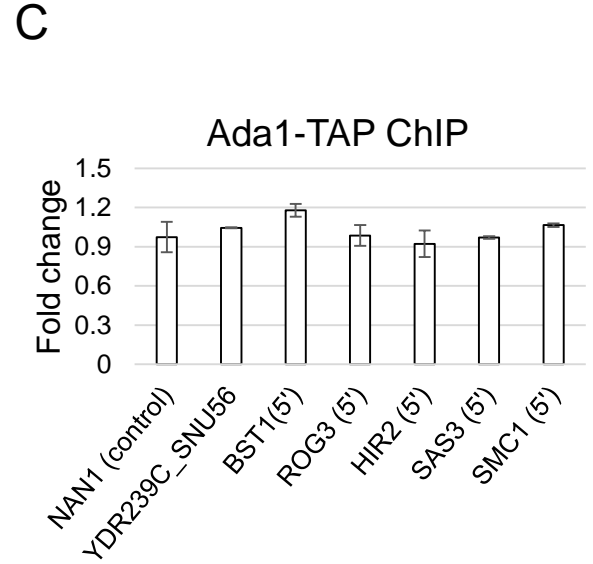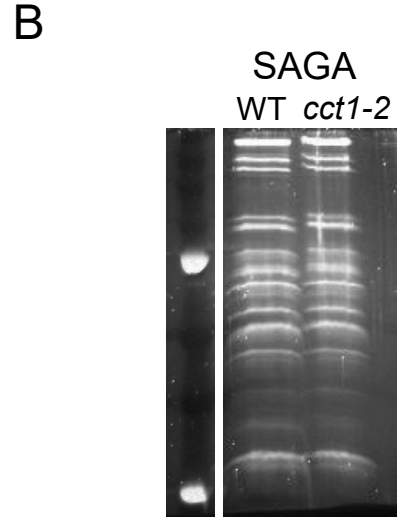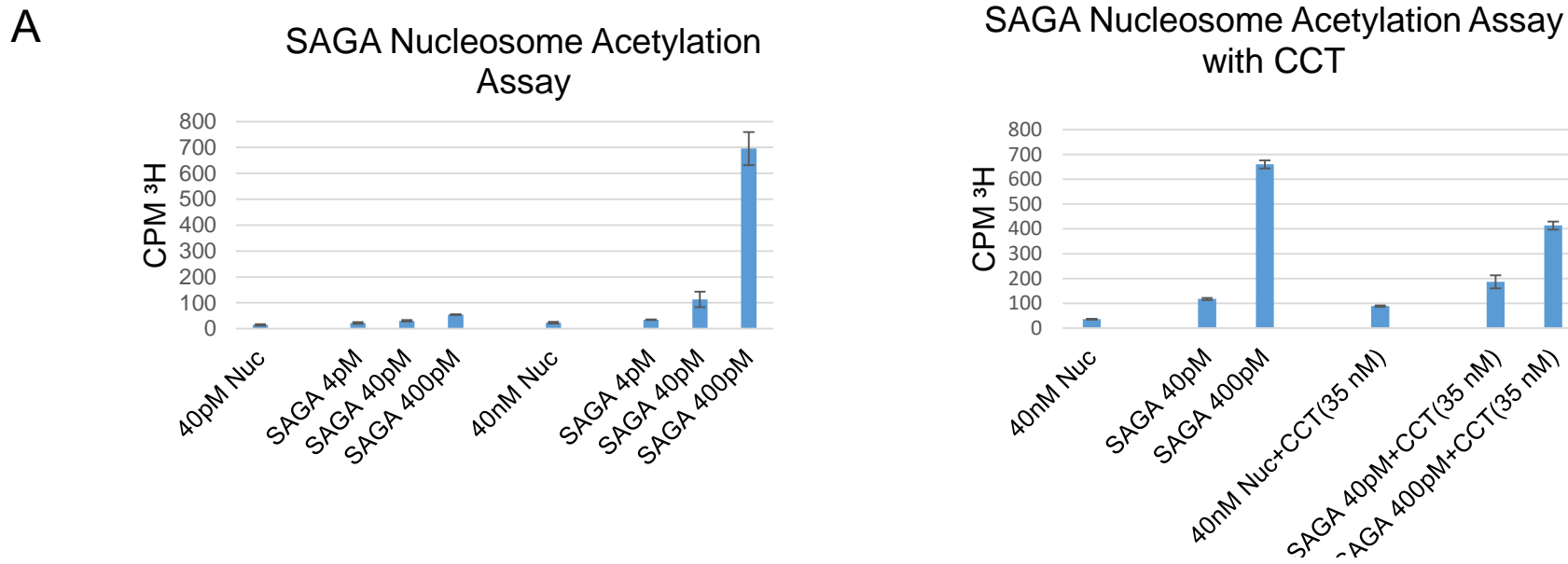
Figure 4.1.24. **CCT does not affect SAGA HAT abilities, nor the complex composition.**
A. *In vitro* SAGA nucleosome acetylation assay with purified CCT, nucleosome and SAGA. (left) Optimizing SAGA usage range. (right) Addition of CCT to the optimized conditions from the left. B. SAGA complex purified from WT and *cct1-2* strains grown at non-permissive temperature stained with Sypro Ruby. C. SAGA occupancy in *cct1-2* grown at 37 °C at the locations affected by 5' bidirectional transcription.
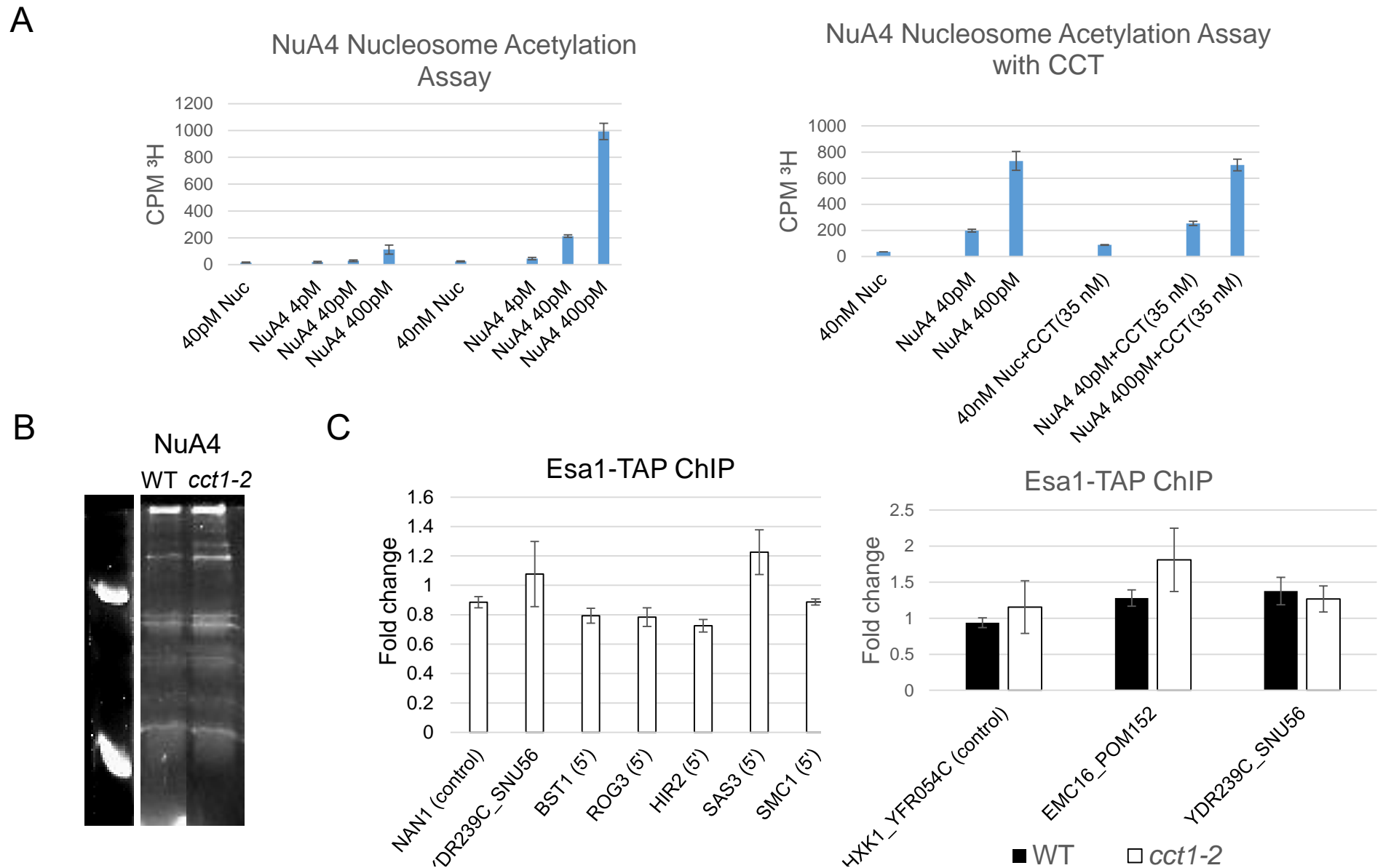
Figure 4.1.25. **CCT does not affect NuA4 HAT abilities, nor the complex composition.**
A. *In vitro* NuA4 nucleosome acetylation assay with purified CCT, nucleosome and NuA4 . (left) Optimizing NuA4 usage range. (right) Addition of CCT to the optimized conditions from the left. B. NuA4 complex purified from WT and *cct1-2* strains grown at non-permissive temperature stained with Sypro Ruby. C. NuA4 occupancy in *cct1-2* and WT grown at 37 ˚C at the locations affected by 5' bidirectional transcription.
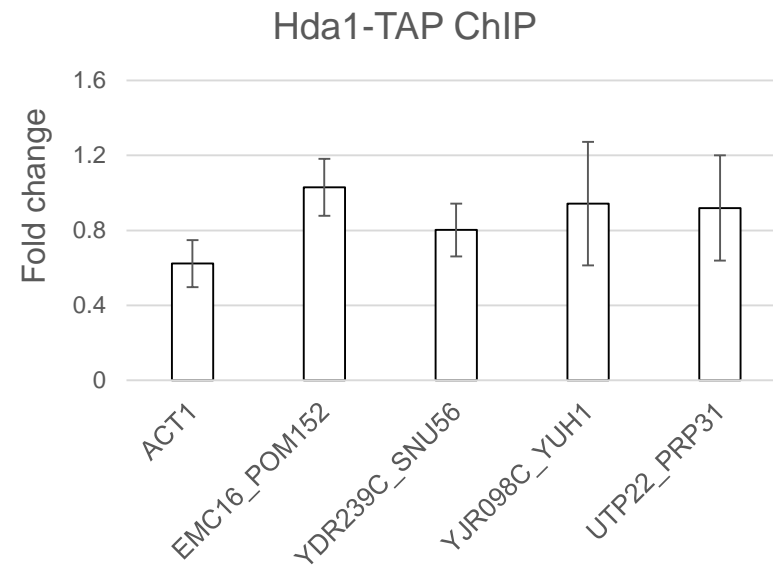
Figure 4.1.26. Hda1-TAP DNA occupancy in *cct1-2* grown at 37 ˚C at the locations with increased 5' bidirectional transcription.

It should be noted that implemented epitope-tagged versions of the subunits carry limitations due to the possibility of false negative results. Instead of the candidate approach, which entails testing vast number of potential effectors, it was further aimed to inspect global change of the DNA occupancy. Prospective alterations at the locations reported to be targeted by certain regulators, together with generalization of the altered pattern upon CCT inactivation, might allow for identification of the targets. To generate global DNA occupancy map, DNaseI Sequencing was utilized (Hesselberth 2009). Before and besides delineating DNA occupancy at target location, this high-throughput assay provides extensive report about open chromatin regions and it allows for the association of described transcriptional anomalies with CCT-dependent modulation of the chromatin landscape. Moreover, because we previously showed that molecular chaperones are able to modulate chromatin via chromatin regulators (Zelin 2012, Echtenkamp 2016), and given CCT's link to diverse chromatin regulators, we were interested whether CCT depletion will affect the chromatin status along the comparable lines.

Similarly to before, reported DNaseI hypersensitivity mapping was employed (Hesselberth 2009, Zelin 2012) on wild type and temperature sensitive strain grown under non-permissive temperature to firstly inspect for the global chromatin structural changes upon CCT depletion (Figure 4.1.27). The results indicate that CCT inactivation did not cause alterations in the total detected open chromatin locations as the number of DNaseI hypersensitive sites (DHSs) stayed approximately the same. There were 4520 DHSs computed for WT and 4492 for *cct1-2*, 80-86% of which are overlapping. However, the sites were lightly yet globally different in their openness, as reflected by differential hotspot z scores that define the extent of hypersensitivity (John 2011) (Figure 4.1.28A). Correspondingly, 38.4 % (1735) of the total overlapping wild type sites displayed 1.5 fold higher z score than mutant, and in *vice versa*, only 4.8% (217) of the mutant sites had higher z score than the wild type, with the total average z scores for CCT 19.5 and *cct1-2* 13.2 (Figure 4.1.28B, left). Moreover, CCT inactivation lead to a decline of the length of the DHSs as 39.3 % (1775) of the total WT DHSs were at least 50 bp longer than in *cct1-2*, whereas *cct1-2* rendered only 15.1 % (677) sites longer than the wild type (Figure 4.1.28B, right). In conclusion, cells devoid of CCT do not lose DHSs but they experience a mild global reduction of the existing open chromatin locations.

	HiSeq 2000	
	WT	*cct1-2*
Reads processed	26411901	23351757
Uniquely mapped reads number	11386429	7262096
Uniquely mapped reads %	43.11%	31.10%
number of reads mapped to too many loci	9195993	6878144
% of reads mapped to too many loci	34.82%	29.45%

Figure 4.1.27. **Quality of DNaseI-Seq reads.**
DNaseI-Seq reads, obtained via deep sequencing DNA derived from partially digested nuclei, aligned with bowtie (Langmead 2009). The nuclei stem from WT and *cct1-2* strains grown at 37 ˚C.
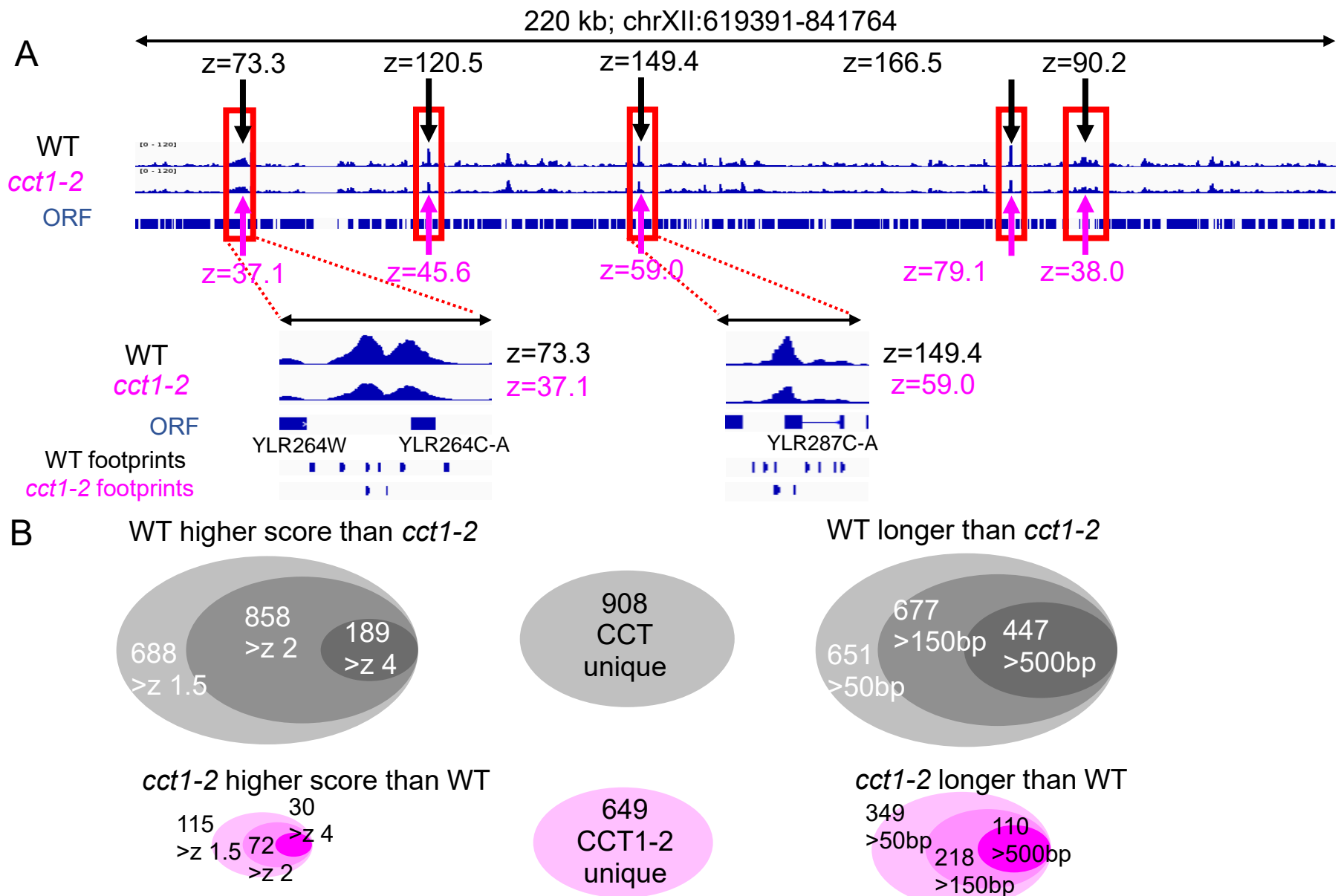
Figure 4.1.28. **CCT inactivation leads to reduction of the open chromatin in terms of hypersensitivity.**
A. Differentially computed DNaseI cleavage rate (fdr=0.01) (John 2011) for WT and *cct1-2* at indicated location reveals decrease in *cct1-2* hypersensitivity (red boxes) as substantiated by the z-score. For select enlarged locations, frequency of footprints detected using footprint finder (Hesselberth 2009) are displayed. B. The number of overlapping DHSs in WT and *cct1-2* with changed z-score or length, as well as non-overlapping DHSs (unique). The darker shades towards the right designate lower threshold in terms of the changed length or z-score.

Our DNaseI hypersensitivity data show that, although mild, there is mostly an increase of nucleosome occupancy in ts *cct1-2* compared to the wild type, however, detected only for 2379 (37%) intergenic locations. For the *vice versa* case, there is merely 1078 (16.9%) intergenic locations that display increased hypersensitivity in mutant with respect to the wild type. Given that 2072 (49%) of transcriptionally affected 5'/intergenic locations overlap with overall chromatin changes filtered according to the low threshold (at least 1.5 times changed z score and at least 50 bp difference in length) (Figure 4.1.29), our data suggest that detectable chromatin alterations are not idiosyncratic to all aberrant transcription. It should be noted here that for divergent intergenic locations, cryptic transcription phenotype from two 5' ORFs (hence one intergenic) was merged into one genomic location when counting the stochiometry of transcriptionally affected location to DHS changes. The 'shared' DHSs could not be assigned to either of the genes' 5' with certainty. This is to clarify that the number of 5' cryptic transcription sites containing changed DHSs might be different than represented depending whether a DHS correlated with only one or both of the two ORFs' transcription phenotypes.

For 1355 (32%) transcriptionally affected locations, increased nucleosomal density is correlated with increased 5' bidirectional transcription, unlike 546 (13%) that displayed decrease (Figure 4.1.29). The results on the whole are contradictory to the studies showing that transcriptionally active regulatory regions are deprived of nucleosomes (Lee 2004). However, global chromatin status of extragenic locations that are subject to pervasive 5' bidirectional transcription has not been studied before. Our data could suggest that, given their transcription, intergenic locations upstream from 5' region of ORFs, in certain instances, perhaps attained configuration of a genic region. It should be emphasizing, however, that chromatin status changes on the whole were not as impactful as the transcriptional changes.

In conjunction with changed chromatin and aberrant transcription, chromatin remodelers' involvement was not identified (Figure 4.1.30).
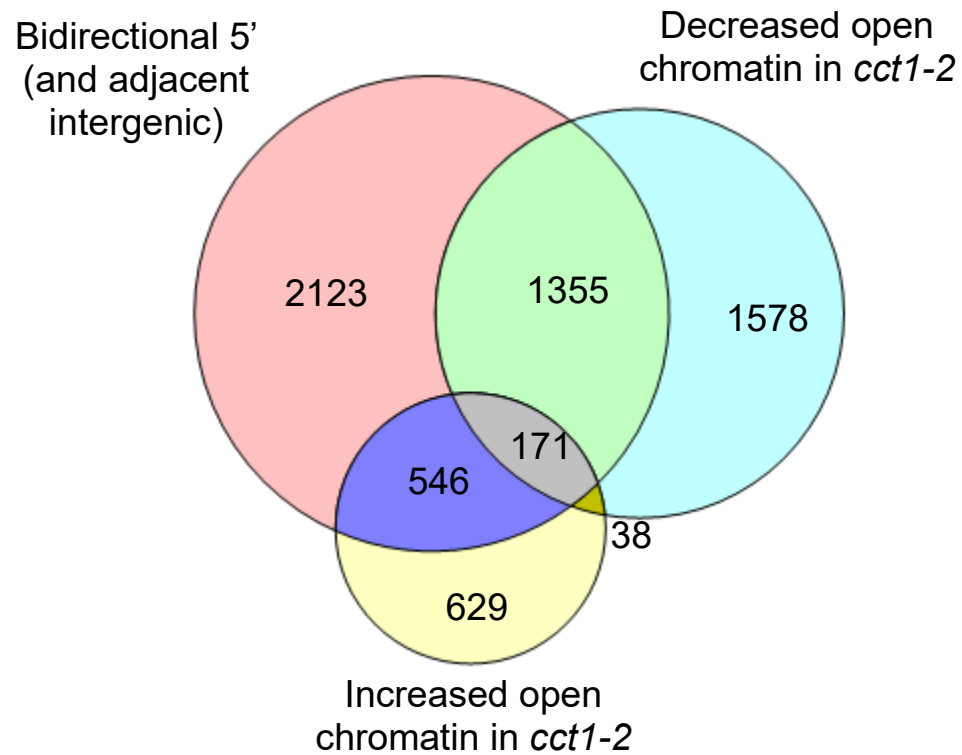
Figure 4.1.29. **More than half of the sites affected by aberrant transcription have no detectable chromatin changes.** Overlap between locations affected by 5' bidirectional transcription according to the RNA-Seq and changed DHSs sites according to the DNaseI-Seq in *cct1-2* with respect to WT (length changed for at least 50 bp and hypersensitivity at least 1.5 fold).
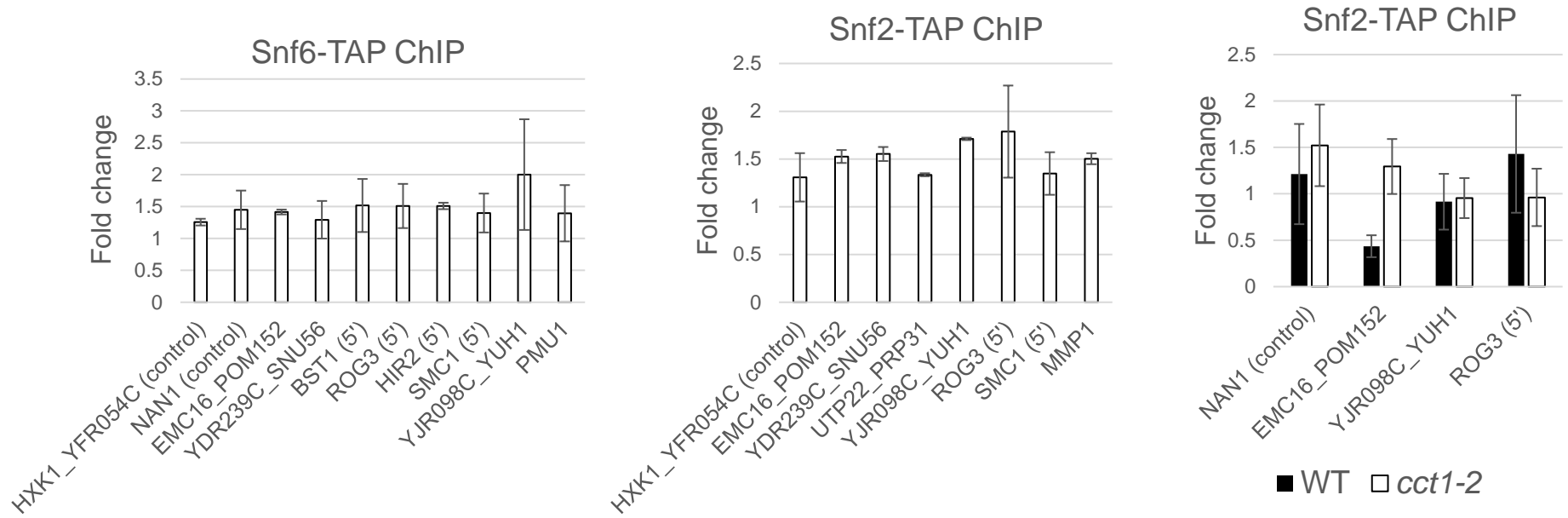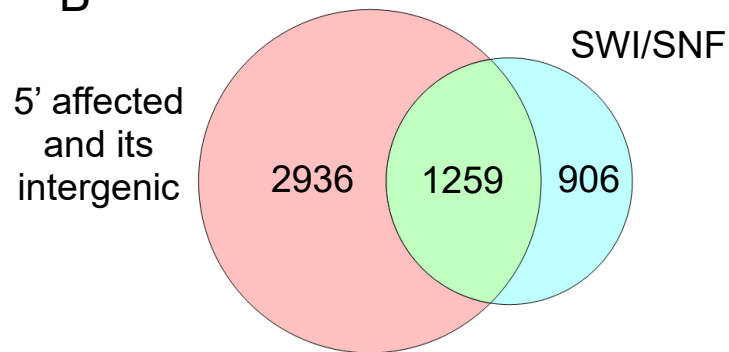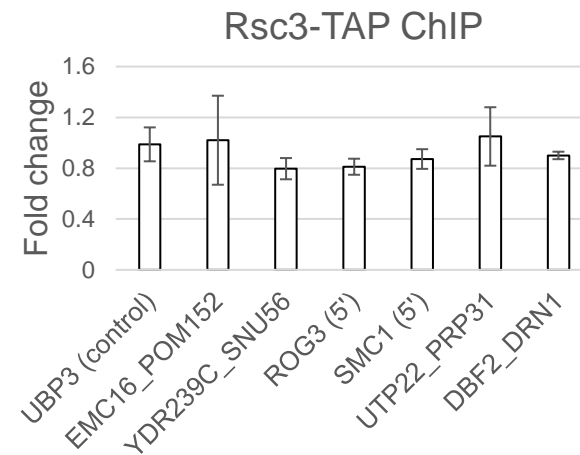
Figure 4.1.30. **Involvement of SWI/SNF and RSC chromatin remodelers at the 5' affected sites.**
A. SWI/SNF occupancy in *cct1-2* grown at 37 ˚C at the locations with increased 5' bidirectional transcription. B. The number of reported SWI/SNF-occupied sites (Dutta 2014) overlapping with *cct1-2* regions affected by 5' bidirectional transcription. C. RSC occupancy in *cct1-2* grown at 37 ˚C at the locations with increased 5' bidirectional transcription.

Next, DHS computation was used further to derive alterations in protein-DNA occupancy. By implementing digital genomic footprinting, it was observed that there was a global reduction of chromatin bound transcription factors (Figure 4.1.28A). Overall, there were 8587 footprints in wild type and 4009 footprints in *cct1-2* according to DNase2TF (fdr 0.001, Sung 2014). Narrowing down the footprints comparison for the sites affected by divergent transcription reveals on average and approximately 50% footprint decline in *cct1-2*, depending on the program (Figure 4.1.31). This corresponded to the general, global decline trend. It should be emphasized again that barely half of the cryptic transcription sites were supported with chromatin status information and the computation about the footprint decline stems only from the detectable subsets. For the footprints associated with 5' cryptic transcription and adjacent intergenic, 1597 and 811 consensus motifs for known transcription factors were identified in the wild type and mutant (DNase2TF, fdr 0.001, Sung 2014). Select computed footprints containing consensus motifs for transcription factors such as Rap1 and Reb1 that were lost in *cct1-2* at the sites affected by cryptic transcription were verified for differential recruitment by ChIP and no positive results were obtained (data not shown). It should be noted here that a single footprint contained several consensus motifs, which complicates the identification process.

Identified consensus motifs for detected footprints covered only ~ 26% of computed footprints, suggesting that 74% identified footprints do not have known protein-binding targets. Considering footprints proximity to the transcriptional regulatory elements (intergenic location plus 150 bp downstream), PIC would be the subsequent intuitive target. RNA polymerase II and basal transcription factors are known to cause conformational chromatin changes in the course of transition between active and inactive conformation (Hahn 2005), which might have contributed to the differential protein accessibility. However, binding of multi-subunit PIC complex within regulatory regions has not been defined in detail, partially due to its non-consensus DNA binding preferences (Afek 2013). Overall, the altered occupancy around TSS could be due to differentially engaged RNA polymerase complex. Detected footprints did not show correlation with reported TATA or TFIIB coordinates (Rhee 2012) (data not shown).

Footprints found within the sites affected by 5' bidirectional transcription and adjacent intergenic

		CCT	*cct1-2*
Hesselberth 2009		4817	3269
Piper 2013	default	3162	775
	dmfp	4891	1282
DNase2TF	0.001	3514	1689
	0.01	21828	11177

Figure 4.1.31. **Footprint changes within the sites affected by 5' bidirectional transcription.**
Footprint numbers detected within WT and *cct1-2* DHSs, computed with three different footprinting programs (Hesselberth 2009, Piper 2009 and Sung 2014) at different thresholds (fdr or p value, Piper 2003 was run under default parameters and also adjusted parameters dmfp where size of the footprints was adjusted to Hesselberth 2009 and merging of the footprints was excluded), that are found within the sites affected by 5' bidirectional transcription and adjacent intergenic according to the RNA-Seq. 5' bidirectional transcription sites were computed from RNA-Seq reads obtained via deep sequencing RNA isolated from WT and *cct1-2* strains grown at non-permissive temperature, by aligning the reads to the reference genome (UCSC, April 2011) with STAR (Dobin 2013), and by assessing gross read number and directionality.

It was interrogated whether changes within the basal transcription machinery upon CCT inactivation lead to the loss of RNA polymerase transcription directionality. Here, according to the H2A.Z anchor away (Figure 4.1.20), H2A.Z loss appeared to be a consequence of pervasive transcription. Pre-initiation complex was already described to evict H2A.Z in a transcription-coupled manner (Hardy 2009, Hardy 2010, Tramantano 2016). Moreover, because other chromatin regulator were negative for the given phenomenon, and a footprint change was detected for a subset of transcriptional regulatory regions, it was intuitive to test RNA polymerase complex itself. The DNA occupancies of various basal transcription machinery components, such as Dst1(TFIIS), Kin28(TFIIH), Sua7(TFIIB) and Taf1(TFIID), were assessed at the location affected by bidirectional transcription in *cct1-2*. The results show no involvement of changed DNA binding of these components (Figure 4.1.32). However, when the total levels of these factors were assessed in wild type and *cct1-2* grown at non-permissive temperature, loss of Taf1-TAP was detected (Figure 4.1.33). Taf1 is a component of an important basal transcription machinery complex TFIID that starts polymerase assembly and remains with polymerase through transcription (Zawel 1993). This result is the first hint that alteration of RNA polymerase holoenzyme complex, particularly TFIID, could contribute to the observed transcription phenotype in the absence of functional CCT.
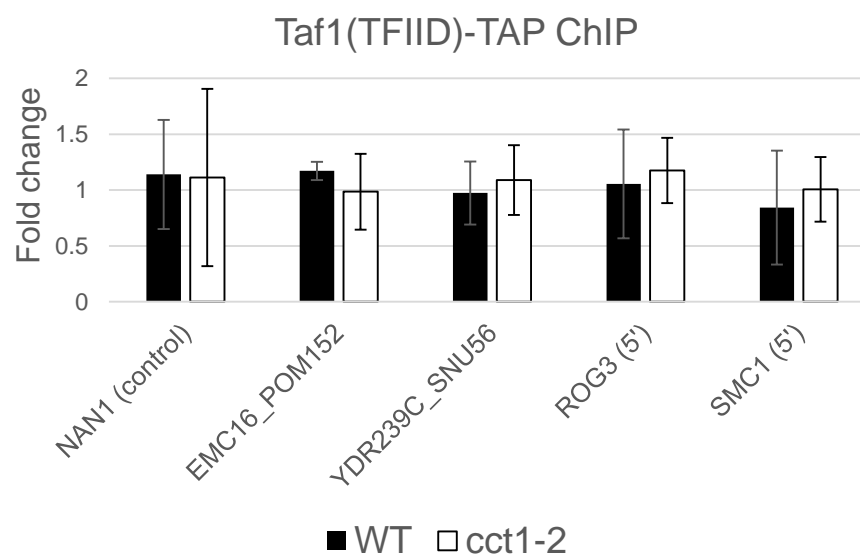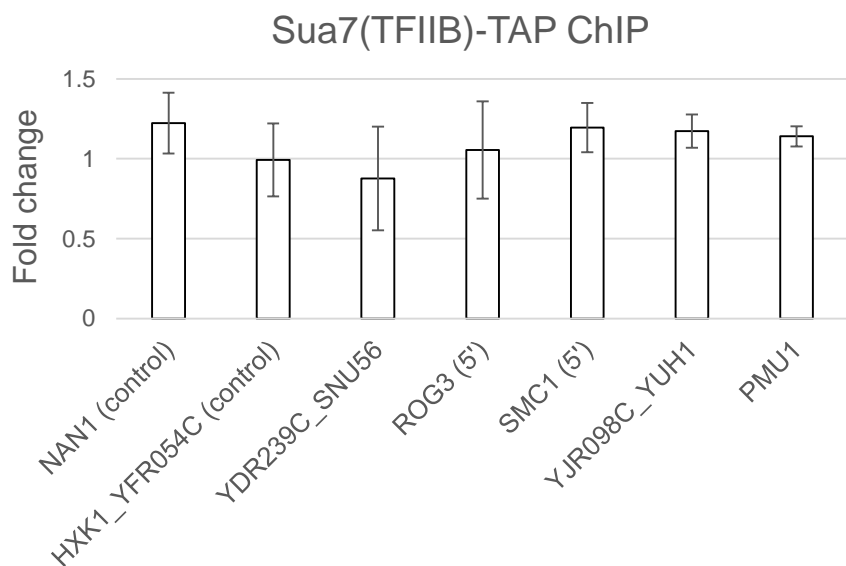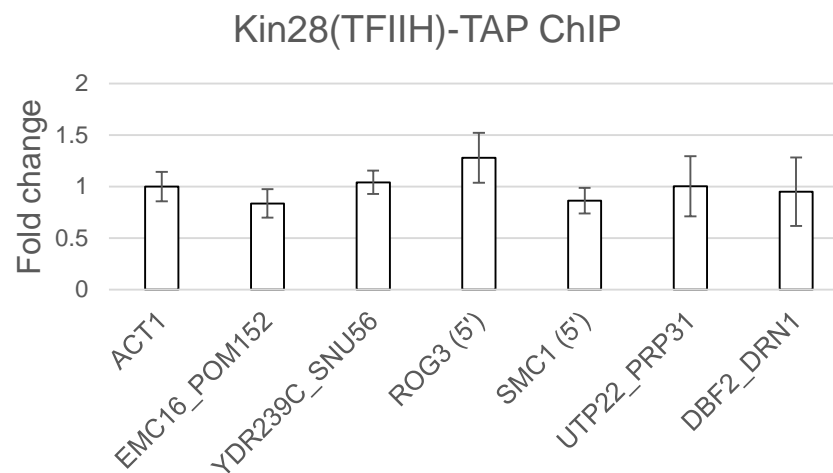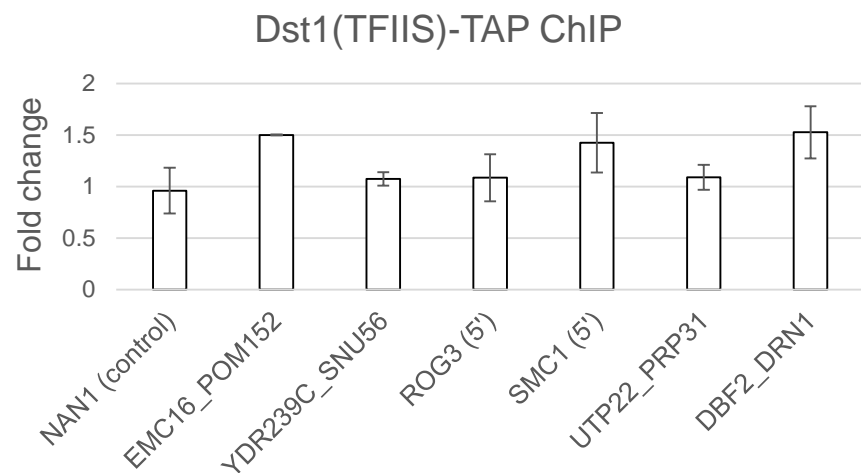
Figure 4.1.32. **Select components of the basal transcription machinery remain unaltered in the course of divergent transcription.**
Dst1(TFIIS)-TAP, Kin28(TFIIH)-TAP, Sua7(TFIIB)-TAP and Taf1(TFIID)-TAP were interrogated for the DNA binding in *cct1-2* grown under non-permissive temperature (37 ˚C) with respect to control (30 ˚C), for Taf1 also wild type control, by utilizing chromatin immunoprecipitation against epitope tagged subunits at the locations affected by bidirectional transcription.

157
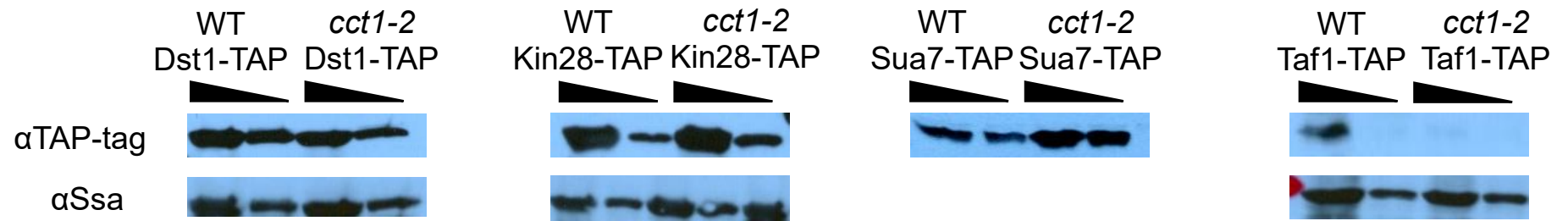
Figure 4.1.33. **Taf1(TFIID)-TAP total protein levels decline in *cct1-2*.**
Dst1(TFIIS)-TAP, Kin28(TFIIH)-TAP, Sua7(TFIIB)-TAP and Taf1(TFIID)-TAP total protein levels in WT and *cct1-2* strains grown at 37 ˚C were assessed by Western blot with αTAP-tag antibodies with respect to loading control with αSsa antibodies.

In the subsequent series of the experiments, the aim was to reconstitute *in vitro* transcription with nuclear extracts generated from the wild type and the ts mutant, in order to inspect for the actively generated divergent transcripts. Since RNA-Seq delivers the information about the steady state RNA levels, the RNA degradation dependencies are not excluded. In addition to eliminating this problem, *in vitro* transcription would allow for possibilities to check whether addition of detected declined components in *cct1-2*, such as TFIID, would reduce the cryptic transcript pools and thereby 'correct' the phenotype.

The *in vitro* transcription reaction with wild type and *cct1-2* nuclear extracts generated from the strains grown under non-permissive temperature, were performed using the amplified DNA templates from the locations shown to lead to 5 ' bidirectional transcription in *cct1-2* (Figure 4.1.6A). The templates were designed so that the sequence upstream from the TSS is shorter than the downstream sequence, which overall would enable tracking of the divergent, differently-sized transcripts. While omission of DNA in negative controls shows no productive transcription for the wild type and little background transcription for *cct1-2*, two radiolabeled transcripts were resolved for the samples in which template DNA was supplemented (red arrows, Figure 4.1.34A, left). The generated transcripts correspond to the longer (higher transcript, presumably downstream from the TSS) and shorter (lower transcript, presumably upstream from the TSS) DNA segments in size. For DRN1 5' DNA template, the intensity of the lower transcript, presumably antisense transcripts, is higher in *cct1-2* with respect to the wild type, whereas the intensity of the higher, presumably sense transcript in *cct1-2* is lower. This implicates propensity of *cct1-2* to produce different transcripts than the wild type. Addition of purified human recombinant CCT to the *in vitro* transcription reaction did not reduce the level of lower transcript in *cct1-2* (Figure 4.1.34A, right). Of note, because *cct1-2* nuclear extract preparations were enriched for DNA contamination, which were in the range of the constructed DRN1 5' DNA template i.e. generated transcript (Figure 4.1.34A), no firmer conclusion about divergent transcription could be drawn. The shorter DNA templates with the same principles as described above were designed, with the aim to generate RNA transcripts that migrate lower than the RNA generated from *cct1-2* nuclear extract's DNA traces. In corroboration, while control DNA, for which identical transcription was observed

according to RNA-Seq, showed no differences in terms of generated transcripts (green arrow for UBP3 control, Figure 4.1.34B), various location affected by bidirectional transcription produced different transcript pools when using wild type and mutant nuclear extracts (red arrows, Figure 4.1.34B). Hence, nuclear extracts obtained from the strains with inactivated CCT transcribe DNA *in vitro* differently than the extract derived from the wild type. This experiments, with further optimizations to remove genomic DNA contamination in *cct1-2* preparations, would be a base for further addition of target purified factors, such as Taf1 or TFIID modules, and examination of transcript pools differences with wild type and *cct1-2*.
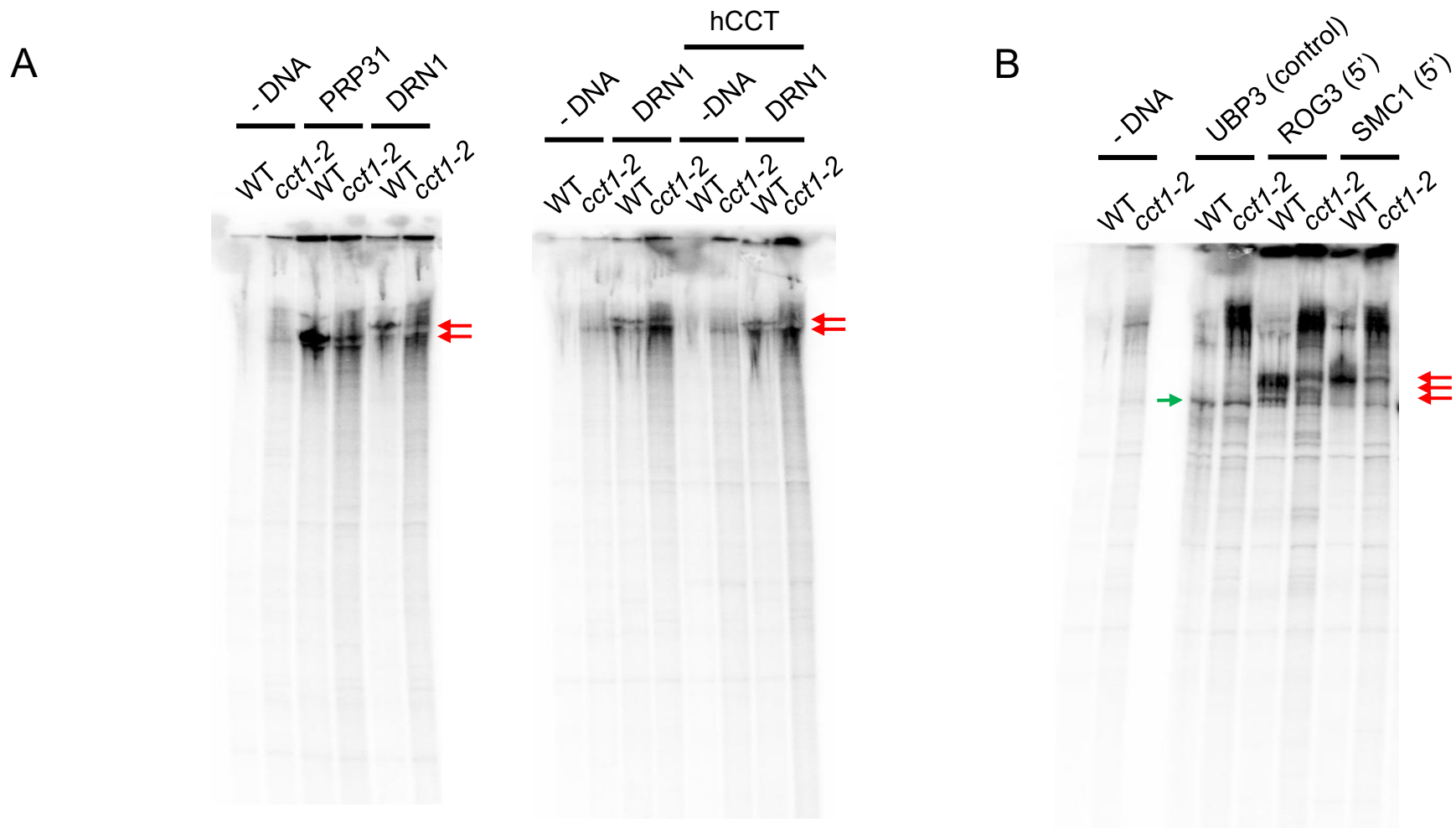
Figure 4.1.34. **WT and *cct1-2* nuclear extracts generate different sets of transcripts in *in vitro* transcription reaction.**
~30 µg/µl CCT and *cct1-2* yeast nuclear extracts, generated from the strains that were grown 4 h at 37 ˚C, were incubated with 30 ng amplified 5' bidirectional transcription site (or no DNA for control), nucleotide mix containing UTP[α-^{32}P] and resolved on 12% acrylamide denaturing urea gel. A. Amplified 5' bidirectional transcription sites for the genes PRP31 and DRN1 contained ~200 bp upstream and ~300 downstream from the TSS. Red arrows point out two different transcripts: higher ~ 300 bp (presumably sense) transcripts and lower (presumably ~200 bp antisense) transcript. (right) Human recombinant CCT was added for indicated reactions at 400 nM (about half of the estimated cellular concentration). B. Templates with total ~200 bp entailed locations affected by 5' bidirectional transcription. Green arrow points out unaltered transcripts WT and *cct1-2* extracts generate when using UBP3 control genic location as a template. Red arrow point out divergent transcripts generated when using ROG3 and SMC1 locations that display 5' bidirectional transcription *in vivo*.

Cryptic transcription phenotype in *cct1-2* could be the consequences of improper cellular proteostasis. Perhaps proteotoxic stress due to malfunctional CCT promoted protein aggregation, which deprived chromatin regulators and affected chromatin equilibrium. One of the severe proteostatic disorders that can be linked to CCT functions, and also implicated in transcriptional dysregulations, is neurodegenerative disease Huntington (Kim 2014, Glajch 2015). While the underlying mechanisms of Huntington pathogenesis are not known, Huntington disease is acknowledged to be caused by the mutations in the gene huntingtin that produces expanded, aggregation-prone stretches of polyglutamine residues (Vonsattel 1998, Arrasate 2012). CCT was identified to suppress polyglutamine aggregation (Nollen 2004). In conjunction with Hsp70, CCT was shown to interfere with polyglutamine fibril formation by promoting assembly of non-toxic oligomers (Behrends 2006, Kitamura 2006). Furthermore, CCT was proposed to sequester short Huntington sequence elements that reinforce nucleation of aggregation, rather than physically blocking polyglutamine repeats (Tam 2009). Huntington, on the other hand, interacts with numerous transcriptional regulators, and one of the speculations is that it leads to nuclear dysregulations through sequestering important chromatin components (Li 2004, Glajch 2015). Huntington was, hence, an interesting model to inspect for transcription targets in relation to proteotoxic stress.

Here, it was tested whether the increase of proteotoxic stress through induced protein aggregation would affect H2A.Z levels, whose loss is viewed as a hallmark of divergent transcription. To test this, aggregation prone Huntington-GFP fusion protein (with 104 polyglutamine repeat) was expressed in the wild type strains and H2A.Z levels were inspected. The results show that expression of Huntington protein led to the loss of H2A.Z at the sites affected by 5' bidirectional transcription (Figure 4.1.35A). Furthermore, the event correlated with the formation of cellular aggregates (Figure 4.1.35B). This potentially suggests that cellular aggregates possibly affecting chromatin regulators in the absence of functional CCT might be the reason for the pervasive transcription. Besides Huntington, both Rnq1 prion and von Hippel-Lindau (VHL) tumor suppression expression led to the H2A.Z decline in the wild type strain (Figure 4.1.36), inferring that the proteotoxic stress is not limited to Huntington.
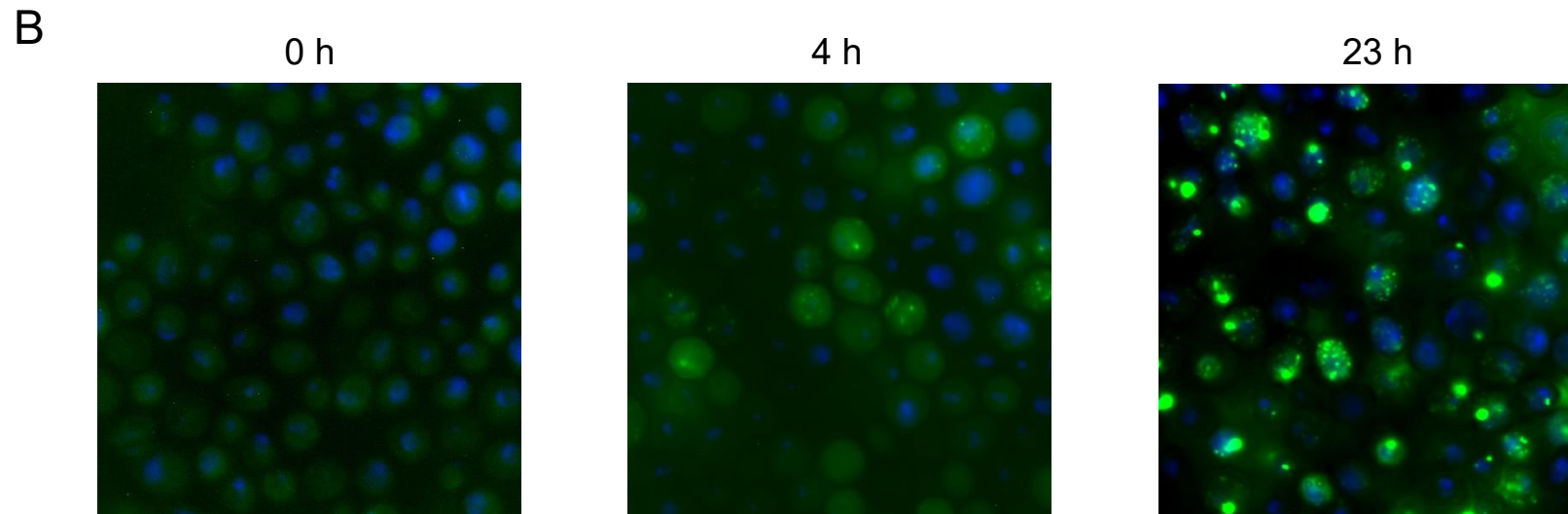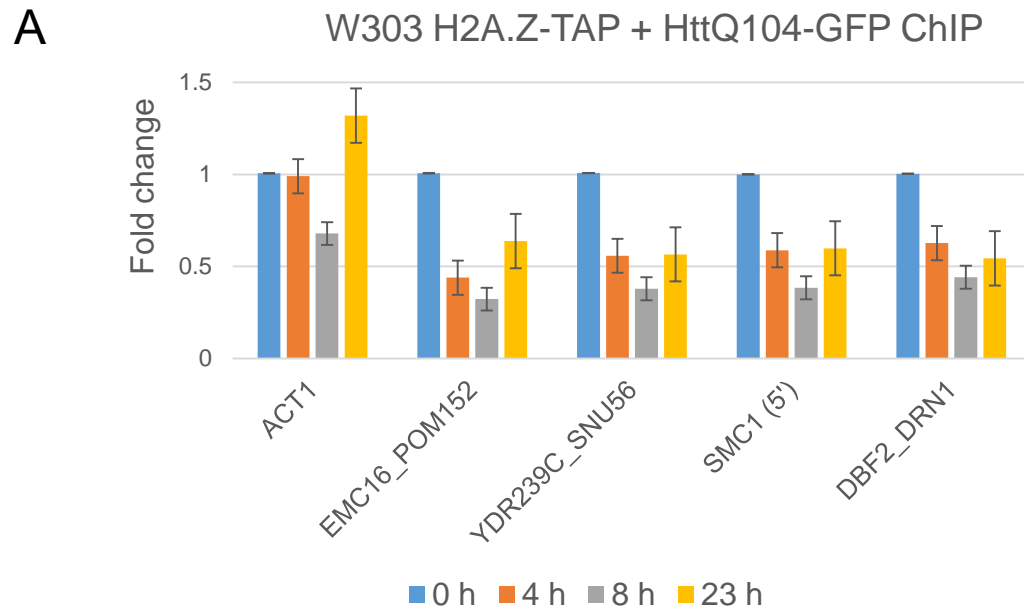
Figure 4.1.35. **Expression of Huntington leads to the loss of H2A.Z at the sites affected by 5' bidirectional transcription.**
A. H2A.Z-TAP DNA occupancy was assessed in W303 *H2A.Z-TAP::His6MX6* strains transformed with vector pESC-URA3 HttQ104-GFP at indicated time points after galactose induction. B. Fluorescence microcopy images depicting increase of cytosolic HttQ104-GFP under the conditions as in A.
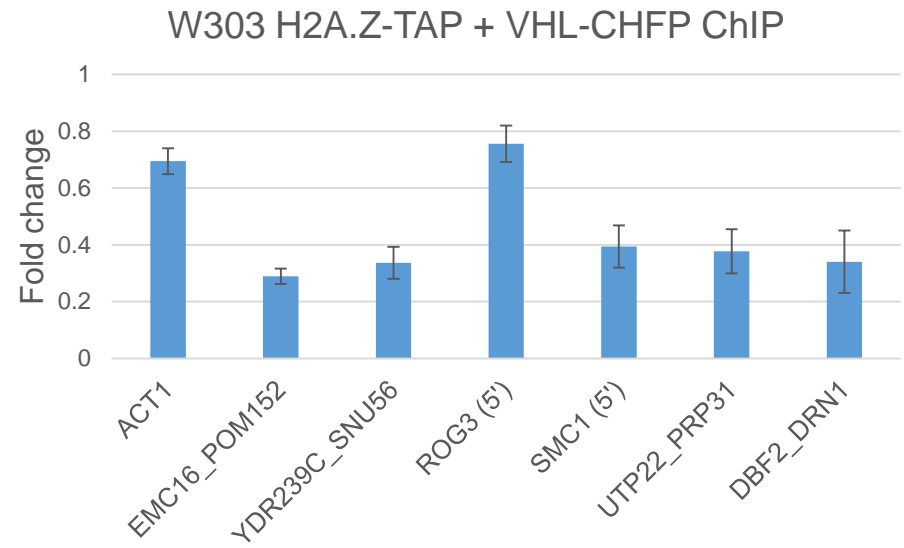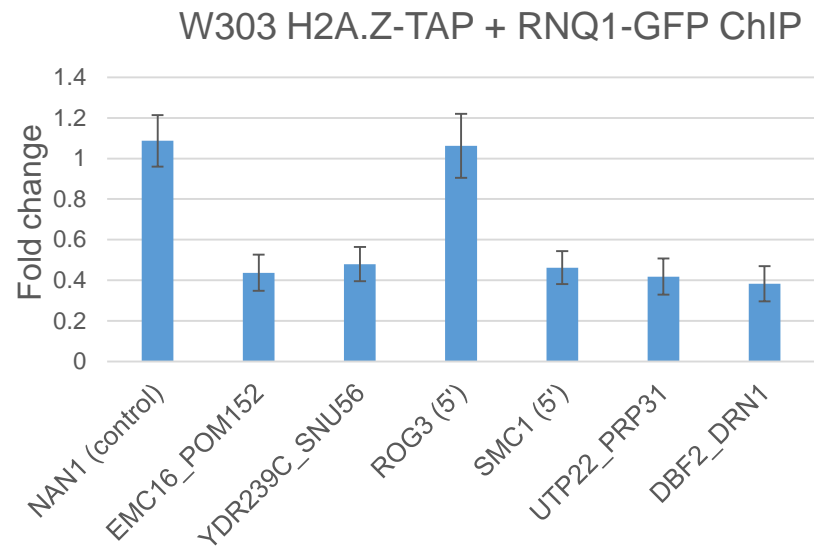
Figure 4.1.36. **Expression of RNQ1 or VHL causes H2A.Z loss at the sites affected by 5' bidirectional transcription.**
H2A.Z-TAP DNA occupancy was assessed in W303 *H2A.Z-TAP::His6MX6* strains transformed with vector pESC-URA3 RNQ1-GFP or pESC-URA3 VHL-CHFP, 8 h after galactose induction.

Not all promoters in *Saccharomyces cerevisiae* contain H2A.Z histone variant – an example are divergent histone promoters that regulate expression of canonical histone gene pairs (Figure 4.1.37A and B). From all four promoters, only HHT2_HHF2 intergenic region displayed notably increased transcription in *cct1-2* (Figure 4.1.37B). The histone gene expression was not affected (GFold values >-1.5 and <1.5). Since reported histone gene regulators were observed to be CCT interactors (Figure 4.1.2), it was appealing to test whether the absence of CCT would affect them. Thereby, the histone promoters were screened for the targets by utilizing epitope tagged *cct1-2* candidate approach in conjunction with ChIP.

A. H2A.Z-TAP ChIP
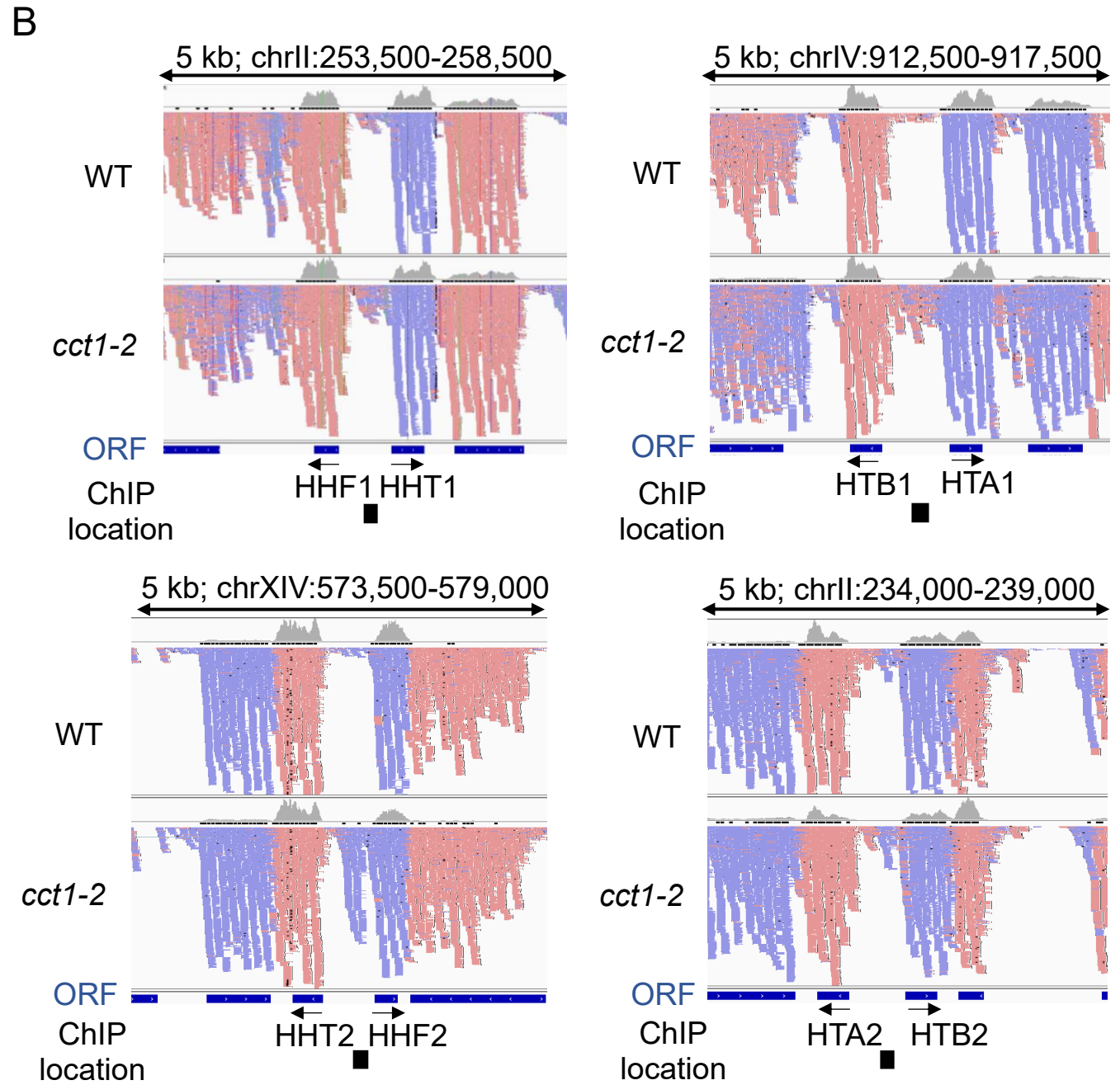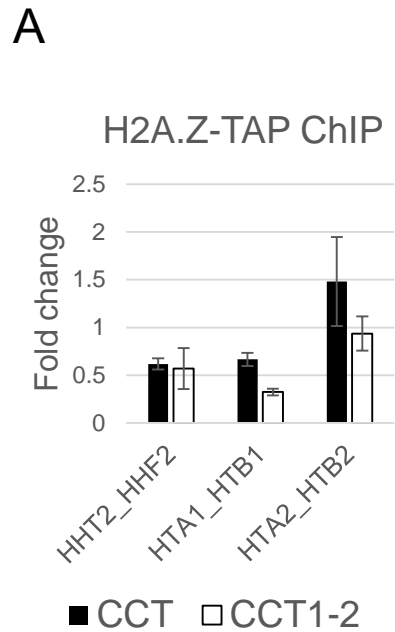
Figure 4.1.37. **CCT affects cryptic transcription at one histone promoter.**
A. H2A.Z occupancy at divergent histone promoters in WT and *cct1-2*. B. Aligned RNA-Seq reads for WT and *cct1-2* at all four divergent histone promoters. Black box represents chipped location.

It was identified that CCT inactivation affected histone promoter-specific regulators – there was an increase of Spt10 HAT and transcriptional activator at all four divergent histone promoters and decline of related Spt21 at three histone promoters with the exception of HTA2_HTB2 (Figure 4.1.38A). Spt10 and Spt21 were shown to be necessary for the histone gene regulation (Dollard 1994, Hess 2004, Eriksson 2005), although Spt21 was more implicated in cell-cycle regulated histone expression (Spellman 1998, Kurat 2014). In particular, Spt10-dependent acetylation of H3K56 at the histone promoters engaged SWI/SNF chromatin remodeler for transcriptional activation (Xu 2005). Because CCT was observed to alters Spt10 binding (Figure 4.1.38A), it was tested whether CCT modulates described pathway. In contrast to increased DNA occupancy of Spt10 in *cct1-2*, a decline of H3K56 acetylation was observed (Figure 4.1.38B), and this was not due to differential recruitment of HDACs Hst3/4 and Hda1 HATs, nor SWI/SNF (Figure 4.1.39A and B). Spt21 on the other hand does not have HAT activities itself but co-purifies Gcn5 (Kurat 2014), yet Gcn5 was not affected at divergent histone promoters either (Figure 4.1.39B). The roles of altered regulators' recruitment at the histone gene promoters in the context of lacking functional CCT, as well as changed H3K56 acetylation status and cryptic transcription of only one out of four histone promoter locations, remain questionable. CCT notably affected some parts of the pathways, yet the outcomes were not as expected, and inquisition of further mechanistic is needed. Nuclear extracts from WT and *cct1-2* displayed completely different band patterns on EMSA with histone promoter probes (Figure 4.1.40A), conforming differential regulator's recruitment. One of newly detected decreased binders in the screens was TFIIB (Sua7-Tap, Figure 4.1.40B). For comparison, changes in TFIID (Taf1-TAP) were not detected within these sites (4.1.40C). Because a basal transcription factor was altered, it is again inferred that CCT affects RNA polymerase complex.
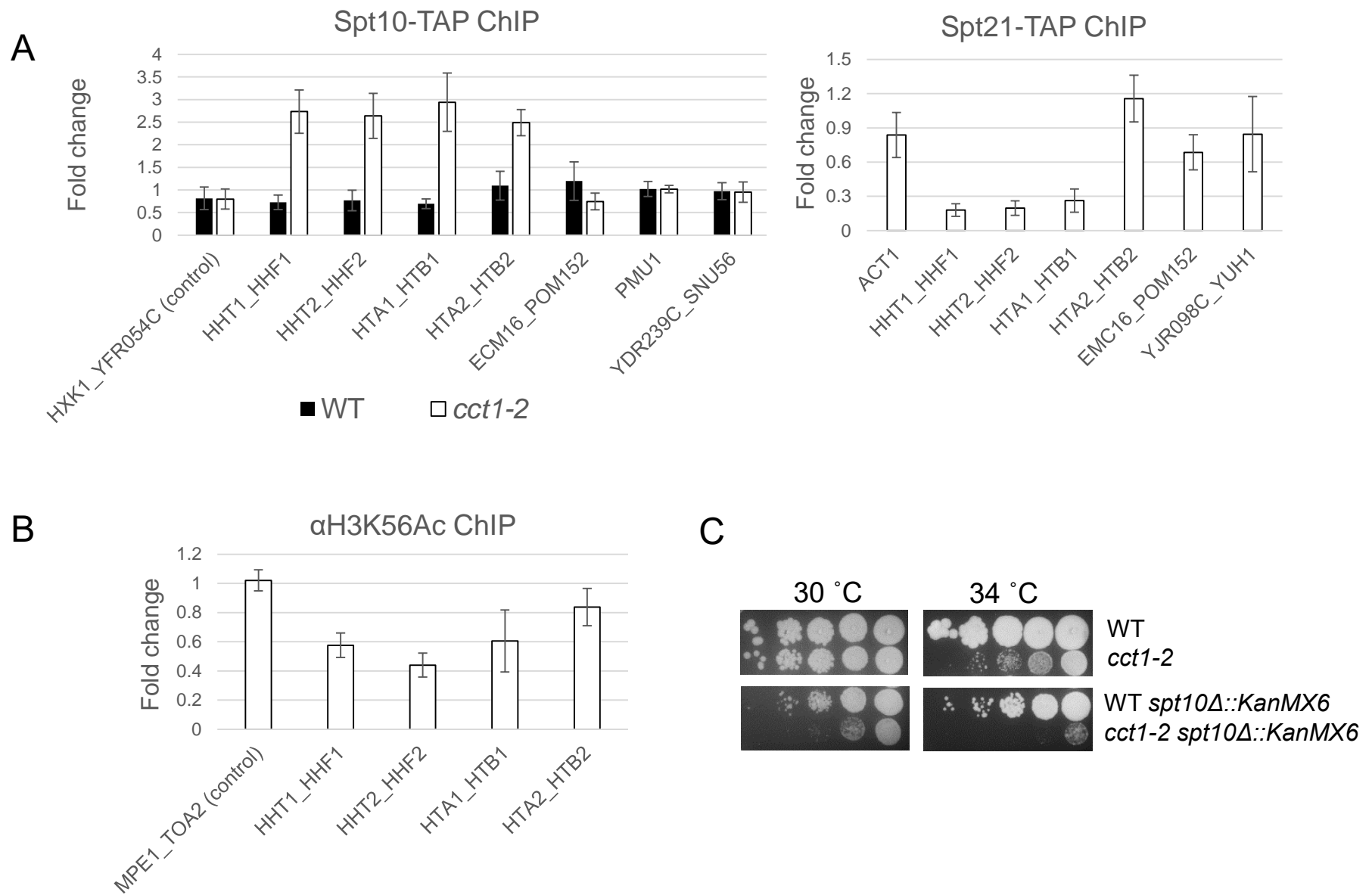
Figure 4.1.38. **Both Spt10 and Spt21 display differential binding at histone promoters in *cct1-2*.**
A. Spt10-TAP DNA occupancy in WT and *cct1-2*, as well as Spt21-TAP DNA occupancy in *cct1-2* at the divergent histone promoters.
B. ChIP in *cct1-2* using αH3K56Ac antibodies at the divergent histone promoters. C. Spot test assay for WT *Δspt10* and *cct1-2 Δspt10* grown at control (30 ˚C) and lethal (34 ˚C) temperature.

168
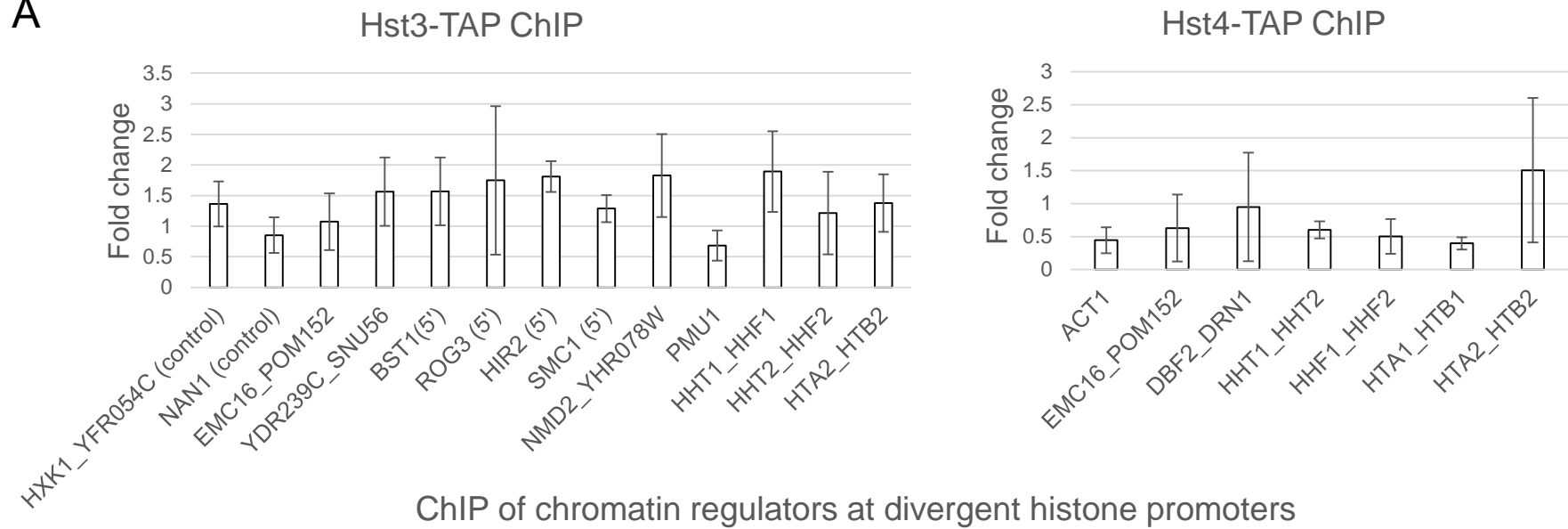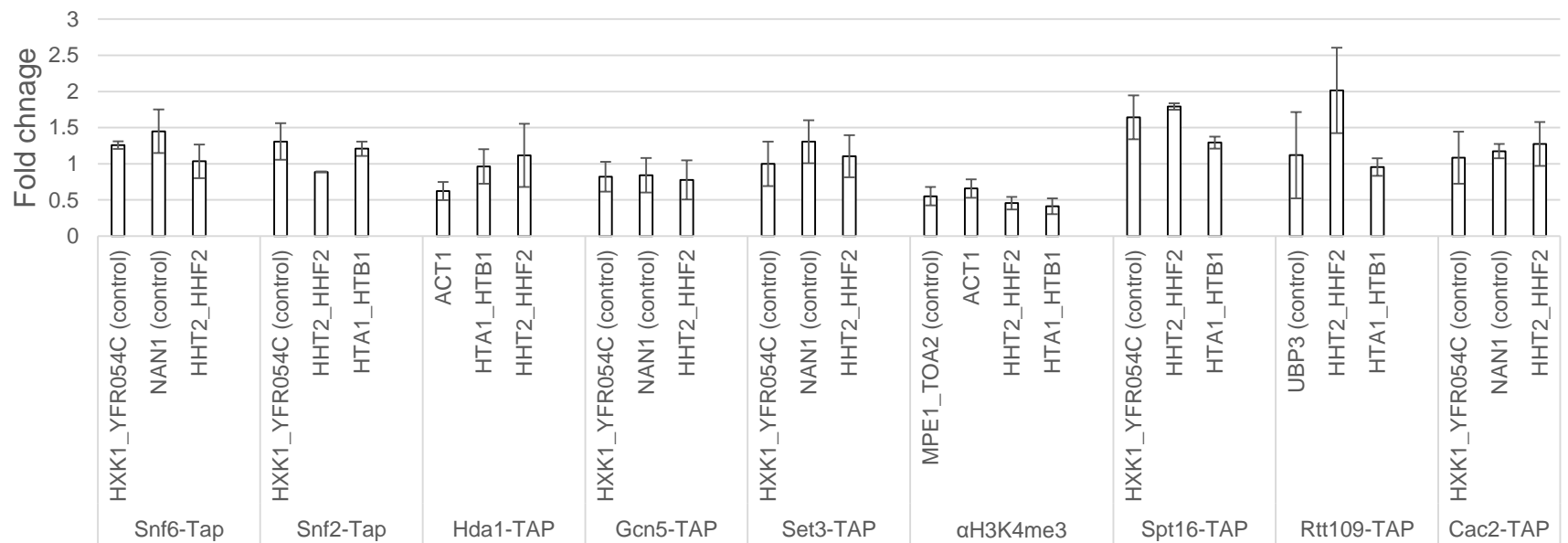
Figure 4.1.39. **Previously implicated chromatin regulators at histone promoters are not affected in in *cct1-2*.**
A. Hst3-TAP and Hst4-TAP DNA occupancy in *cct1-2* at the divergent histone promoters, and as a control other locations affected by 5' bidirectional transcription. B. ChIP of the *cct1-2* TAP-tagged strains at the divergent histone promoters, as well as H2K4me3 methylation mark.

169
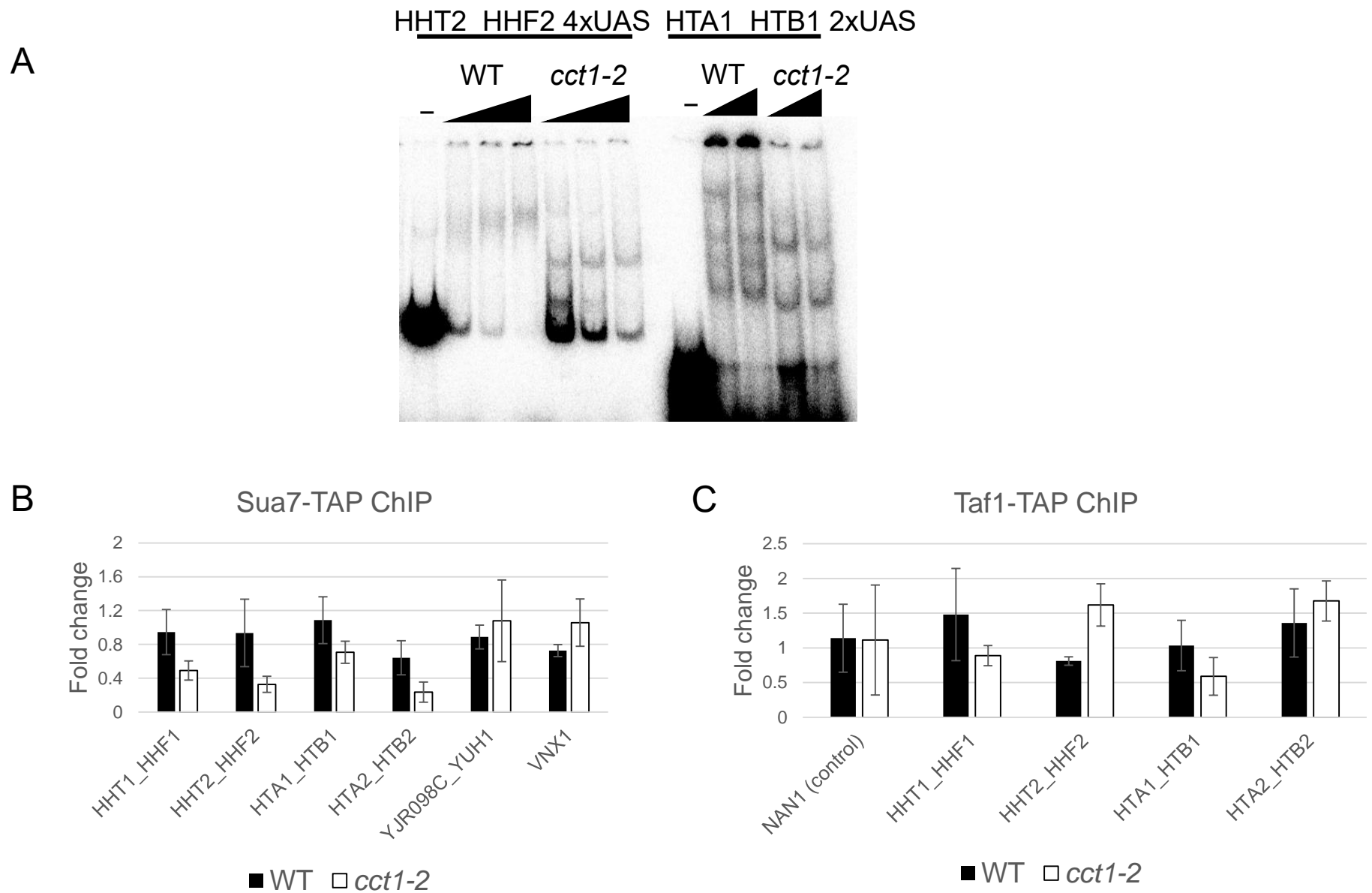
Figure 4.1.40. **Novel targets at histone promoters in *cct1-2*.**
A. EMSA with WT and *cct1-2* nuclear extracts, obtained from the cells grown at non-permissive temperature, probed to radiolabeled histone promoters. B. Sua7-TAP DNA occupancy in WT and *cct1-2* grown at 37 ˚C at the divergent histone promoters. C. Taf1-TAP DNA occupancy in WT and *cct1-2* at the divergent histone promoters.

CCT inactivation, besides globally affecting H2A.Z promoters to cause bidirectional transcription, and local promoters by causing differential regulator enrichment, also led to termination failures of selective genes. CCT depletion caused termination defects at snoRNA genes, as reflected by the increase of transcripts in the intergenic locations past the 3' region of the ORFs (Figure 4.1.41A). Nrd1 termination complex, was reported to be responsible for proper maturation of snoRNA, as well as release of RNAPII (Steinmetz 2001). It was thereby tested whether Nrd1 is affected upon CCT inactivation. The results show that increased termination defects correlated with impaired Nrd1 recruitment in *cct1-2* (Figure 4.1.41B). This was not due to decline of total Nrd1 cellular levels (Figure 4.1.42A). Unlike the genes *snR13* and *snR5*, where failed termination leads to cryptic transcription of the after 3' intergenic region, *snR42* defective readthrough leads to the antisense transcription of the convergent upstream gene. At *snR42*, however, Nrd1 could not be detected (Figure 4.1.41B), likely because different antisense transcription mechanism are involved.

As CCT involvement in Nrd1-metidated termination pathway at snoRNAs was positive, the details of the mechanism were explored further. Kin28, yeast TFIIH, phosphorylates serine 5 on the CTD of RNA polymerase II largest subunit (Rodriguez 2000). Ess1, Ser-Pro isomerase that isomerizes preferentially phosphorylated serine 5 from RNA polymerase II CTD (Gemmill 2005), and modulates transcription (Wilcox 2004, Wu 2000, Wu 2003, Krishnamurthy 2009), was shown to be necessary for the effective termination of snoRNA genes through Nrd1 pathway (Singh 2009). Given that CCT physically interacts with both CTD-Ser5 kinase Kin28 and Ess1, it was examined whether CCT modulates snoRNA termination via these players. The results showed that, whereas Kin28 (TFIIH) total cellular levels were unaltered (Figure 4.1.33), its recruitment at snoRNA terminator declined (Figure 4.1.42B). The fact that Kin28 total cellular levels were unaltered and only recruitment at snoRNA was affected would be in agreement with TFIIH affecting only local instances, such as snoRNAs, and not being global target factor at all the 5' locations subjected to pervasive bidirectional transcription. On the other hand, total cellular levels of Ess1 Ser5-Pro isomerase were unaltered and the protein displayed no differential recruitment at snoRNA terminators (Figure 4.1.42A and B). It should be

noted that Ess1-TAP implemented in ChIP studies before displayed only a mild occupancy change (Singh 2009) and the results here would perhaps need further verifications. On the whole, the termination failure at snoRNA occurs due to CCT-dependent Nrd1 response, with underlying downregulation of kinase TFIIH.

In addition, it is speculate that CCT inactivation also leads to splicing anomalies due to the surged antisense intron transcription compared to the wild type (Figure 4.1.43). Splicing incongruities could be fortuitous effect following 5' bidirectional transcription, because the affected introns were close to these 5' locations.
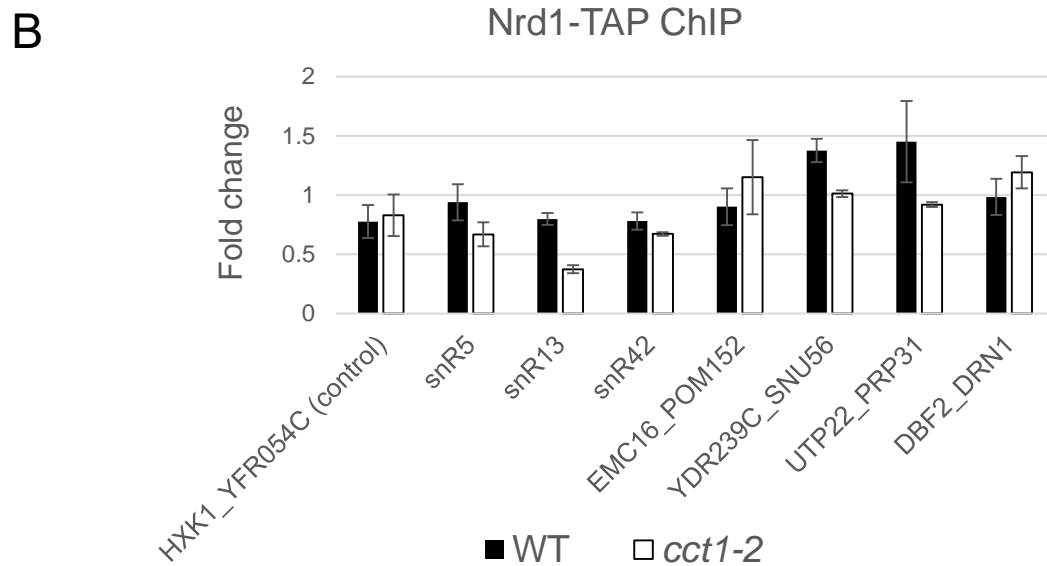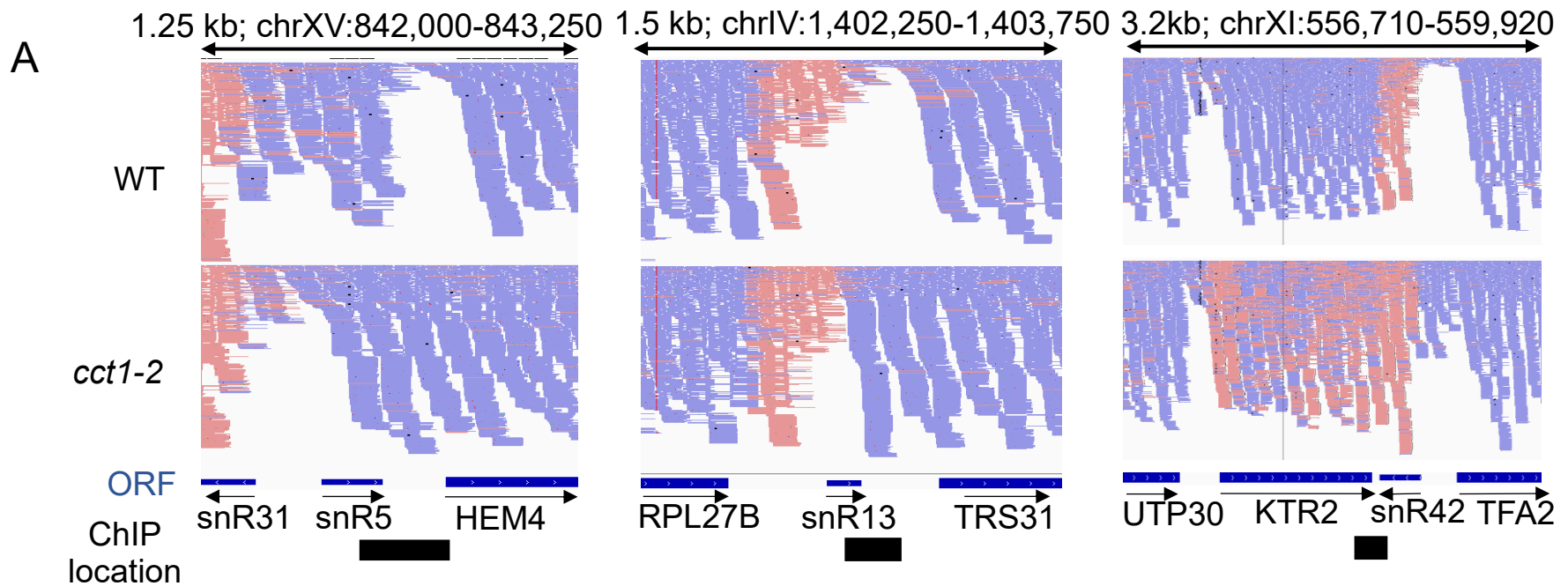
Figure 4.1.41. **CCT affects termination at snoRNA genes via Nrd1.**
A. RNA-Seq reads, derived from WT and *cct1-2* grown at 37 ˚C, representing increase of reads in *cct1-2* at snoRNA genes past the 3' termination point at indicated locations. B. Nrd1-TAP DNA occupancy at snoRNA terminators in WT and *cct1-2*.

173
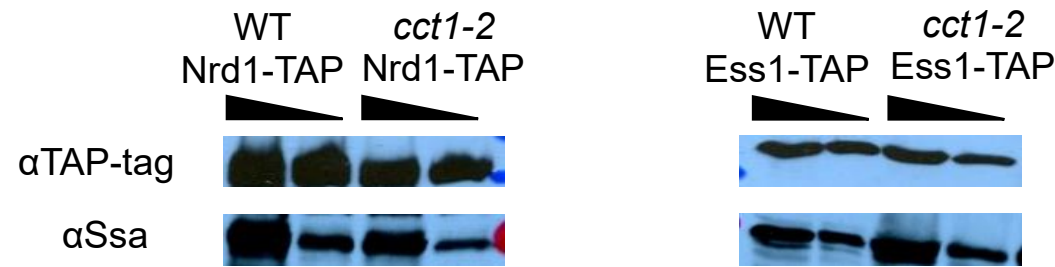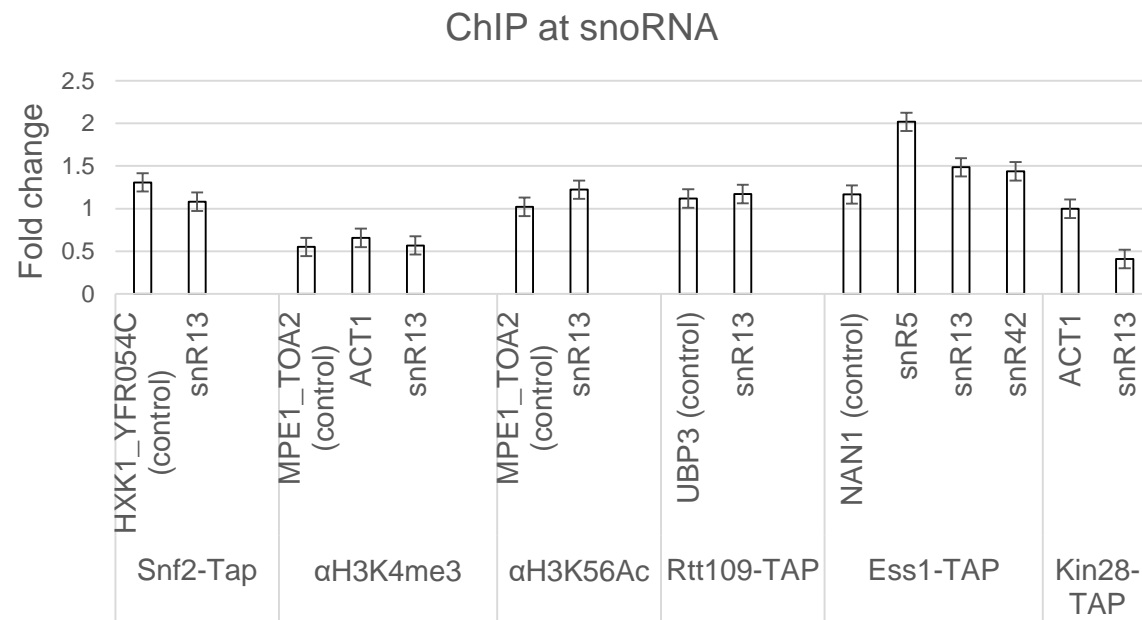
Figure 4.1.42. **Testing array of chromatin regulators at snoRNA in *cct1-2*.**
A. Nrd1-TAP and Ess1-TAP total protein levels in WT and *cct1-2* strains grown at 37 ˚C were assessed by Western blot with αTAP-tag antibodies with respect to loading control with αSsa antibodies. B. ChIP of the TAP-tagged strains, as well as modification marks H3K4me3 and H3K56ac at snoRNA genes' terminators in *cct1-2* grown at non-permissive temperature (37 ˚C) with respect to control (30 ˚C).
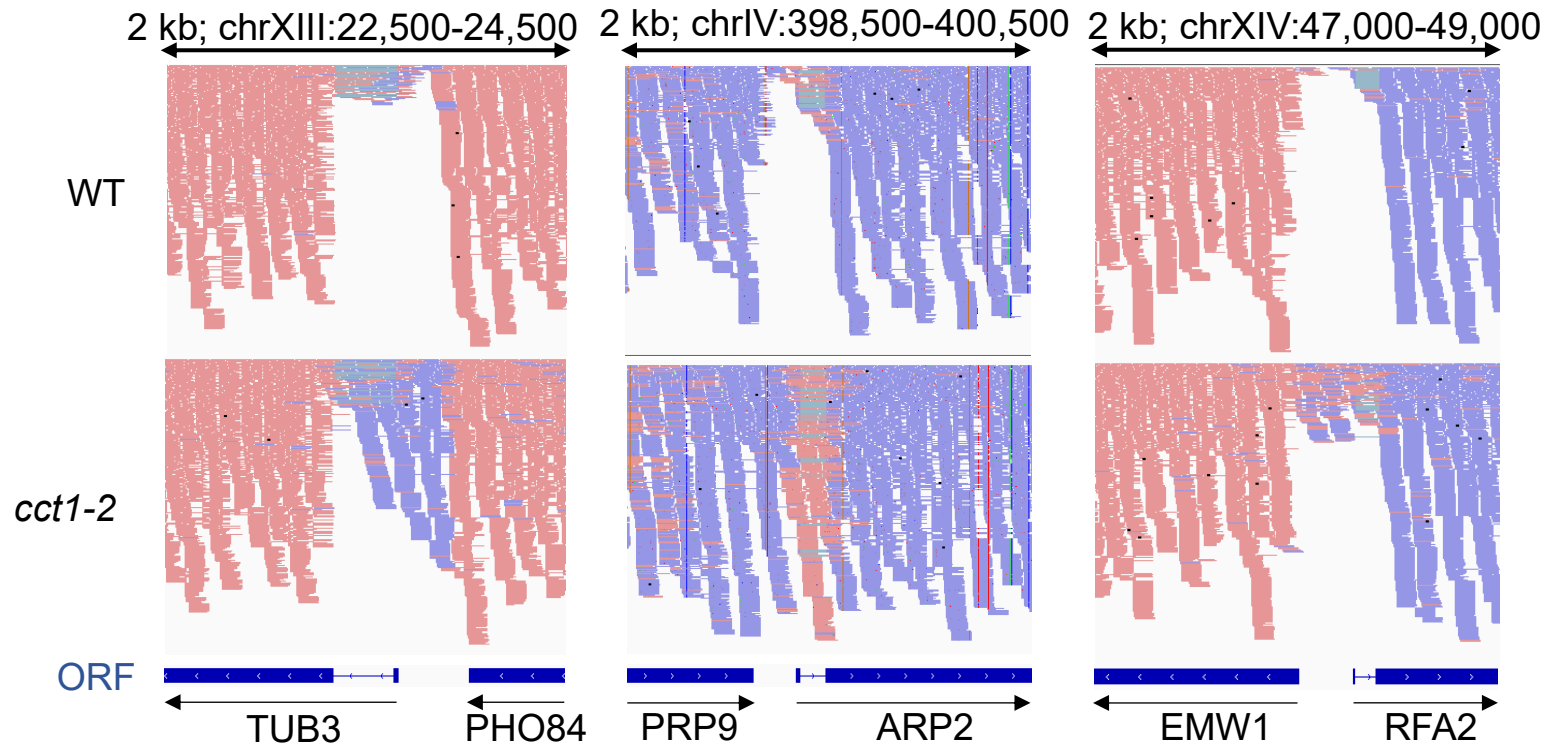
Figure 4.1.43. **CCT is likely involved in splicing.**
RNA-Seq reads, derived from WT and *cct1-2* grown at 37 ˚C, depicting increase of (antisense) reads in *cct1-2* at introns, which are demarcated as thin lines within ORFs (thick blue box) at select locations.

175

4.2. Hsp90

Hsp90 was shown to contribute to differential gene expression via affecting specific promoter-proximal chromatin regulators (Tariq 2009, Hamamoto 2004). Active gene promoters are some of the areas known to be marked by differential chromatin status (Bell 2011). Even though Hsp90 was shown to globally colocalize with nucleosome depleted regions near TSS (Sawarkar 2012), it was not interrogated whether Hsp90 is capable of modulating chromatin structure comparable to transcriptional status. To investigate the influence of Hsp90 on chromatin architecture *in vivo*, DNaseI-Seq assay was used to map DHS sites across the genome in yeast expressing WT Hsp90 or ts mutant G170D, which inactivates at 37 °C (Nathan 1995), similarly to approach for CCT. Analysis of the DHS pattern following 15-min incubation at 37 °C revealed a general dependence on Hsp90 as ~27% of the DHSs in the WT background were lost in G170D and ~10% novel sites appeared (Figure 4.2.1A). Importantly for this data set, DHSs with excessively increased hypersensitive were detected, as reflected by the increased average chromatin openness for G170D specific overlapping and unique sites, quantified via z score (John 2011) (Figure 4.2.1A). Due to pronounced DNaseI cleavage rate, these sites are visually trackable on the genome browser (Figure 4.2.1B). Footprint detection was used to discover relative DNA occupancy within the DHSs (Hesselberth 2009) and motif scan (Sandelin 2004) was implemented on the cognate DNA elements to identify potentially bound transcription factors. We revealed that the sites with increased hypersensitivity in G170D are enriched in Rsc3 and Rsc30 consensus elements (Figure 4.2.1B). Overall there were 136 Rsc3 and 137 Rsc30 sites in WT and 275 and 272 in G170D. Further chromatin immunoprecipitation experiments were performed to confirm colocalization of increased Rsc3 occupancy at the sites with increased hypersensitivity upon 15-min Hsp90 inactivation (Figure 4.2.2).
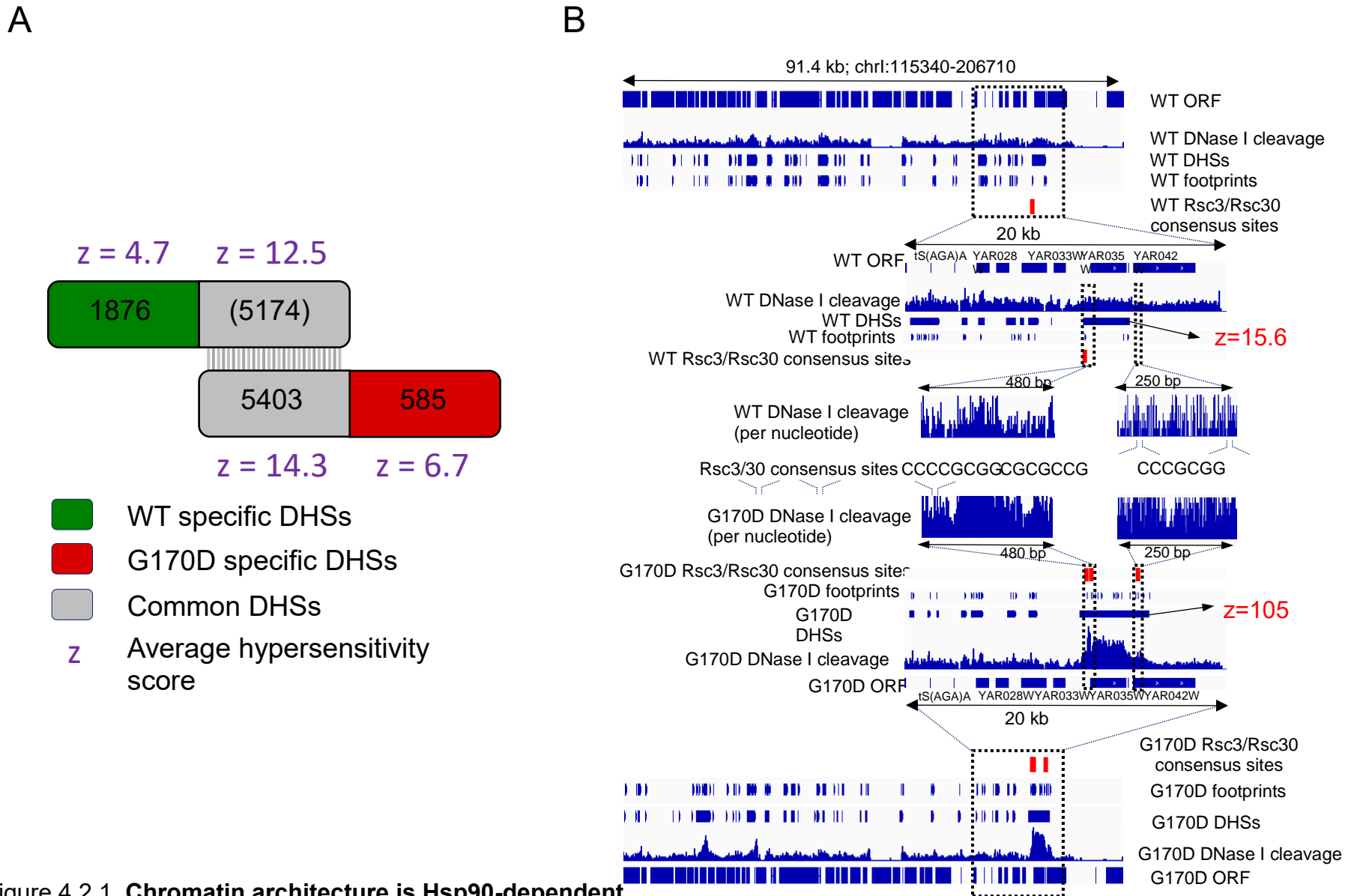
Figure 4.2.1. **Chromatin architecture is Hsp90-dependent.**
A. Bar graph representing overlap between WT and G170D DHSs (grey), as well as WT (green) and G170D (red) unique sites. Z is average z-score, a hypersensitivity measure (John 2011) for the give DHS group. B. Differentially computed DNaseI cleavage rate (fdr=0.01) for WT (top) and G170D (bottom) at indicated location, revealing peaks with increased hypersensitivity in G170D as quantified by the z-score. Enlargements of the dashed location point towards short DNaseI-protected regions detected by footprinting (Hesselberth 2009), where Rsc3/30 consensus motifs were identified.
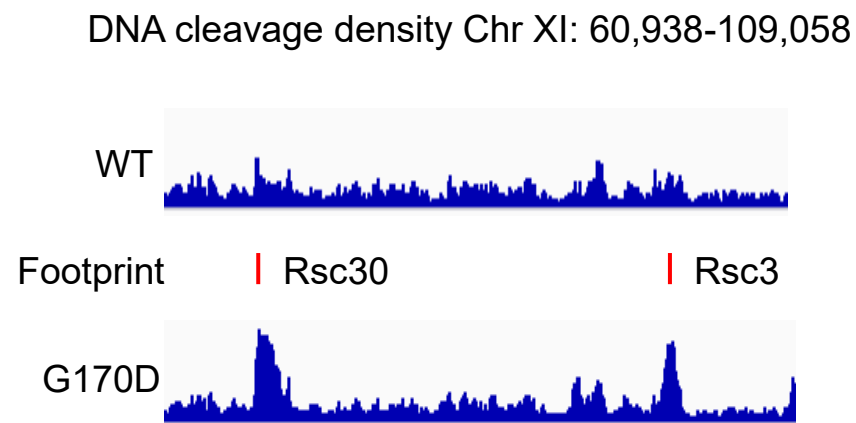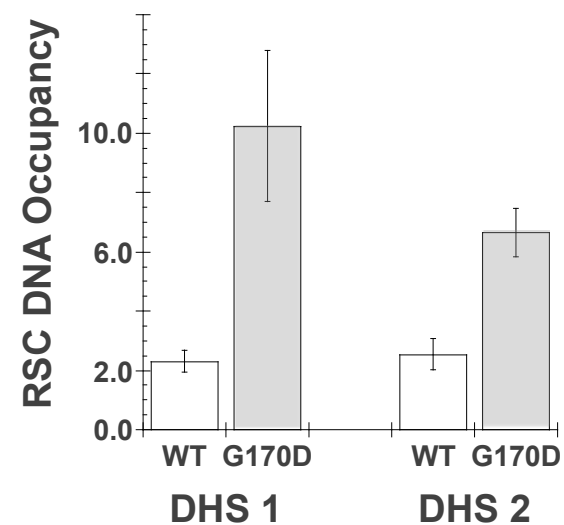
Figure 4.2.2. **Increased hypersensitive sites upon Hsp90 inactivation correlate with increased Rsc3 occupancy.**
A. DNaseI cleavage rate for WT and ts G170D at select location that contains two sites with increased hypersensitivity in G170D. These sites also colocalize with Rsc3 or Rsc30 consensus motif (positions marked in red) as identified with digital genomic footprinting. B. DNA occupancy of Rsc3-TAP in WT and G170D, grown at 37 ˚C for 15 min, at the locations from A.

Rsc3 and Rsc30 transcription factors are DNA binding subunits of the RSC, an ATP-dependent chromatin remodeler capable of perturbing local chromatin structure (Angus-Hill 2001, Tsukiyama, Lorch 1999). Given the observed phenotype in G170D and previous findings that Hsp90 genetically connects to RSC (Zhao 2005), it was postulated that Hsp90 is able to displace entire RSC from its target location and thereby terminate its remodeling actions. Continued RSC remodeling would otherwise lead to displacement of nucleosomes and generation of the locations with elevated DNaseI cleavage rate. *In vitro* results were in agreement with the postulations derived from deep DHS sequencing and digital genomic footprinting. In a concentration dependent manner, purified recombinant Hsp90 was able to release RSC complex from its cognate DNA (Figure 4.2.3A). To further test whether Hsp90 is able to affect RSC's remodeling activity, a nucleosome EMSA was used. Thereby, a centrally positioned mononucleosome was reconstituted using recombinant *Xenopus* octamer and radiolabeled 601 DNA fragment (Luger 1999, Lowary 1998). RSC bound nucleosome without ATP, whereas ATP addition lead to the formation of activated RSC complex (complex 2, Figure 4.2.3B) (Lorch 1998). Addition of Hsp90 abolished RSC-nucleosome interaction regardless of ATP. The released mononucleosome was still centrally positioned, indicating that it was not subject to remodeling reaction. This confirmed that Hsp90 is able to dissociate RSC from its target DNA and nucleosome, hampering its remodeling.
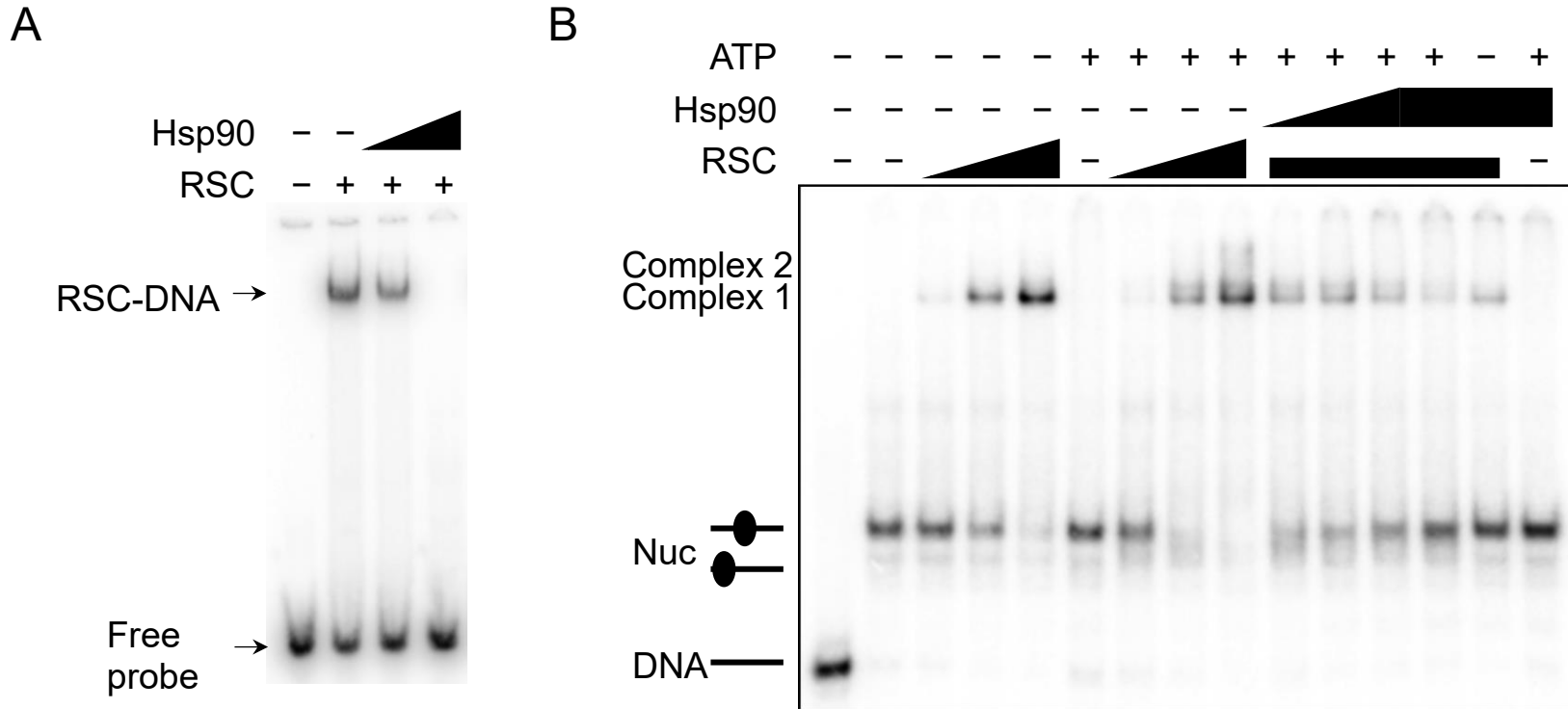
Figure 4.2.3. **Hsp90 displaces RSC from the DNA and from the nucleosome without enhancing remodeling activity.**
A. RSC DNA-binding activity monitored by EMSA using purified RSC and radiolabeled PHO8 promoter DNA. The influence of Hsp90 on RSC-DNA structures was determined by titrating in Hsp90 (0, 2, or 20 µM). B. RSC nucleosome binding and remodeling activity was checked by EMSA using nucleosomes prepared with radiolabeled 601-positioning DNA, titrations of purified RSC (1, 5, and 10 nM) and Hsp90. The influence of ATP (1 mM) and Hsp90 (4 µM) were assessed, as indicated. The migration points of free DNA, nucleosome with centrally or terminally positioned histones, and RSC-nucleosome structures (complex1 and 2) are marked.

To examine which RSC subunits are targeted by Hsp90, two-hybrid assay was employed. Out of 17 screened RSC subunits, 2 displayed relationship with Hsp90 (Figure 4.2.4). No subunit had a standard positive result because there was no *HIS3* reporter activation upon coexpressing the bait (DBD-Hsp90) and either prey (AD-RSC subunits). However, AD-Rsc3 and AD-Sfh1 both autoactivated *GAL1-HIS3* reporter, yet coexpression of DBD-Hsp90 abrogated the autoactivation. *GAL1* promoter system used in the two-hybrid assay is known to hold Rsc3/30 binding sites used by RSC to activate the downstream gene (James 1996, Floer 2010). We suspected that the change in HIS3 expression stems from the fact that AD-Rsc3 and likely AD-Sfh1 lead to autoactivation which was abolished by the increased local Hsp90 concentration in the form of DBD-Hsp90. These results suggest that Hsp90 dissociates RSC from the DNA by targeting Rsc3 and likely Sfh1 subunits.
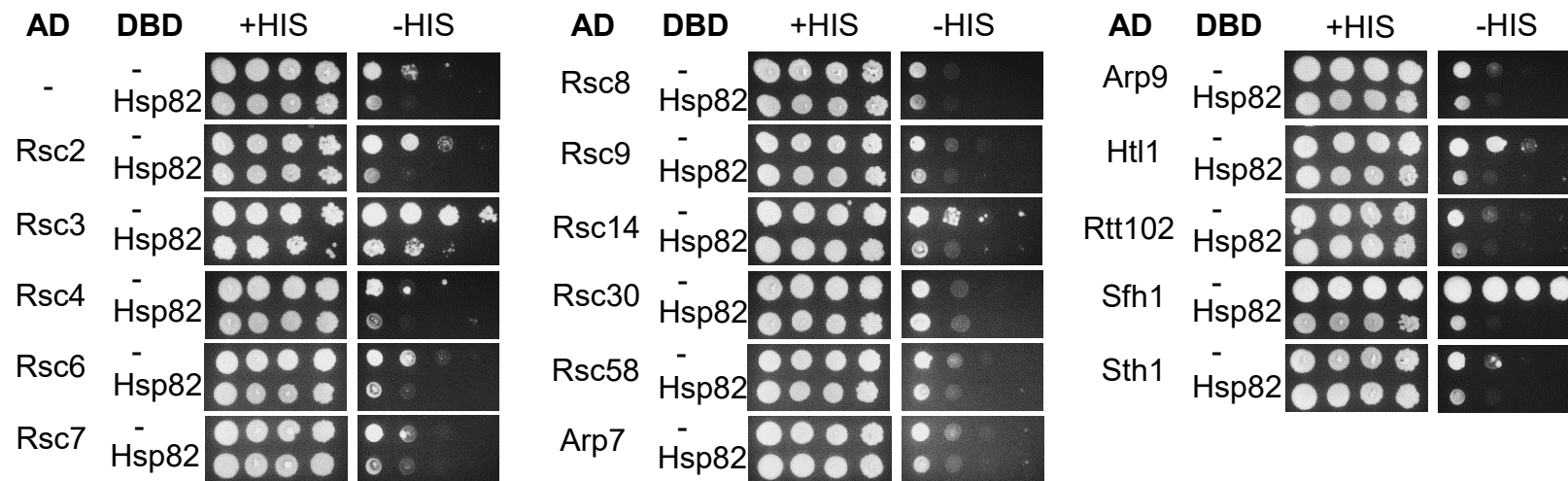
Figure 4.2.4. **Two-hybrid screening identified an ability of Hsp82 to suppress Rsc3 and Sfh1 autoactivation of the *GAL1*-reporter.**
Yeast 2-hybrid analysis performed using the Gal4 DNA binding domain (DBD), fusion of the DBD with Hsp82 (DBD-Hsp82), Gal4 activation domain (AD), or fusions of the AD with RSC subunits, as indicated. Yeast (AH109) transformants plated onto complete media (+HIS) or selection media (-HIS) to test activation of the *HIS3* ORF through a minimal *GAL1* promoter containing *GAL4* UAS (James *et al*., 1996).

Apart from the sites with increased hypersensitivity, analysis of the DNaseI-Seq data revealed another characteristic: there was a genome-wide reduction of the open chromatin as reflected by the decrease of the DHSs numbers (15% less in G170D) and total length of the open chromatin (13% less in G170D) (Figure 4.2.5A). These results suggested that chromatin is subject to two different perturbations upon Hsp90 inactivation. Interestingly, for DNaseI-Seq upon prolonged Hsp90 depletion (6 h) no DHSs with significantly increased hypersensitivity were detected anymore, as well as no Rsc3/30 footprints (Figure 4.2.5B). Because the group of DHSs with abnormal hypersensitivity disappeared, the long-term effect proposes presence of the compensatory mechanisms that allowed circumvention of the anomalous hypersensitive site formation observed for the short-term Hsp90 inactivation. However, long-term inactivation of Hsp90 resulted merely in the genome-wide shortening of the open chromatin (Figure 4.2.6A), similarly to the short-term depletion. Majority of the G170D DHSs are smaller (2362, 62.9%) according to their length or hypersensitivity z score; 883 (23.5%) sites are lost and only 513 (13.6 %) are gained in mutant with respect to the wild type (Figure 4.2.6B). Given the global decline, we wanted to address the functional causes that led to these chromatin alterations in the cells devoid of Hsp90.
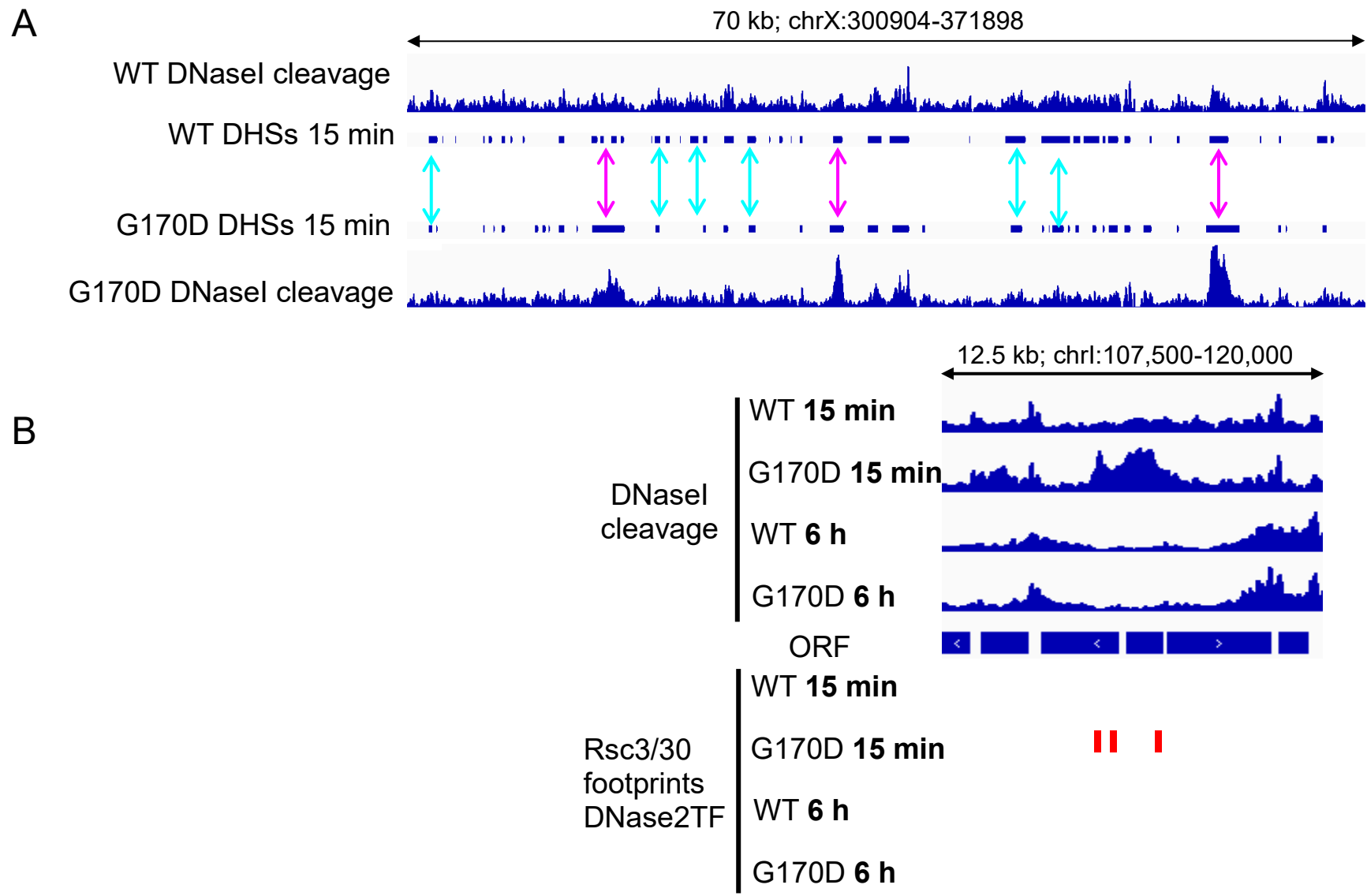
Figure 4.2.5. **Two characteristics of the chromatin upon short-term Hsp90 depletion – open chromatin regions disappear after long-term Hsp90 depletion.**
A. DNaseI cleavage rate (fdr=0.01) computed with hotspot (John 2011) in WT and ts G170D at the select location upon short-term (15 min) Hsp90 inactivation. Pink arrows point out DHSs with excessively increased hypersensitivity and light blue arrows point out reduced length/loss of G170D DHSs with respect to WT. B. DNaseI cleavage rate upon short-term (15 min) and long-term (6 h) Hsp90 inactivation and Rsc3/30 footprints (red) detected with DNase2TF (Sung 2014) for the given Hsp90 data sets at the select location.
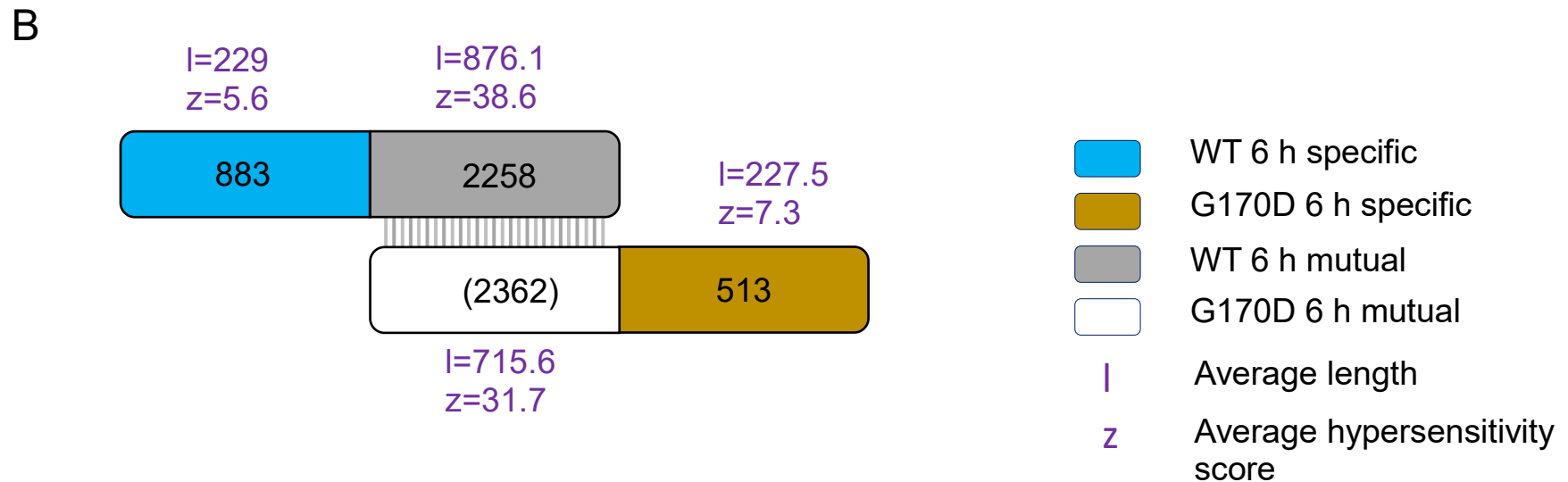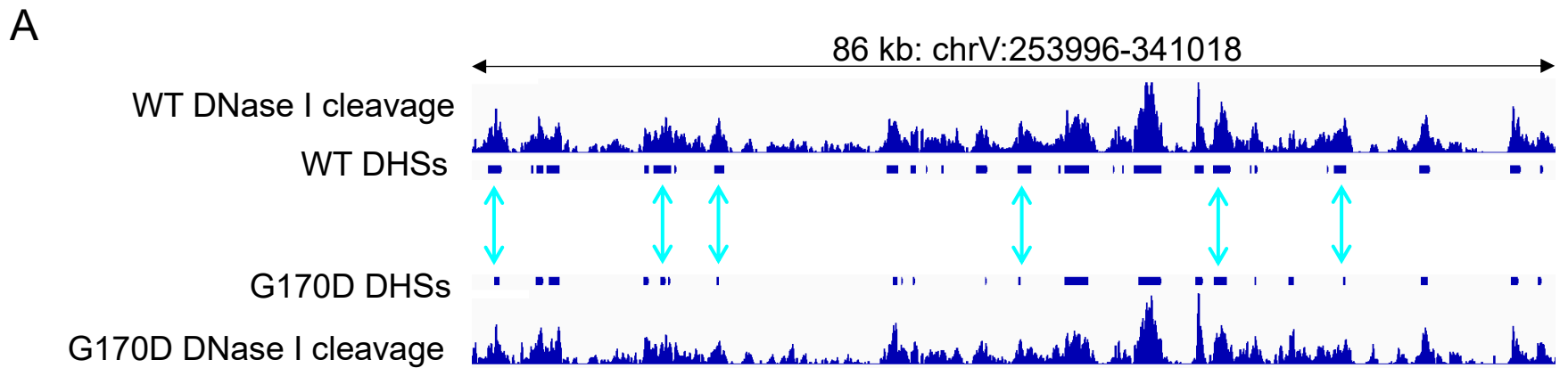
Figure 4.2.6. **Long-term Hsp90 depletion leads to mild global closure of the open chromatin.**
A. DNaseI cleavage rate (fdr=0.01) in WT and ts G170D upon long-term (6 h) Hsp90 inactivation. Light blue arrows point out reduced length (or hypersensitivity) of the G170D DHSs with respect to WT. B. Bar graph representing the number of overlapping (grey/white) and WT (blue) or G170D (bronze) specific DHSs. Average length (l) and average z score (z) for the given DHSs groups.

It was further observed that overall reduction of the open chromatin upon long-term Hsp90 depletion was followed by the decline of the total bound transcription factors, as revealed by utilizing digital genomic footprinting (false discovery rate (fdr) = 0.01) on computed DHSs (Hesselberth 2009) (Figure 4.2.7). The footprint reduction was confirmed by comparing the results with newer footprint detection programs that were reporting higher recapitulation rates, based on updated models and footprint detection algorithms (Piper 2013, Sung 2014). The programs provided different computing depths (p scores at 10^{-30} to 10^{-10} and fdr at 0.01 and 0.1) and hence different overall numbers of detected potential transcription factor binding sites. However, the declining trends in G170D are consistent. The loss of G170D footprints is reflected by the altered DNaseI cleavage, which is visualized in Figure 4.2.8. for select intergenic locations. Because DHSs are characterized by their length and z score (John 2011), subpeak architectures are not ramified – the mentioned footprint occupancies defined as a short protections within DHSs (Hesselberth 2009) offer DHS structural characterizations instead. Even though the magnitude of the profile change is not prominent, its reproducibility was notable. Initial DNaseI-Seq analysis were based on 40 and 28 millions of reads for WT and G170D – 12 and 7 million of which were successfully mapped due to unique mapability. By resequencing created libraries to rise the input read numbers to 126 million for WT and 85 million for mutant, 38 and 21 million of which were successfully aligned, DNaseI cleavage profiles were identical.

		WT	G170D	WT	G170D	WT	G170D
Hesselberth 2009		fdr 0.1		fdr 0.2			
		3540	2686	6350	5059		
Piper 2013		p-value10^{-30}		p-value10^{-20}		p-value10^{-10}	
	defualt	4460	3736	11072	9230	29770	24177
	dmfp	4838	4024	12185	9778	32346	25519
Sung 2014		fdr 0.01		fdr 0.1			
		45019	33585	73146	59093		

Figure 4.2.7. **Open chromatin correlates with the loss of potentially bound transcription factors.**
Footprint numbers detected within WT and G170D DHSs computed with three different footprint detection programs (Hesselberth 2009, Piper 2009 and Sung 2014) at different thresholds (fdr or p value). Piper 2003 was run under default parameters and also adjusted parameters (dmfp: size of the footprints adjusted to Hesselberth 2009 and merging of the footprints was excluded).
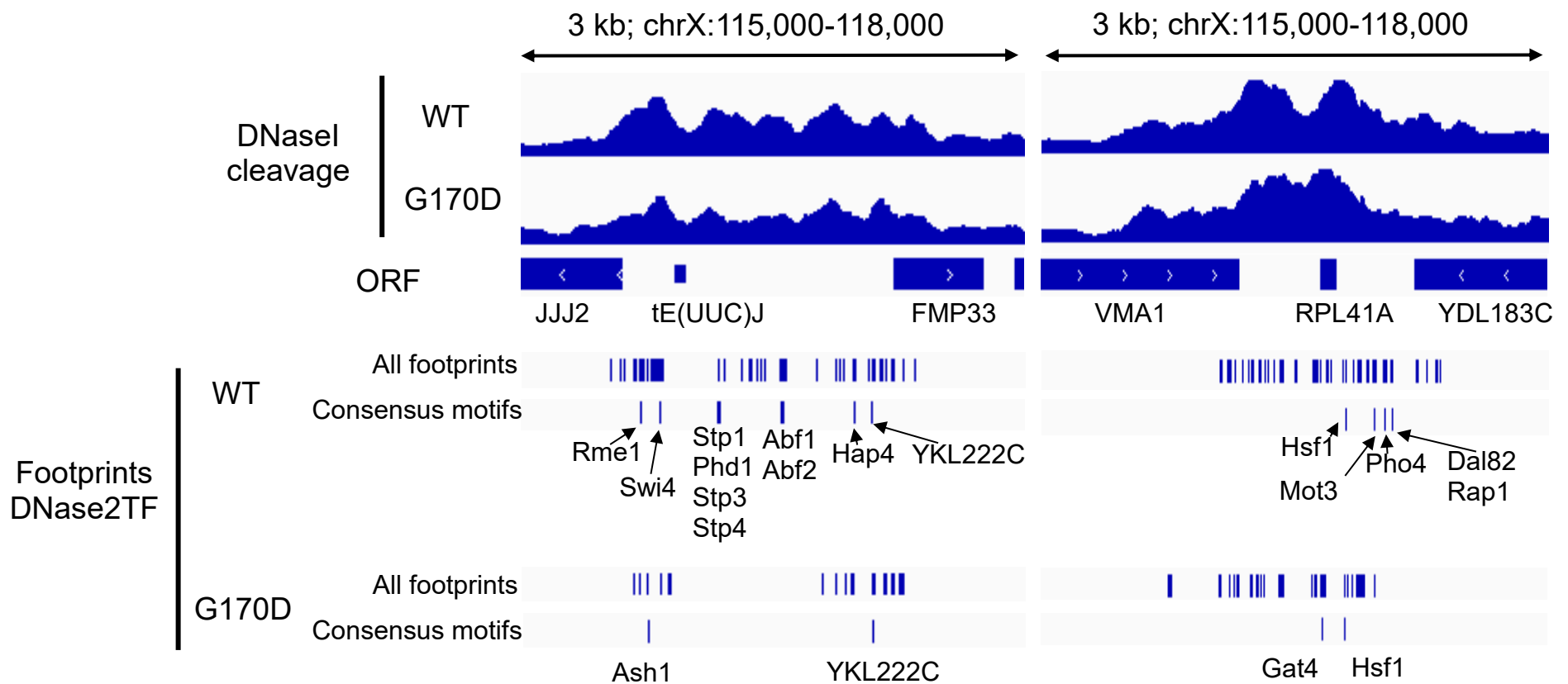
Figure 4.2.8. **Altered cleavage rates at DHSs correlate with loss of G170D-specific footprints.**
DNaseI cleavage rate (fdr=0.01) for WT and G170D DHSs demonstrating altered cleavage profiles at indicated genomic locations. Footprints are computed for the give locations using DNase2TF (fdr=0.01) (Sung 2014). Motif scan on identified footprints was performed via RSA-tools (van Helden 2000) using frequency matrices obtained from JASPAR (Sandelin 2004).

Loss of hypersensitivity and transcription factors advocate for the increased nucleosomal occupancy. It is known that transcription factors and nucleosomes are in competition – one will impede the other in its association with the DNA (Workman 1992, Morse 2003, Ganapathi 2011, Afek 2011). Hsp90 could be aiding functions of both antagonists differently. Previous findings in this chapter and other report showed that Hsp90 absence is followed by impaired nucleosome displacement (Floer 2008), and an *in vitro* experiment demonstrated Hsp90's ability to enable DNA-binding activity of bHLH transcription factors MyoD1 and E11 (Shaknovich 1992, Shue 1994). The later case would carry more weight here – we suspected that Hsp90 inactivation negatively influenced DNA occupancy of transcription factors, which allowed for higher nucleosomal habitation in G170D and thereby smaller DHSs. To posit this hypothesis, select recombinant yeast transcription factors were tested for their DNA binding in the presence of yeast recombinant Hsp90. Thereby, purified transcription factors were incubated with radiolabeled probe containing transcription-factor specific consensus motif, with varied Hsp90 concentration, and reaction was resolved on EMSA. As seen from the Figure 4.2.9A, Hsp90 enhanced DNA binding of Abf1, Cbf1, Met31 and Rap1 in a concentration dependent manner. However, Hsp90 did not affect Reb1 DNA-binding ability. Hsp90 specifically enhanced binding of Ino2/4 heterodimer, and poorly also Ino4 (Figure 4.2.9B, left). As a control, Hsp90 did not reinforce binding of Ino2/4 heterodimer to cognate element specific for other transcription factors such as Ino2, Mcm1, Rap1 and Abf1 (Figure 4.2.9B, right). This suggests that, by specifically maintaining DNA occupancy of various transcription factors, Hsp90 could affect the open chromatin. In agreement with mentioned transcription factors, Rsc3, Rsc30 as well as Rsc3/30 heterodimer DNA-binding was supported by Hsp90 titration (Figure 4.2.10A). This is however in contradiction with our previous RSC data and it remains to be examined whether Hsp90 is able to reinforce antagonizing events of the same process. Because different Hsp90 preparations were used for the two different experiments, the later result will be subject to further verification. Besides Rsc3/30, Hsp90 modulated binding of purified recombinant Sfh1 subunit, another RSC subunits that showed an interaction with Hsp90 in two-hybrid screen, likely through favoring discrete oligomerization states (4.2.10B).
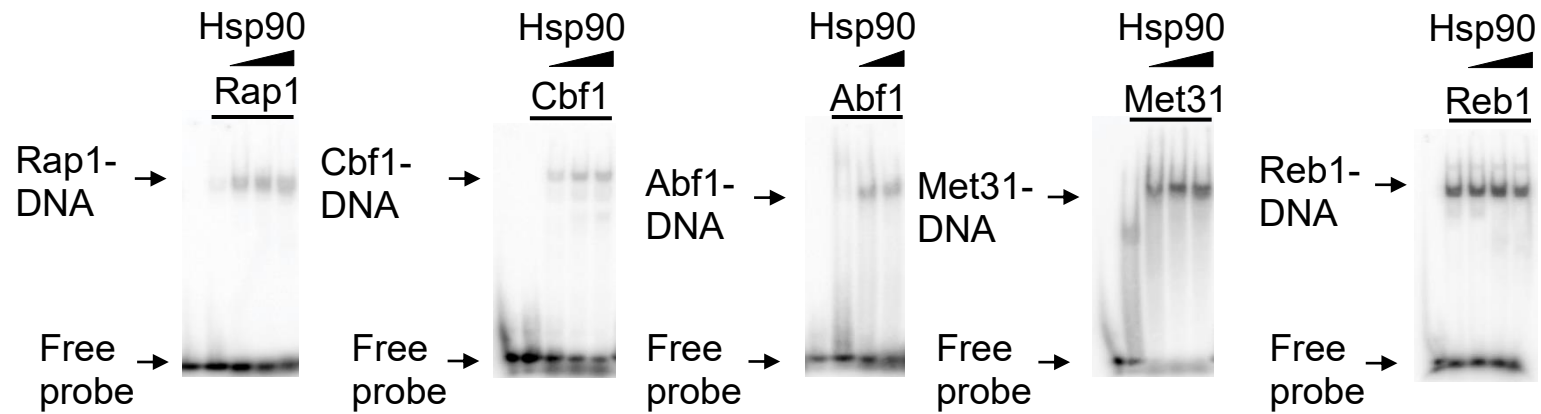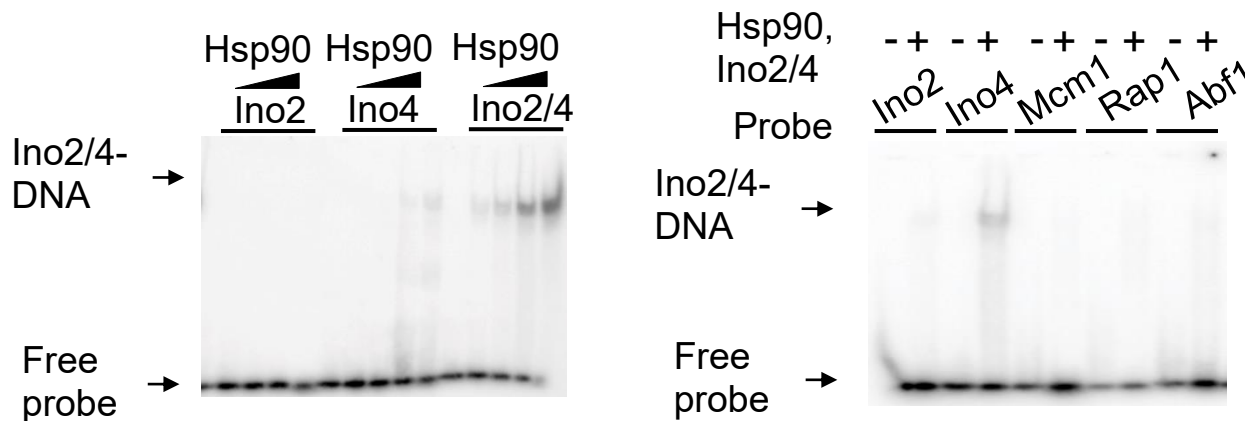
Figure 4.2.9. **Hsp90 enhances binding of transcription factors to their cognate DNA *in vitro.***
Transcription factors binding activity to their cognate DNA elements in the presence of Hsp90, monitored with EMSA using recombinant yeast transcription factors, radiolabeled DNA probe (20 nM) and increasing concentration of recombinant purified yeast Hsp90 (4, 12 and 34 µM). A. Rap1 (250 pM), Cbf1 (1 nM), Abf1 (100 nM), Met31 (1 µM) and Reb1 (113 nM), DNA binding. B. Ino2 (1.25 µM), Ino4 (1.25 µM), and heterodimer Ino2/4 (300 nM), DNA binding, as well as control EMSA testing Hsp90 enhancement of Ino2/4 binding to DNA probe containing Ino2, Ino4, Mcm1, Rap1 and Abf1 consensus elements.
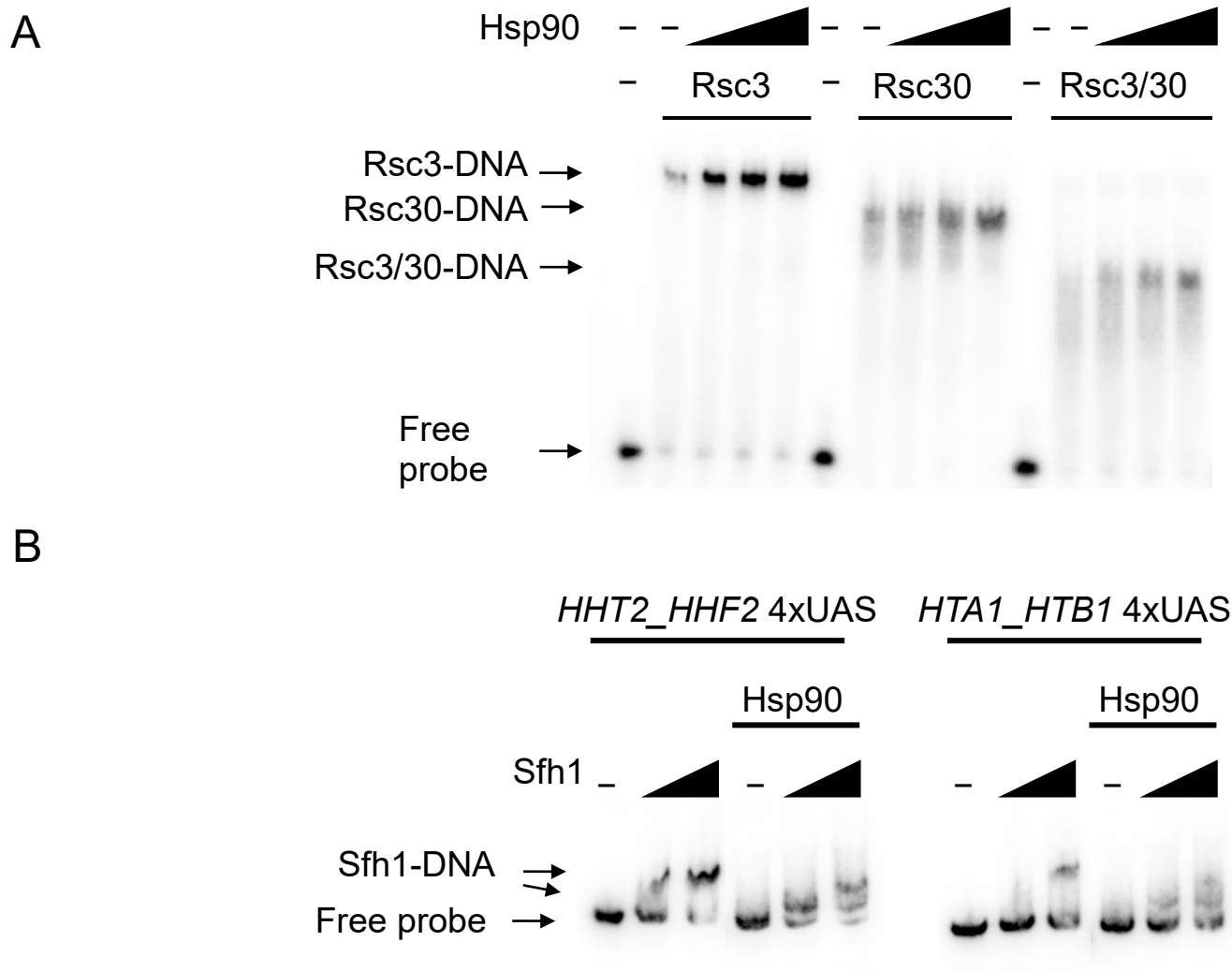
Figure 4.2.10. **Hsp90 enhances binding of Rsc3, Rsc30, Rsc3/30 and alters DNA binding of Sfh1.**
A. DNA-binding activity of recombinantly purified Rsc3 and Rsc30 (70 nM), as well as Rsc3/30 heterodimer, to radiolabeled *ACC1_TIM23* promoter probe (20 nM) with applied Hsp90 titration (4, 12 and 34 µM) was examined via EMSA. B. Purified Sfh1 (100 and 600 nM) DNA-binding was tested using radiolabeled histone promoters (*HHT2_HHF2*, *HTA1_HTB1*, 20 nM) in the presence of Hsp90 (40 µM).

191

Hsp90 was reported to support stability and activity of various chromatin-binding regulators (Tariq 2009, Hamamoto 2004). We wanted to assess whether decline of open chromatin and computed footprints could also be assigned to reduced cellular levels of transcription factors upon Hsp90 depletion. Thereby, wild type and ts mutant strain grown under non-permissive temperature were subject to cycloheximide treatment, which inhibits protein synthesis, and the total protein levels were inspected (Figure 4.2.11). Monitoring existing levels of transcription factors revealed degradation of the transcription factors in the absence of functional Hsp90 confirming that Hsp90 is involved in maintenance of their stability and hence overall half-life. Furthermore, the ability of Hsp90 to preserve transcription factor stability was inspected for conservation. To test generalized theme of Hsp90 inhibition as means to affect stability of transcription factors, vSRC 3T3 mouse fibroblastoma cells were treated with radicicol. The levels of various transcription factors in the presence of Hsp90 inhibitor were assessed with Western blotting. The results show that, while Hsp90 control levels remained the same, transcription factor Hsf1, c-Myc1 and GATA-5 levels declined (Figure 4.2.12).
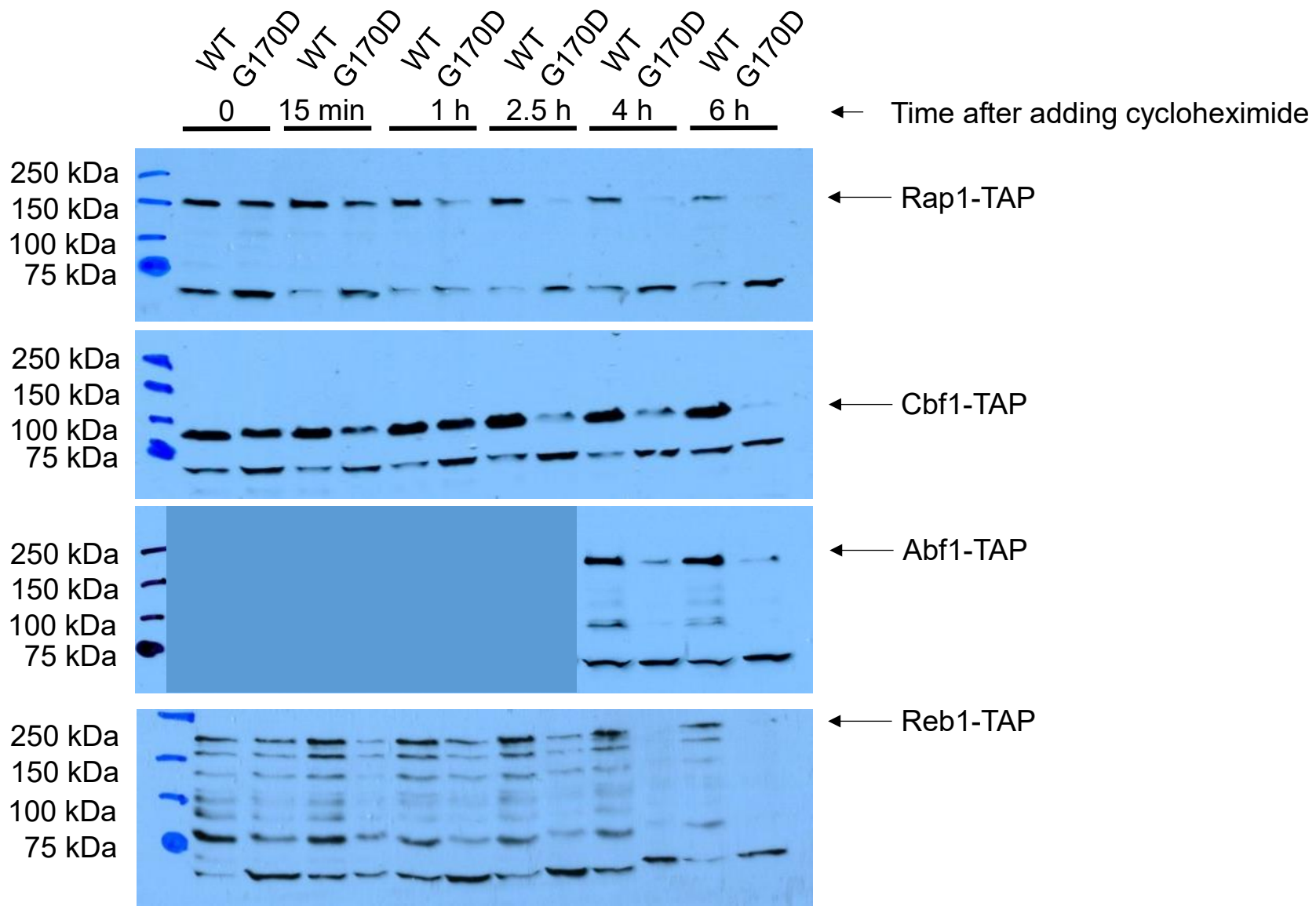
Figure 4.2.11. **Hsp90 supports transcription factor longevity.**
The levels of the TAP-tagged transcription factors in WT and G170D strains grown at non-permissive temperature in the presence of cycloheximide, monitored by Western blotting for αTAP-tag at indicated time points after cycloheximide addition.
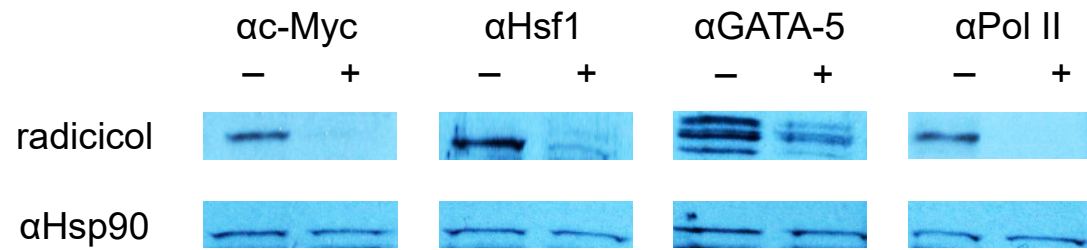
Figure 4.2.12. **Hsp90-supported transcription factor stability is conserved.**
The levels of the transcription factors in vSRC 3T3 cell lines in the presence of radicicol (10 μM), monitored by Western blotting with antibodies directed against indicated transcription factors: c-Myc, Hsf1, GATA-5, and also Pol II.

Modulation of transcription factor functional equilibrium entails the next question – how is the transcriptional outcome affected in the absence of functional Hsp90? To answer this question, RNA-Seq was utilized on RNA isolated from WT and G170D grown at 37 °C for 6 h, similarly to CCT. Read analysis according to GFold computation (Feng 2012) reveals that there were only 114 upregulated and 152 downregulated genes (GFold ≥1.5, or GFold ≤-1.5) (Appendix 7.7.2). The list of differentially expressed genes as well as their GO annotations were similar to results obtained from CCT depletion experiments and hence not Hsp90 specific. Loss of footprints within intergenic locations was further correlated with transcriptional response. The Figure 4.2.13. displays select transcription factors known to bind at the regulatory regions and modulate the target gene expression. Along with this, cleavage rate at the affected regulatory region containing TF-specific consensus motif in G170D and wild type, and GFold computation that stands for differential gene expression, were provided. Interestingly, even though transcription factor footprints were lost from their target genes' regulatory regions in G170D according to the computed cleavage rate, transcriptional outcome was unaltered (GFold ≤1.5, or GFold ≥-1.5). Hence, even though Hsp90 is shown here to modulate transcription factor binding and their stability, the cells circumvented and/or accustomed to the Hsp90-dependent loss of bound transcription factors, thereby not changing the gene expression status.

Exploration of the nuclear characteristics under the conditions of inactivated Hsp90 encompassed a question whether differential gene expression and whether chromatin large-scale landscape activities would correlate with these events. Comparison of changed DHSs regions (at least 50 bp longer or 1.5 changed z-score) with differentially expressed genes (and their adjacent intergenic intervals) revealed only 7.5% colocalization from the total DHSs pool (Figure 4.2.14). Hence, the structural chromatin changes were not idiosyncratic to the differential gene expression.

Footprint: Abf1
Gene: YOR357C
Intergenic:
YOR357C_YOR358W
GFold: 0.38
Cited in: Yarragudi 2006

chrXV:1,009,575-1,010,000

Footprint: Mcm1
Gene: YDR146C
Intergenic:
YDR146C_YDR147W
GFold: 0.36
Cited in: Lee 2002

chrIV:750,950-751,100

Footprint: Gcn4
Gene: YCL030C
Intergenic:
YCL030C_YCL029C
GFold: 0
Cited in: Yarragudi 2004

chrIII:68,450-68,600

Footprint: Rap1
Gene: YJL117W
Intergenic:
YJL1178C_YJL117W
GFold: -0.08
Cited in: Yarragudi 2006

chrX:90,200-90,300

Footprint: Reb1
Gene: YBR049C
Intergenic:
YBR049C_YBR050C
GFold: -0.17
Cited in: Wang 1988

chrII:336,750-337,250

Figure 4.2.13. **Transcription factors at the target genes' regulatory regions with reported gene expression dependencies – the same factors are lost in G170D but do not correlate with the differential gene expression.** Transcription factors lost from the reported target genes' regulatory location and the fold gene expression change upon Hsp90 inactivation are listed. DNaseI cleavage and footprints computed were for the given locations (Hesselberth 2009, Piper 2013, Sung 2014) in WT and G170D. Motif scan on identified footprints was performed via RSA-tools (van Helden 2000) using frequency matrices obtained from JASPAR (Sandelin 2004). Differential gene expression for the indicated genes was computed with GFold (Feng 2012). Lost footprint with identified consensus motifs in G170D is indicated with dashed red box and red arrow.
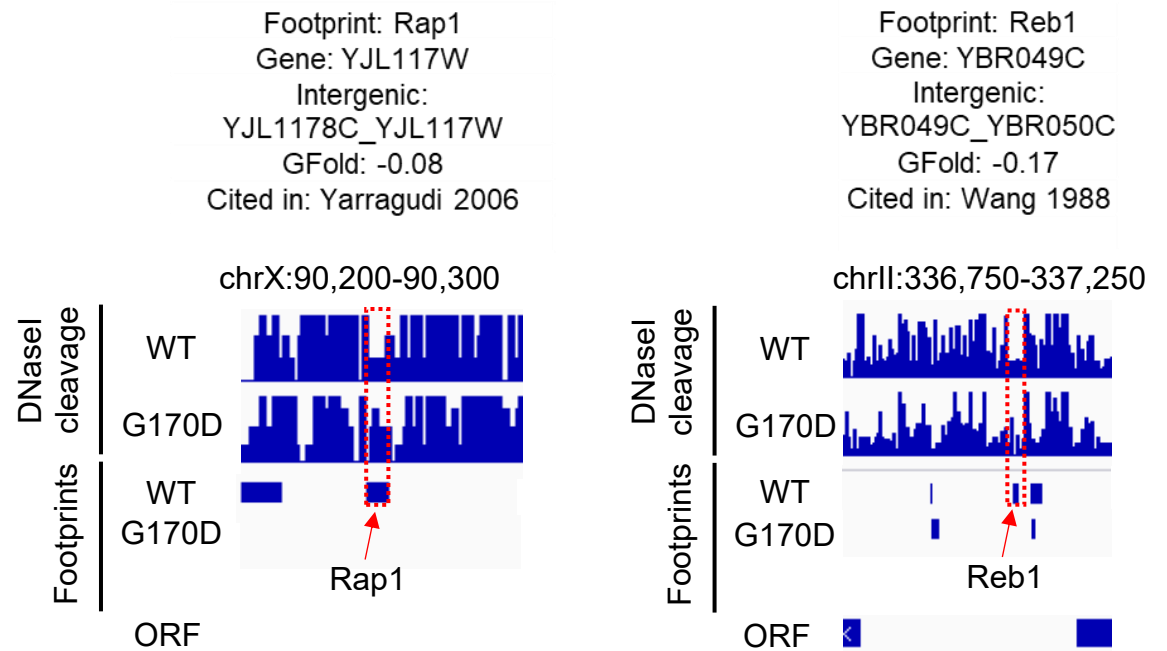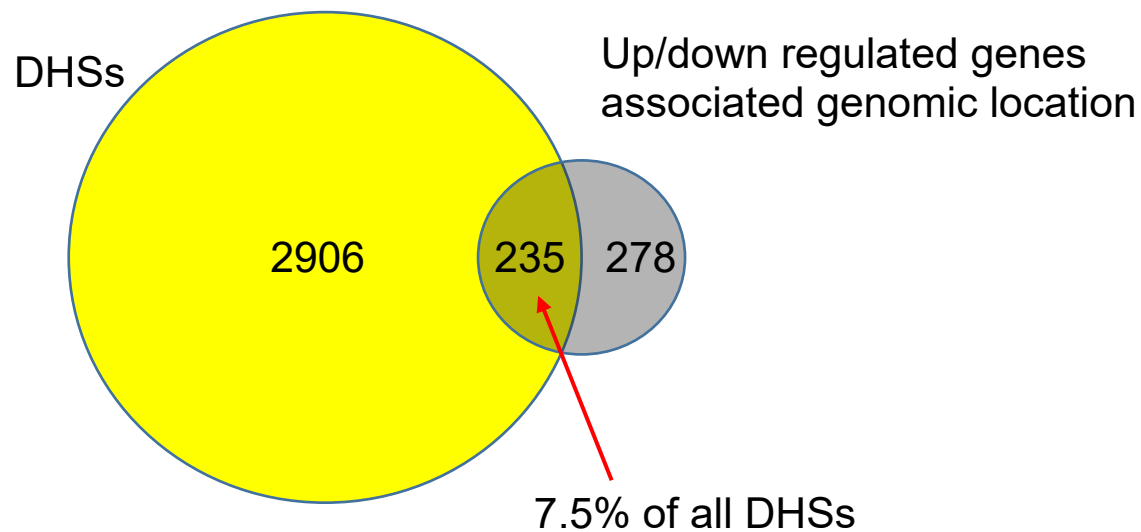
Figure 4.2.14. **Chromatin changes are not linked to differential gene expression.**
Venn diagram depicting overlap between the sites of the changed chromatin (increased/decreased – at least 50 bp changed length or 1.5 fold z-score – lost and gained DHSs in both WT and G170D) with the regions of differentially expressed genes (ORFs and their associated intergenic locations) according to Gfold (Feng 2012).

The magnitude of the non-coding transcriptome alterations further led to discoveries that the most prominent phenotype for extended Hsp90 depletion was not chromatin landscape. There was a global increase in 5' bidirectional transcripts in G170D (Figure 4.2.15) for ~56% (3966) ORFs (≥2 fold changed read directionality at the 5'), comparable to *cct1-2*. Altered chromatin correlated with only ~31% (1228) of the 5' bidirectional sites and their adjacent intergenic regions, suggesting that majority of these events are not directly related. Besides the main 5' cryptic transcription phenotype, Hsp90 inactivation also caused the antisense transcription of certain subtelomeric genes (Figure 4.2.16). All the events were correlated with H2A.Z histone variant loss, as described for CCT (Figure 4.2.15 and 4.2.16). This indicates the two chaperones are involved in the same process, and they perhaps regulate the same involved clients.
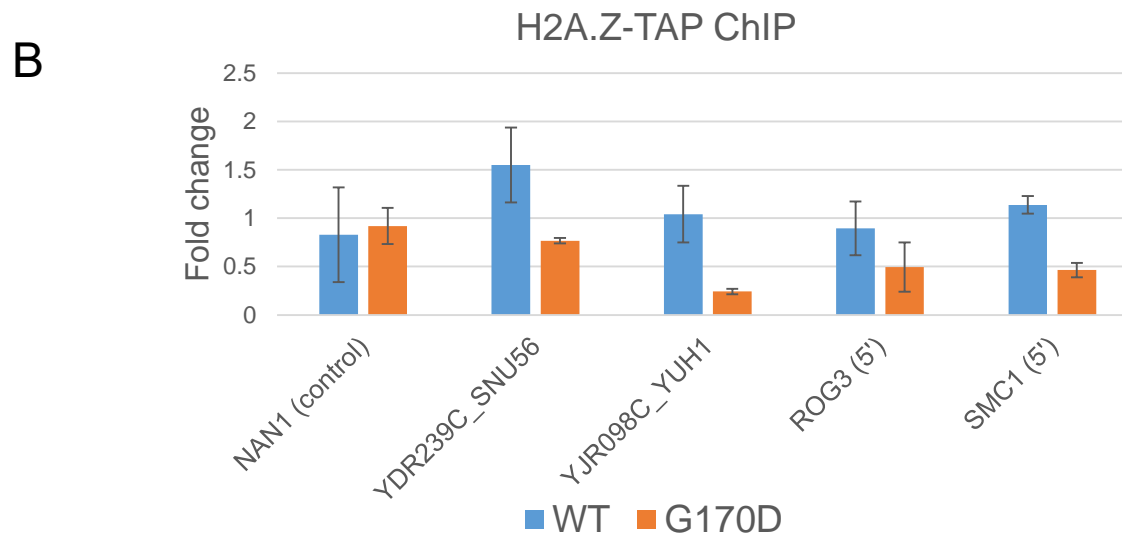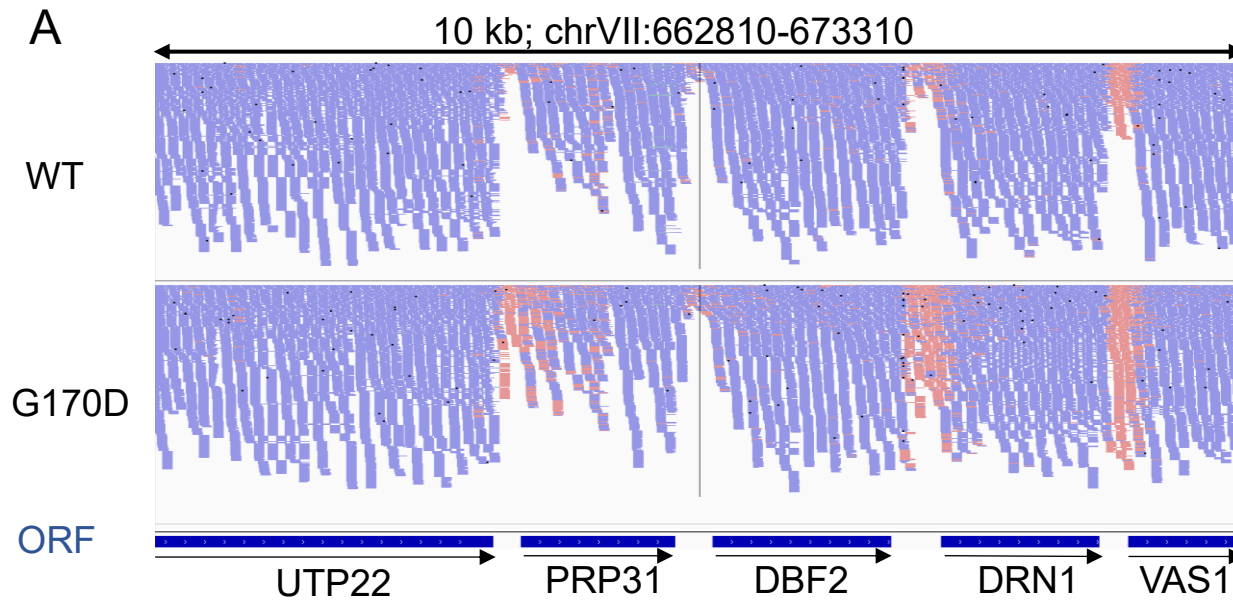
Figure 4.2.15. **Hsp90 depletion leads to 5' bidirectional transcription, which correlates with H2A.Z loss.**
A. RNA-Seq reads, obtained from RNA isolated from WT and G170D grown at non-permissive temperature, aligned to the reference genome sacCer3 (UCSC, April 2011) with STAR (Dobin 2013), as represented in collapsed form in IGV. ORFs are given as boxes with arrows indicating gene directionality, and intergenic regions are blank between gene boxes; sense reads are represented in blue and antisense reads in red. B. H2A.Z-TAP DNA occupancy at the locations affected by 5' bidirectional transcription in WT and G170D strains grown at 37 ˚C for 6 h.
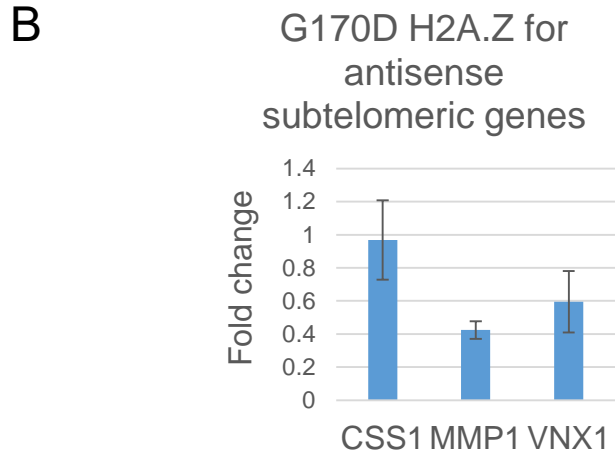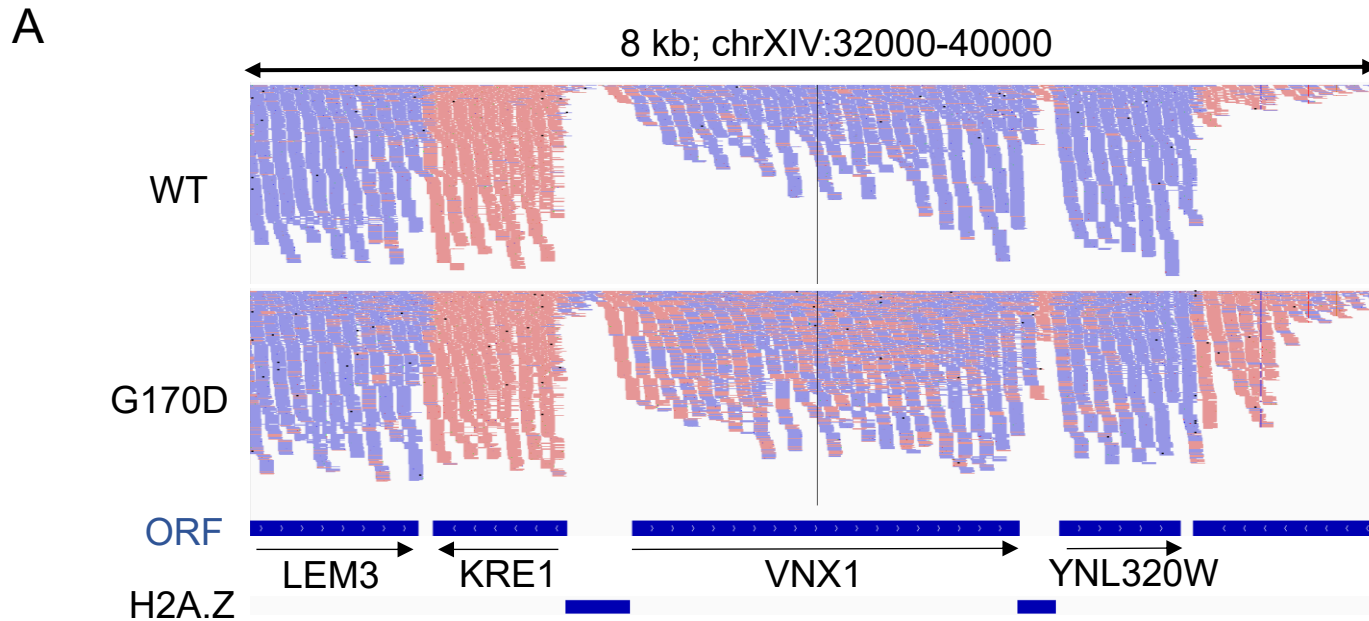
Figure 4.2.16. **Hsp90 depletion leads to antisense transcription of the subtelomeric genes associated to H2A.Z loss.**
A. RNA-Seq reads for RNA derived from WT and G170D, grown at 37 ˚C for 6 h, at subtelomeric location around the gene VNX1 that leans towards antisense transcription in G170D, as represented by the increase of antisense reads (red) with respect to WT that mostly has sense reads (blue). H2A.Z colocalized with VNX1 gene according to the H2A.Z map by Zhang 2005. B. H2A.Z-TAP DNA occupancy in G170D grown at 37 ˚C for 6 h at the subtelomeric genes that colocalize with H2A.Z nucleosome variant and are subject to antisense transcription upon Hsp90 inactivation.

The regions affected by 5' bidirectional transcription upon Hsp90 inactivation are targeted by numerous chromatin regulators (Figure 4.2.17), comparable to CCT. This would be expected as differences between CCT and Hsp90 5' affected locations represent less than 10% of all 5' events, most of which carry very poor score. In fact, the only observed difference between CCT and Hsp90 transcriptome data is that the absence of Hsp90 did not affect transcription termination at snoRNA genes, nor concomitant presence of the Nrd1 at the respective termination sites (Figure 4.2.18). Hence, Hsp90 does not regulate transcription termination. Another similarity between the states where Hsp90 or CCT were deprived is the increase of DNA occupancy of Spt10 transcriptional activators at divergent histone promoters, together with decline of TFIIB (Figure 4.2.19). Overall, these results suggest mutual ties between Hsp90 and CCT in controlling pervasive global 5' bidirectional transcription as well as affecting divergent histone promoters' regulators.
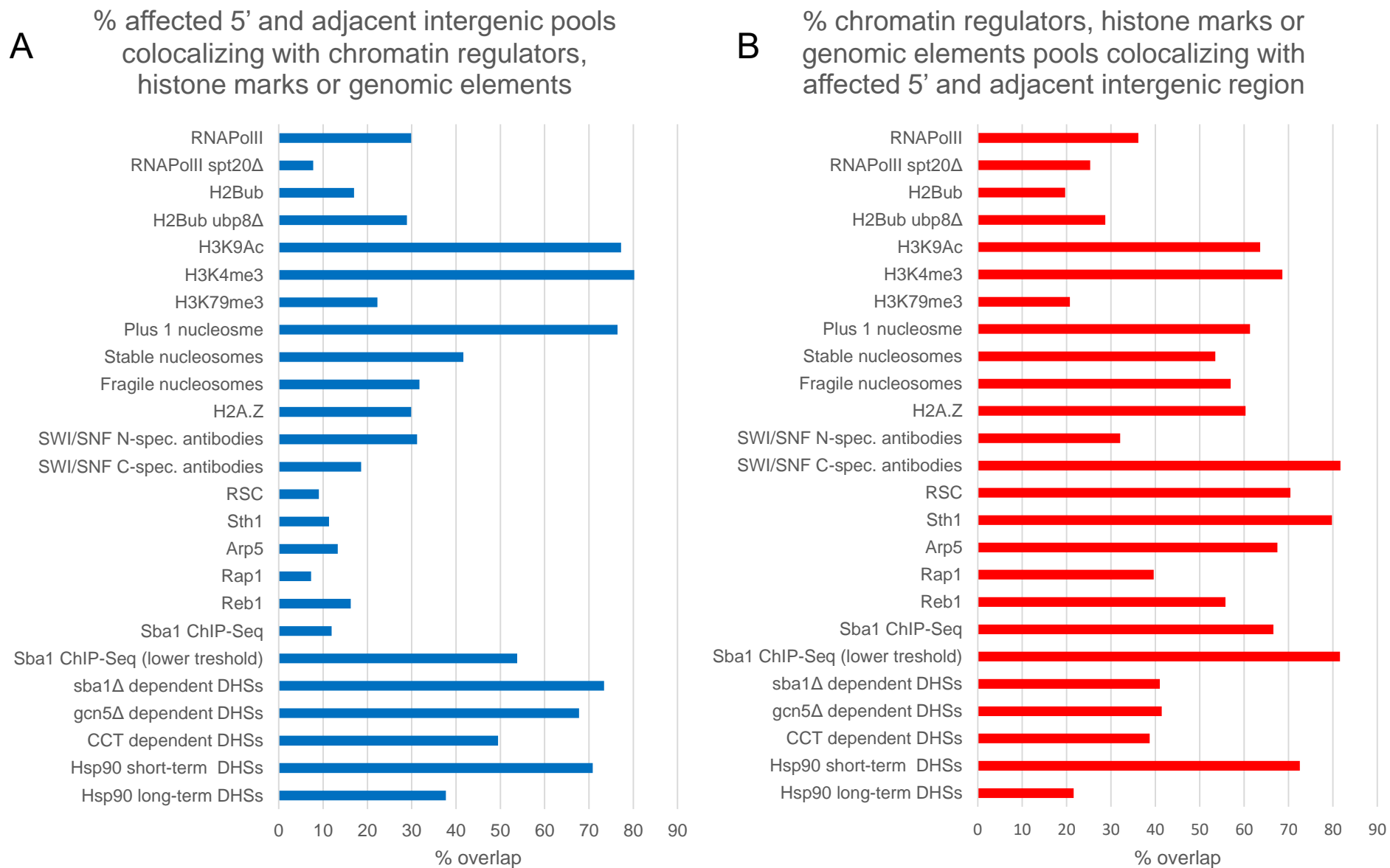
Figure 4.2.17. **5' bidirectional transcription locations in G170D are targeted by crucial chromatin regulators.**
A. Percent 5' sites with bidirectional transcription with adjacent intergenic location (subject to cryptic transcription due to 5' effect) that are covered by respective chromatin regulators, histone marks or other genomic elements. B. Percent detected sites for the given chromatin regulators, histone marks or other elements that have 5' bidirectional transcription phenotype in G170D. Raw data were retrieved via GEO accession number and analyzed as described in Methods, or if provided, genomic coordinates were taken directly: Bonnet 2014, Xue 2015, Kubik 2015, Zhang 2005, Rhee 2012, Dutta 2014, Zelin 2012, Parnell 2015, Ng 2002, Lieb 2001.
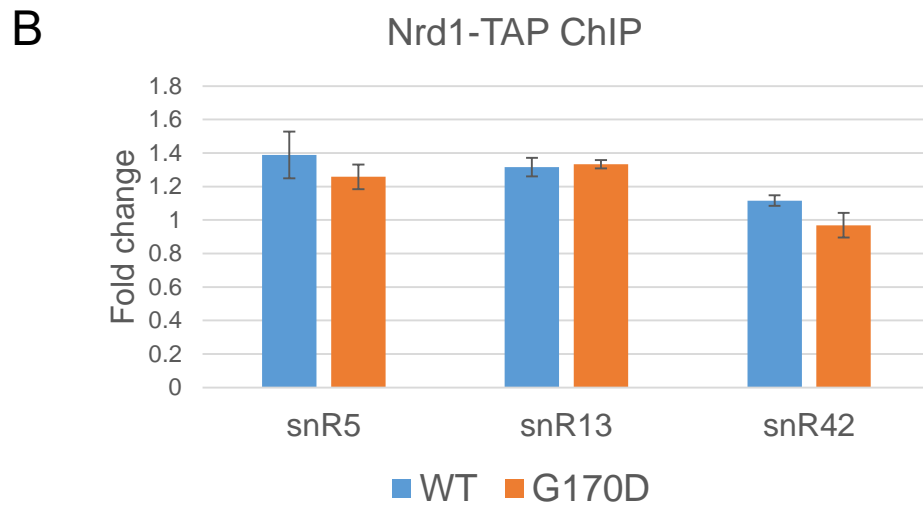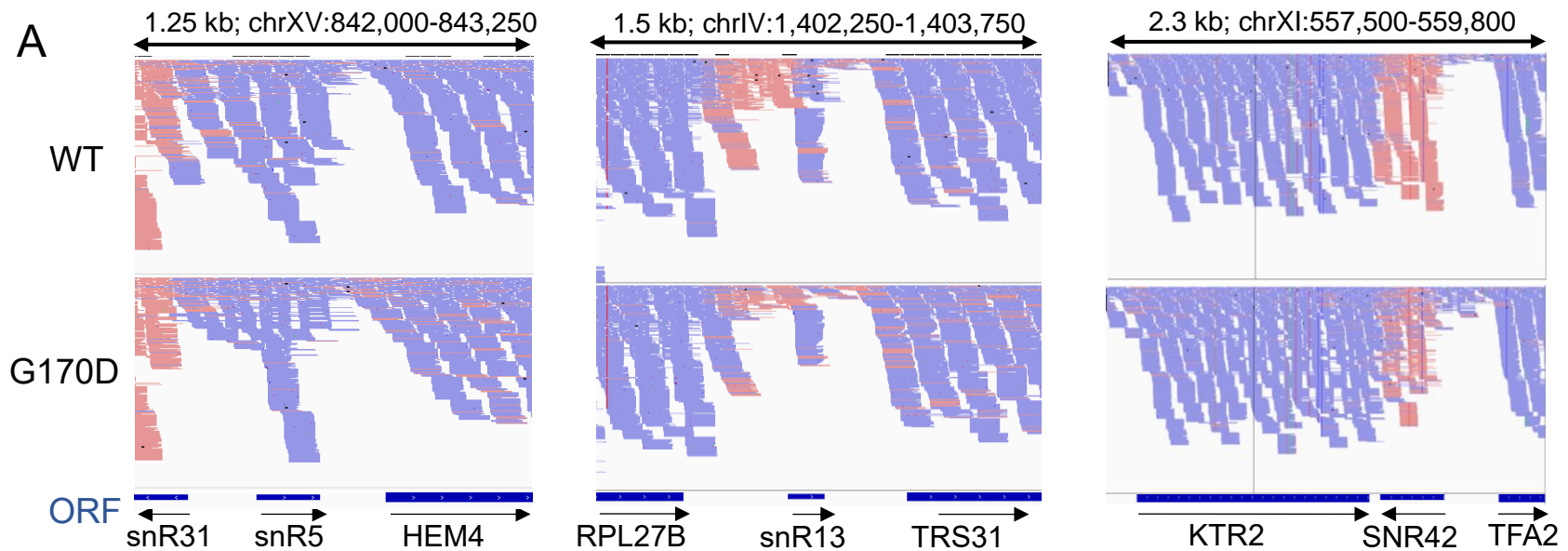
Figure 4.2.18. **Hsp90 inactivation does not cause transcription termination defects at snoRNA genes.**
A. Aligned RNA-Seq reads obtained from RNA isolated from WT and G170D strains grown at non-permissive temperature (6 h at 37 ˚C) depicting unaltered reads at snoRNA genes' terminators. B. Nrd1-TAP DNA occupancy measured for WT and G170D at the 3' locations of the given snoRNA genes in A. under the same conditions.
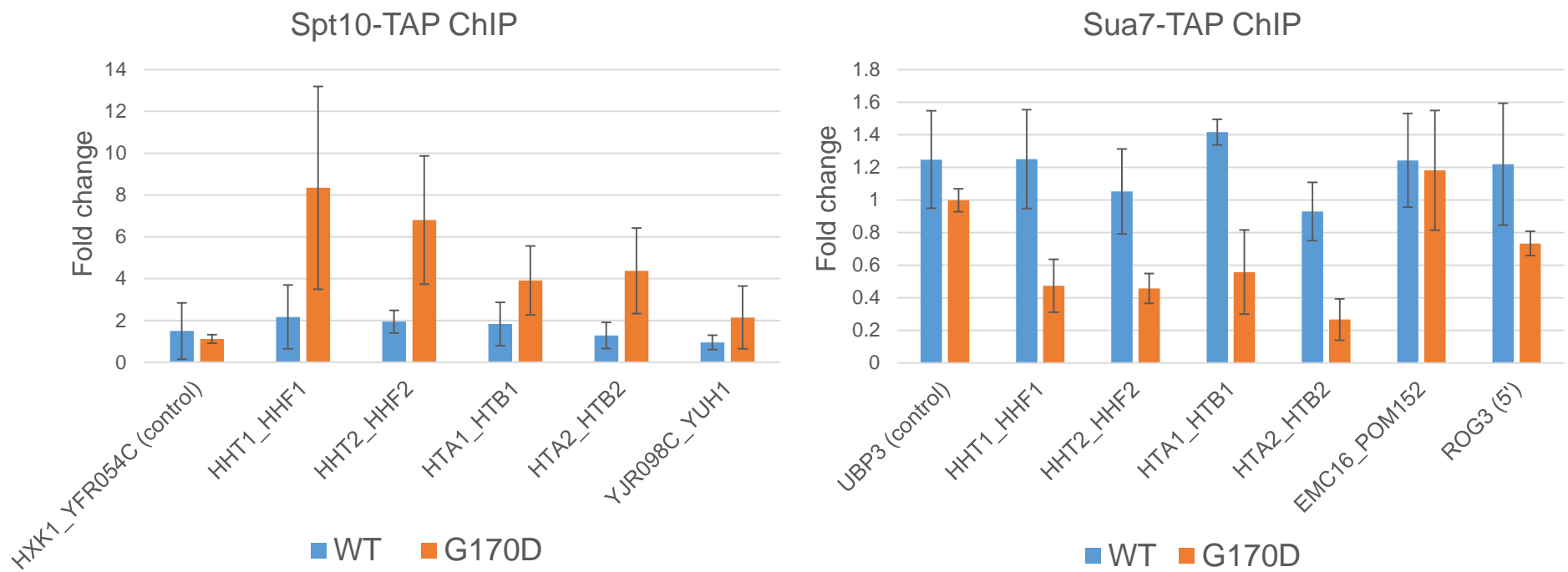
Figure 4.2.19. **Hsp90 inactivation leads to enrichment of Spt10 and loss of Sua7 at divergent histone promoters.**
Spt10-TAP and Sua7-TAP DNA occupancy at the divergent histone promoters in WT and G170D strains grown at non-permissive temperature (6 h at 37 ˚C).

| Merged | Anti-Hsp90 (rabbit) + anti-rabbit-FITC | DAPI |
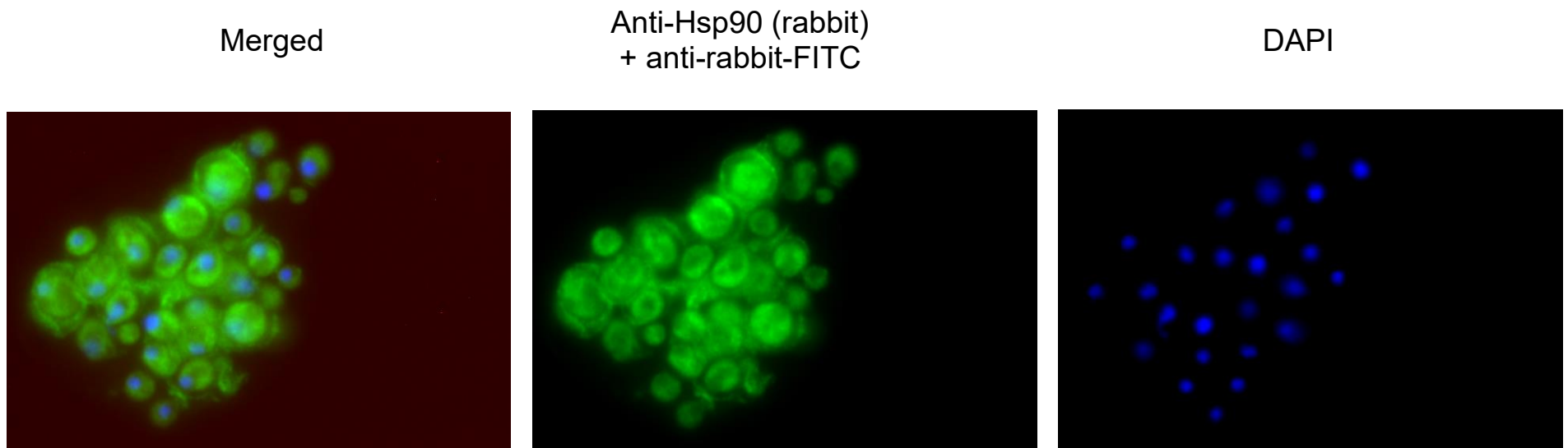
Figure 4.2.20. **Hsp90 is a nuclear protein**.
The cellular localization of yeast Hsp90 was determined by indirect immunofluorescence on spheroplasts using primary antibodies raised against Hsp90 and an AlexaFluor488-conjugated secondary α-rabbit antibodies. ImageJ was used to determine the percent area of each nuclei relative to the total spheroplasts area along with the relative Hsp90 signal intensity. In conjunction with the established copy number of Hsp90 molecules per cell (Ghaemmaghami *et al*., 2003), the nuclear concentration of Hsp90 was calculated to be 1.87 μM.

4.3. P23

Even before CCT and Hsp90, implementation of DNaseI-Seq high-throughput technique mentioned in the previous chapters revealed that chromatin architectural changes are dependent on p23 (Zelin 2012). One of the features was gain of the open chromatin locations – increased cleavage density in p23 deletion strain compared to the WT was shown for a select location (Figure 5B in Zelin 2012). It was substantiated that in the absence of p23 altered transcription factor DNA occupancy contributed to the observed phenotype. By inspecting identified consensus motifs within the sites of increased hypersensitivity, it is evident that Rsc3 and Rsc30 are some of the enriched transcription factors as well (Figure 4.3.1). In addition to this, genome-wide physically detectable p23 and RSC target genomic locations suggested about 40% colocalization with the total RSC detectable pools (Figure 4.3.2). Used RSC data stem from two different maps based on different experimental approaches (Ng 2002, Parnell 2015). Even though Fisher's exact test confirmed the high correlation between p23 and RSC maps (p value $1x10^{-104}$ and $1x10^{-71}$), the two RSC data sets correlate poorly with each other by giving only 80 mutual locations. This observation was attributed to the possibility that RSC as a very dynamic chromatin remodeling complex is difficult to re-locate under different experimental settings whereas p23 could consistently target RSC, provided p23 is able to do so.
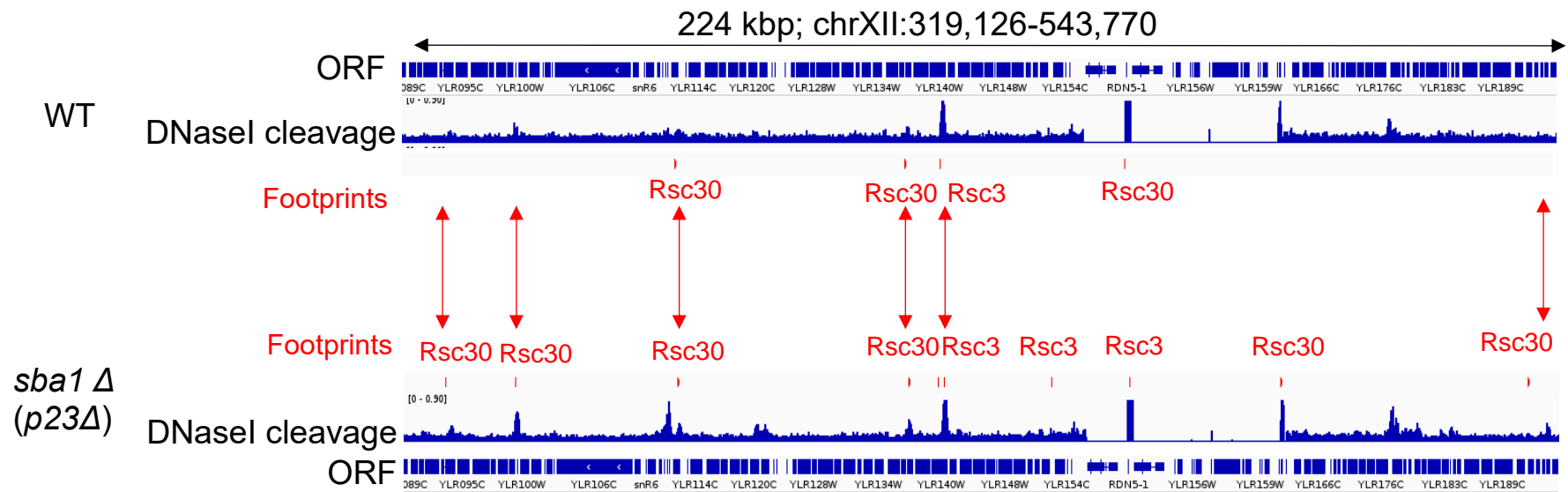
Figure 4.3.1. **P23 loss correlates with gained RSC footprints at select locations with increased hypersensitivity.**
DNaseI cleavage rate for WT and *Δsba1* (Zelin 2012) and footprints identified with the program from Hesselberth 2009, for which Rsc3/30 motifs were detected using RSAT (van Helden 2000) with frequency matrices obtained from JASPAR (Sandelin 2004)
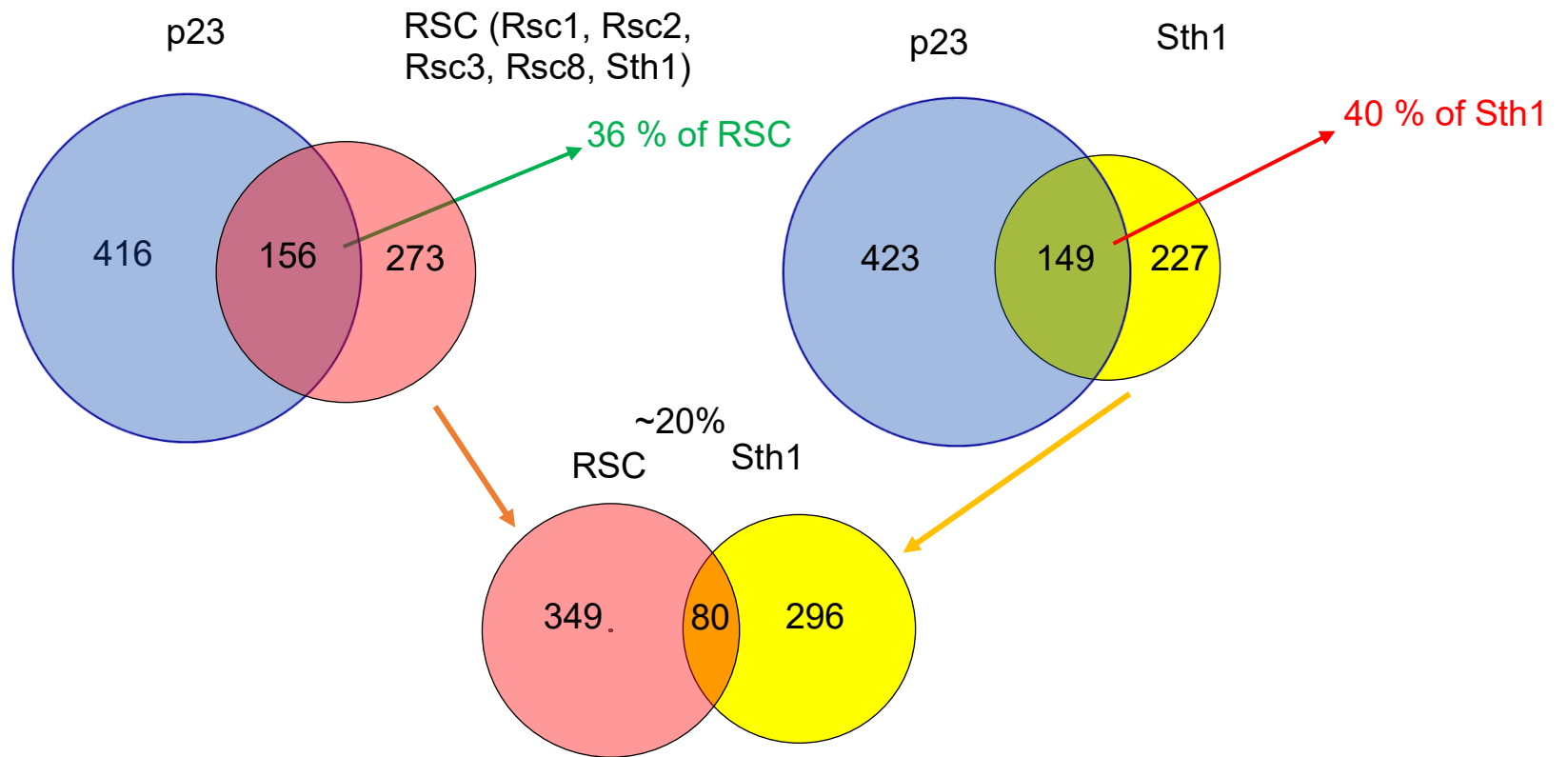
Figure 4.3.2. **P23 and RSC target genomic locations colocalize, but different RSC data sets do not.**
Overlap between p23 Chip-Seq data and different RSC data sets: (left) Ng 2002, (right) Parnell 2015.

Given the changed chromatin at the locations where RSC and p23 physical co-occur and finding about their genetic interaction (Echtenkamp 2011), it was further inspected how p23 could affect RSC, as a multi-subunit complex, functionally. To check whether p23 is able to alter RSC-DNA structure, recombinant purified RSC complex was titrated to the reaction containing radiolabeled *PHO8* promoter probe, a prominent RSC target location (Wippo 2011) (Figure 4.3.3A). P23 was able to dissociate RSC from the DNA in a concentration-dependent manner, with noticeable effect at 4 µM, which corresponds to the nuclear p23 concentration. As a control, titration of p23Δ84 protein defective in chaperone activity did not affect RSC-DNA complex (Figure 4.3.3A). As mentioned earlier for Hsp90, the next step entailed usage of two-hybrid assay to test whether p23 physically associates with any of the RSC subunits to release entire complex from the DNA. The assay suggested negative interaction between p23 and Rsc3, as well as Sth1 (Echtenkamp 2016), comparable to Hsp90. In addition and different than for Hsp90, the assay revealed a positive interaction between p23 and Rsc30. The two-hybrid results were further substantiated via EMSA using purified recombinant Rsc3, Rsc30 and Sfh1 (shown later) to which p23 titration was applied. P23 was able to displace Rsc3 from the DNA, and not Rsc30 (Figure 4.3.3B). Rsc3 and Rsc30 are capable of forming a heterodimer (Angus-Hill 2001) and this was reconstituted *in vitro* with equimolar amounts of proteins that migrated as a single band (Figure 4.3.3C). P23 was able to release Rsc3/30 heterodimer indicating that Rsc3 was sufficient for p23 to act on the DNA-bound complex. Finally, the application of anisotropy in which reactions, similarly to EMSA, were monitored for the ability of the protein or complex to bind fluorescein-labeled DNA and p23 to foster transitions were examined over time (Figure 4.3.4). Whereas unlabeled competitor DNA did not significantly alter the occupancy of the RSC to its pre-bound DNA, p23 readily accelerated its off rate. It was also apparent that p23 reinforced the off-rate of Rsc3 and it did not affect Rsc30, which is in corroboration with two-hybrid and EMSA. Based on these findings, we concluded that p23 is capable of physically associating with Rsc30 to displace RSC complex via Rsc3 subunit.
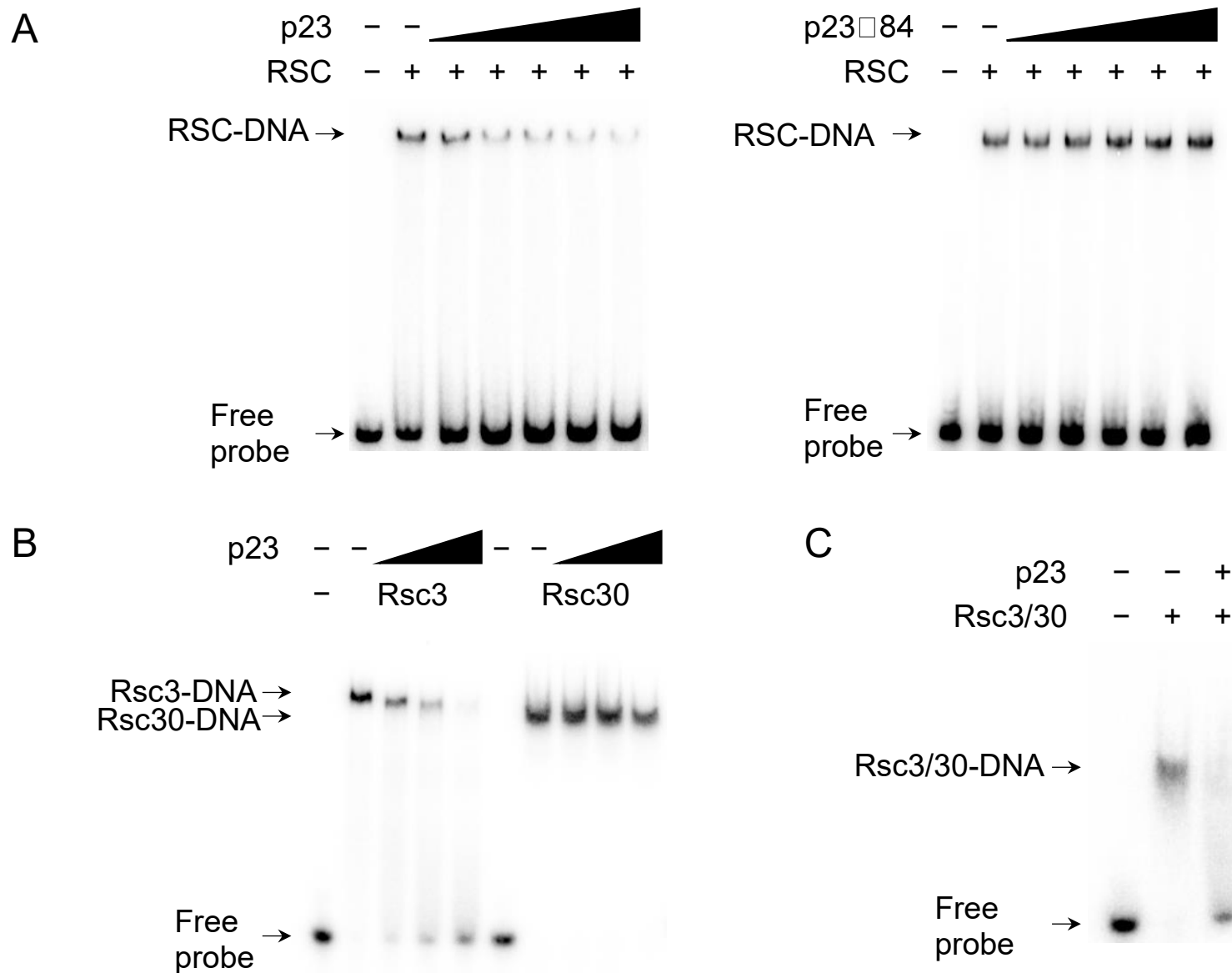
Figure 4.3.3. **P23 dissociate RSC from the DNA targeting select subunits.**
A. RSC-DNA binding activity monitored by EMSA using purified RSC (5 nM) and radiolabeled *PHO8* promoter DNA (12.5 nM). The influence of p23 on RSC-DNA structure determined using a titration (0, 1, 2, 4, 8 and 16 µM) of full length p23 or mutant p23Δ84. B. The influence of p23 (0, 4, 12 and 32 µM) on DNA binding activities (*ACC1_TIM23* promoter probe, 20 nM) of purified recombinant Rsc3 and Rsc30 (180 nM). C. The effect of p23 (6 µM) on Rsc3/30 heterodimer bound to *ACC1_TIM23* promoter probe (20 nM).
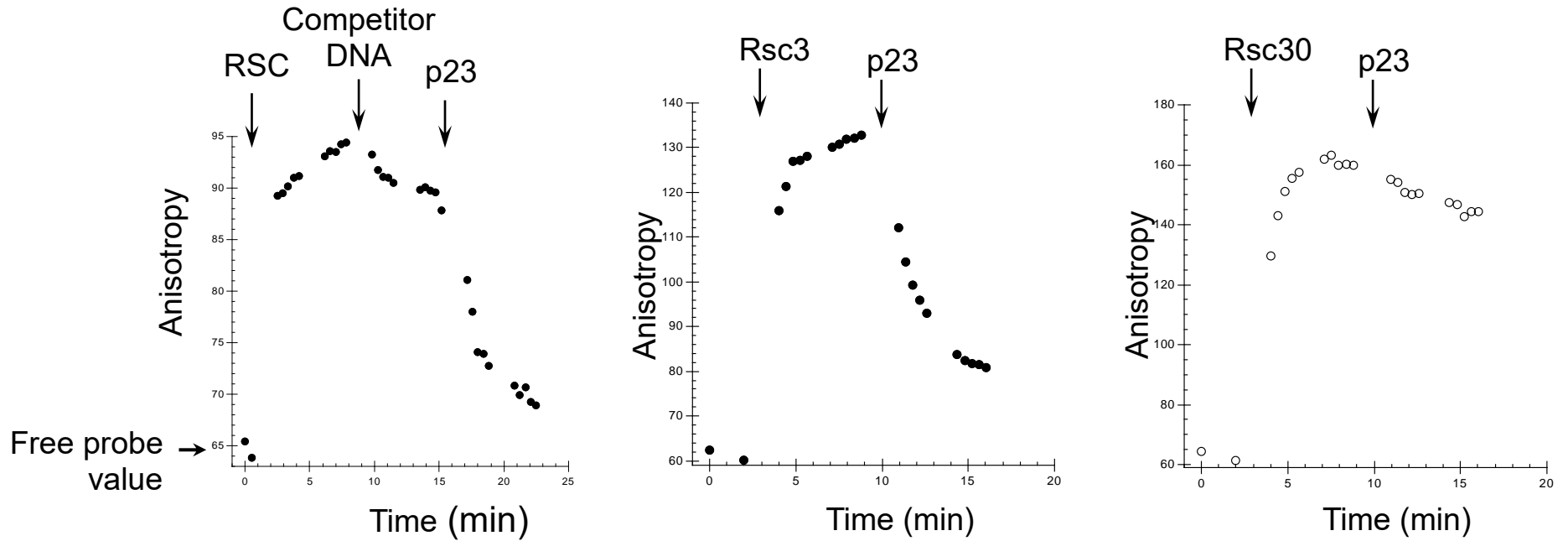
Figure 4.3.4. **P23 fosters off-rate of RSC and Rsc3.**
P23's ability to dissociate RSC-, Rsc3- and Rsc30-DNA complex was monitored by fluorescence anisotropy using fluorescein-labeled oligonucleotide (*ACC1_TIM23* promoter, 80 nM). Free probe value represents anisotropy (mAU) before protein addition and the proteins, purified RSC (5 nM), purified recombinant Rsc3 or Rsc30 (180 nM) and p23 (20 µM), or unlabeled competitor probe (1.25 µM) were added at indicated time points.

Despite binding DNA and nucleosomes with comparable affinities, RSC's more physiological target is a nucleosome (Sengupta 2001). Similarly as described for Hsp90, it was studied whether p23 impacts RSC remodeling activities using centrally positioned mononucleosomes resolved on EMSA. RSC bound the nucleosome independent of ATP and formed an activated nucleosome structure upon ATP addition (complex 2) (Lorch 1998) (Figure 4.3.5). In the presence of p23, the remodeling reaction was driven to completion, as evidenced by the release of terminally localized mononucleosomes and/or free DNA (lanes 10-13) (Figure 4.3.5). In the absence of ATP, p23 triggered dissociation of RSC from the unremodeled mononucleosomes (lane 14) (Figure 4.3.5). Thus, p23 differentially impacts RSC in an ATP-dependent manner (i.e., in the presence of ATP, p23 fosters the remodeling reaction, but in the absence of ATP, p23 dissociates the idle complex). For a comparison, Hsp90 dissociated RSC-nucleosome structure without affecting the state of the nucleosome (4.2.3B), as described in the previous chapter. Perhaps due to p23's physical docking to Rsc30, one of the RSC subunit, p23 exerted greater modulatory effects on RSC than Hsp90 – it fostered its remodeling in addition to separation of the RSC-nucleosome structure.
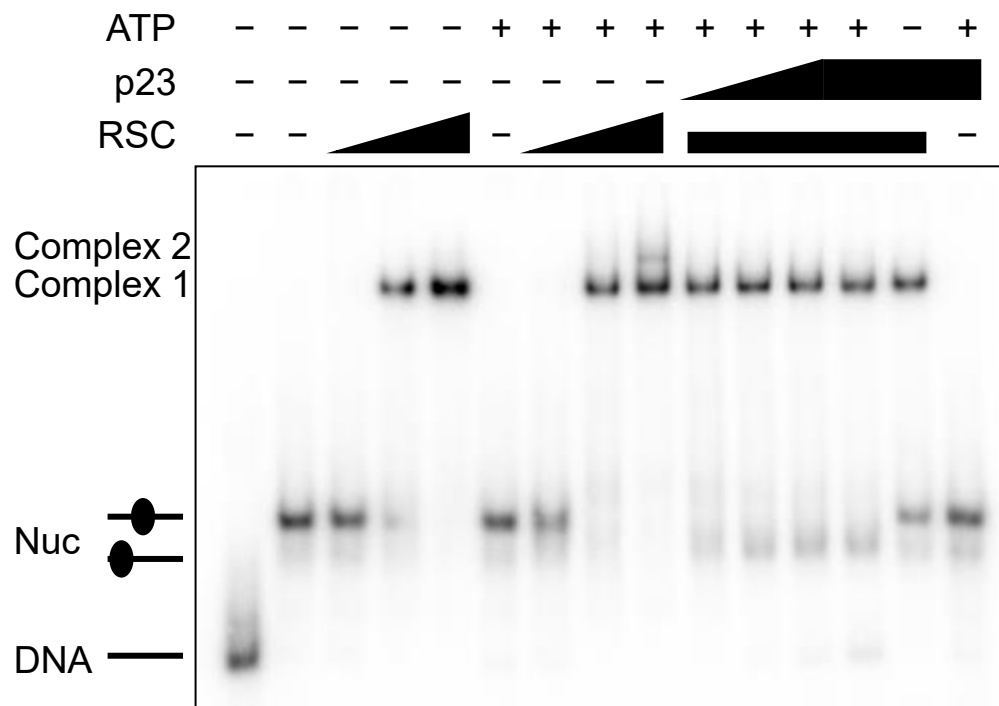
Figure 4.3.5. **P23 promotes RSC remodeling *in vitro.***
RSC nucleosome binding and remodeling activity was checked by EMSA using nucleosomes prepared with radiolabeled 601-positioning DNA and titrations of purified RSC (1, 5, and 10 nM). The influence of ATP (1 mM) and p23 (1, 3, 5, 15 µM) were assessed, as indicated. The migration points of free DNA, nucleosome with centrally or terminally positioned histones, and RSC-nucleosome structures (complex1 and 2) are marked.

The ways in which p23 regulates RSC lay beyond targeting Rsc3/30 heterodimer. P23 readily displaced purified RSC complex lacking Rsc3, Rsc30 or even Rsc7 (Figure 4.3.6) – the crucial subunit which was proposed to hold entire complex together (Wilson 2006). RSC*Δrsc30* and especially RSC*Δrsc7* conferred weaker EMSA signal than the WT RSC at the same protein concentrations, indicating problems with the DNA binding, likely due to impaired complex integrity. These complexes were correspondingly more easily displaced from the DNA by p23. RSC apparently binds DNA through several subunits and p23 abolishes all these interaction. P23 was shown to dissociate recombinantly purified Sfh1 (Figure 4.3.7A). Interestingly, partially cleaved Rsc3, Rsc30 and Rsc3/30 heterodimer that retained DNA binding potential were still targeted by p23 (Figure 4.3.8). This would indicate that p23 suffices DNA binding domains or other robust domains that remained unaltered after proteolytic cleavage.

In miscellaneous EMSA screens, p23 was shown to release close to almost any protein or complex. Amongst discovered targets were SAGA histone methyltransferase – another multi-subunit complex, Ino2 and Ino4 transcription factors and maybe Ino2/4 heterodimer as well (Figure 4.3.7). It is unclear whether CCT has DNA binding activities or rather its unavoidable co-purifying clients gave DNA binding signal, which is eliminated by p23. Hence, p23 seems to hold a role of a universal DNA displacer.

Because main chaperones showed strong involvement in intergenic cryptic transcription due to impaired directionality at the 5', it was appealing to check whether this extends on p23, as a part of Hsp90 system or independently. In this work, H2A.Z loss was viewed as an indirect hallmark of the sites affected by divergent transcription. The absence of p23 did not alter H2A.Z levels at the locations previously shown to be subject to cryptic transcription in the cells lacking CCT, Hsp90 and likely Hsp70 (Figure 4.3.9). This might indicated that p23 absence does not empower aberrant transcription. However, further RNA quantification in the cells with triggered p23 loss, rather than deletion strains, would be required to rule out this possibility.
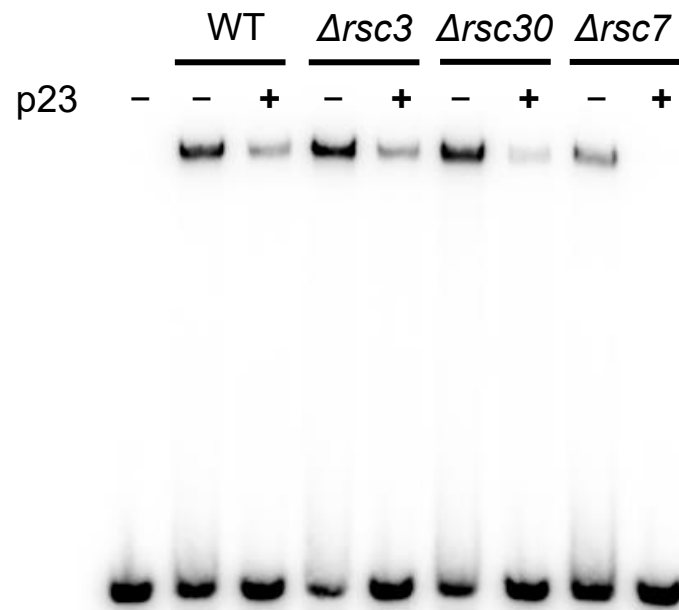
Figure 4.3.6. **P23 dissociate RSC-DNA complex despite RSC lacking crucial subunits.**
A. DNA binding activity of RSC complexes deleted for subunits (*Δrsc3*, *Δrsc30*, *Δrsc7*) monitored by EMSA using purified RSCs (WT, *Δrsc3*, *Δrsc30*, *Δrsc7*) (5 nM) and radiolabeled PHO8 promoter DNA (12.5 nM) without or with p23 (8 μM).
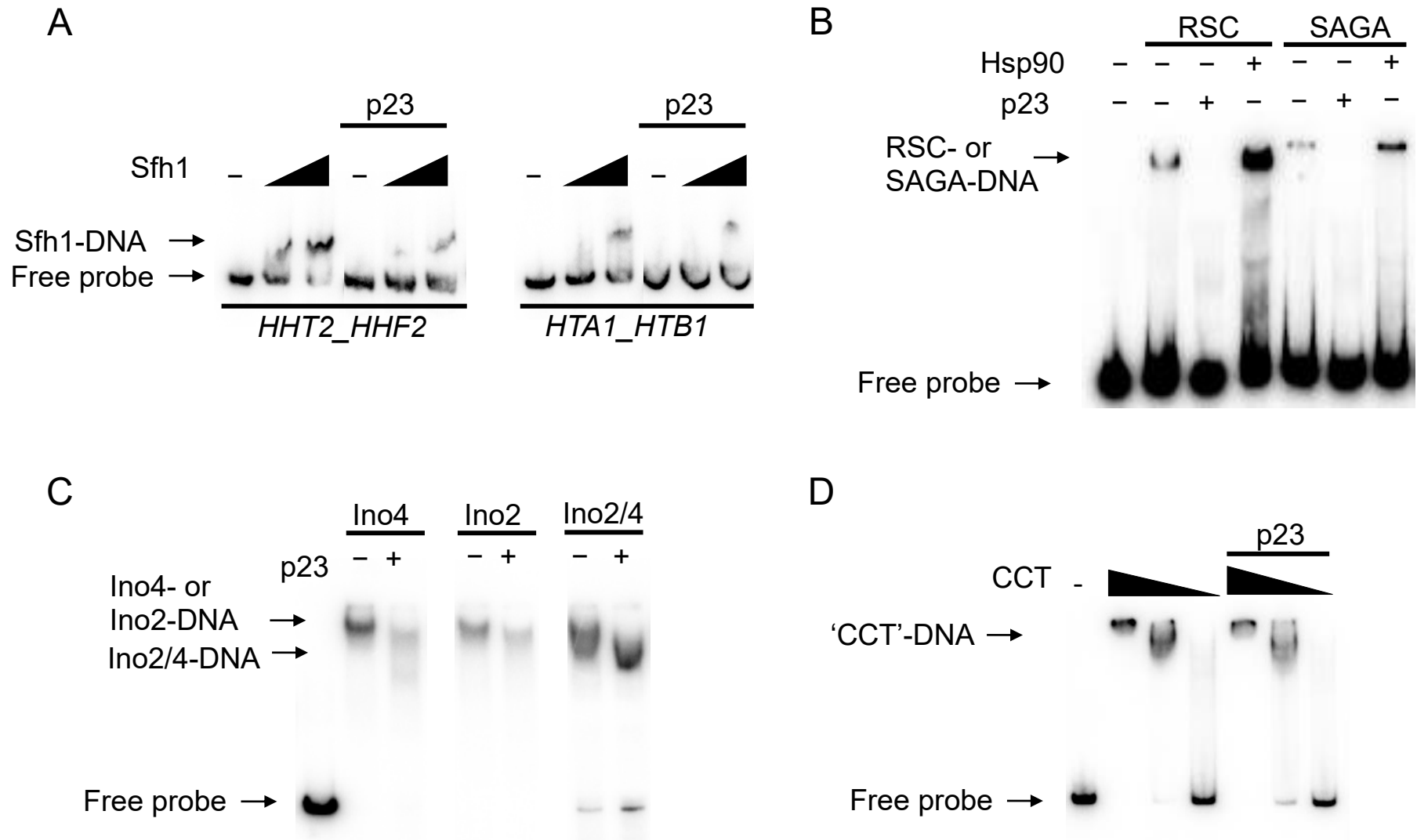
Figure 4.3.7. **P23 dissociate various proteins and complexes from DNA *in vitro*.**
A. Binding of recombinant purified Sfh1 at histone promoter probes (*HHT2_HHF2* and *HTA1_HTB1*) containing 4x upstream activating sequence was monitored by EMSA in the presence of p23. B. The ability of p23 to dissociate SAGA-DNA complex, similarly to RSC-DNA, was examined with purified yeast SAGA complex (20 nM), radiolabeled INO1 promoter (50 nM) and p23 (20 μM). C. DNA binding of recombinant Ino2, Ino4 or Ino2/4 heterodimer was tested using radiolabeled INO1 promoter (20 nM) in the presence of p23 (20 μM). D. Human recombinant CCT (400, 40, 4 nM) or its co-purifying components bind DNA (20 nM), which is affected upon p23 addition (20 μM).
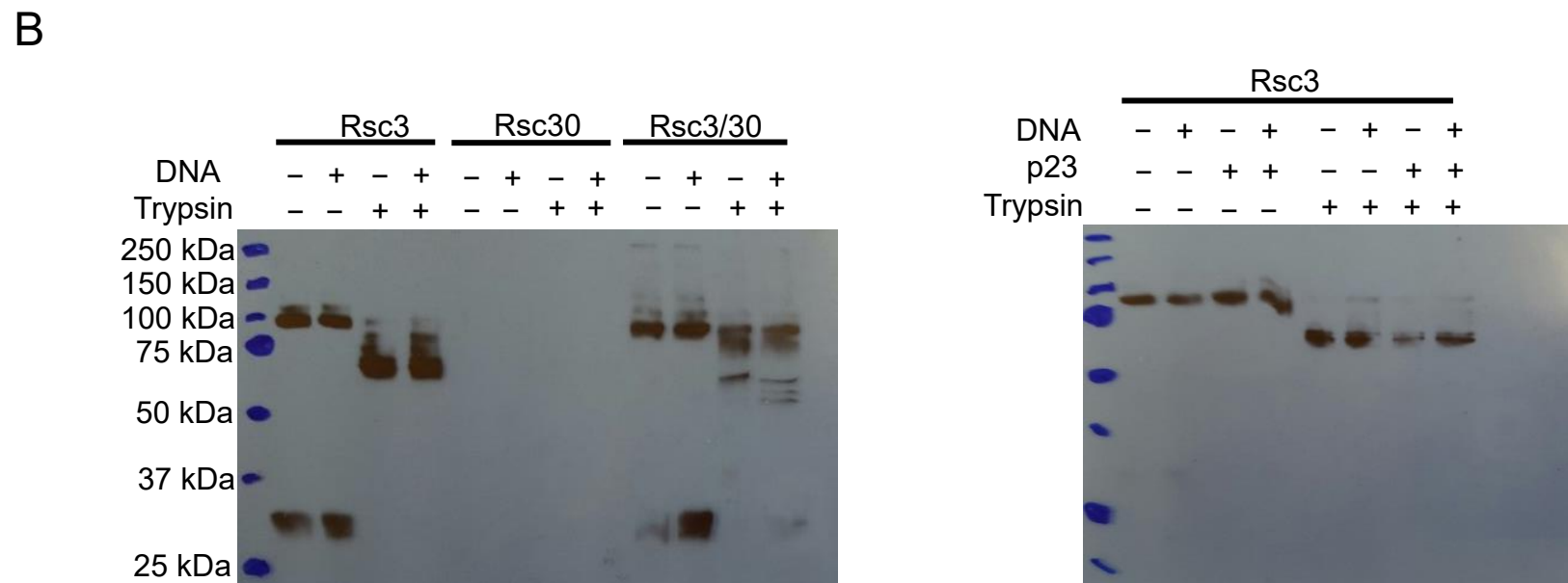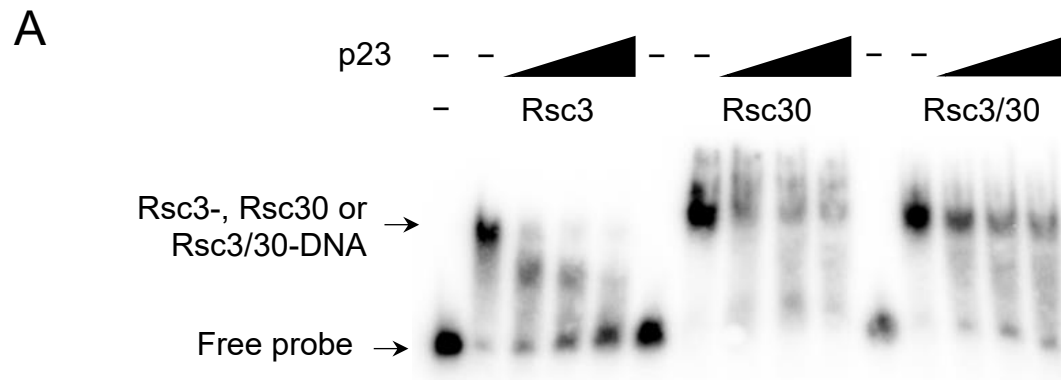
Figure 4.3.8. **Partially cleaved Rsc3 and also Rsc3, Rsc3/30 are still subject to p23-mediated displacement from DNA.**
A. The ability of p23 (0, 4, 12 and 32 μM) to dissociated purified recombinant and tryptically digested Rsc3, Rsc30 and Rsc3/30 (200 nM) from the *ACC1_TIM23* probe (20 nM) was examined via EMSA. B. The effect of partial digestion of Rsc3 in the presence of DNA, Rsc30 and p23 was examined by Western blotting against αRsc3 antibodies.

Δp23 H2A.Z-TAP/ WT H2A.Z-TAP ChIP
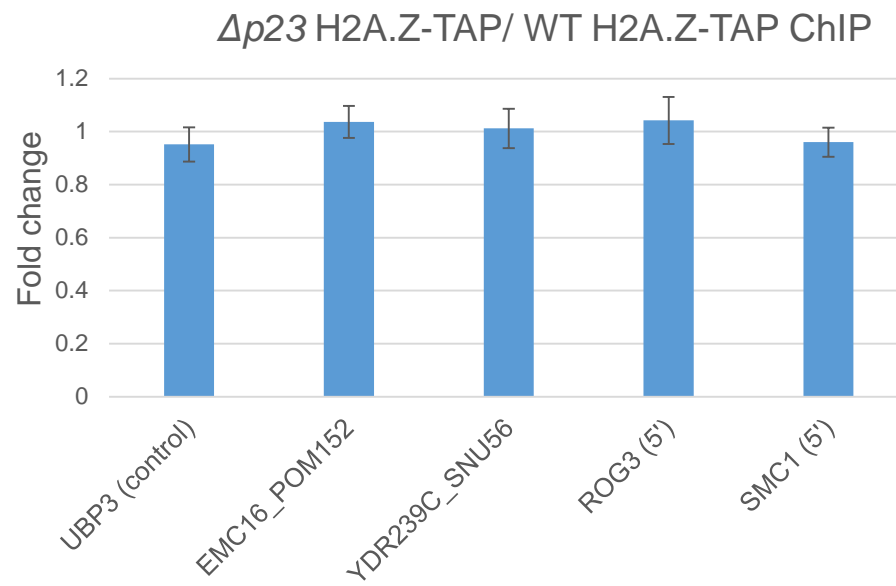
Figure 4.3.9. **P23 does not affect H2A.Z levels like other chaperones.**
H2A.Z occupancy measured in *Δp23* against WT using αH2A.Z antibodies at the locations that are subject to 5' bidirectional transcription upon CCT, Hsp90 and likely Hsp70 depletion.

4.4. Hsp70

Hsp70 temperature sensitive strain *ssa1-45* (Taxis 2003) was used to study how Hsp70 connects to chromatin, comparable to previously described chaperones. DNaseI-Seq was to be implemented as a startup to investigate whether Hsp70 is also involved in modulation of the chromatin architecture. For the purpose of this experiment, WT and *ssa1-45* were grown at non-permissive temperature for 4 h and DNaseI titration was applied to the isolated nuclei. The concentration range reaching partial digestion of the chromatin was suitable to proceed with. It was observed that chromatin from *ssa1-45* strain was over-digested at three times lower DNaseI concentration than WT's chromatin (6 U/ml for WT vs. 2 U/ml for mutant). The strong effect was not the case for other chaperone strains – CCT WT did necessitate lightly higher DNaseI concentration than *cct1-2* to obtain the equal partially digested chromatin (WT 4-5 U/ml, *cct1-2* 2-3 U/ml) and no change for Hsp90 WT and G170D was needed (2 U/ml for both Hsp90 WT and G170D). This indicates that chromatin in the absence of functional Hsp70 is rather sensitive to DNaseI digestion, excessively open due to loss of nucleosome/histones or subject to other processes which led to this result.

Because both CCT and Hsp90 delivered very similarly results in terms of 5' bidirectional cryptic transcription and associated H2A.Z loss at the affected locations, it was quickly checked whether Hsp70 absence has the potential to generate the same phenotype. This would imply that all three major molecular chaperones connect to the same nuclear process or maybe even the identical clients to control the global propensity of the RNA polymerase to fire in both directions. As seen from the Figure 4.4.1, H2A.Z loss and increase in H3K79me3 transcriptional marker were detected upon Hsp70 depletion at the identical locations used to test other chaperones. Hence, there is a good chance that Hsp70 is involved in cryptic intergenic and/or 5' transcription events as well.
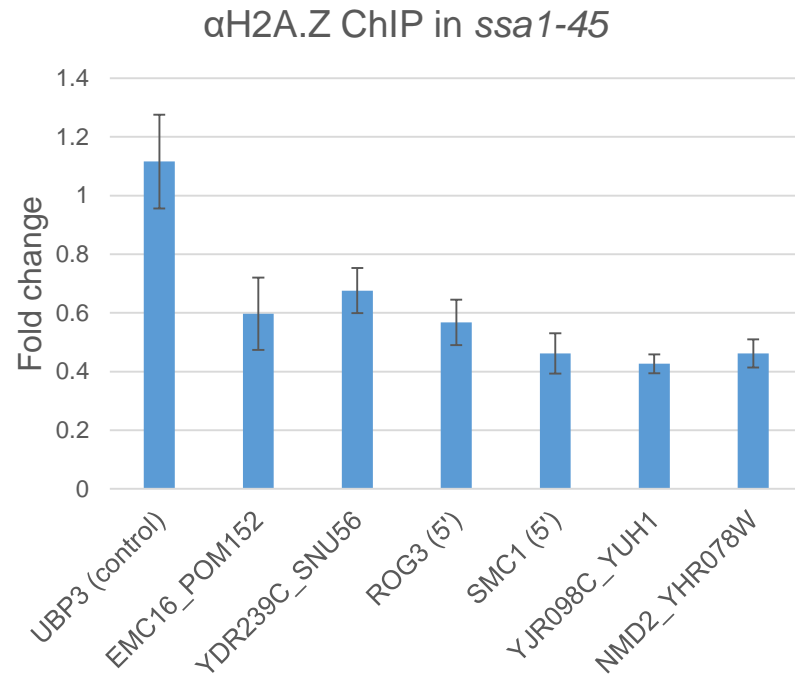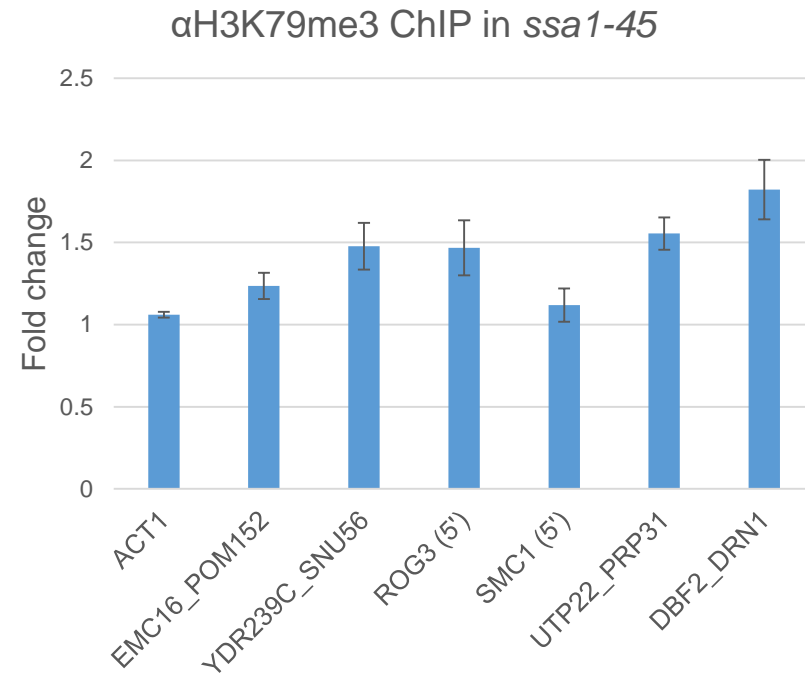
Figure 4.4.1. **Hsp70 inactivation leads to H2A.Z loss and likely 5' bidirectional transcription.**
A. H2A.Z DNA occupancy measured in the temperature sensitive Hsp70 strain, *ssa1-45*, grown at non-permissive temperature, normalized against control (strains grown at 30 ˚C), at the locations previously shown to be affected by 5' bidirectional transcription upon inactivating either CCT or Hsp90. B. Chromatin immunoprecipitation in *ssa1-45* with H3K79me3 antibodies at the location affected by 5' bidirectional/intergenic transcription in CCT and Hsp90.

5. Summary and Discussion

5.1. CCT

CCT (TRiC) is traditionally a cytosolic chaperonin that primarily contributes to protein homeostasis by facilitating the assembly of protein complexes. The work presented here explored CCT's roles in the nucleus, both literature-wise and experimentally. Historical overview of bacterial CCT homolog pointed out, previously less pronounced, essentiality of GroEL/ES in bacterial transcription and replication. Regarding eukaryotes, CCT was observed in the nucleus yet its functional nuclear roles remained unexplored. With the rise of high-throughput interactome maps, CCT's connection to the nucleus appeared more relevant. Here, for the first time, nuclear functions of CCT were addressed empirically in detail. Thereby, three high-throughput approaches suitable for *de novo* nuclear protein characterization were implemented in conjunction with the temperature sensitive CCT strain *cct1-2*.

RNA-Seq, as mean to evaluate transcription dependencies, revealed that CCT inactivation resulted in intergenic cryptic transcription. The intergenic transcripts were located close to or within the same canonical promoter, and were divergent in directionality to canonical ORF transcripts. This classifies the process as 5' bidirectional transcription, by which 70% of all ORFs were affected. Thereby, no impactful gross gene expression changes were correlated with 5' bidirectional transcription. CCT inactivation also led to the antisense transcription for the subset of subtelomeric genes, as well as termination defects at snoRNA genes.

Unravelling CCT roles in 5' bidirectional transcription entailed examination of CCT interactors. Since CCT interacts with numerous crucial chromatin regulators that are implicated in transcription, the aim was to detect CCT dependencies therein. Because

one prominent group of CCT interactors were histone modifiers, histone code changes were inspected. Thereby, specialized histone mass spectrometry, which focuses only on histone post-translational modifications, was utilized on the histones obtained from wild type and *cct1-2* strain grown under non-permissive temperature. The results revealed increase of H3K79me3 mark in *cct1-2* – a mark catalyzed by Dot1 methyltransferase (Feng 2002, Ng 2002, van Leeuwen 2002). H3K79me3 mark is known to demarcate regions of active transcription (Im 2003, Jaskelioff 2003, Martin 2005, Vakoc 2006, Kitada 2012, Xue 2015, Xue 2017). Hence, it is not expected within intergenic regions. Increase of H3K79me3 in combination with increased cryptic intergenic transcription in *cct1-2* suggested that H3K79me3 surge could be within intergenic locations. Although mild, the increase of H3K79me3 within intergenic locations or regions affected by 5' bidirectional transcription was validated. However, preceding steps to H3K79me3, such PAF1-complex mediate elongation, and further examination of Dot1-mediated H3K79me3 itself, could not offer the mechanistic explanation for the cause of the 5' bidirectional transcription in *cct1-2*. In simplicity, deletion of Dot1 – the sole enzyme responsible for H3K79 methylation, did not affect events associated with 5' bidirectional transcription, such as H2A.Z decline. H3K79me3 thereby appeared to be the end result of the transcription event. H3K79me3 could offered other lines of conclusions. Because H3K79me3 is transcriptionally concomitant mark, the results were in favor of hypothesis that intergenic cryptic transcripts in ts *cct1-2* were rather a direct consequence of the cryptic transcription than a result of defective RNA degradation and changed steady-state RNA levels.

H3K79me3 was mentioned to be mutually exclusive with H2A.Z histone variant (Li 2005) and H2A.Z-containing, +1 nucleosome, locations (Zhang 2005) overlapped with the sites affected by 5' bidirectional transcription upon CCT inactivation. In addition, assessing H2A.Z occupancy revealed two-fold decline at the affected sites in *cct1-2*. Due to its previous implications in both canonical transcriptional regulation and cryptic transcription (Zlatanova 2008, Jeronimo 2015), it was hypothesized that H2A.Z was linked to the 5' transcriptional anomaly. Chromatin remodelers and histone chaperones that mediate H2A.Z removal and deposition, and histone chaperones involved in general

histone turnover, were interrogated for their DNA occupancy at affected locations and general protein complex compositions, as well as steady state protein levels. Since tested regulators were not involved and since the sole decline of total H2A.Z levels was observed, the dependence of bidirectional transcription on H2A.Z was tested using anchor away method. Triggered nuclear H2A.Z depletion did not alter 5' or any other transcription event. Because of the genetic connection, CCT and H2A.Z are still anticipated to show partitions within the same pathways, and details are to be elucidated in the future. The results here, although negative for CCT phenotype, are a contributory observation for the transcription field. H2A.Z transcriptional roles have been vaguely defined, especially since the evolutionary conserved histone variant holds contradictory functions. H2A.Z is believed to serves as a transcriptional activator by posing for transcription initiation or it allows for nucleosomal susceptibility (Zhang 2005, Adam 2001, Santisteban 2011). On the other hand, transcriptionally inhibitory effects of H2A.Z were reported, in terms of global gene downregulation or negatively affected recruitment of transcriptional apparatus (Adam 2001, Meneghini 2003). Adding on to this now – H2A.Z occupancy and total levels decline correlate with 5' bidirectional cryptic transcription upon CCT inactivation. Furthermore, the transcriptome does not change by forcing H2A.Z out of the nucleus. The unaltered transcriptome profile upon triggered H2A.Z depletion, and not complete HTZ1 depletion, was not anticipated, but also never interrogated or at least not reported. It remains to be answered, why H2A.Z remains involved, but it is not essential for the above processes. Perhaps H2A.Z presence within +1 nucleosome and operation on the transcription level undermine its traditional physical involvement at the affected locations and are linked to aiding remote signaling events within the same process.

Histone mass spectrometry on the histones derived from the wild type and *cct1-2* strain also revealed a mild decline of H3 and H4 histone tail acetylations in *cct1-2*. According to the interactome map, CCT interacts with almost all histone acetyltransferases and deacetylase complexes. It was thereby examined whether HATs SAGA and NuA4, as well as HDACs Rdp3S/L, Set3C and Hda1 are altered in *cct1-2* with respect to the wild type. As an oligomer-assembly chaperonin, it was expected that the

protein complexes would be affected, yet this was not the case. CCT was not able to alter occupancy at the target locations, nor enzymatic abilities of the select tested components. Other targets famous for cryptic transcription, such as Rpd3S-Set1 and Set3C-Set2 histone deacetylase-histone methyltransferase pairs were unaffected as well. The question remains whether the mild acetylation decline is significant, and if so, whether indirect events led to such an outcome. Often times it is reported that deprivation of an HAT (or an HDAC) leads to both increase of acetylation at some and decline at the other gene targets (Robyr 2002, Roh 2004), suggesting compensatory mechanisms within the complex regulatory network. Examination of genetic connection undoubtedly points out the existing parallels between CCT and histone modifiers, and CCT deprivation might have affected the histone code balance indirectly.

Since none of the chromatin regulators reported within transcription field, as well as many other CCT chromatin interactors, turned out positive, the intuitive next target was RNA polymerase holoenzyme itself. PIC was already described to evict H2A.Z in a transcription-coupled manner (Hardy 2009, Hardy 2010, Tramantano 2016), and increased cryptic transcription here could have enhanced the effect. According to this, PIC would be a target, not H2A.Z. RNA polymerase II holoenzyme is a complex entity consisting of 10-12 subunits (Myer 1998). Adding to this is an array of basal transcription factors, such as TFIID, TFIIB, TFIIA, TFIIH, TFIIF, TFIIE, and coactivators such as mediator or SAGA (Hahn 2005) – each of which vary in subunit number, hence size, recruitment timing and overall function. According to the interactome maps, CCT does connect to RNA polymerase, select basal factors and activators. The challenging question is – who would be affected within transcription complex by CCT such that transcriptional directionality is lost upon CCT depletion? TFIID subunit was discovered to have reduced protein levels in *cct1-2*. TFIID is required for the formation of a pre-initiation complex as it recruits downstream factors (Shen 2003). In yeast, it consists of fourteen TATA associated factors (TAFs) and one TATA binding protein (TBP) (Sanders 2002). Unlike for TBP, whose role is to recognize and bind TATA box, the contributions of the TFIID TAF components have not been fully dissected. Yet, 84% of the yeast genes are known to be transcriptionally dependent on TAFs (Shen 2003) and TAFs are believed to serve

as promoter-recognition factors and coactivators (Albright 2000). It could be that CCT aids TAF assembly within TFIID. Promoter-specific variations of TFIID were reported (Maston 2012) and CCT might be responsible for the assembly of differential TFIID modules. It should be emphasized that not all components of RNA polymerase complex were tested and it remains to be verified whether the phenotype in *cct1-2* would actually be only due to TFIID. Hallmark transcription models propose an elegant sequence of events, such as recruitment of studied factors, for effective transcription initiation and elongation. The rising number of 'exception'-like findings might slowly dissuade these models and argue for the existence of promoter-specific requirements, perhaps promoter-specific modules of RNA polymerase-associated factors. RNA polymerase holoenzyme together with numerous other aiding factors would readily require folding assistance to meet the needs of specialized promoters or other genomic regions for the purpose of gene regulation. This process would be easily accomplished by molecular chaperones. In support of this notion, CCT inactivation was shown here to affect different RNA polymerase basal transcription factors at different regulatory locations: TFIIB at divergent histone promoters, TFIIH at snoRNA terminators and perhaps TFIID at 5' locations of majority of ORFs. While indirect contributions are possible, planned CCT/*cct1-2* ChIP-Seq experiments will hopefully deduce altered genome-wide CCT localization pattern, along with direct CCT involvement and the target genomic locations.

Antisense transcription was also observed for the subset of subtelomeric (or certain centromeric) locations in the absence of functional CCT. The cause for the phenotypes according to the RNA-Seq reads seemed to vary: (i) the terminator might have served as a promoter; or (ii) the upstream gene was transcribed reversely due to downstream 5' bidirectional transcription of the canonical promoter; or (iii) defective termination for canonical gene did not discontinue read-through. H2A.Z loss colocalized with antisense subtelomeric genes in *cct1-2*. H2A.Z was observed to colocalize with clustered subtelomeric genes and it has been believed to regulate their transcription and maintain the heterochromatin in general (Shia 2006). From the data in this work, aberrant transcription happened regardless of H2A.Z. If the antisense transcription in *cct1-2* occurs irrespective of H2A.Z presence, revision of previously assigned H2A.Z subtelomeric

regulatory roles would be needed. Subtelomeric genes are subject to different regulation compared to other genomic locations. SIR complex is known to be engaged at the telomeric locations to reinforce the spread of heterochromatin – this event is antagonized by SAS histone acetyltransferase complex (Grunstein 1997, Kimura 2002). SAS complex interact with CCT according to the newly obtained CCT E-MAP (epistatic miniarray profile, data kindly shared by J. Frydman). It is speculated that, similarly as proposed, CCT deprivation interfered with the transcriptional balance due to impaired location-specific chromatin regulators, in this case maybe SIR-SAS and concomitant factors.

CCT inactivation led to differential recruitment of histone-promoter specific activators. Regulation of four divergent histone promoters in fact is essential for entire genome – inappropriate amounts of histones would subvert both chromatin landscape and DNA processes such as transcription, replication and repair. In corroboration, despite the fact that Spt10, and also Spt21, bind only to the pairs of UAS at the divergent histone promoters, Spt10 was shown to be a global regulator affecting hundreds of genes (Hess 2004, Eriksson 2005). The cells devoid of SPT10 gene display sever growth defects (Natsoulis 1994) and in the absence of CCT, the effect is exacerbated, as shown via spot test assay in ts *cct1-2* strain with *Δspt10* grown at the lethal temperature. CCT seems to connect to Spt10 in various way. Deleted genes that caused double-mutant lethality or extreme sickness in combination with *Δspt10* are some of the prominent CCT interactors, such as SAGA, Rpd3-Sin3 and NuA4/Swr1 (Chang 2011). In contrary to this and quite interesting, genes whose deletion suppresses *Δspt10* growth phenotype are the ones involved in H2A.Z chromatin homeostasis, such as INO80 subunit IES3 and Nap1; then also Hda2 and Set3 HDACs (Chang 2011). Along with this, *Δspt10* cells have defective subtelomeric silencing as well (Braun 2007). Hence, it seems that Spt10, even though physically binding to non-H2A.Z promoters, is physiologically woven to H2A.Z-containg locations. The results about differential recruitment of histone promoter specific regulators could be also a pleiotropic or chaperone-dependent side effect. As CCT is essential, perhaps decline of cell-cycle specific regulator Spt21 prevailed due to underlying signaling to inhibit division. H3K56 acetylation declined within the promoters, signifying

that the synthesis of histones does not need to happen, and in this scenario, increase of Spt10 HAT occupancy was observed maybe due to hypoacetylated regulatory regions.

Positive correlation between increase of Huntington-driven aggregation and H2A.Z loss, hallmark of cryptic transcription, inferred that perhaps increase of proteotoxic stress under the conditions of inactivated CCT led to aberrant transcription. It would be worth testing whether cellular declining H2A.Z, and maybe other changed components, colocalizes with aggregation foci. Subverted transcriptional equilibrium could be assigned to the deprivation of the chromatin regulators, which might have ended up in misfolded foci. Other aggregation-prone chromatin targets within huntingtin interactome could be affected by Huntington and potentially contribute to the 5' bidirectional transcription. Interestingly and in corroboration with this, when comparing CCT nuclear interactome map with huntingtin transcriptional targets or interactors (Li 2004), Taf1 mammalian homolog, which declined in *cct1-2*, was listed. The proteotoxic stress and cryptic transcription hallmarks did not co-occur due to specific aggregation-reinforcing protein, as overexpression of Rnq1 and VHL tumor suppressor were tailed by the same cryptic transcription mark. It is called into question whether the proteotoxic stress affected specific components or a random collection. If CCT inactivation led to dysregulation of random components, amongst which unselected chromatin regulators were affected, it would be unlikely to observe specific aberrant transcription, such as 5' bidirectional/intergenic transcription for most of the genome or transcription termination at snoRNA genes. Hence, even though aggregation is maybe viewed as a non-selective process, susceptible protein structures attacked with preference are connected to the 5' transcriptional regulation. These results highlight parallels between the increase of proteotoxic stress due to cellular aggregation (via overexpression of aggregation-prone proteins or CCT inactivation), involvements of specific chromatin regulators and 5' bidirectional transcription.

How did aberrant transcription events correlate with the chromatin state? The third high-throughput technique utilized to examine the effects of CCT on the chromatin status was DNaseI-Seq. This data revealed that the magnitude of chromatin changes did not

meet transcriptional changes. While more than half of the sites affected by cryptic transcription did not deliver information about the chromatin status, the other locations suggested mainly mild chromatin closure upon CCT inactivation – ~32% cryptic transcription sites declined in openness and ~13% increased. The result that 5' bidirectional transcription was correlated with mild increased nucleosomal density is opposite from the expectations. The traditional dogma delineates that transcription correlates with openness of the chromatin, particularly regulatory regions (Hirschhorn 1992, Grunstein 1997, Adkins 2004, Hesselberth 2009, Voong 2017). Unlike regulatory regions that are nucleosome depleted depending on the context, ORF are nucleosome enriched (Hesselberth 2009, Voong 2017). Here, intergenic regions in terms of transcription could 'behave' like ORFs. The chromatin status upon bidirectional or in general cryptic transcription has not been defined. Our data could propose that in those cases, inadvertent nucleosomal accumulation could have happened due to cryptic transcription-coupled nucleosome turnover. Nucleosome turnover is correlated with H3K56 acetylation mark (Rufiange 2007, Tsubota 2007, Kaplan 2008). As there was no increase of H3K56 acetylation, alternative mechanism such as incorporation of histones from a milieu devoid of this mark could have taken place. Maybe such nucleosome events also led to exclusion of H2A.Z histone variant. In the absence of functional CCT, H2A.Z total levels are declining, as H2A.Z maybe misses an opportunity to get incorporated back onto the chromatin.

In this work, chaperonin CCT, a cytosolic machinery is shown to be a crucial regulator of nuclear events. Absence of functional CCT lead mainly to subverted transcript equilibrium instigated by the RNA polymerase bidirectional firing. Different regulatory regions might recruit different modules of the RNA polymerase complex and different functional modules might require assistance by the molecular chaperones. This work addressed only certain aspects of CCT-dependent nuclear phenotypes. CCT was shown to regulate termination at snoRNA genes via Nrd1 termination complex. Because Nrd1 termination events were also functionally dependent on exosome (van Hoof 2000, Vasiljeva 2006), the possible connection between CCT and exosome is brought up. In

addition, the increase of reads within introns in *cct1-2* compared to wild type indicates that CCT is involved in splicing event, hence RNA processing besides transcription.

5.2. Hsp90

Hsp90 has been the most popular molecular chaperone. Hsp90 interacts with about 10% of the whole proteome, as estimated from the genome wide studies in *Saccharomyces cerevisiae* (Zhao 2005). Using indirect immunofluorescence staining, nuclear Hsp90 concentration was calculated to be 1.87 µM, according to which above 8% of the entire cellular Hsp90 are localized in the nucleus (Figure 4.2.20). For a comparison, RNA polymerase II dispersed nuclear pool in HeLa cells is present at the concentration of only ~ 1 µM. Broad functional nuclear implications were assigned to Hsp90 – it was associated with chromosome segregation during mitosis (Stemmann 2002), telomerase complex (Holt 1999) and receptor mediated transcriptional regulatory complex (Freeman 2002). Even though Hsp90 catalytic domain is structurally rather related to the nuclear homodimeric ATPases such as DNA gyrases, topoisomerase II and the DNA mismatch repair proteins (Bergerat 1997, Dutta 2000, Young 2001), its direct DNA activities have not been observed. Instead, it affected nuclear events via modulating many nuclear regulators. Unlike acknowledged Hsp90 chaperone's roles in modulating chromatin regulators, the global dependencies of underlying chromatin landscape on Hsp90 were not known. This work elucidates different types of global chromatin changes upon Hsp90 depletion, as well as the associated affected targets.

DNaseI hypersensitivity mapping (Hesselberth 2009) was implemented to study chromatin landscape under the conditions of inactive Hsp90, by means of using temperature sensitive strain G170D (Nathan 1995), with respect to control. Two main features were observed: (i) brief (15 min) Hsp90 inactivation led to an excessive hypersensitivity increase of a small group of hypersensitive sites associated with a chromatin remodeler; and (ii) brief (15 min) and long-term (6 h) Hsp90 depletion lead to a mild yet global decline of open chromatin in length. In the first case, it was shown that the anomalous openness effect is due to the failure to abolish DNA-RSC chromatin remodeler interaction in the absence of functional Hsp90. Failure to comply with timewise efficient RSC removal allowed for its prolonged remodeling activity and hence creation of

misplaced open chromatin regions. These perturbations within the short time elucidated crucial importance of Hsp90 chaperone to maintain proper chromatin dynamics. In the second case, it was shown that decline of open chromatin correlated with transcription factor loss. Hsp90 supported DNA-binding and half-life of transcription factors in a conserved fashion. Here, Hsp90 depletion mirrored its stabilizing chaperone functions in regard to chromatin upkeep – it is suggested that Hsp90 is able to support globally both DNA binding and stability of various transcription factors, maintaining thereby open chromatin state. Together these two broad divisions reveal distinct levels of Hsp90 time-dependent effects on global chromatin modulation.

Hsp90-mediated transcription factor DNA binding and stability would have a great physiological relevance within the field of oncology. Transcription factors are one of the main class of misregulated cancer cell dependencies due to their potential to alter gene expression and thereby drive cellular transformations (Bhagwat 2015). Hsp90, on the other hand, is a renowned oncological target that supports stability of numerous oncogenic proteins, including transcription factors (Khurana 2015). Prominent onco-transcription factors that belong to Hsp90 client network are NF-κB, STATs, p53, and Bcl-6 (Khurana 2015). Pharmacological inhibition of Hsp90 has been widely proposed as one of the approaches to sensitize cancer cells (Sidera 2014). The therapy was, for instance, shown to lead to destabilization of steroid hormone receptors in breast cancer (Bagatell 2001). Hsp90 inhibition was shown to affect stability of upregulated transcription factors, such as c-Myc in breast cancer cell lines (Lee 2017) and transcription factor Hsf1 was brought into relation with Hsp90 and cancer (Chen 2013, Donnelly 2014, Engerud 2014). Generalized theme of Hsp90 inhibition as means to affect stability of transcription factors was tested in cancer cell, vSRC 3T3 mouse fibroblastoma, via radicicol treatment. The levels of various transcription factors in the presence of Hsp90 inhibitor declined. This confirmed that Hsp90 globally regulates stability of DNA binding proteins under afflicting conditions, in addition to the regular, i.e. healthy cells.

The findings about Hsp90-mediated modulation of transcription factor, together with the gene expression program, could also contribute to the pool of Hsp90-centered

evolutionary biology niches. Hsp90 was shown to influence relationship between genotype and phenotype, intervening in evolutionary pathways (Jarosz 2010). In theory, accumulation of genetic variations does not meet the magnitude of phenotypic variations – following only little variation in the gene expression, such traits are buffered or canalized (de Visser 2003). Hsp90 is believed to be a buffering protein that stabilizes key developmental proteins, which however, might allow for the accumulation of genotypic variations (Rutherford 1998). It was observed that under the conditions of compromised Hsp90 and depending on the genotype, an array of morphological, heritable phenotypes emerged (Sollars 2002, Queitsch 2002). Hsp90 was proposed to act both as a potentiator, allowing oncoming genetic variations to create new Hsp90-dependent phenotypes, and a capacitor, suppressing phenotypes that are released under compromisation of Hsp90 (Jarosz 2010). Here, the global loss of transcription factors upon Hsp90 depletion did not alter the gene expression program – cells seemingly circumvented Hsp90 inactivation. The preconditioned to Hsp90 loss, hence previously grown under the conditions of inactivated Hsp90 (6 h at 37 °C), are currently examined for the capability to overcome various stresses upon Hsp90 reactivation (shift to 30 °C after 37 °C exposure). Several pathways specific for the lost transcription factors in G170D are inspected under the conditions of compound starvation or under different carbon or nonmetallic sources. For instance, as Ino2/4 transcription factors, which regulate phospholipid metabolism (Loewen 2004), declined in G170D, the cells would be inspected for their growth under inositol starvation. Then, Met31 transcription factors that regulate Sulphur metabolism (Carrillo 2012) declined in G170D – the cells previously grown at 37 °C would be shifted to 30 °C media containing different Sulphur sources. This would reveal whether undermining of global Hsp90-modulated transcription factor functions would carry long-term, heritable implications.

It should be noted that, besides footprint decline in G170D, the programs suggest redistribution of the footprinting populations – G170D is escorted by the footprints not present in the wild type. This could be either because some transcription factors escaped Hsp90' dependence or the cell came up with the complement footprints forcing not to change the gene expression program. DHS contain subpeaks that reflect averaged

nucleosomal deprivation and different semi-present nucleosomal periodicity could have manifested upon Hsp90 depletion as well. In other words, the average signal might have captured the meta-state in which nucleosome positioning was not fixed for all cells or for the average of different populations. This would correlate well with different footprint landscape. Nucleosome 'breathing', which is believed to be sporadic nucleosomal unspooling, or fragile nucleosome species, different than canonical ones in their biochemical properties, were all mentioned entities that influence chromatin landscape status (Kubik 2015, Culkin 2017), but underlying factors remained concealed. We would suggest here that Hsp90 is able to contribute to the modulation of this chromatin landscape fine-tuning both through transcription factors and chromatin remodelers.

It is not exclusive that chromatin remodelers are engaged only at the sites of increase hypersensitivity, but they could also be involved at the DHS with reduced length in G170D. Under the circumstance of long-term Hsp90 absence, chromatin regulators could have been impacted structurally due to the lack of traditional chaperoning, and closure of the chromatin or obstructed nucleosome positioning that lead to the closure was favored. Besides the option that remodeling complex integrity as a whole might have been impaired, single domains or residues are equally likely. Mutations in the RSC remodeler that foster its continuous remodeling are detected (Clapier 2016), and it would be worth investigating whether these are the sites targeted by Hsp90. Alternatively, it could be that opposing machineries not affected by Hsp90 took over to close the chromatin. ISW1 chromatin remodeler are reported to antagonize RSC at promoter regions and negatively impact the open chromatin (Parnell 2015).

It was found here that excessively large open chromatin regions within short-term Hsp90 depletion were not present within the long-term Hsp90 depletion data set. Very aberrant chromatin changes could be compensated upon longer inactivation of Hsp90, yet, this was not the case for transcriptome. Hsp90 inactivation, just like CCT, led to global 5' cryptic bidirectional transcription. Similar factors that were checked in *cct1-2* were also tested in G170D for the contributions to cryptic bidirectional transcription. In G170D, there was a strong co-occurrence of conspicuous 5' bidirectional transcription phenotype within

or close to the promoter with H2A.Z-containing nucleosome where H2A.Z drops. Along with this, transcription directionality of certain H2A.Z-containing subtelomeric genes is also affected upon Hsp90-induced loss of H2A.Z. Hsp90 depletion also affected recruitment of histone-promoter specific regulators and affected transcripts within introns, likely showing implications in splicing. As the only difference, Hsp90 inactivation did not lead to read-through defects at snoRNA genes, unlike CCT. From these results, it appears that CCT and Hsp90 are both required for the regulation of the same chromatin targets or they parallel within the same cellular pathway that reassures correct orientation of RNA polymerase at the transcription initiation sites. Eukaryotic cells evolved to have three major chaperone machineries – each of which are rather different in their mechanisms and functional scopes. The same client perhaps requires different chaperones to reach and maintain completeness of functional settings. Even though this is favored in theory, the examples of the three chaperones raising up the same client to the complete functionality have been scarce.

5.3. P23

A lot of attention has been devoted to the early proposal about chaperones' roles in folding and assembly of protein complexes (Ellis 1987). While the generation of the protein structures is essential, the maintenance of the functional system is equally important, as effective upkeep of a healthy proteome lowers the energy usage. Importantly, it was shown here that such upkeep of the proteome is not restricted to the cytosol. By using RSC chromatin remodeling complex as a model, it was revealed that p23 elevated functionality of an assembled nuclear protein complex.

The tight genome package challenges the accessibility of underlying DNA. Chromatin remodelers are acknowledged factors that modulate chromatin openness through nucleosome remodeling (Clapier 2009). The total number of assessed chromatin remodelers in the cell is in the range of 5-50 times lower than the number of nucleosomes. The onset of the DNA replication or transcription as a response to physiological needs would certainly require extensive and effective nucleosome repositioning actions, which might challenge the remodeler-nucleosome stoichiometry. We propose that this is overcome with the help of molecular chaperones, such as p23 and Hsp90. P23 was shown here to prompt RSC's remodeling reaction, displacing it thereby from the nucleosome. Such released RSC complex would be set free for new locations that require remodeling assistance. *In vitro*, RSC was shown to remodel only about two arrays within 120 min (Logie 1999). This is not the case for chromatin remodelers *in vivo* which act efficiently by transitioning onto new targets quickly to manage the genome. We propose that p23 impedes the longevity of high-affinity remodeler-nucleosome reaction, which, although required, interferers with the biological timing (Echtenkamp 2014). P23, hence, managed the pool of available proteins, elevated its functionality and reduced the energy usage.

How does p23 'know' which protein (complexes) to target? Perhaps astonishing observation is how a small, 22 kDa chaperone manages to disassemble from the DNA

huge, above 1 MDa complexes, such as transcriptional regulatory complexes (Freeman 2002) and now RSC and SAGA. In the case of RSC, p23 was proposed here to dock onto Rsc30 DNA binding subunit of the RSC chromatin remodeler to target and displace Rsc3, and thereby entire complex. However, when used above physiological concentration, p23 displaced Rsc30 as well (data not shown). In addition, p23 was able to free from the DNA RSC lacking DNA binding subunits, suggesting complementary DNA binding domains, which are yet equally targeted by p23. RSC is known to bind DNA promiscuously (Floer 2010), which increases the complexity of assigning all DNA binding domains precisely. Apart from RSC, SAGA HAT – the complex with very little sequence similarity with RSC and completely different nuclear function – is equally targeted by p23 and released from cognate DNA. P23 was even able to affect DNA binding activities of partially cleaved Rsc3/30 transcription factors. All these observations suggest that, despite specificity of the chromatin remodeling function or DNA-binding function, there does not seem to be universal physical neither protein nor DNA sequence favored by p23. It could be that p23 in a specialized yet non-selective manner speeds up the flow of the crowded, dynamic nuclear milieu. Ongoing crosslinking studies, with p23 construct for which photocrosslinkable resides are placed within C-terminal chaperoning domain might reveal some answers to these questions. As p23 was able to displace almost any transcription factor or DNA-binding protein, this work assigns p23 a role of a universal 'DNA displacer'.

6. Outlooks

Perhaps the most inspirational long-term goal would be to show that major heat shock proteins actually assemble transcription machinery and dictate precise transcription in eukaryotes. 'Assemble' here could have several meanings. The mechanism might be chaperone-like transient touch-and-go or it might not belong to the traditional, catalogued chaperone approaches we are aware of. It would be appealing to deduce whether chaperones' cytosolic, nuclear, or both implications are a major determinant for the RNA polymerase holoenzyme functionality. Chaperones are certainly needed during and post protein synthesis in the cytoplasm. Yet, what is the extent to which they assemble RNA polymerase holoenzyme in the cytoplasm, and how much of the job is weighted in the nucleus, where actual functionality is needed?

The chromatin-integrated information together with the multifaceted transcription machinery has been believed to dictate transcription directionality. Decades of work have supported hypothesis about basal transcription machinery and promoter, transcription start site, +1 nucleosome, post-translational modifications, nucleosome depleted regions – all the conducive *cis* and *trans* elements that dictate transcription initiation, and thus, in the right direction. Suddenly, deprivation of a single major chaperone subverts chromatin landscape status and identity of transcriptional directionality. Rather than affecting a single element, chaperones contributions are laid out on several levels and defining all those contributions would improve our understanding of target DNA processes.

Crucial chromatin regulators such as SAGA or RSC, including RNA polymerase complex, are multi-subunit oligomers composed of evolutionary conserved subunits whose function is not known, or general necessity still questionable. It is alluded that, since the subunits were retained, cells likely need them. It is expected from the chaperones to aid these complexes in attaining correct protein structure or maintain functionality. In doing so, they could come into touch with these 'undefined' subunits. Dissecting characteristics of single subunits might be challenging as proteins denature in

the absence of the rest of the macromolecular complex. With chaperones, single subunits might operate stand-alone. Chaperones might be a good starting gate towards defining the unknown variables – revealing what functionality chaperones elevate for the subunit or complex might allow for unraveling complete regulators' contributions.

7. Appendices

7.1. Bacterial Strains

XL1-Blue
Rossetta (DE3)
BL21-GroEL (DE3)
BL21-CodonPlus (DE3)-RIPL, Agilent Technologies
CH184, Siller 2010

7.2. Yeast Strains

Ts G170D and parental WT W303 (Nathan 1995) were obtained from S. Lindquist group. All below strains were made in this work.

WT Ino2-TAP*::His6MX*
G170D Ino2-TAP*::His6MX*
WT Ino4-TAP*::His6MX*
G170D Ino4-TAP*::His6MX*
WT Met31-TAP*::His6MX*
G170D Met31-TAP*::His6MX*
WT Cbf1-TAP*::His6MX*
G170D Cbf1-TAP::*His6MX*
WT Abf1-TAP*::His6MX*
G170D Abf1-TAP*::His6MX*
WT Rgt1-TAP*::His6MX*
G170D Gal4-TAP*::His6MX*
WT Ecm22-TAP*::His6MX*
G170D Ecm22-TAP*::His6MX*
WT Mcm1-TAP*::His6MX*
G170D Mcm1-TAP*::His6MX*
WT Sut1-TAP*::His6MX*
G170D Sut1-TAP*::His6MX*
WT Asg1-TAP*::His6MX*
G170D Asg1-TAP*::His6MX*
WT Rap1-TAP*::His6MX*
G170D Rap1-TAP*::His6MX*
WT Reb1-TAP*::His6MX*
G170D Reb1-TAP*::His6MX*
WT Rsc3-TAP*::His6MX*
G170D Rsc3-TAP*::His6MX*
WT Spt10-TAP:*:His6MX*
G170D Spt10-TAP*::His6MX*
WT Nrd1-TAP*::His6MX*
G170D Nrd1-TAP*::His6MX*
WT H2A.Z-TAP*::His6MX*
G170D H2A.Z-TAP*::His6MX*

Temperature sensitive *cct1-2* and parental WT W303 (Ursic 1994) were obtained from J. Frydman group. All below strains were made in this work.

WT Pho23-TAP*::His6MX*	WT *dot1Δ::KanMX6* H2A.Z-TAP*::His6MX6*
cct1-2 Pho23-TAP::His6MX	*cct1-2 dot1Δ::KanMX6* H2A.Z-TAP*::His6MX6*
WT Rxt2-TAP*::His6MX*	WT *dot1Δ::KanMX6*
cct1-2 Rxt2-TAP*::His6MX*	*cct1-2 dot1Δ::KanMX6*
WT Sif2-TAP*::His6MX*	WT *set1Δ::KanMX6*
cct1-2 Sif2-TAP*::His6MX*	*cct1-2 set1Δ::KanMX6*
WT Ada2-TAP*::His6MX*	WT *vps75Δ::KanMX6*
cct1-2 Ada2-TAP*::His6MX*	*cct1-2 vps75Δ::KanMX6*
WT Spt3-TAP*::His6MX*	WT *cac2Δ::KanMX6*
cct1-2 Spt3-TAP*::His6MX*	*cct1-2 cac2Δ::KanMX6*
WT Ubp8-TAP*::His6MX*	WT *spt10Δ::KanMX6*
cct1-2 Ubp8-TAP*::His6MX*	*cct1-2 spt10Δ::KanMX6*
cct1-2 Sap30-TAP*::His6MX*	WT *swr1Δ::KanMX6*
WT Hos2-TAP*::His6MX*	*cct1-2 swr1Δ::KanMX6*
cct1-2 Hos2-TAP*::His6MX*	WT *htz1Δ::KanMX6*
WT Snt1-TAP*::His6MX*	*cct1-2 htz1Δ::KanMX6*
cct1-2 Snt1-TAP*::His6MX*	WT *asf1Δ::KanMX6*
WT Set3-TAP*::His6MX*	*cct1-2 asf1Δ::KanMX6*
cct1-2 Set3-TAP*::His6MX*	WT *rtt109Δ::KanMX6*
WT Asg1-TAP*::His6MX*	WT *hst3Δ::KanMX6*
WT Ecm22-TAP*::His6MX*	WT *hst1Δ::KanMX6*
cct1-2 Ecm22-TAP::His6MX*	*cct1-2 hst1Δ::KanMX6*
WT Rgt1-TAP*::His6MX*	WT *sif1Δ::KanMX6*
cct1-2 Rgt1-TAP*::His6MX*	*cct1-2 sif1Δ::KanMX6*
WT Snt1-TAP*::His6MX*	WT *snt1Δ::KanMX6*
cct1-2 Snt1-TAP*::His6MX*	*cct1-2 snt1Δ::KanMX6*
WT Gal4-TAP*::His6MX*	WT *cti6Δ::KanMX6*
WT Met31-TAP*::His6MX*	*cct1-2 cti6Δ::KanMX6*
WT Ino2-TAP*::His6MX*	WT *dep1Δ::KanMX6*
cct1-2 Ino2-TAP*::His6MX*	*cct1-2 dep1Δ::KanMX6*
WT Ino4-TAP*::His6MX*	WT *ume1Δ::KanMX6*
cct1-2 Ino4-TAP*::His6MX*	*cct1-2 ume1Δ::KanMX6*
WT Rap1-TAP*::His6MX*	WT *rxt1Δ::KanMX6*
cct1-2 Rap1-TAP*::His6MX*	*cct1-2 rxt1Δ::KanMX6*
WT Reb1-TAP*::His6MX*	WT *rxt3Δ::KanMX6*
cct1-2 Reb1-TAP*::His6MX*	*cct1-2 rxt3Δ::KanMX6*
WT Mcm1-TAP*::His6MX*	WT *pho23Δ::KanMX6*
cct1-2 Mcm1-TAP*::His6MX*	*cct1-2 pho23Δ::KanMX6*
WT Cbf1-TAP*::His6MX*	WT *sap30Δ::KanMX6*
cct1-2 Cbf1-TAP*::His6MX*	*cct1-2 sap30Δ::KanMX6*
WT Abf1-TAP*::His6MX*	WT *sds3Δ::KanMX6*
cct1-2 Abf1-TAP*::His6MX*	*cct1-2 sds3Δ::KanMX6*

WT Ada1-TAP*::His6MX*   WT *ume6Δ::KanMX6*
cct1-2 Ada1-TAP*::His6MX*   *cct1-2 ume6Δ::KanMX6*
WT Asf1-TAP*::His6MX*   WT *rco1Δ::KanMX6*
cct1-2 Asf1-TAP*::His6MX*   *cct1-2 rco1Δ::KanMX6*
WT Cac2-TAP*::His6MX*   WT *spt8Δ::KanMX6*
cct1-2 Cac2-TAP*::His6MX*   *cct1-2 spt8Δ::KanMX6*
WT Dot1-TAP*::His6MX*   WT *spt3Δ::KanMX6*
cct1-2 Dot1-TAP*::His6MX*   *cct1-2 spt3Δ::KanMX6*
WT Esa1-TAP*::His6MX*   WT *eaf3Δ::KanMX6*
cct1-2 Esa1-TAP*::His6MX*   *cct1-2 eaf3Δ::KanMX6*
WT Hst3-TAP*::His6MX*   WT *ada3Δ::KanMX6*
cct1-2 Hst3-TAP*::His6MX*   *cct1-2 ada3Δ::KanMX6*
WT Nrd1-TAP*::His6MX*   WT *set3Δ::KanMX6*
cct1-2 Nrd1-TAP*::His6MX*   *cct1-2 set3Δ::KanMX6*
WT Set1-TAP*::His6MX*   WT *hos2Δ::KanMX6*
cct1-2 Set1-TAP*::His6MX*   *cct1-2 hos2Δ::KanMX6*
WT Vps75-TAP*::His6MX*   WT *sgf29Δ::KanMX6*
WT Gcn5-TAP*::His6MX*   *cct1-2 sgf29Δ::KanMX6*
cct1-2 Gcn5-TAP*::His6MX*   WT *ubp8Δ::KanMX6*
WT Rtt109-TAP*::His6MX*   *cct1-2 ubp8Δ::KanMX6*
cct1-2 Rtt109-TAP*::His6MX*   WT *ada2Δ::KanMX6*
WT Snf6-TAP*::His6MX*   *cct1-2 ada2Δ::KanMX6*
cct1-2 Snf6-TAP*::His6MX*   WT *hos4Δ::KanMX6*
WT Ino80-TAP*::His6MX*   *cct1-2 hos4Δ::KanMX6*
cct1-2 ino80-TAP*::His6MX*   WT *rtg2Δ::KanMX6*
WT Spt10-TAP*::His6MX*   *cct1-2 rtg2Δ::KanMX6*
cct1-2 Spt10-TAP*::His6MX*   WT *gcn5Δ::KanMX6*
WT Swr1-TAP*::His6MX*   *cct1-2 gcn5Δ::KanMX6*
cct1-2 Swr1-TAP*::His6MX*   WT *sgf79Δ::KanMX6*
WT Arp5-TAP*::His6MX*   *cct1-2 sgf79Δ::KanMX6*
cct1-2 Arp5-TAP*::His6MX*   WT *cpr1Δ::KanMX6*
WT Rsc3-TAP*::His6MX*   *cct1-2 cpr1Δ::KanMX6*
cct1-2 Rsc3-TAP*::His6MX*   WT *rpd3Δ::KanMX6*
CCT HHT2-TAP*::His6MX*   *cct1-2 rpd3Δ::KanMX6*
cct1-2 HHT2-TAP*::His6MX*   WT *ash1Δ::KanMX6*
CCT HTA2-TAP*::His6MX*   *cct1-2 ash1Δ::LEU2*
cct1-2 HTA2-TAP*::His6MX*   WT *ada5Δ::KanMX6*
CCT Snf2-TAP*::His6MX*   WT *spt7Δ::KanMX6*
cct1-2 Snf2-TAP*::His6MX*   WT *sin3Δ::KanMX6*
CCT Nap1-TAP*::His6MX*
cct1-2 Nap1-TAP*::His6MX*
CCT Spt21-TAP*::His6MX*
cct1-2 Spt21-TAP*::His6MX*
CCT Taf1-TAP*::His6MX*
cct1-2 Taf1-TAP*::His6MX*

CCT Hda1-TAP*::His6MX*
cct1-2 Hda1-TAP*::His6MX*
CCT Ess1-TAP*::His6MX*
cct1-2 Ess1-TAP*::His6MX*
CCT Kin28-TAP*::His6MX*
cct1-2 Kin28-TAP*::His6MX*
CCT Dst1-TAP*::His6MX*
cct1-2 Dst1-TAP*::His6MX*
CCT Sua7-TAP*::His6MX*
cct1-2 Sua7-TAP*::His6MX*
CCT Set3-TAP*::His6MX*
cct1-2 Set3-TAP*::His6MX*
CCT Paf1-TAP*::His6MX*
cct1-2 Paf1-TAP*::His6MX*
CCT H2A.Z-TAP*::His6MX*
cct1-2 H2A.Z-TAP*::His6MX*
CCT Sin3-TAP*::His6MX*
cct1-2 Sin3-TAP*::His6MX*
CCT Hst4-TAP*::His6MX*
cct1-2 Hst4-TAP*::His6MX*
CCT Set1-TAP*::His6MX*
cct1-2 Spt16-TAP*::His6MX*

Other strains

BY4741 TAP-tag library, Open Biosystems
VDY1874, Euroscarf
VDY1874 H2A.Z-FRB*::KanMX6,* this work
YSC001 RPB3-3xFLAG::*NAT,* J. Weissman group
W303 *cct2Δ* pCCT2-CBP::LEU2, Dan Gestaut, J. Frydman group
Ssa1 WT, Taxis 2003
ssa1-45, Taxis 2003
NDY05, J. Brickner group
NDY05 *ino2Δ*, this work
NDY05 *ino4Δ*, this work
NDY05 *cbf1Δ*, this work

 AH109 (two-hybrid strain, Clontech) transformed with indicated plasmids:
'-' on the left means pGBKT7 plasmid has no Hsp82 insert
-' on the right means pGADT7 has no RSC subunit insert

-/Rsc30	-/Rsc6
Hsp82/Sfh1	Hsp82/Rsc7
Hsp82/Sth1	Hsp82/Rsc4
-/Sth1	Hsp82/Rsc30
-/Rsc58	-/Rsc8
Hsp82/R58	Hsp82/Rsc8
-/Arp7	-/Rsc9
-/Arp9	Hsp82/Rsc9
Hsp82/Arp7	-/Rsc30
Hsp82/Arp9	Hsp82/Ldb7
-/Rtt102	-/-
Hsp82/Rtt102	Hsp82/-
Hsp82/Htl1	-/Rsc2
-/Htl1	Hsp82/Rsc2
-/Ldb7	-/Rsc3
-/Sfh1	Hsp82/Rsc3
Hsp82/Rsc6	-/Rsc1
-/Rsc7	-/Rsc4

7.3. Plasmids

pFA6a-HIS3MX6, Longtine 1998
pFA6a-TRP1MX6, Longtine 1998
pFA6a-KanMX6, Longtine 1998
pFA6a-LEU2MX6, Noguchi 2013
pET28a-Hsp82, Freeman group
pET23a-Sba1, Freeman group
pET28a-SUMO-Abf1, this work
pET28a-SUMO-Rap1, this work
pET28a-SUMO-Reb1, this work
pET28a-SUMO-Cbf1, this work
pET28a-SUMO-Met31, this work
pET28a-SUMO-Ino2, this work
pET28a-SUMO-Ino4, this work
pET28a-SUMO-Rsc3, this work
pET28a-SUMO-Rsc30, this work
pET28a-SUMO-Sth1, this work
pET28a-SUMO-Sfh1, this work
pET28a-SUMO-H2A, this work
pET28a-SUMO-H2B, this work
pET28a-SUMO-H3, this work
pET28a-SUMO-H4, this work
pET28a-SUMO-Sba1, this work
pET28a-SUMO-Hsp82, this work
pET28a-Sumo-protease, Brieher group
pTEV-protease, Brieher group
CP7171 (H2A), Peterson group
CP718 (H2B), Peterson group
CP719 (H3), Peterson group
CP720 (H4), Peterson group
CP1024 (pGEM-3Z/601), Lowary 1998
pEVOL-pBpF, Chin 2002
pET23a-Sba1-F164BPA, this work
pET23a-Sba1-F198BPA, this work
pET28a-SUMO-Sba1-F164BPA, this work
pET28a-SUMO-Sba1-F198BPA, this work
pBAD-His6-Sumo-TEV-LIC, Scott Gradia group
pBAD-His6-Sumo-TEV-LIC-Sba1, this work

pBAD-His6-Sumo-TEV-LIC-Sba1-F164BPA, this work
pBAD-His6-Sumo-TEV-LIC-Sba1-F198BPA, this work
pFA6a-FRB-KanMX6, Haruki 2008
pET28a-SUMO-hFOXM1, this work
pGBKT7, Clontech
pGADT7, Clontech
pESC-URA3 HttQ104-GFP, Frydman group
pESC-URA3 RNQ1-GFP, Frydman group
pESC-URA3 VHL-CHFP, Frydman group

7.4. Chemicals

Chemical Name	Company
1-methyl-2-pyrrolidinone	Aldrich
2,2-Thiodiethanol	Aldrich
2-mercaptoethanol	Acros Organics
30% Acrylamide (37.5:1)	BioRad
4-(2-Aminoethyl)Benzene Sulfonyl Fluoride	MP Biomedicals
40% Acrylamide (19:1)	BioRad
40% Acrylamide (37.5:1)	BioRad
5-bromo-2-Deoxyuridine-5-Triphosphate	Sigma-Aldrich
Acetic Acid Glacial	J.T. Baker Avantor
Acetone	Acros Organics
Adenine Sulfate	Acros Organics
Adenosine-5-triphosphate Sodium Salt	USB
Agarose	Fisher
Agarose Low Melting	Fisher
Ammonium Acetate	Fisher, VWR
Ammonium Hydroxide	Fisher
Ammonium persulfate	Acros Organics
Ammonium Sulfate	USB
Ampicillin	Gold Biotechnology
Antifoam A	Spectrum
Aprotinin	Gold Biotechnology
ATPγ	MP Biomedicals, Perkin Elmer
Bacto Agar	BD
Bacto Peptone	BD
Bacto Tryptone	BD
Bacto Yeast Extract	BD
Blasticidin S Hydrochloride	Fisher
Boric Acid	Fisher
Brilliant Blue	USB
Bromophenol Blue Sodium Salt	Acros Organics
BSA	Fisher
Caffeine	Fisher
Calcium Acetate hydrate	ACROS
Calcium Chloride	Sigma-Aldrich
CAPS	Acros Organics
Cesium Chloride	Fisher

Chloramphenicol	Fisher
Chloroform	Sigma-Aldrich
Cobalt(III)chloride hexahydrate	Acros Organics
Creatine Kinase	Gold Biotechnology
Crystal Violet	Acros Organics
Cycloheximide	Fisher
D+Sucrose	Fisher
Deoxycholic Acid Sodium Salt	USB
Deoxyribonucleic Acid, highly polymerized	USB
Dextrose Monohydrate	Fisher
D-Galactose	Fisher
Difico Yeast Nitrogen Base w/o AA	Fisher
DMSO	Fisher
dNTP	NEB
D-Sorbitol	Acros Organics
DTT	Gold Biotechnology
EDTA	Acros Organics
EGTA	Fisher
Ekono Hybridization Buffer	RPI Research Products
Ethanol	Decon Laboratories
Ethidium Bromide Tablets	USB
Ethylene glycol	Acros Organics
Ficoll PM400	GE Healthcare
Formaldehyde	Sigma-Aldrich
Formamide	Acros Organics
Formic Acid	Sigma-Aldrich
G418 Sulfate	Gold Biotechnology
Gentamicin Sulfate	USB
Glycerol	Fisher
Glycine	Fisher
Glycogen	ICN Biomedicals
Glycylglycine	Acros Organics
Glycyl-glycyl-glycine	Acros Organics
Guanidine Chloride	USB
Guanidine hydrochloride	Fisher
Guanidine Thiocyanate	USB
Heparin Sodium	Acros Organics
HEPES	USB
Herring Sperm DNA	Promega
Hydrochloric Acid	Fisher
Hydroxylamine Hydrocloride	Acros Organics

Imidazole	USB
Inositol	Acros Organics
IPTG	Gold Biotechnology
Isopropyl Alcohol	Macron
L+Glutamic Acid	Acros Organics
Lactic Acid	Fisher
L-Alanine	Acros Organics
L-Aminobenzoic Acid	Acros Organics
L-Apartic Acid	Acros Organics
L-Arginine	Fisher
L-Aspargine	Acros Organics
LB Medium	BD
L-Cysteine	Acros Organics
Leupeptin Sulfate	Gold Biotechnology
L-Glutamine	Acros Organics
L-Histidine	Acros Organics
L-Isoleudin	Acros Organics
Lithium Acetate Dihydrate	Acros Organics
Lithium chloride	Fisher
Lithium Sulfate	Acros Organics
L-Leucine	Fisher
L-Lysine	Acros Organics
L-Methionine	Acros Organics
L-Phenylalanine	Acros Organics
L-Proline	Acros Organics
L-Serine	Acros Organics
L-Threonine	Acros Organics
L-Tryptophan	Acros Organics
L-Tyrosine	Acros Organics
L-Valine	Acros Organics
Lysozyme	Fisher
Magnesium Acetate	Fisher
Magnesium Chloride Hexahydrate	Acros Organics
Magnesium Chloride tetrahydrate	Fisher
Magnesium Sulfate	USB
MES Free Acid Monohydrate	Fisher
Methyl Alcohol	Macron
MOPS	Fisher
Myo-Inositol	Alfa Aesar
N, N, N, N-tetramethyl-ethylenediamine	Aldrich
Natural Red	Acros Organics

Neomycin Sulfate	Fisher
N-Lauroylsarcosine Sodium Salt	Acros Organics
Nonidet P40 Substitute	USB
Ovalbumine	Fisher
Paraformaldehyde	Fisher
PEG 3350	Fisher
Pepstatin A	Gold Biotechnology
Phenol, Chloroform, Isoamylalcohol	Fisher
Phosphocreatine	Sigma-Aldrich
PMSF	Gold Biotechnology
poly(dG-dC)	Sigma-Aldrich
poly(dI-dC)	Thermo Scientific
Poly-L-Lysine	Sigma-Aldrich
Polyvinylalcohol, 80% hydrolized	Aldrich
Polyvinylpyrrolidone	Fisher
Potassium Acetate	Alfa Aesar
Potassium Chloride	USB
Potassium Glutamate	ICN Biomedicals
Potassium hydroxide	Fisher
Potassium Phosphate Dibasic	USB
Potassium Phosphate Monobasic	USB
Progesterone	USB
Propidium iodide	Invitrogen Molecular Probes
Proteinase K	Fisher
Prtoeinase K (from Tritrachium Album)	Fisher
Radicicol	AG Scientific
Ribonuclease A	Sigma-Aldrich
Ribonucleic Acid	Fisher
Saturated phenol	Fisher
Sodium Acetate trihydrate	Fisher
Sodium Azide	USB
Sodium Bicarbonate	ACROS
Sodium Borate	Fisher
Sodium butyrate	Alfa Aesar
Sodium Carbonate Anhydrous	Fisher
Sodium Carbonate Monohydrate	Sigma-Aldrich
Sodium Chloride	Fisher
Sodium Citrate	Fisher
Sodium Dodecyl Sulfate	Fisher
Sodium hydroxide	Sigma-Aldrich
Sodium Hydroxyde	Sigma-Aldrich

Sodium Metavanadate	Aldrich
Sodium Molybdate Dihydrate	Acros Organics
Sodium Phosphate Dibasic	USB
Sodium Phosphate Monobasic	USB
Sodium Pyrophosphate	Acros Organics
Sodium Sulfate	Sigma-Aldrich
Spectinomycin-Dihydrochloride Pentahydrate	MP Biomedicals
Spermidine	Acros Organics
Spermine	Acros Organics
ssDNA	Ambion Invitrogen
Streptomycin	Fisher
Succinic anhydride	Aldrich
Sucrose certified ACS	Fisher
Sucrose crystal	Fisher
Sulforhodamine B Sodium Salt	Sigma-Aldrich
Sulfuric Acid	Fisher
Taurine	Acros Organics
TEMED	Fisher, BioRad
Trichloroacetic Acid	Fisher
Triethylamine	Acros Organics
Tris Base	Fisher
Tris Hydrochloride	Fisher
Triton X-100	USB
tRNA	Sigma-Aldrich
Trypsine	USB
Tween	Fisher
Ultrapure dNTP set	Amersham Biosceinces, Thermo Fisher
Ultrapure NTP Set	Amersham Pharmacia Biotech
Uracil	Acros Organics
Urea	Fisher
Xylene Cyanol	Acros Organics
Yeast Extract	BD
Yeast Nitrogen Base w/o AA	BD
YPD Broth Traditional Formulation with peptone	USB
Zinc Acetate Dihydrate	Acros Organics
Zinc Chloride	Acros Organics
Zymolyase 100T	USB
Zymolyase 20T	MP Biomedicals

7.5. Chipped Locations
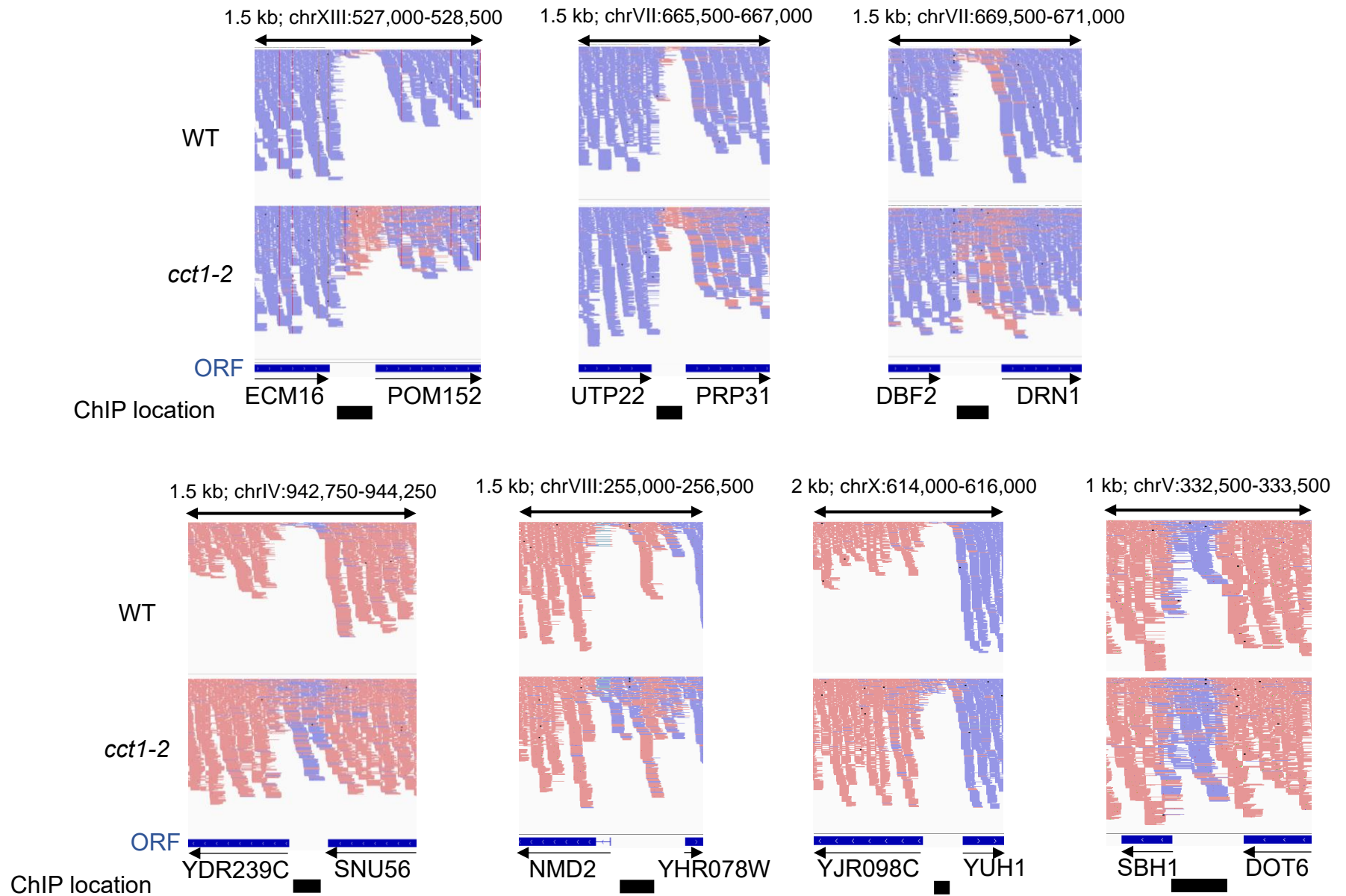
Figure 7.5.1. Intergenic locations used for chromatin immunoprecipitation assay
RNA-Seq reads obtained via deep sequencing RNA isolated from WT and *cct1-2* strains grown at non-permissive temperature, aligned to the reference genome (UCSC, April 2011) with STAR (Dobin 2013). Black boxes represent to be qPCRed product from the ChIPed DNA.
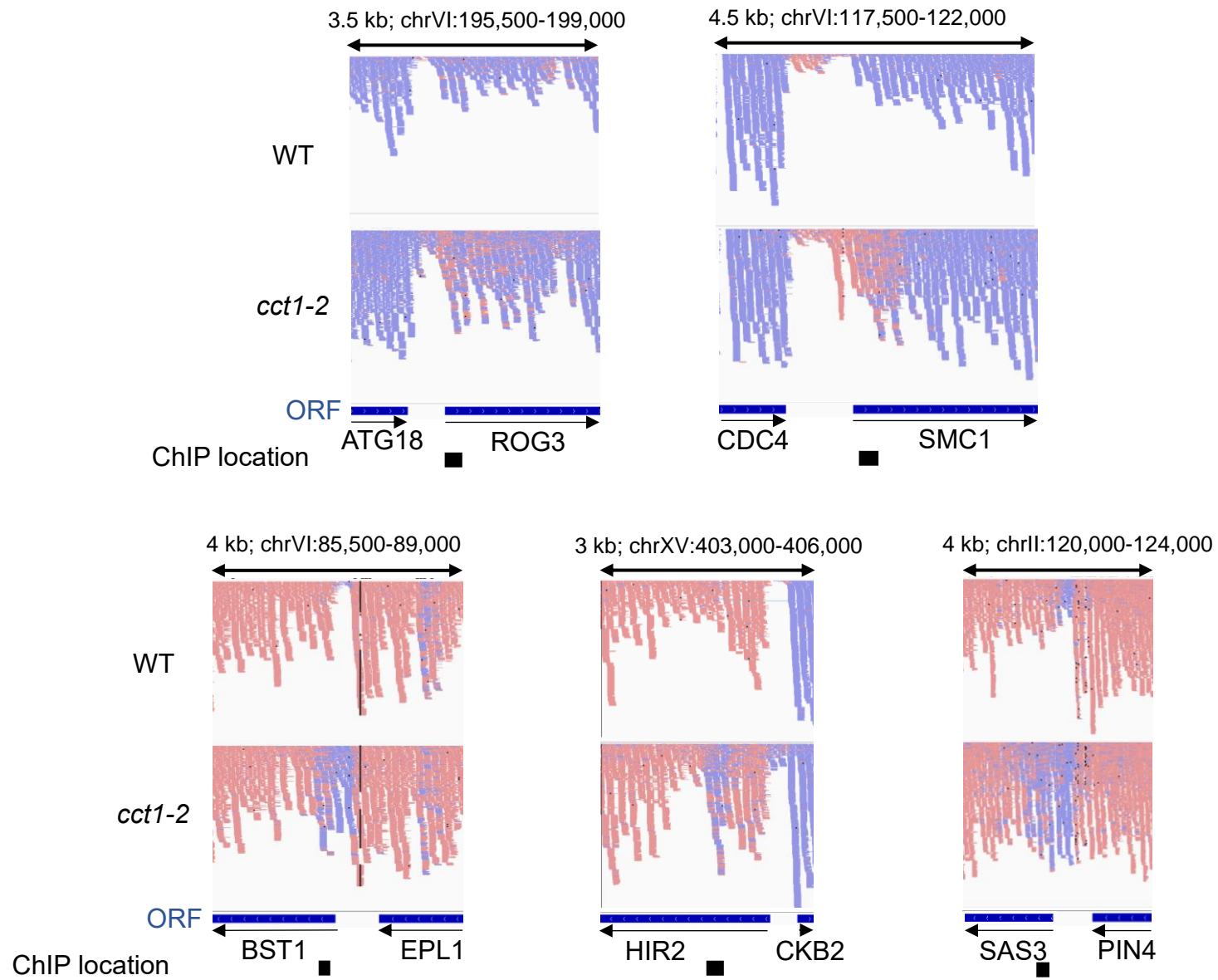
Figure 7.5.2. **5' locations used for chromatin immunoprecipitation assay**
RNA-Seq reads obtained via deep sequencing RNA isolated from WT and *cct1-2* strains grown at non-permissive temperature, aligned to the reference genome (UCSC, April 2011) with STAR (Dobin 2013). Black boxes represent to be qPCRed product from the ChIPed DNA.
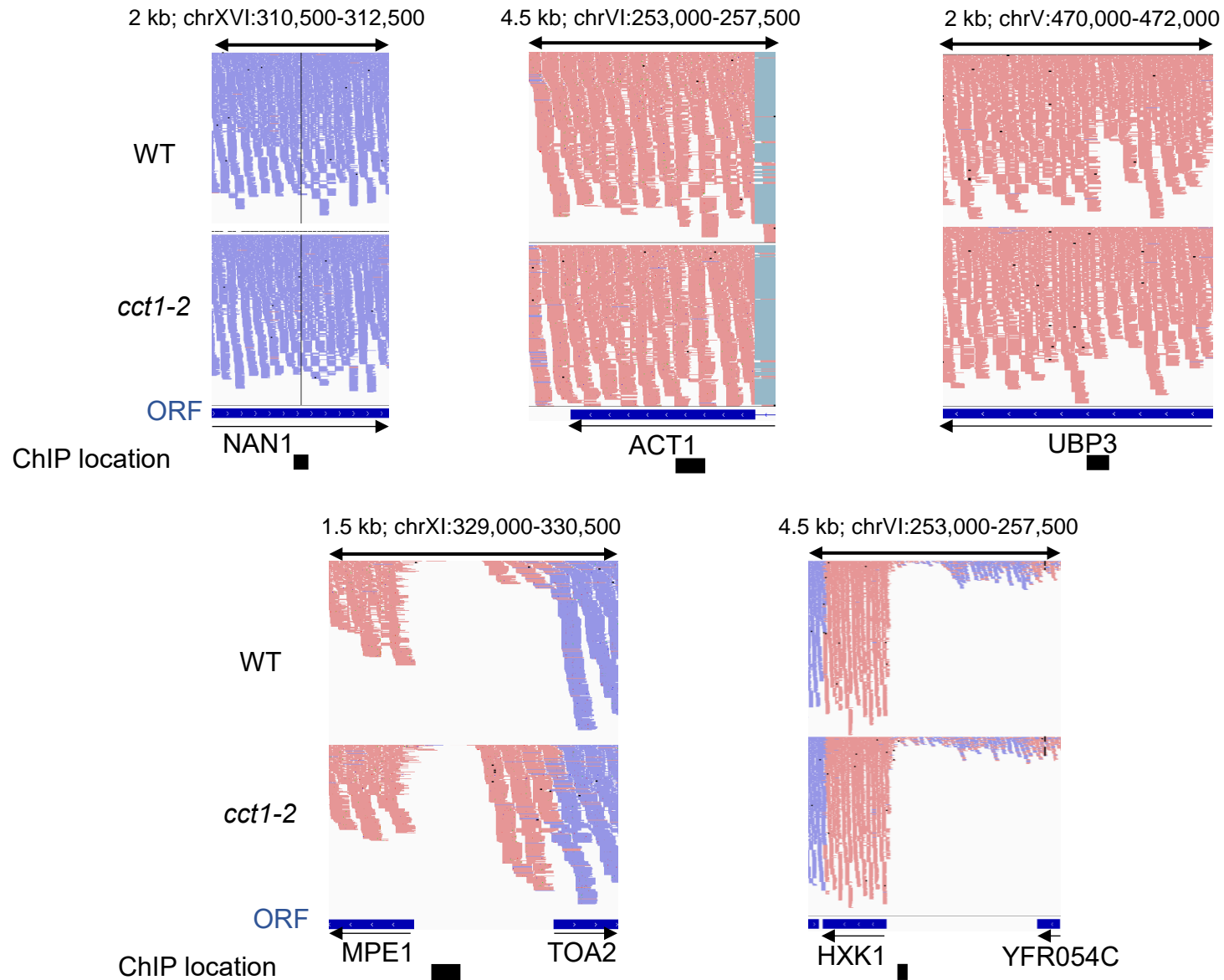
Figure 7.5.3. **Control (inter)genic locations used for chromatin immunoprecipitation assay**
RNA-Seq reads obtained via deep sequencing RNA isolated from WT and *cct1-2* strains grown at non-permissive temperature, aligned to the reference genome (UCSC, April 2011) with STAR (Dobin 2013). Black boxes represent to be qPCRed product from the ChIPed DNA.
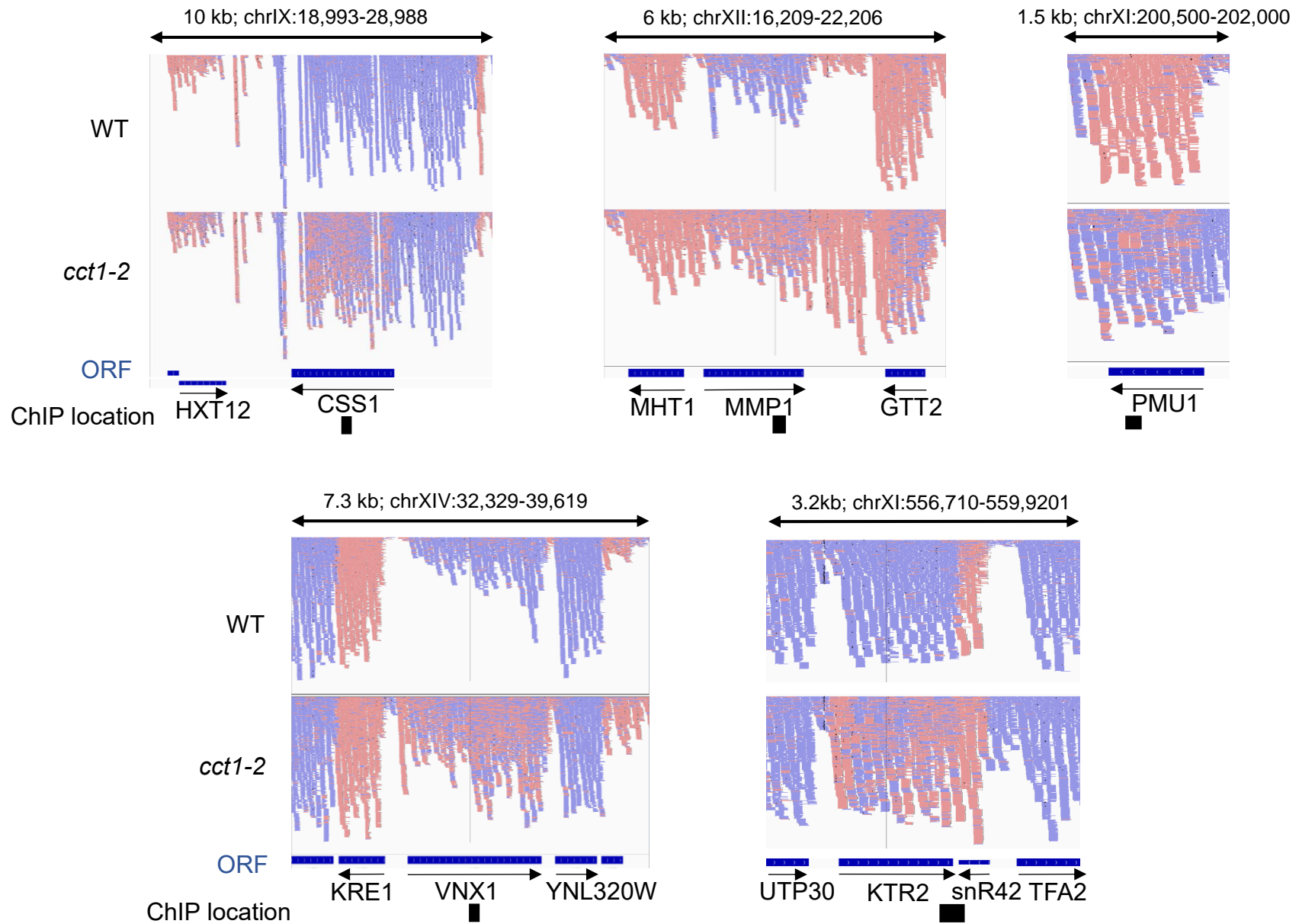
Figure 7.5.4. **Locations used for chromatin immunoprecipitation assay for the genes with switched directionality**
RNA-Seq reads obtained via deep sequencing RNA isolated from WT and *cct1-2* strains grown at non-permissive temperature, aligned to the reference genome (UCSC, April 2011) with STAR (Dobin 2013). Black boxes represent to be qPCRed product from the ChIPed DNA.

7.6. Genes with Changed Directionality in *cct1-2*

```
YAL067C chrI:7235-9016

YBL106C chrII:10847-13879

YBR069C chrII:376574-378433

YBR283C chrII:768943-770415

YCR106W chrIII:310958-313456

YDL216C chrIV:68997-70319

YDL194W chrIV:111580-114234

YR132C chrIV:718816-720303

YDL104C chrIV:273653-274876

YDR076W chrIV:598468-599688

YDR185C chrIV:831934-832473

YDR498C chrIV:1445843-1446994

YGL209W chrVII:95858-97006

YGL113W chrVII:295932-297938

YGL101W chrVII:312193-312840

YGR109C chrVII:705359-706501

YGL143C chrVII:234717-235958

YGR041W chrVII:577487-579130

YHR048W chrVIII:204607-206151

YHR061C chrVIII:221534-222478

YHR177W chrVIII:456591-457952

YIL169C chrIX:23119-26106

YIL115C chrIX:144327-148709

YJL193W chrX:71366-72574

YJL157C chrX:123836-126328

YJL156C chrX:126853-128952

YKL221W chrXI:6107-7528

YKL128C chrXI:200884-201771

YKR061W chrXI:557677-558954
```

YLL061W chrXII:17956-19707

YML116W chrXIII:38196-39824

YML118W chrXIII:32334-33851

YML017W chrXIII:236588-238731

YMR006C chrXIII:277561-279681

YMR069W chrXIII:407709-408566

YML027W chrXIII:221406-222563

YNL321W chrXIV:34696-37422

YNR048W chrXIV:711630-712811

YNR056C chrXIV:731618-733303

YNR067C chrXIV:755746-759099

YNR069C chrXIV:761123-762592

YOL153C chrXV:36822-38567

YOR011W chrXV:349679-353863

YOR049C chrXV:422668-423732

YOR071C chrXV:459480-461276

YOR301W chrXV:880965-882272

YPR162C chrXVI:866715-868304

YPR194C chrXVI:924304-926937

YPL018W chrXVI:517651-518760

YPR027C chrXVI:620425-621258

YPL016W chrXVI:521014-524958

7.7. Up/Down Regulated Genes

7.7.1. CCT

Upregulated (GFold >1.5), Illumina HiSeq4000

YJR005C-A	YBL065W	YMR175W-A	YHR007C-A	YKL106C-A	YOR121C
SPG4	HSP104	MEI5	YEL045C	YGR127W	AAD16
YDR250C	UGX2	ANS1	YER079W	GCD6	SEC26
GRE1	RTC3	SSE2	DCS2	YBR201C-A	YLR366W
YBR072C-A	YER066C-A	XBP1	TMA10	HXT14	YJR098C
SSA3	NCE103	BUD26	YIL100W	YOR072W-A	TMA17
BTN2	OM45	YLR307C-A	SMA1	YKL091C	YMR247W-A
YDR220C	YGL138C	RPN4	RNP1	OPI10	YBR116C
SPG1	YGL015C	KAR2	TRS23	ATG32	TDH1
HSP42	ECM11	EMP46	ECM4	RRD2	ATG33
SSA4	YDR249C	YBL008W-A	YKL107W	YLR410W-B	YGR122C-A
YDR215C	YLR149C	UIP4	USV1	YBR178W	ECL1
GND2	HSP26	DDR2	ACH1	NUR1	YDR379C-A
SRX1	CHA1	YMR085W	YKR073C	FMP48	YDL022C-A
INO1	SPR28	YFL015W-A	TKL2	PMA2	YNR001W-A
SIP18	ATG8	SNU56	YML100W-A	YDR248C	YMR141C
RGI1	YPL205C	PHM7	YER085C	YOR020W-A	YAL016C-B
YDL218W	PCF11	YDR239C	YER084W-A	YJL136W-A	GSP2
RTN2	PDC6	YJR008W	LEE1	YIM2	RCK1
YDR194W-A	FMP16	YMR084W	AIM17	YNL013C	YMR173W-A
YER067C-A	PAM1	FYV12	YLL047W	YGR273C	DBP1
HSP78	CTA1	HMX1	SDP1	FYV10	IDP3
CTT1	MFB1	YJR115W	ULI1	HXT5	SPS100
YPL261C	YBR284W	SAF1	YDL114W	YDR182W-A	YMR013W-A
ADR1	YLR012C	YDR015C	YGL034C	CPR6	YOR053W
NDE2	SHC1	YPL185W	YNL115C	YLR202C	YNR034W-A
NQM1	IVY1	YIL046W-A	ZRT1	YER135C	YHL037C
MSC1	ATG3	HED1	YIL100C-A	YOR289W	YJR157W
ECM23	PIR3	YDR114C	YOL114C	YMR114C	AAD10
YMR031W-A	IDP2	ERO1	HEF3	YDL118W	PTP2
HSP30	DIA3	COX20	YKL123W	HES1	
YJL144W	CHL4	HPA2	YKL151C	YNL171C	
YOR186W	YGR066C	SPG5	YMR007W	ANB1	
YML084W	YBL071C-B	YDR246W-A	MAM1	ATG9	
RRT7	YLR311C	SOL4	FMP45	TOS8	
YAP6	YOR214C	EXG2	GDB1	GTT1	
OSW1	YOR329W-A	GGA1	HXT10	YJL015C	

YFL032W	YIL032C	SNZ1	GPH1	YJL150W
YDR261W-B	SGA1	YHR138C	FUN19	BIO3
GAD1	SER3	ALD3	YPR160C-A	YJL027C
YJR120W	YLR312C	YJR096W	YPR074W-A	IML2
YOR024W	GIP2	HSP12	YPL102C	PSH1
YFL015C	MOH1	SIL1	ATG7	SSH4
HSP82	SIR4	YDR426C	ADH2	YJL163C
AIM26	CRG1	YKL050C	FMN1	YCR022C
YBR200W-A	YOL024W	URA10	YPR096C	TRR2
YJL045W	YCL041C	BIO4	FRT2	HEM1
CRF1	PRM6	UBC8	YDL007C-A	DDR48
YDL159W-A	YDR034C-D	YIL055C	MRPL7	FDH1
RMD5	CYC7	ARO9	GLC3	YDR042C
YDR048C	YET2	CAT2	YPR064W	UGA2
HBT1	TFS1	YMR244W	RGI2	YBR226C
PEX5	YDR230W	YDR261W-A	THI20	YOL085C
PAU12	RAD9	MET32	SNX41	YOR072W
ALD2	AMS1	SPO19	PFK26	PRP28
YML007C-A	URA8	YHR137C-A	YMR196W	YBR221W-A
YLL006W-A	GAL7	YGR201C	GCY1	YDL119C
YOR186C-A	YDR034W-B	YLR124W	YOR292C	YLR217W
YKL065W-A	TSA2	YER091C-A	YGR053C	YOL131W

Downregulated (GFold <-1.5), Illumina HiSeq4000

YDR274C	EGD2	RPS11A	YGR017W	YDR524W-C	HO
CWC21	RPS4B	YGR018C	RPS6A	RPS18A	AAH1
CWP2	RPS7A	GUK1	RPS27A	RPL16A	YPR202W
YJR018W	FET3	RPS26A	RPL40A	BUD28	MFA2
GPD2	RPL14B	RPS8B	RPS19B	RPS21B	HXT4
STM1	GLN1	RPL43A	RPS16A	RPS19A	OAC1
YER156C	POP8	SUR7	RPS2	RPL40B	IMD2
YBL012C	YOR390W	RPS10A	YMR272W-A	CCS1	BSC3
RPS25A	TAL1	RPP2A	ICY1	BAP3	RDS1
SSB2	RPL31A	CWP1	RPS24B	GAP1	YKL223W
ERG1	ENT4	RPL37B	AAD15	YOR314W	RPL9A
BAT1	HOM2	RPS5	RPS23A	TRX1	YFL067W
VEL1	YAR064W	MDJ2	RPL30	RPL33A	YRF1-4
COS2	RPS1B	YBR300C	RPP0	RPS12	YHR214C-B
TAT1	SML1	RPP1B	RPS8A	YPL142C	SPL2
YLR264C-A	RPS27B	YDR354C-A	YEL032C-A	RPS16B	YHR219W
YER189W	RPL43B	YGL258W-A	UTR2	RPS6B	YER188W
YOL014W	YIR042C	YBL113W-A	RPL18A	YLR462W	PHM6
HXK2	YGR265W	RPS1A	RPS14A	PCL1	YFL064C
YLR099W-A	TRP4	YBR191W-A	YGL123C-A	RPL5	YNR075C-A

SOL3	ARR1	RPL19B	ILV3	OPT2	PHO11
VBA4	GAS1	SAM1	YHL050C	TOS6	YFL066C
YLR232W	RPS30A	RPP2B	RPL23A	OLE1	YPR204W
TSC10	YLR179C	RPS0A	FET4	RPL15A	COS8
YOR108C-A	SUN4	RPS23B	YFL065C	VTC1	PHO12
SNM1	SUR1	RPS21A	DUT1	RPL18B	PHO84
HMS2	BNA5	RPS24A	RPL17A	PDR5	COS10
YMR307C-A	MES1	RPL32	SFG1	YLL044W	YML133C
RGS2	RPS9A	SCW4	SNO2	RPL26B	YHR214C-C
MNP1	GLY1	RKI1	RPL2B	RPL8B	YLL066W-A
YHL050W-A	RPL36A	RPS11B	RPL21B	RPS3	YLL066C
YPL279C	RPS10B	LEU2	RPL20A	RPS29A	
YJR129C	RPL42B	RPL7A	GGC1	SNO3	
YOL164W-A	RPL13A	RPL13B	RPL3	ASC1	
YPR036W-A	RPS15	RPL12A	HIS1	RPL8A	
RPL19A	RPL42A	ALD6	RPL2A	RPS20	
SRP40	CTS1	RPL24A	RPL24B	RPS26B	
RPL11B	SPS4	RPL4A	RPL20B	MRH1	
COX19	DED81	RPL14A	YHR214C-E	PTR2	
SYC1	AGP1	YGR176W	RPS4A	RPL27B	
YDL241W	RPL16B	RPL23B	ARR2	RPS22A	
NMA1	ILV2	ELO1	DSE2	YBL113C	
RPS30B	RPS0B	RPL25	RPS17B	DPS1	
CBR1	YDR524C-B	BAR1	RPL1B	BSC1	
TIM9	RPL22B	YPS5	ADH7	STE2	
EFT2	RPL27A	RPS18B	YDR417C	HTB2	
YLR126C	RPL6B	RPS9B	BNA1	RPL31B	
MRPL8	YBL107C	YLR339C	CLN1	PMA1	
PDR16	RPL6A	GCV3	PRM7	YLR413W	
RPS25B	HMO1	ATF2	RPL12B	YGR259C	
TMA19	RPL37A	RPL36B	RPL26A	MEP2	
RPL17B	RPL34A	YPL250W-A	RPS13	GDH1	
PUT4	SCS7	RPL4B	RPS17A	DBP2	
RFU1	LEU9	YHB1	RPS31	HTA2	
SEC53	PRO3	FUI1	FCY2	YDL041W	
YER023C-A	PHO5	RPL29	RPS7B	GIT1	
YGL069C	OPI11	AAD3	RPP1A	ARR3	
PPA2	TNA1	YEL053W-A	RPL21A	ALD5	
RPL38	FMP41	COS1	RPL22A	ASN1	

7.7.2. Hsp90

Upregulated (GFold >1.5)

SSA3	PUG1	YOX1	BUD20
BTN2	HSP78	FUS1	YHR086W-A
MF(ALPHA)1	YFR052C-A	GDB1	SFH5
SSA4	YNL034W	YOR379C	HEM3
HSP42	YNR034W-A	RNR3	APT1
JLP1	GSY1	DAL7	RPL14B
HSP30	SIS1	DCS2	GPD2
TMA10	CPR6	SSA1	RPS12
HXT6	SPS22	TPO4	PIR3
AAD6	TIP1	RGI1	ASC1
SIP4	ARG1	YSW1	RPS19A
AAD16	PIN3	SPO71	RPS22A
DAL80	YLR217W	YOL162W	RPL23A
YJR005C-A	PIG2	YKL177W	YLR171W
OSW1	SPO21	GAD1	FLX1
YKR033C	REC104	YER067C-A	IES6
MEP2	DAL5	MDJ1	RPC34
BSC5	UGA1	STI1	RPL35B
YDL114W	PRM6	YCT1	TRM112
RPN4	UIP4	YGL010W	RPL8A
GLC3	HES1	XKS1	NOG2
SSE2	PEX18	FIT1	SRP40
HXT10	ANS1	CUP1-1	RPS31
PDR11	GDH3	RAD59	YGL117W
HSP26	SPO1	WSC4	YEF3
MLS1	ALD3	POX1	YAT1
ALY1	YLR012C	FLO10	YLR280C
YNR068C	YGL138C	MAL31	YDR509W
HSP104	YML047W-A	GAP1	PHS1
YNL018C	YDR119W-A	OPI10	RPL1B
FES1	YFR020W	OYE3	COX19
YJL144W	YKL123W	CDA2	FCY2
UGA4	YAL004W	YDL026W	YER034W
SIP18	FAR11	YBR184W	FTR1
SPG4	RRT5	GRE1	YOL085W-A
HXK1	SPG1	SEO1	YPL067C
IME2	SGT2		RRN5
GRE3	ACH1		YLR169W
DUR1,2	PES4		YPL025C

Downregulated (Gfold <-1.5)

DIF1	YOL114C	YOR248W
YNR066C	PDC1	YOL085C
RPL26A	HMF1	EXG1
HOP2	PGM1	YLR179C
REX2	RPL40B	YMR315W-A
URA2	HMT1	RFU1
SFG1	ARI1	RPL9A
RPS21A	YMR122W-A	YNL024C
SAM1	YGR121W-A	POC4
FCY1	PSA1	YDR374W-A
SSU72	SRL1	FUI1
KTR3	ICY1	CMC4
RPL16A	YPR078C	DSE2
HXT2	ALD6	SPL2
SNF11	GDT1	POP8
RPL33A	MNP1	DPM1
RPS25B	CCS1	LOT5
MCH5	AIM4	AQR1
RPS3	YDR274C	RPL31B
TRP1	DFR1	YOL118C
FUR1	YCH1	RAS1
RPL21B	RKI1	YGR039W
YPL142C	YGL069C	HTA2
NAT4	APS1	YLR413W
YPR036W-A	MRH1	YKE4
RPS26B	FEN1	MER1
YCL049C	GNP1	HXT1
YOL155W-A	YGR160W	YLR112W
HTB2	YPR050C	YKL069W
RPL43B	YKL102C	RHR2
RPS18A	NSR1	HOR2
YDR008C	YJL152W	HUG1
GTT3	DBP2	YHR022C-A
RPS9B	ATF2	HXT3
NHP6A	YBR200W-A	PHO84
CYC3	SNA3	CWP1
YDL071C	RPS29A	
RPL15A	YGL088W	
RPL2A	MAK3	

7.8. Other Unintegrated Results

In vitro methylation assay with synthetic peptides, purified Dot1 and purified human recombinant CCT.
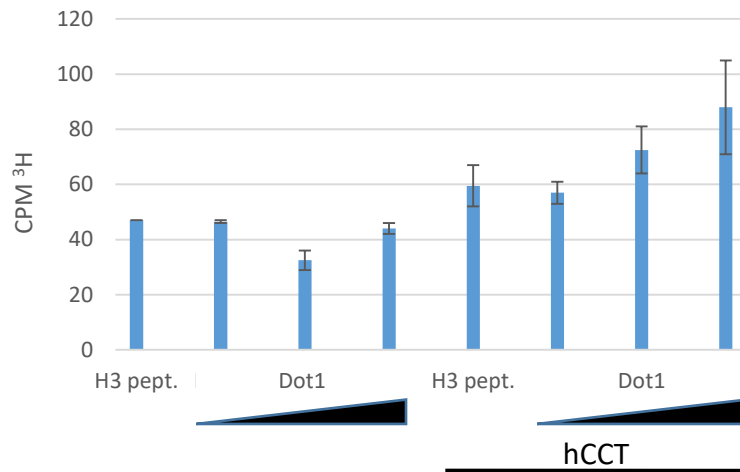
In vitro acetylation assay with reconstituted nucleosomes as substrate and purified Spt10, SWI/SNF and human recombinant CCT
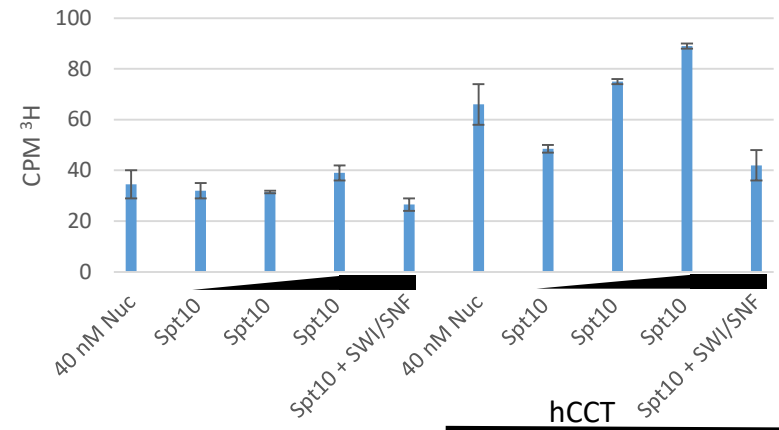
Steady state protein levels in WT and *cct1-2* grown at 37 ˚C.
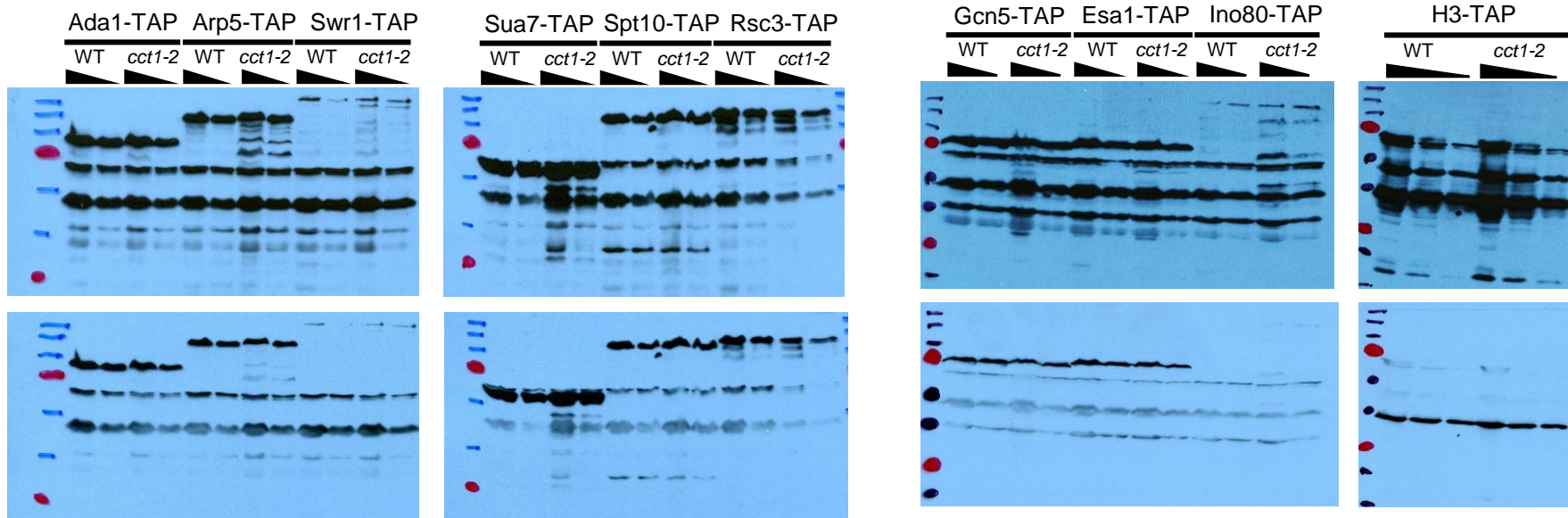
7.9. Codes

7.9.1. SplitterForPeakAnnotator.py

-Zeno-Dan Barcutean-

```
#process the file into a table
tableFile = raw_input("Enter the name of the file containing the table: ")
with open(tableFile) as f:
    lines = f.readlines()
data = []
for i in range(0, len(lines)):
    line = lines[i].split()
    data.append(line)
#split the table into two tables
table1 = []
table2 = []
dict1 = {}
dict2 = {}
for i in range(2, len(data)):
    line = data[i]
    line1 = []
    line2 = []
    line1.append(line[0])
    line1.append(line[1])
    line1.append(line[2])
    someString = ''.join(line1)
    if(someString not in dict1):
        dict1[someString] = None
        line1.append(line[3])
        table1.append('\t'.join(line1))
    line2.append(line[0])
    line2.append(line[4])
    line2.append(line[5])
    if(len(line2) > 6):
        line2.append(line[6])
    someString = ''.join(line2)
    if(someString not in dict2):
        dict2[someString] = None
        if(len(line2) > 7):
            line2.append(line[7])
```

```
            table2.append('\t'.join(line2))
#create the output files
resultFileName = raw_input("Enter the filename for the first table: ")
resultFile = open(resultFileName, 'w')
for i in table1:
    print>>resultFile, i
resultFileName = raw_input("Enter the filename for the second table: ")
resultFile = open(resultFileName, 'w')
for i in table2:
    print>>resultFile, i
```

7.9.2. UsingPeakAnnotator.py

-Zeno-Dan Barcutean-

```
import os
import subprocess

#this function splits a table into two tables
def splitTables(tableFile, splitFile1, splitFile2, outputFolder):
    with open(tableFile) as f:
        lines = f.readlines()
    data = []
    for i in range(0, len(lines)):
        line = lines[i].split()
        data.append(line)
    #split the table into two tables
    table1 = []
    table2 = []
    dict1 = {}
    dict2 = {}
    for i in range(2, len(data)):
        line = data[i]
        line1 = []
        line2 = []
        line1.append(line[0])
        line1.append(line[1])
        line1.append(line[2])
        someString = ''.join(line1)
        if(someString not in dict1):
            dict1[someString] = None
            line1.append(line[3])
            table1.append('\t'.join(line1))
```

```python
            line2.append(line[0])
            line2.append(line[4])
            line2.append(line[5])
            if(len(line2) > 6):
                line2.append(line[6])
            someString = ''.join(line2)
            if(someString not in dict2):
                dict2[someString] = None
                if(len(line2) > 7):
                    line2.append(line[7])
                table2.append('\t'.join(line2))
    #create the output files
    fromFileName = splitFile1.split('.')[0] + '_' + splitFile2
    printTable(table1, splitFile1, fromFileName, outputFolder)
    printTable(table2, splitFile2, fromFileName, outputFolder)
#this function outputs a table after splitting
def printTable(table, splitFile, fromFileName, outputFolder):
    splitFile = outputFolder + '/' + splitFile.split('.')[0] + '_from_' + fromFileName
    resultFile = open(splitFile, 'w')
    for i in table:
        print>>resultFile, i


    #first, get the path for the three folders and for the PeakAnnotator
    inputFolder1 = raw_input("Enter the name of the first input folder: ")
    inputFolder2 = raw_input("Enter the name of the second input folder: ")
    outputFolder = raw_input("Enter the name of the output folder: ")
    print("You must enter the path for the Peak Annotator; it is something like
/home/zlata/Software/PeakAnnotator_Cpp_1.4/PeakAnnotator_Linux64/")
    peakAnnotatorPath = raw_input("Enter the path for the Peak Annotator: ")
    peakAnnotatorPath += "PeakAnnotator"
    #parse the folders
    for file1 in os.listdir(inputFolder1):
        inputFile1 = inputFolder1 + '/' + file1
        for file2 in os.listdir(inputFolder2):
            inputFile2 = inputFolder2 + '/' + file2
            outputFile = outputFolder + '/' + file1.split('.')[0] + '_' + file2.split('.')[0]
            #replace with the path to your PeakAnnotator
            subprocess.call([peakAnnotatorPath, "ODS", inputFile1, inputFile2, outputFile])
            splitTables(outputFile, file1, file2, outputFolder)
```

7.9.3. DHS Searcher for Genes/Intergenic

-Zeno-Dan Barcutean-

```
files = []
data = []
fileName = ""
name = ""
while True:
    fileName = raw_input("Enter a filename (or Enter to quit): ")
    if not fileName:
        break
    with open(fileName) as f:
        lines = f.readlines()
    for i in range(0, len(lines)):
        line = lines[i].split()
        line.append (fileName)
        data.append(line)
while True:
    name = raw_input("Enter a name to search (or Enter to quit): ")
    if not name:
        break
    for line in data:
        names = line[3].split('_')
        if names[0] == name or names[1] == name:
            if line[len(line) - 1] == 'intergenic.bed':
                print 'File - intergenic.bed:    ' + line[0] + ', ' + line[1] + ', ' + line[2] + ', ' +
line[3]
            else:
                print 'File - ' + line[len(line) - 1] +':    ' + line[0] + ', '
```

7.10. Special Topic: Overview of Digital Genomic Footprinting Development and a Brief Evaluation of Reliability

Understanding genomic events on a global scale, such as binding of transcription factors along the entire genome, requires reliable techniques that enable their tracking under a given condition. The most widely used method to study interactions between transcription factors and DNA has been chromatin immunoprecipitation (ChIP) assay (Solomon 1985). ChIP was later advanced to the ChIP coupled to microarray hybridization (ChIP-chip) (Ren 2000) and to the ChIP sequencing (ChIP-Seq) (Johnson 2007, Robertson 2007). The main downside of the ChIP remains the fact that its information content has been mostly restricted to the binding sites of the single transcription factor per experiment. Before ChIP was introduced, traditional footprinting was present as an antagonistic method with the impact on identifying various *cis*-regulatory DNA binding sites rather than the target protein (Galas 1978, Gilbert 1971). ChIP however gained in popularity due to its simplicity over daunting footprinting protocols (Kuwabara 1987, Brenowitz 1986). In the recent years, sequencing accompanied by the computational add-ons in the footprinting field significantly simplified its usage. After its first application on the yeast genome, DNase I high throughput sequencing (DNaseI-Seq) in conjunction with digital genomic footprinting was introduced as a tool to study transcription factor occupancy at the single nucleotide resolution level (Hesselberth 2009). The central aspect was the implementation of novel computational methods to detect genome-wide footprint positions from a single DNaseI experiment.

The application of DNaseI-Seq in combination with digital footprinting increased due to its convenience to manage millions of reads and provide informative transcription factor pools. Yet, the accurate computational inferring of binding sites was not always guaranteed and it urged novel algorithms. Challenged by the detection accuracy,

development of various computational methods with the modifications that would tackle this problem followed (Chen 2010, Boyle 2011, Neph 2012, Piper 2013, Sung 2014), together with the expansion of the applicable model genomes. The newer algorithmic approaches argued to enhance precision of the footprint detection with respect to the previously published footprinting programs (Chen 2010, Piper 2013, Sung 2014). The specificity appears promising due to the high recapitulation rate of the regions predicted to be protected from the DNase I cleavage, but discordances still occur (Piper 2013, Sung 2014, He 2014). The question remains, given a new yeast DNase I sequencing sample and a choice of free open source footprinting software packages, how much a non-expert can rely on the digital genomic footprinting models to analyze the DNaseI-Seq data and how much the results obtained using different programs overlap. Here, theoretical scopes of the footprinting models were compared, performance of several programs were evaluated on a DNaseI-Seq sample and the outcomes were compared with the published data that contain known transcription factor binding sites.

Before the onset of computational analysis, the first experimental step of the DNaseI-Seq is to amplify the "signals" where the DNaseI was able to cut genomic DNA. For this purpose, short DNA sequences that have undergone 2 or more proximally close cleavages are released from the limited DNasaI digestion of the nuclei. These size selected sequences (<300 bp) are Illumina sequenced to generate millions of sequencing reads (Hesselberth 2009). Uniquely mappable reads are aligned to the reference genome and further background normalized. Number of aligned reads or precisely tags at specific base are used to compute DNaseI cleavage counts at that position. The classical approach from Hesselberth 2009 defines footprint as a short DNaseI protected nucleotide sequence, manifested by the transcription factor binding, which is flanked by the DNaseI unprotected sites, i.e. sites with the high cleavage rate. The binomial distribution based algorithm scans for short, 8-30 bp, non-overlapping footprints and returns the ones with defined statistical significance. The same group developed algorithm based on dynamic Bayesian network and Hidden Markov model that leveraged Hesselberth's binomial test, but it retained the same footprint architecture (Chen 2010). Using Hesselberth's model it was supported that the footprint-like protected sequences are enriched in intergenic

regions mostly upstream of transcriptional start sites (TSSs) and they contain numerous known and functional transcription factor consensus motifs. Furthermore, footprints detected by their program showed correspondence with chromatin architecture, i.e. 175 bp nucleosome caused periodicity was mirrored by the presence and absence of transcription factors. In addition, it agreed with the evolutionary conservation for some transcription factors. On the whole, it made it very consistent with the *in vivo* situation.

Hesselberth's program omits the possibility to delineate local enrichment of sequencing tags over a broader regulatory regions – DNaseI accessible genomic sequences, termed DNaseI hypersensitive sites (DHSs) – without clustering footprints to deduce this information. Several years before digital genomic footprinting, few studies analyzed DHSs by either identifying sequence outliers with respect to the background DNaseI hits (Sabo 2004) or by using simple strategy of clustering DNaseI sequence tags, and hence, accounting for the ones that are in close proximal vicinity as DHSs (Crawford 2006). The problem was the usage of defined primer pairs to analyze only selected regions. Attention was paid to the algorithm that would deduce DHSs from the entire high throughput sequencing data, where the footprints are then to be scanned from. This is important because transcription factor binding sequences are within the open chromatin, which represents only a small portion of the total chromatin. F-seq algorithm enabled easier calling of genomic regions with high DNaseI-cleavage density using kernel density estimation (Boyle 2008). As the algorithm faced the problem by using inflexible same-sized scanning windows across the entire genome, it got replaced by hotspot (John 2011). While its primary task was to detect peaks enriched in cleavage for a region, hotspot considered highly cleaved regions and poorly cleaved regions differently with respect to their local background information. Hence, an open promoter of highly transcribed genes and heterochromatin would be treated differently while the maximal cleavage information is deduced from both. In the study by Neph 2012, footprints were successfully scanned from the hotspot deduced DHSs to expand the human *cis*-regulatory lexicon. They used a simpler strategy, footprint occupancy score (FOS), that calculates contrast between the average tags within the central footprint occupied region and its flanking components. For this purpose, footprint format was stereotyped as 50-bp

protected region flanked on each side by 15-bp highly cleaved tag counts. Similarly to Hesselberth's study on yeast, this footprint feature was found to prevail in most of the mammalian promoters and is argued to direct transcriptional initiation.

Further application of digital genomic footprinting went through redefinition, expansion or change of the footprinting procedures and models. Study by Piper 2013 introduced importance of the cleavage imbalance in the two strands for the first time. Their program Wellington considers so called shoulder regions, i.e. the regions surrounding the footprint, as one of the key factors for the footprint call decision. This is because it is anticipated that DNaseI activity on one strand could be inhibited. Namely, Wellington predicts footprints with respect to the 5' sequence tag for each strand and it assumes that the number of reads aligning 5' and 3' footprint edges can be asymmetrical. The observation comes from the fact that DNase I generated fragments, especially the ones that extend away from the DHS regions, usually do not undergo second cleavage and get lost. Therefore, strand direction was regarded to be highly informative factor. In the latest comparative evaluation, Wellington was reported to outperform programs such as Neph 2012 and Nadrigal 2014 (Barozzi 2014). As digital genomic footprinting was further evolving, the complexity of the footprint nature got more obvious. Hesselberth 2009 did shortly account for the importance of the affinity of transcription factor to its cognate DNA, but not enough attention was paid to the cleavage bias and footprint was still scaffolded into a static format. Newer approaches demonstrated importance of the sequence bias, signal dependency on a transcription factor and dynamic nature of footprints (He 2014, Sung 2014). Study by Sung 2014 made a clear distinction between factor independent DNase I cut signature and protection from transiently bound transcription factor, which is then as a footprint depth dependent on the factor residence time. Their algorithm is also based on a binomial distribution, yet the footprint estimation starts from the raw cut counts simplifying the computation strategy even more than predecessors. While having reduced computation time, Sung 2014 suggested higher reproducibility. Lastly, machine-learning protein interaction quantitation (PIQ) technique was developed to scan the DNaseI-Seq data for the previously 'learned' footprint cleavage profiles and to assess a footprint impact on the local hypersensitivity (Sherwood

2014). Unlike traditional works that firstly detect DHS (Boyle 2008, Baek 2012) and then search for the footprints *de novo*, PIQ enables prediction of the status of the chromatin surrounding the footprints, which were initially detected through the data base implemented knowledge (Boyle 2011).

To take a comparative look on the performance of developed models, three different footprint detection programs (Hesselberth 2009, Piper 2013, Sung 2014) were applied on the *Saccharomyces cerevisiae* data set (Zelin 2012). This data set was chosen because we found it to be a high quality yeast DNaseI-Seq data available, based on the criteria of total number of obtained sequencing reads, reads aligned to unique genomic locations, reads that were suppressed due to multiple alignment and reads that failed to align. Footprinting programs were run on the hypersensitive sites from the wild type DNaseI-Seq sample, obtained via hotspot (John 2011). Motif scan on identified footprints was performed using frequency matrices obtained from JASPAR (Sandelin 2004).

The total numbers of identified footprints according to Hesselberth 2009 and Piper 2013 are similar (8311 and 8642) at the same false discovery rate (FDR) of 0.01; the program from Sung 2014 gives higher number (11074) at much more stringent FDR of 0.001. When weighted to the open chromatin, Hesselberth's footprints cover 7 % and Piper's and Sung's 8.4 % and 8.3 %. Despite this similarity, the ratio of intersecting base pairs between either program's footprints is only 0.2, based on the bedtools jaccard statistics (Quinlan 2010), and 30% of the footprints have any overlapping coordinates, which is very low. Hence, the programs deliver different footprint pools and the next question would be whether these results concur with the binding sites form the literature.

Computationally detected footprints are reported to cluster on promoters or other intergenic regions (Hesselberth 2009, Chen 2010, Neph 2012, Piper 2013, He 2014). However, more than 50 % of the footprints detected using either of the above programs do not have any overlap with the intergenic regions. Furthermore, it is suggested that transcription factors and nucleosomes compete for the DNA sequence and it was shown that most of the functional transcription factor binding sites are nucleosome depleted

(Segal 2006). When compared with the nucleosomal maps (Yuan 2005, Jiang 2009), only 20 % of the total detected footprints are found within non-nucleosomal DNA. It appears that regardless of different footprint sets obtained by each program, their deviations from the expected intergenic or non-nucleosomal sequences is similar.

Predicted footprints were further correlated with the targets available in the *Saccharomyces* Genome Database (SGD), that come from ChIP-Seq, ChIP-chip, microarray RNA expression levels and computational-combinatorial evidences. As summarized in the Table 7.10. below, the percentages of detected footprints, containing consensus motifs with literature relevant locations, are transcription factor dependent: Rap1 and Reb1, which are known to be strong binders, have higher recapitulation with all programs (40-50%), whereas Azf1, Cbf1, Ino2, Ino4 and Met31 very low (0-10%). The small subset of computationally detected footprints supported by the literature evidences are actually the only footprint pools that are similar between all three programs. This however represents only a small portion of the total computationally derived footprints with either of the tested programs.

In summary, several footprinting models based on different algorithms are proposed to ease identification of target transcription factors from the high-throughput data. Despite them being a valuable prediction tool within target locations, they are always to be used with caution, in supplement with other either theoretical or experimental tools.

	Table 7.10.	total detected	detected that are literature relevant	**% detected that are literature relevant**	not found in the literature
Abf1	Hesselberth 2009	156	47	**30**	109
	Piper 2013	140	23	**16**	117
	Sung 2014	179	52	**29**	127
Azf1	Hesselberth 2009	225	0	**0**	225
	Piper 2013	224	0	**0**	224
	Sung 2014	313	0	**0**	313
Gal4	Hesselberth 2009	17	3	**18**	14
	Piper 2013	22	4	**18**	18
	Sung 2014	25	7	**28**	18
Cbf1	Hesselberth 2009	66	0	**0**	66
	Piper 2013	87	3	**3**	84
	Sung 2014	60	2	**3**	58
Ino2	Hesselberth 2009	19	1	**5**	18
	Piper 2013	23	1	**4**	22
	Sung 2014	18	2	**11**	16
Ino4	Hesselberth 2009	10	0	**0**	10
	Piper 2013	12	0	**0**	12
	Sung 2014	7	2	**29**	5
Mcm1	Hesselberth 2009	42	5	**12**	37
	Piper 2013	40	7	**18**	33
	Sung 2014	39	6	**15**	33
Met31	Hesselberth 2009	76	2	**3**	74
	Piper 2013	64	1	**2**	63
	Sung 2014	68	2	**3**	66
Rap1	Hesselberth 2009	61	26	**43**	35
	Piper 2013	50	25	**50**	25
	Sung 2014	55	24	**44**	31
Reb1	Hesselberth 2009	233	111	**48**	122
	Piper 2013	159	60	**38**	99
	Sung 2014	186	94	**50**	92

8. References

Abravaya, K., Myers, M.P., Murphy, S.P., and Morimoto, R.I. (1992). The human heat shock protein hsp70 interacts with HSF1, the transcription factor that regulates heat shock gene expression. Genes Dev. *6*, 1153–1164.

Adam, M., Robert, F., Larochelle, M., and Gaudreau, L. (2001). H2A.Z is required for global chromatin integrity and for recruitment of RNA polymerase II under specific conditions. Mol. Cell. Biol. *21*, 6270–6279.

Adkins, M.W., Howar, S.R., and Tyler, J.K. (2004). Chromatin disassembly mediated by the histone chaperone Asf1 is essential for transcriptional activation of the yeast PHO5 and PHO8 genes. Mol. Cell *14*, 657–666.

Afek, A., and Lukatsky, D.B. (2013). Genome-wide organization of eukaryotic preinitiation complex is influenced by nonconsensus protein-DNA binding. Biophys. J. *104*, 1107–1115.

Afek, A., Sela, I., Musa-Lempel, N., and Lukatsky, D.B. (2011). Nonspecific transcription-factor-DNA binding influences nucleosome occupancy in yeast. Biophys. J. *101*, 2465–2475.

Akner, G., Mossberg, K., Sundqvist, K.-G., Gustafsson, J.-A., and Wikstrom, A.-C. (1992). Evidence for reversible, non-microtubule and non-microfilament-dependent nuclear translocation of hsp90 after heat shock in human fibroblasts. Eur. J. Cell Biol. *58*, 356–364.

Alberts, B.M., Amodio, F.J., Jenkins, M., Gutmann, E.D., and Ferris, F.L. (1968). Studies with DNA-cellulose chromatography. I. DNA-binding proteins from *Escherichia coli*. Cold Spring Harb. Symp. Quant. Biol. *33*, 289–305.

Albright, S.R., and Tjian, R. (2000). TAFs revisited: More data reveal new twists and confirm old ideas. Gene *242*, 1–13.

Allard, S., Utley, R.T., Savard, J., Clarke, A., Grant, P., Brandl, C.J., Pillus, L., Workman, J.L., and Côté, J. (1999). NuA4, an essential transcription adaptor/histone H4 acetyltransferase complex contains Esa1p and the ATM-related cofactor Tra1p. EMBO *18*, 5108–5119.

Allfrey, V.G., Littau, V.C., and Mirsky, E. (1963). On the role of histones in regulating ribonucleic acid synthesis in the cell nucleus. Proc. Natl. Acad. Sci. U. S. A. *49*, 414–421.

Amberg, D. C., Burke, D., Strathern, J. N. (2005). Cold Spring Harbor Laboratory **Methods in yeast genetics: a Cold Spring Harbor Laboratory course manual.** Cold Spring Harbor Laboratory Press.

Andrews S. (2010). FastQC: a quality control tool for high throughput sequence data. Available online at: http://www.bioinformatics.babraham.ac.uk/projects/fastqc

Angus-Hill, M.L., Schlichter, A., Roberts, D., Erdjument-Bromage, H., Tempst, P., and Cairns, B.R. (2001). A Rsc3/Rsc30 zinc cluster dimer reveals novel roles for the chromatin remodeler RSC in gene expression and cell cycle control. Mol. Cell *7*, 741–751.

Arrasate, M., and Finkbeiner, S. (2012). Protein aggregates in Huntington's disease. Exp. Neurol. *238*, 1–11.Arrigo,

A.P., Fakan, S., and Tissières, A. (1980). Localization of the heat shock-induced proteins in *Drosophila melanogaster* tissue culture cells. Dev. Biol. *78*, 86–103.

Artzt, K. (2012). Mammalian developmental genetics in the twentieth century. Genetics *192*, 1151–1163.

Ashburner, M., and Bonnert, J.J. (1979). The Induction of Gene Activity in *Drosophila* by Heat Shock. Cell *17*, 241–254.

Bagatell, R., Khan, O., Paine-Murrieta, G., Tayor, C.W., Akinaga, S., and Whitsell, L. (2001). Destabilization of steroid recepors by heat shock protein 90 binding drugs: A ligand independent approach to hormonal therapy for breast cancer. Clin. Cancer Res. *7*, 2076–2084.

Bak, A.L., Bak, P., and Zeuthen, J. (1979). Higher levels of organization in chromosomes. J. Theor. Biol. *76*, 205–217.

Baker, T.A., Grossman, A.D., and Gross, C.A. (1984). A gene regulating the heat shock response in *Escherichia coli* also affects proteolysis. Proc. Natl. Acad. Sci. U. S. A. *81*, 6779–6783.

Balchin, D., Hayer-Hartl, M., and Hartl, F.U. (2016). In vivo aspects of protein folding and quality control. Science *353*, 42.

Baltimore, D., (1970). Central dogma reversed. Nature *226*, 1198–1199.

Bardwell, J.C.A., and Craig, E.A. (1988). An ancient heat shock gene is dispensable. J.Bacteriol. *170*, 2977–2983.

Bardwell, J.C., and Craig, E.A. (1984). Major heat shock gene of *Drosophila* and the *Escherichia coli* heat-inducible dnaK gene are homologous. Proc. Natl. Acad. Sci. *81*, 848–852.

Barr, M.L. (1966). The significance of the sex chromatin. Int. Rev. of Cyt. *19*, 35-95.

Barraclough, R., and Ellis, R.J. (1980). Protein synthesis in chloroplasts IX. Assembly of newly-synthesized large subunits into ribulose bishopshate carboxylase in isolated intact pea chloroplasts. BBA Sect. Nucleic Acids Protein Synth. *608*, 19–31.

Bases, R. (2006). Heat shock protein 70 enhanced deoxyribonucleic acid base excision repair in human leukemic cells after ionizing radiation. Cell Stress Chaperones *11*, 240–249.

Baulieu, E. E., Binart, N., Buchou, T., Catelli, M. G., Garcia, T., Gasc, J. M., Groyer, A., Joab, I., Moncharmont, B., Radanyi, B., Renoir, M., Tuohimaa, P., and Mester., J, (1983). In *Steroid Hormone Receptors: Structure and Function* (Ericksson, H. and Gustaffson, J. A., eds) Nobel Symposium, *57*, 45–72, Elsevier Scientific Publishing Co., Amsterdam.

Behrends, C., Langer, C.A., Boteva, R., Böttcher, U.M., Stemp, M.J., Schaffar, G., Rao, B.V., Giese, A., Kretzschmar, H., Siegers, K., et al. (2006). Chaperonin TRiC Promotes the Assembly of polyQ Expansion Proteins into Nontoxic Oligomers. Mol. Cell *23*, 887–897.

Bell, O., Tiwari, V.K., Thomä, N.H., and Schübeler, D. (2011). Determinants and dynamics of genome accessibility. Nat. Rev. Genet. *12*, 554–564.

Belotserkovskaya, R., Oh, S., Bondarenko, V.A., Studitsky, V.M., Reinberg, D., Bondarenko, V.A., Orphanides, G., Studitsky, V.M., and Reinbergl, D. (2003). FACT facilitates transription-dependent nucleosomes alteration. Science *301*, 1090–1093.

Belotserkovskaya, R., Saunders, A., Lis, J.T., and Reinberg, D. (2004). Transcription through chromatin: Understanding a complex FACT. Biochim. Biophys. Acta - Gene Struct. Expr. *1677*, 87–99.

Berbers, G.A.M., Kunnen, R., van Bergen en Henegouwen, P.M.P., and Wijk, R. van (1988). Localization and quantitation of hsp84 in mammalian cells. Exp. Cell Res. *177*, 257–271.

Bergen en Henegouwen, P. M. P., Berbers, Guy, Linnemans, Wilbert, Roeland, W. (1987). Subcellular localization of the 84,000 dalton heat-shock protein in mouse neuroblastoma cells: evidence for a cytoplasmic and nuclear location. Eur. J. of Cell Biol. *43*, 78–469.

Bergerat, A., De Massy, B., Gadelle, D., Varoutas, P.C., Nicolas, A., and Forterre, P. (1997). An atypical topoisomerase II from archaea with implications for meiotic recombination. Nature *386*, 414–417.

Berlowitz, B.Y.L. (1964). Differential genetic activity, heterochromatization and RNA metabolism. Proc. N. A. S. Genet. *53*, 68–73.

Bernstein, B.E., Humphrey, E.L., Erlich, R.L., Schneider, R., Bouman, P., Liu, J.S., Kouzarides, T., and Schreiber, S.L. (2002). Methylation of histone H3 Lys 4 in coding regions of active genes. Proc. Natl. Acad. Sci. *99*, 8695–8700.

Bhagwat, A.S., and Vakoc, C.R. (2015). Targeting transcription factors in cancer. Trends in Cancer *1*, 53–65.

Bian, C., Xu, C., Ruan, J., Lee, K.K., Burke, T.L., Tempel, W., Barsyte, D., Li, J., Wu, M., Zhou, B.O., et al. (2011). Sgf29 binds histone H3K4me2/3 and is required for SAGA complex recruitment and histone H3 acetylation. EMBO J. *30*, 2829–2842.

Bigotti, M.G., and Clarke, A.R. (2008). Chaperonins: The hunt for the Group II mechanism. Arch. Biochem. Biophys. *474*, 331–339.

Biophys, S.H.B., Commun, R., Baltimore, S.H.E., Biophys, B., Renoir, J., Buchou, T., Mester, J., Radanyi, C., and Baulieu, E. (1984). Oligomeric structure of molybdate-stabilized, nontransformed 8S progesterone receptor from chicken oviduct cytosol. Am. Chem. Soc. *23*, 6016–6023.

Birnbaumer, M.E., Schrader, W.T., and O'Malley, B.W. (1979). Chemical cross-linking of chick oviduct progesterone-receptor subunits by using a reversible bifunctional cross-linking agent. Biochem. J. *181*, 201–213.

Blackwood, E., and Eisenman, R. (1991). Max: a helix-loop-helix zipper protein that forms a sequence-specific DNA-binding complex with Myc. Science *251*, 1211–1217.

Bolger, A.M., Lohse, M., and Usadel, B. (2014). Trimmomatic: A flexible trimmer for Illumina sequence data. Bioinformatics *30*, 2114–2120.

Bonnet, J., Wang, C.Y., Baptista, T., Vincent, S.D., Hsiao, W.C., Stierle, M., Kao, C.F., Tora, L., and Devys, D. (2014). The SAGA coactivator complex acts on the whole transcribed genome and is required for RNA polymerase II transcription. Genes Dev. *28*, 1999–2012.

Bose, S., Weikl, T., Bugl, H., Buchner, J., Weiki, T., and Bogi, H. (1996). Chaperone function of Hsp90-associated proteins. Science *274*, 1715–1717.

Boulon, S., Marmier-Gourrier, N., Pradet-Balade, B., Wurth, L., Verheggen, C., Jády, B.E., Rothé, B., Pescia, C., Robert, M.C., Kiss, T., et al. (2008). The Hsp90 chaperone controls the biogenesis of L7Ae RNPs through conserved machinery. J. Cell Biol. *180*, 579–595.

Boyle, A.P., Davis, S., Shulha, H.P., Meltzer, P., Margulies, E.H., Weng, Z., Furey, T.S., and Crawford, G.E. (2008). High-resolution mapping and characterization of open chromatin across the genome. Cell *132*, 311–322.

Braun, M.A., Costa, P.J., Crisucci, E.M., and Arndt, K.M. (2007). Identification of Rkr1, a Nuclear RING domain protein with functional connections to chromatin modification in *Saccharomyces cerevisiae*. Mol. Cell. Biol. *27*, 2800–2811.

Braunstein, M., Sobel, R.E., Allis, C.D., Turner, B.M., and Broach, J.R. (1996). Efficient transcriptional silencing in *Saccharomyces cerevisiae* requires a heterochromatin histone acetylation pattern. Mol. Cell. Biol. *16*, 4349–4356.

Briggs, S.D., Bryk, M., Strahl, B.D., Cheung, W.L., Davie, J.K., Dent, S.Y., Winston, F., and Allis, C.D. (2001). Histone H3 lysine 4 methylation is mediated by Set 1 and required for cell growth and rDNA silencing in *Saccharomyces cerevissiae*. Genes Dev. *15*, 3286–3295.

Brown, S.W. (1966). Heterochromatin. Science *151*, 417–425.

Buchner, J. (1999). Hsp90 and Co. - A holding for folding. Trends Biochem. Sci. *24*, 136–141.

Bukau, B., and Walker, G.C. (1989). Cellular defects caused by deletion of the *Escherichia coli* dnaK gene indicate roles for heat shock protein in normal metabolism. J. Bacteriol. *171*, 2337–2346.

Bull, E.E.A. (2004). Enhanced tumor cell radiosensitivity and abrogation of G2 and S-phase arrest by the Hsp90 inhibitor 17-(dimethylaminoethylamino)-17-demethoxygeldanamycin. Clin. Cancer Res. *10*, 8077–8084.

Buratowski, S. (2009). Progression through the RNA Polymerase II CTD Cycle. Mol. Cell *36*, 541–546.

Burke, J.M., Spencer, S.L., Lauffenburger, D.A., Sorger, P.K., Young, J.W., Alon, U., Swain, P.S., Elowitz, M.B., Swain, P.S., Kaern, M., et al. (2007). Dynamics of replication-independent histone turnover in budding yeast. Science *315*, 1405–1409.

Burns, L.G., and Peterson, C.L. (1997). Protein complexes for remodeling chromatin. Biochim. Biophys. Acta - Gene Struct. Expr. *1350*, 159–168.

Butt, T.R., Edavettal, S.C., Hall, J.P., and Mattern, M.R. (2005). SUMO fusion technology for difficult-to-express proteins. Protein Expr. Purif. *43*, 1–9.

Cairns, B.R. (2007). Chromatin remodeling: Insights and intrigue from single-molecule studies. Nat. Struct. Mol. Biol. *14*, 989–996.

Cairns, B.R., Lorch, Y., Li, Y., Zhang, M., Lacomis, L., Erdjument-Bromage, H., Tempst, P., Du, J., Laurent, B., and Kornberg, R.D. (1996). RSC, an essential, abundant chromatin-remodeling complex. Cell *87*, 1249–1260.

Carbajal, M.E., Valet, J.-P., Charest, P.M., and Tanguay, R.M. (1990). Purification of *Drosophila* hsp83 and immunoelectron microscopic localization. Eur. J. Cell Biol. *52*, 147–156.

Carrillo, E., Ben-Ari, G., Wildenhain, J., Tyers, M., Grammentz, D., and Lee, T.A. (2012). Characterizing the roles of Met31 and Met32 in coordinating Met4-activated transcription in the absence of Met30. Mol. Biol. Cell *23*, 1928–1942.

Carrozza, M.J., Li, B., Florens, L., Suganuma, T., Swanson, S.K., Lee, K.K., Shia, W.J., Anderson, S., Yates, J., Washburn, M.P., et al. (2005). Histone H3 methylation by Set2 directs deacetylation of coding regions by Rpd3S to suppress spurious intragenic transcription. Cell *123*, 581–592.

Catelli, M., Binart, N., Jung-Testas, I., Renoir, J., Baulieu, E., Feramisco, J., and Welch, W. (1985). The common 90kd component of nontransformed "8S" steroid receptors is a heat shock protein. Eur. Mol. Biol. Organ. J. *4*, 3131–3135.

Chamberlin, M.J. (1974). The selectivity of transcription. Annu. Rev. Biochem. *43*, 721–775.

Chang, J.S., and Winston, F. (2011). Spt10 and Spt21 are required for transcriptional silencing in *Saccharomyces cerevisiae*. Eukaryot. Cell *10*, 118–129.

Chen, Y., Chen, J., Loo, A., Jaeger, S., Bagdasarian, L., Yu, J., Chung, F., Korn, J., Ruddy, D., Guo, R., et al. (2013). Targeting HSF1 sensitizes cancer cells to HSP90 inhibition. Oncotarget *4*, 816–829.

Churchman, L.S., and Weissman, J.S. (2011). Nascent transcript sequencing visualizes transcription at nucleotide resolution. Nature *469*, 368–373.

Clapier, C.R., and Cairns, B.R. (2009). The biology of chromatin remodeling complexes. Annu. Rev. Biochem. *78*, 273–304.

Clapier, C.R., Kasten, M.M., Parnell, T.J., Viswanathan, R., Szerlong, H., Sirinakis, G., Zhang, Y., and Cairns, B.R. (2016). Regulation of DNA translocation efficiency within the chromatin remodeler RSC/Sth1 potentiates nucleosome sliding and ejection. Mol. Cell *62*, 453–461.

Clarke, A.S., Lowell, J.E., Jacobson, S.J., and Pillus, L. (1999). Esa1p is an essential histone acetyltransferase required for cell cycle progression. Mol Cell Biol *19*, 2515–2526.

Collier, N.C., and Schlesinger, M.J. (1986). The dynamic state of heat shock proteins in chicken embryo fibroblasts. J. Cell Biol. *103*, 1495–1507.

Comings, D.E. (1967). Histones of genetically active and inactive chromatin. J. Cell Biol. 35, 699-708.

Crawford, G.E., Davis, S., Scacheri, P.C., Renaud, G., Halawi, M.J., Erdos, M.R., Green, R., Meltzer, P.S., Wolfsberg, T.G., and Collins, F.S. (2006). DNase-chip: A high-resolution method to identify DNase I hypersensitive sites using tiled microarrays. Nat. Methods *3*, 503–509.

Culkin, J., de Bruin, L., Tompitak, M., Phillips, R., and Schiessel, H. (2017). The role of DNA sequence in nucleosome breathing. Eur. Phys. J. E *40*.

David, K., and Kevin, S. (1997). Repression by Ume6 involves recruitment of a complex containing Sin3 corepressor and Rpd3 histone deacetylase to target promoters. Cell *89*, 365–371.

de Visser, J.A.G.M., Hermisson, J., Wagner, G.P., Meyers, L.A., Bagheri-Chaichian, H., Blanchard, J.L., Chao, L., Cheverud, J.M., Elena, S.F., Fontana, W., et al. (2003). Perspective: Evolution and detection of genetic robustness. Int. J. Org. Evol. *57*, 1959–1972.

DeFranco, D.B., and Csermely, P. (2000). Steroid receptor and molecular chaperone encounters in the nucleus. Sci STKE *42*.

DeGennaro, C.M., Alver, B.H., Marguerat, S., Stepanova, E., Davis, C.P., Bahler, J., Park, P.J., and Winston, F. (2013). Spt6 regulates intragenic and antisense transcription, nucleosome positioning, and histone modifications genome-wide in fission teast. Mol. Cell. Biol. *33*, 4779–4792.

Dekker, C., Stirling, P.C., McCormack, E.A., Filmore, H., Paul, A., Brost, R.L., Costanzo, M., Boone, C., Leroux, M.R., and Willison, K.R. (2008). The interaction network of the chaperonin CCT. EMBO J. *27*, 1827–1839.

DeZwaan, D.C., Toogun, O.A., Echtenkamp, F.J., and Freeman, B.C. (2009). The Hsp82 molecular chaperone promotes a switch between unextendable and extendable telomere states. Nat. Struct. Mol. Biol. *16*, 711–716.

Dion, M.F., Altschuler, S.J., Wu, L.F., and Rando, O.J. (2005). Genomic characterization reveals a simple histone H4 acetylation code. Proc. Natl. Acad. Sci. *102*, 5501–5506.

Dobin, A., Davis, C.A., Schlesinger, F., Drenkow, J., Zaleski, C., Jha, S., Batut, P., Chaisson, M., and Gingeras, T.R. (2013). STAR: Ultrafast universal RNA-seq aligner. Bioinformatics *29*, 15–21.

Dobrovolskaia-Zavadskaia, N. (1933). Preliminary symbols for a tail-mutation in mice. The American Naturalist *67*, 186-188.

Dobson, C.M. (1999). Protein misfolding, evolution and disease. TIBS *0004*, 329–332.

Dodson, M., Echols, H., Wickner, S., Alfano, C., Mensa-Wilmot, K., Gomes, B., LeBowitz, J., Roberts, J.D., and McMacken, R. (1986). Specialized nucleoprotein structures at the origin of replication of bacteriophage lambda: localized unwinding of duplex DNA by a six-protein reaction. Proc. Natl. Acad. Sci. U. S. A. *83*, 7638–7642.

Dodson, M., McMacken, R., and Echols, H. (1989). Specialized nucleoprotein structures at the origin of replication of bacteriophage l. J.Biol.Chem. *264*, 10719–10725.

Dodson, M., Roberts, J., McMacken, R., and Echols, H. (1985). Specialized nucleoprotein structures at the origin of replication of bacteriophage lambda: complexes with lambda O protein and with lambda O, lambda P, and *Escherichia coli* DnaB proteins. Proc. Natl. Acad. Sci. U. S. A. *82*, 4678–4682.

Dollard, C., Ricupero-Hovasse, S.L., Natsoulis, G., Boeke, J.D., and Winston, F. (1994). SPT10 and SPT21 are required for transcription of particular histone genes in *Saccharomyces cerevisiae*. Mol. Cell. Biol. *14*, 5223–5228.

Donnelly, N., Passerini, V., Durrbaum, M., Stingele, S., and Storchova, Z. (2014). HSF1 deficiency and impaired HSP90-dependent protein folding are hallmarks of aneuploid human cells. EMBO J. *33*, 2374–2387.

Dote, H., Burgan, W.E., Camphausen, K., and Tofilon, P.J. (2006). Inhibition of Hsp90 compromises the DNA damage response to radiation. Cancer Res. *66*, 9211–9220.

Dronamraju, R., Ramachandran, S., Jha, D.K., Adams, A.T., Difiore, J. V., Parra, M.A., Dokholyan, N. V., and Strahl, B.D. (2017). Redundant functions for Nap1 and Chz1 in H2A.Z deposition. Sci. Rep. *7*, 1–10.

Dudley, A.M., Rougeulle, C., and Winston, F. (1999). The Spt components of SAGA facilitate TBP binding to a promoter at a post-activator-binding step in vivo. Genes Dev. *13*, 2940–2945.

Dunn, A.Y., Melville, M.W., and Frydman, J. (2001). Review: Cellular substrates of the eukaryotic chaperonin TRiC/CCT. J. Struct. Biol. *135*, 176–184.

Dutta, A., Gogol, M., Kim, J.H., Smolle, M., Venkatesh, S., Gilmore, J., Florens, L., Washburn, M.P., and Workman, J.L. (2014). Swi/Snf dynamics on stress-responsive genes is governed by competitive bromodomain interactions. Genes Dev. *28*, 2314–2330.

Dutta, R., and Inouye, M. (2000). GHKL, an emergent ATPase/kinase superfamily. Trends Biochem. Sci. *25*, 24–28.Ebrahimi-Fakhari, D., Wahlster, L., and McLean, P.J. (2011). Molecular chaperones in Parkinson's disease – present and future. J Park. Dis *1*, 299–320.

Echtenkamp, F.J., Zelin, E., Oxelmark, E., Woo, J.I., Andrews, B.J., Garabedian, M., and Freeman, B.C. (2011). Global functional map of the p23 molecular chaperone reveals an extensive cellular network. Mol. Cell *43*, 229–241.

Edery, I., and Sonenberg, N. (1985). Cap-dependent RNA splicing in a HeLa nuclear extract. Proc. Natl. Acad. Sci. U. S. A. *82*, 7590–7594.

Elgin, S.C.R., and Weintraub, H. (1975). Further 1975. Annu. Rev. Biochem. *44*, 725–774.Ellis, R. (1987). Proteins as molecular chaperones. Nature *328*, 378–379.

Engerud, H., Tangen, I.L., Berg, A., Kusonmano, K., Halle, M.K., Øyan, A.M., Kalland, K.H., Stefansson, I., Trovik, J., Salvesen, H.B., et al. (2014). High level of HSF1 associates with aggressive endometrial carcinoma and suggests potential for HSP90 inhibitors. Br. J. Cancer *111*, 78–84.

Eriksson, P.R., Mendiratta, G., McLaughlin, N.B., Wolfsberg, T.G., Mariño-Ramírez, L., Pompa, T. a, Jainerin, M., Landsman, D., Shen, C.-H., and Clark, D.J. (2005). Global regulation by the yeast Spt10 protein is mediated through chromatin structure and the histone upstream activating sequence elements. Mol. Cell. Biol. *25*, 9127–9137.

Fan, X., Geisberg, J. V., Wong, K.H., and Jin, Y. (2011). Conditional depletion of nuclear proteins by the Anchor Away system. Curr. Protoc. Mol. Biol. 1–8.

Farr, G.W., Scharl, E.C., Schumacher, R.J., Sondek, S., and Horwich, A.L. (1997). Chaperonin-mediated folding in the eukaryotic cytosol proceeds through rounds of release of native and nonnative forms. Cell *89*, 927–937.

Fayet, O., Ziegelhoffer, T., and Georgopoulos, C. (1989). The groES and groEL heat shock gene products of *Escherichia coli* are essential for bacterial growth at all temperatures. J. Bacteriol. *171*, 1379–1385.

Feldman, D.E., Thulasiraman, V., Ferreyra, R.G., and Frydman, J. (1999). Formation of the VHL-elongin BC tumor suppressor complex is mediated by the chaperonin TRiC. Mol. Cell *4*, 1051–1061.

Felts, S.J., and Toft, D.O. (2003). P23, a simple protein with complex activities. Cell Stress and Chaperones *8*, 108–113.

Feng, J., Meyer, C.A., Wang, Q., Liu, J.S., Liu, X.S., and Zhang, Y. (2012). GFOLD: A generalized fold change for ranking differentially expressed genes from RNA-seq data. Bioinformatics *28*, 2782–2788.

Feng, Q., Wang, H., Ng, H.H., Erdjument-Bromage, H., Tempst, P., Struhl, K., and Zhang, Y. (2002). Methylation of H3-lysine 79 is mediated by a new family of HMTases without a SET domain. Curr. Biol. *12*, 1052–1058.

Fini, M.E., Bendena, W.G., and Pardue, M.L. (1989). Unusual behavior of the cytoplasmic transcript of hsrω: An abundant, stress-inducible RNA that is translated but yields no detectable protein product. J. Cell Biol. *108*, 2045–2057.

Flahertu, K.M., DeLuca-Flaherty, C., and McKay, D.B. (1990). Three-dimesnional structure of the ATPase fragment of 70K heat-shock cognate protein. Nature *346*, 623–628.

Flemming, W. (1882). Zell-Substanz, Kern und Zellteilung. F.C.W. Vogel in Leipzig.

Floer, M., Bryant, G.O., and Ptashne, M. (2008). HSP90/70 chaperones are required for rapid nucleosome removal upon induction of the GAL genes of yeast. Proc. Natl. Acad. Sci. *105*, 2975–2980.

Floer, M., Wang, X., Prabhu, V., Berrozpe, G., Narayan, S., Spagna, D., Alvarez, D., Kendall, J., Krasnitz, A., Stepansky, A., et al. (2010). A RSC/nucleosome complex determines chromatin architecture and facilitates activator binding. Cell *141*, 407–418.

Flom, G., Weekes, J., and Johnson, J.L. (2005). Novel interaction of the Hsp90 chaperone machine with Ssl2, an essential DNA helicase in *Saccharomyces cerevisiae*. Curr. Genet. *47*, 368–380.

Fraction, N. (1977). Progesterone receptors in the chick oviduct. Eur. J. Biochem. *72*, 405–414.

Freeman, B.C. (2002). Disassembly of transcriptional regulatory complexes by molecular chaperones. Science *296*, 2232–2235.

Freeman, B.C., Felts, S.J., Toft, D.O., and Yamamoto, K.R. (2000). The p23 molecular chaperones act at a late step in intracellular receptor action to differentially affect ligand efficacies. Genes Dev. *14*, 422–434.

Freeman, B.C., Toft, D.O., and Morimoto, R.I. (1996). Molecular chaperone machines: Chaperone activities of the cyclophilin Cyp-40 and the steroid aporeceptor-associated protein p23. Science *274*, 1718–1720.

Freeman, B.C., and Yamamoto, K.R. (2001). Continuous recycling: A mechanism for modulatory signal transduction. Trends Biochem. Sci. *26*, 285–290.

Frietze S., Farnham P.J. (2011). Transcription Factor Effector Domains. In: Hughes T. (eds) A Handbook of Transcription Factors. Subcellular Biochemistry, *52*, Springer, Dordrecht.

Frydman, J., Nimmesgern, E., Ohtsuka, K., and Hartl, F.U. (1994). Folding of nascent polypeptide chains in a high molecular mass assembly with molecular chaperones. Nature *370*, 111–117.

Frydman, J., Nimmesgern, E., Erdjument-Bromage1, H., Wall2, J.S., Tempst1, P., and Hartl3, F.-U. (1992). Function in protein folding of TRiC, a cytosolic ring complex containing TCP-1 and structurally related subunits. EMBO J. *1*, 4767–4778.

Gamer, J., Bujard, H., and Bukau, B. (1992). Physical interaction between heat shock proteins DnaK, DnaJ, and GrpE and the bacterial heat shock transcription factor sigma 32. Cell *69*, 833–842.

Gamer, J., Multhaup, G., Tomoyasu, T., McCarty, J.S., Rüdiger, S., Schönfeld, H.J., Schirra, C., Bujard, H., and Bukau, B. (1996). A cycle of binding and release of the DnaK, DnaJ and GrpE chaperones regulates activity of the *Escherichia coli* heat shock transcription factor sigma32. EMBO J. *15*, 607–617.

Ganapathi, M., Palumbo, M.J., Ansari, S.A., He, Q., Tsui, K., Nislow, C., and Morse, R.H. (2011). Extensive role of the general regulatory factors, Abf1 and Rap1, in determining genome-wide chromatin structure in budding yeast. Nucleic Acids Res. *39*, 2032–2044.

Gao, Y., Thomas, J.O., Chow, R.L., Lee, G.H., and Cowan, N.J. (1992). A cytoplasmic chaperonin that catalyzes β-actin folding. Cell *69*, 1043–1050.

Garbe, J.C., and Pardue, M.L. (1986). Heat shock locus 93D of *Drosophila melanogaster*: a spliced RNA most strongly conserved in the intron sequence. Proc. Natl. Acad. Sci. USA *83*, 1812–1816.

Gasc, J.M., Renoir, J.M., Radanyi, C., Joab, I., Tuohimaa, P., and Baulieu, E.E. (1984). Progesterone receptor in the chick oviduct: An immunohistochemical study with antibodies to distinct receptor components. J. Cell Biol. *99*, 1193–1201.

Gasc, J.M., Renoir, J.M., Faber, L.E., Delahaye, F., and Baulieu, E.E. (1990). Nuclear localization of two steroid receptor-associated proteins, hsp90 and p59. Exp. Cell Res. *186*, 362–367.

Gatenby, A.A., and Viitanen, P. V (1994). Structural and functional aspects of chaperonin-mediated protein folding. Annu Rev Plant Physiol *45*, 469–491.

Gemmill, T.R., Wu, X., and Hanes, S.D. (2005). Vanishingly low levels of Ess1 prolyl-isomerase activity are sufficient for growth in *Saccharomyces cerevisiae*. J. Biol. Chem. *280*, 15510–15517.

Georgopoulos, C.P. (1977). A new bacterial gene (groPC) which affects lambda DNA replication. Mol. Gen. Genet. *151*, 35–39.

Georgopoulos, C.P. (1971). Bacterial mutants in which the gene N function of bacteriophage lambda is blocked have an altered RNA polymerase. Proc. Natl. Acad. Sci. U. S. A. *68*, 2977–2981.

Georgopoulos, C.P., Hendrix, R.W., Casjens, S.R., and Kaiser, A.D. (1973). Host participation in bacteriophage lambda head assembly. J. Mol. Biol. *76*, 45–60.

Gerhold, C.B., and Gasser, S.M. (2014). INO80 and SWR complexes: Relating structure to function in chromatin remodeling. Trends Cell Biol. *24*, 619–631.

Gerner, C., Gotzmann, J., Fröhwein, U., Schamberger, C., Ellinger, A., and Sauermann, G. (2002). Proteome analysis of nuclear matrix proteins during apoptotic chromatin condensation. Cell Death Differ. *9*, 671–681.

Gerner, C., Holzmann, K., Meissner, M., Gotzmann, J., Grimm, R., and Sauermann, G. (1999). Reassembling proteins and chaperones in human nuclear matrix protein fractions. J. Cell. Biochem. *74*, 145–151.

Ghaemmaghami, S., Huh, W.-K., Bower, K., Howson, R.W., Belle, A., Dephoure, N., O'Shea, E.K., and Weissman, J.S. (2003). Global analysis of protein expression in yeast. Nature *425*, 737–741.

Gietz, R.D., and Schiestl, R.H. (2008). High-efficiency yeast transformation using the LiAc/SS carrier DNA/PEG method. Nat. Protoc. *2*, 31–35.

Gilbert, C.S., van den Bosch, M., Green, C.M., Vialard, J.E., Grenon, M., Erdjument-Bromage, H., Tempst, P., and Lowndes, N.F. (2003). The budding yeast Rad9 checkpoint complex: Chaperone proteins are required for its function. EMBO Rep. *4*, 953–958.

Glajch, K.E., and Sadri-Vakili, G. (2015). Epigenetic mechanisms Involved in Huntington's disease pathogenesis. J. Huntingtons. Dis. *4*, 1–15.

Goldfless, S.J., Morag, A.S., Belisle, K.A., Sutera, V.A., and Lovett, S.T. (2006). DNA repeat rearrangements mediated by DnaK-dependent replication fork repair. Mol. Cell *21*, 595–604.

Goldman, L., Franke, E.K., Kindel, D.J., Blaney, D.J., and Richfield, D. (1963). Histones and gene functions. Nature *197*, 912–914.

Goodfellow, S. J., and Zomerdijk, J. C. B. M. (2013). Basic mechanisms in RNA polymerase I transcription of the ribosomal RNA Genes. In: Kundu T. (eds) Epigenetics: Development and Disease. Subcellular Biochemistry, *61*, Springer, Dordrecht.

Goodrich, J.A., and Tjian, R. (1994). TBP-TAF complexes: selectivity factors for eukaryotic transcription. Curr. Opin. Cell Biol. *6*, 403–409.

Gorski, J., Toft, D., Shyamala, G., Smith, D., Notides, A. (1968). Hormone receptors: studies on the interaction of estrogen with the uterus. Recent Prog. Horm. Res. *24*, 45–80.

Govind, C.K., Qiu, H., Ginsburg, D.S., Ruan, C., Hofmeyer, K., Hu, C., Swaminathan, V., Workman, J.L., Li, B., and Hinnebusch, A.G. (2010). Phosphorylated Pol II CTD recruits multiple HDACs, including Rpd3C(S), for methylation-dependent deacetylation of ORF nucleosomes. Mol. Cell *39*, 234–246.

Grant, P.A., Schieltz, D., Pray-Grant, M.G., Yates, J.R., Workman, J.L., Amati, B., Dalton, S., Brooks, M.W., Littlewood, T.D., Evan, G.I., et al. (1998). The ATM-related cofactor Tra1 is a component of the purified SAGA complex. Mol. Cell *2*, 863–867.

Grant, P.A., Duggan, L., Côté, J., Roberts, S.M., Brownell, J.E., Candau, R., Ohba, R., Owen-Hughes, T., Allis, C.D., Winston, F., et al. (1997). Yeast Gcn5 functions in two multisubunit complexes to acetylate nucleosomal histones: Characterization of an ADA complex and the SAGA (SPT/ADA) complex. Genes Dev. *11*, 1640–1650.

Grant, P.A., Eberharter, A., John, S., Cook, R.G., Turner, B.M., and Workman, J.L. (1999). Expanded lysine acetylation specificity of Gcn5 in native complexes. J. Biol. Chem. *274*, 5895–5900.

Gross, J.D. (1957). Incorporation of phosphorus-32 into salivary-type chromosomes which exibit "Puffs." Nature *180*, 440.

Grudniak, A.M., Markowska, K., and Wolska, K.I. (2015). Interactions of *Escherichia coli* molecular chaperone HtpG with DnaA replication initiator DNA. Cell Stress Chaperones *20*, 951–957.

Grunstein, M. (1997). Histone acetylation in chromatin structure and transcription. Nature *389*, 349–352.

Grunstein, M. (1997). Molecular model for telomeric heterochromatin in yeast. Curr. Opin. Cell Biol. *9*, 383–387.

Guenther, M.G., Yu, J., Kao, G.D., Yen, T.J., and Lazar, M.A. (2002). Assembly of the SMRT-histone deacetylase 3 repression complex requires the TCP-1 ring complex. Genes Dev. *16*, 3130–3135.

Guillemette, B., Bataille, A.R., Gévry, N., Adam, M., Blanchette, M., Robert, F., and Gaudreau, L. (2005). Variant histone H2A.z is globally localized to the promoters of inactive yeast genes and regulates nucleosome positioning. PLoS Biol. *3*, 1–11.

Hackam, A.S., Singaraja, R., Zhang, T., Gan, L., and Hayden, M.R. (1999). In vitro evidence for both the nucleus and cytoplasm as subcellular sites of pathogenesis in Huntington's disease. Hum. Mol. Genet. *8*, 25–33.

Hahn, S. (1998). The role of TAFs in RNA polymerase II transcription. Cell *95*, 579–582.

Hahn, S., and Young, E.T. (2011). Transcriptional regulation in *Saccharomyces cerevisiae*: Transcription factor regulation and function, mechanisms of initiation, and roles of activators and coactivators. Genetics *189*, 705–736.

Hamamoto, R., Furukawa, Y., Morita, M., Iimura, Y., Silva, F.P., Li, M., Yagyu, R., and Nakamura, Y. (2004). SMYD3 encodes a histone methyltransferase involved in the proliferation of cancer cells. Nat. Cell Biol. *6*, 731–740.

Hardy, S., Jacques, P.É., Gévry, N., Forest, A., Fortin, M.È., Laflamme, L., Gaudreau, L., and Robert, F. (2009). The euchromatic and heterochromatic landscapes are shaped by antagonizing effects of transcription on H2A.Z deposition. PLoS Genet. *5*.

Hardy, S., and Robert, F. (2010). Random deposition of histone variants: A cellular mistake or a novel regulatory mechanism? Epigenetics *5*, 368–372.

Hartl, F.U., Bracher, A., and Hayer-Hartl, M. (2011). Molecular chaperones in protein folding and proteostasis. Nature *475*, 324–332.

Hartley, P.D., and Madhani, H.D. (2009). Mechanisms that specify promoter nucleosome location and identity. Cell *137*, 445–458.

Haruki, H., Nishikawa, J., and Laemmli, U.K. (2008). The anchor-away technique: rapid, conditional establishment of yeast mutant phenotypes. Mol. Cell *31*, 925–932.

Haussler, E. P., Festschrift Hevn. Basel, Reinhardt, *1936*, 339–341.

Hayes, S.A., and Dice, J.F. (1996). Roles of molecular chaperones in protein degradation. J. Cell Biol. *132*, 255–258.

Heitz, E. (1928). **Das heterochromatin der Moose.** I. Jahrb. Wiss. Botanik, *69*, 762–818.

Hemmingsen, S.M., Woolford, C., van der Vies, S.M., Tilly, K., Dennis, D.T., Georgopoulos, C.P., Hendrix, R.W., and Ellis, R.J. (1988). Homologous plant and bacterial proteins chaperone oligomeric protein assembly. Nature *333*, 330–334.

Henikoff, S. (2000). Heterochromatin function in complex genomes. Biochim. Biophys. Acta *1470*, O1–O8.

Hennig, B.P., Bendrin, K., Zhou, Y., and Fischer, T. (2012). Chd1 chromatin remodelers maintain nucleosome organization and repress cryptic transcription. EMBO Rep. *13*, 997–1003.

Henry, K.W., Wyce, A., Lo, W.S., Duggan, L.J., Emre, N.C.T., Kao, C.F., Pillus, L., Shilatifard, A., Osley, M.A., and Berger, S.L. (2003). Transcriptional activation via sequential histone H2B ubiquitylation and deubiquitylation, mediated by SAGA-associated Ubp8. Genes Dev. *17*, 2648–2663.

Herrmann, B.G., Barlow, D.P., and Lehrach, H. (1987). A large inverted duplication allows homologous recombination between chromosomes heterozygous for the proximal t complex inversion. Cell *48*, 813–825.

Herrmann, B.G., Labeit, S., Poustka, A., King, T.R., and Lehrach, H. (1990). Cloning of the T gene required in mesoderm formation in the mouse. Nature *343*, 617–622.

Hess, D., Liu, B., Roan, N.R., Sternglanz, R., and Winston, F. (2004). Spt10-dependent transcriptional activation in *Saccharomyces cerevisiae* requires both the Spt10 acetyltransferase domain and Spt21. Mol. Cell. Biol. *24*, 135–143.

Hesselberth, J.R., Chen, X., Zhang, Z., Sabo, P.J., Sandstrom, R., Reynolds, A.P., Thurman, R.E., Neph, S., Kuehn, M.S., Noble, W.S., et al. (2009). Global mapping of protein-DNA interactions in vivo by digital genomic footprinting. Nat. Methods *6*, 283–289.

Hirschhorn, J.N., Brown, S.A., Clark, C.D., and W, F. (1992). Evidence that SNF2/ WI2 and SNF5 activate transcription in yeast by altering chromatin structure Genes Dev. 2288–2298.

Ho, Y., Gruhler, A., Heilbut, A., Bader, G.D., Moore, L., Adams, S.L., Millar, A., Taylor, P., Bennett, K., Boutilier, K., et al. (2002). Systematic identification of protein complexes in *Saccharomyces cerevisiae* by mass spectrometry. Nature *415*, 180–183.

Holt, S.E., Aisner, D.L., Baur, J., Tesmer, V.M., Dy, M., Ouellette, M., Trager, J.B., Morin, G.B., Toft, D.O., Shay, J.W., et al. (1999). Functional requirement of p23 and Hsp90 in telomerase complexes. Genes Dev. *13*, 817–826.

Horwich, A.L., Willison, K.R., Cowan, N.J., Viitanen, P., Micklethwaite, P., Gething, M.-J., Saibil, H., Georgopoulos, C., Hartl, F.-U., Welch, W.J., et al. (1993). Protein folding in the cell: Functions of two families of molecular chaperone, hsp 60 and TF55-TCP1. Philos. Trans. R. Soc. Lond. B *339*, 313–326.

Horwich, A.L., Fenton, W.A., Chapman, E., and Farr, G.W. (2007). Two families of chaperonin: physiology and mechanism. Annu. Rev. Cell Dev. Biol. *23*, 115–145.

Hsu, T.C. (1962). Differential rate in RNA sythesis between euchromatin and heterochromatin. Exp. Cell Res. *27*, 332–334.Hu, J., and Anselmo, D. (2000). *In vitro* reconstitution of a functional duck hepatitis B virus reverse transcriptase: posttranslational activation by Hsp90. J. Virol. *74*, 11447–11455.

Hu, J., and Seeger, C. (1996). Hsp90 is required for the activity of a hepatitis B virus reverse transcriptase. Proc. Natl. Acad. Sci. U. S. A. *93*, 1060–1064.

Hu, J., O.Toft, D., and Seeger, C. (1997). Hepadnavirus assembly and reverse transcription require a multi-component chaperone complex which is incorporated into nucleocapsids. EMBO J. *16*, 59–68.

Hummel, B., Hansen, E.C., Yoveva, A., Aprile-Garcia, F., Hussong, R., and Sawarkar, R. (2017). The evolutionary capacitor HSP90 buffers the regulatory effects of mammalian endogenous retroviruses. Nat. Struct. Mol. Biol. *24*, 234–242.

Hunt, C.R., Dix, D.J., Sharma, G.G., Pandita, R.K., Gupta, A., Funk, M., and Pandita, T.K. (2004). Genomic instability and enhanced radiosensitivity in Hsp70.1- and Hsp70.3-deficient mice. Mol. Cell. Biol. *24*, 899–911.

Hwang, D.S., Crooke, E., and Kornberg, A. (1990). Aggregated dnaA protein is dissociated and activated for DNA replication by phospholipase or dnaK protein. J. Biol. Chem. *265*, 19244–19248.

Im, H., Park, C., Feng, Q., Johnson, K.D., Kiekhaefer, C.M., Choi, K., Zhang, Y., and Bresnick, E.H. (2003). Dynamic regulation of histone H3 methylated at lysine 79 within a tissue-specific chromatin domain. J. Biol. Chem. *278*, 18346–18352.

Ingvarsdottir, K., Krogan, N.J., Emre, N.C.T., Wyce, A., Thompson, N.J., Emili, A., Hughes, T.R., Greenblatt, J.F., and Berger, S.L. (2005). H2B ubiquitin protease Ubp8 and Sgf11 constitute a discrete functional module within the *Saccharomyces cerevisiae* SAGA complex. Mol. Cell. Biol. *25*, 1162–1172.

Ishihama, A., Ikeuchi, T., and Yura, T. (1976). A novel adenosine triphosphatase isolated from RNA polymerase preparations of *Escherichia coli*. J. Biochem. *79*, 917–925.

Itikawa, H., and Ryu, J.-I. (1979). Isolation and characterization of a temperature-sensitive dnak mutant of *Escherichia coli*. B. J. Bacteriol. *138*, 339–344.

Jacob, F., Ullman, A., and Mond, J. (1964). The promoter, a genetic element necessary for the expression of an operon. CR Acad. Sci. *258*, 3125–28.

James, P., Halladay, J., and Craig, E. a (1996). Genomic libraries and a host. Genetics *144*, 1425–1436.

Jarosz, D.F., and Lindquist, S. (2010). Hsp90 and environmental stress transform the adaptive value of natural genetic variatio. Science *330*, 1820–1824.

Jarosz, D.F., Taipale, M., and Lindquist, S. (2010). Protein Homeostasis and the Phenotypic Manifestation of Genetic Diversity: Principles and Mechanisms. Annu. Rev. Genet. *44,* 189–216.

Jaskelioff, M., and Peterson, C.L. (2003). Chromatin and transcription: Histones continue to make their marks. Nat. Cell Biol. *5*, 395–399.

Jenkins, A.J., March, J.B., Oliver, I.R., and Masters, M. (1986). A DNA fragment containing the groE genes can suppress mutations in the *Escherichia coli* dnaA gene. Mol. Gen. Genet. *202*, 446–454.

Jensen, E. V (2017). On the Mechanism of Estrogen Action. Perspect. Biol. Med. *6*, 47–60.

Jeronimo, C., Watanabe, S., Kaplan, C.D., Peterson, C.L., and Robert, F. (2015). The Histone Chaperones FACT and Spt6 Restrict H2A.Z from Intragenic Locations. Mol. Cell *58*, 1113–1123.

Jin, Y., Eser, U., Struhl, K., and Churchman, L.S. (2017). The Ground State and Evolution of Promoter Region Directionality. Cell *170*, 889–898.

Joab, I., Radanyi, C., Renoir, M., Buchou, T., Catelli, M.-G., Binart, N., Mester, J., and Baulieu, E.-E. (1984). Common non-hormone binding component in non-transformed chick oviduct receptors of four steroid hormones. Nature *308*, 850–853.

John, S., Sabo, P.J., Thurman, R.E., Sung, M.H., Biddie, S.C., Johnson, T.A., Hager, G.L., and Stamatoyannopoulos, J.A. (2011). Chromatin accessibility pre-determines glucocorticoid receptor binding patterns. Nat. Genet. *43*, 264–268.

Johnson, J.L., and Toft, D.O. (1994). A novel chaperone complex for steroid receptors involving heat shock proteins, immunophilins, and p23. J. Biol. Chem. *269*, 24989–24993.

Joly, E.C., Tremblay, E., Tanguay, R.M., Wu, Y., and Bibor-Hardy, V. (1994). TRiC-P5, a novel TCP1-related protein, is localized in the cytoplasm and in the nuclear matrix. J. Cell Sci. *107*, 2851–2859.

Jorgensen, P., Edgington, N.P., Schneider, B., Rupes, I., Tyers, Mike, and Flutcher, B. (2010). The size of the nucleus increases as yeast cells grow. Mol. Biol. Cell *18*, 3523–3532.

Josling, G.A., Selvarajah, S.A., Petter, M., and Duffy, M.F. (2012). The role of bromodomain proteins in regulating gene expression. Genes *3*, 320–343.

Kabakov, A.E., Malyutina, Y. V., and Latchman, D.S. (2006). Hsf1-mediated stress response can transiently enhance cellular radioresistance. Radiat. Res. *165*, 410–423.

Kadosh, D., and Struhl, K. (1998). Targeted recruitment of the Sin3-Rpd3 histone deacetylase complex generates a highly localized domain of repressed chromatin in vivo. Mol. Cell. Biol. *18*, 5121–5127.

Kang, K.I., Devin, J., Cadepond, F., Jibard, N., Guiochon-Mantel, a, Baulieu, E.E., and Catelli, M.G. (1994). In vivo functional protein-protein interaction: nuclear targeted hsp90 shifts cytoplasmic steroid receptor mutants into the nucleus. Proc. Natl. Acad. Sci. U. S. A. *91*, 340–344.

Kang, K.I., Meng, X., Devin-Leclerc, J., Bouhouche, I., Chadli, a, Cadepond, F., Baulieu, E.E., and Catelli, M.G. (1999). The molecular chaperone Hsp90 can negatively regulate the activity of a glucocorticosteroid-dependent promoter. Proc. Natl. Acad. Sci. U. S. A. *96*, 1439–1444.

Kaplan, C.D., Laprade, L., and Winston, F. (2003). Transcription Elongation Factors Repress Transcription Inititaion from Cryptic Sites. Science *239*, 17–18.

Kaplan, T., Liu, C.L., Erkmann, J.A., Holik, J., Grunstein, M., Kaufman, P.D., Friedman, N., and Rando, O.J. (2008). Cell cycle- and chaperone-mediated regulation of H3K56ac incorporation in yeast. PLoS Genet. *4*.

Karmodiya, K., Krebs, A.R., Oulad-Abdelghani, M., Kimura, H., and Tora, L. (2012). H3K9 and H3K14 acetylation co-occur at many gene regulatory elements, while H3K14ac marks a subset of inactive inducible promoters in mouse embryonic stem cells. BMC Genomics *13*.

Kasten, M., Szerlong, H., Erdjument-Bromage, H., Tempst, P., Werner, M., and Cairns, B.R. (2004). Tandem bromodomains in the chromatin remodeler RSC recognize acetylated histone H3 Lys14. EMBO J. *23*, 1348–1359.

Kelley, P.M., and Schlesinger, M.J. (1982). Antibodies to two major chicken heat shock proteins cross-react with similar proteins in widely divergent species. Mol. Cell. Biol. *2*, 267–274.

Kenny, M.K., Mendez, F., Sandigursky, M., Kureekattil, R.P., Goldman, J.D., Franklin, W.A., and Bases, R. (2001). Heat Shock Protein 70 Binds to Human Apurinic/Apyrimidinic Endonuclease and Stimulates Endonuclease Activity at Abasic Sites. J. Biol. Chem. *276*, 9532–9536.

Keogh, M.C., Kurdistani, S.K., Morris, S.A., Ahn, S.H., Podolny, V., Collins, S.R., Schuldiner, M., Chin, K., Punna, T., Thompson, N.J., et al. (2005). Cotranscriptional Set2 methylation of histone H3 lysine 36 recruits a repressive Rpd3 complex. Cell *123*, 593–605.

Khurana, N., and Bhattacharyya, S. (2015). Hsp90, the Concertmaster: Tuning Transcription. Front. Oncol. *5*, 1–7.

Kim, H.J., Seol, J.H., Han, J.W., Youn, H.D., and Cho, E.J. (2007). Histone chaperones regulate histone exchange during transcription. EMBO J. *26*, 4467–4474.

Kim, J.H., Lee, B.B., Oh, Y.M., Zhu, C., Steinmetz, L.M., Lee, Y., Kim, W.K., Lee, S.B., Buratowski, S., and Kim, T.S. (2016). Modulation of mRNA and lncRNA expression dynamics by the Set2-Rpd3S pathway. Nat. Commun. *7*, 1–11.

Kim, S., and Kim, K.-T. (2014). Therapeutic Approaches for Inhibition of Protein Aggregation in Huntington's Disease. Exp. Neurobiol. *23*, 36–44.

Kim, S., Willison, K.R., and Horwich, A.L. (1994). Cystosolic chaperonin subunits have a conserved ATPase domain but diverged polypeptide-binding domains. Trends Biochem. Sci. *19*, 543–548.

Kim, T., and Buratowski, S. (2009). Dimethylation of H3K4 by Set1 Recruits the Set3 Histone Deacetylase Complex to 5′ Transcribed Regions. Cell *137*, 259–272.

Kimura, A., Umehara, T., and Horikoshi, M. (2002). Chromosomal gradient of histone acetylation established by Sas2p and Sir2p functions as a shield against gene silencing. Nat. Genet. *32*, 370–377.

Kitada, T., Kuryan, B.G., Tran, N.N.H., Song, C., Xue, Y., Carey, M., and Grunstein, M. (2012). Mechanism for epigenetic variegation of gene expression at yeast telomeric heterochromatin. Genes Dev. *26*, 2443–2455.

Kitamura, A., Kubota, H., Pack, C.G., Matsumoto, G., Hirayama, S., Takahashi, Y., Kimura, H., Kinjo, M., Morimoto, R.I., and Nagata, K. (2006). Cytosolic chaperonin prevents polyglutamine toxicity with altering the aggregation state. Nat. Cell Biol. *8*, 1163–1170.

Kloetzel, P., and Bautz, E.K.F. (1983). Heat-shock proteins are associated with hnRNA in *Drosophila melanogaster* tissue culture cells. EMBO J. *2*, 705–710.

Knoblauch, N.T.M., Rüdiger, S., Schönfeld, H.J., Driessen, A.J.M., Schneider-Mergener, J., and Bukau, B. (1999). Substrate specificity of the SecB chaperone. J. Biol. Chem. *274*, 34219–34225.

Kobor, M.S., Venkatasubrahmanyam, S., Meneghini, M.D., Gin, J.W., Jennings, J.L., Link, A.J., Madhani, H.D., and Rine, J. (2004). A protein complex containing the conserved Swi2/Snf2-related ATPase Swr1p deposits histone variant H2A.Z into euchromatin. PLoS Biol. *2*.

Koch, F., Jourquin, F., Ferrier, P., and Andrau, J.C. (2008). Genome-wide RNA polymerase II: not genes only! Trends Biochem. Sci. *33*, 265–273.

Kornberg, R.D. (1977). Structure of Chromatin. Ann. Rev. Biochem *46*, 931–954.

Kornberg, R.D. (1974). Chromatin Structure : A Repeating Unit of Histones and DNA. Sci *184*, 868–871.

Kornberg, R.D., and Thomas, J.O. (1974). Chromatin Structure : Oligomers of the Histones. Science *184*, 865–868.

Kotoglou, P., Kalaitzakis, A., Vezyraki, P., Tzavaras, T., Michalis, L.K., Dantzer, F., Jung, J.U., and Angelidis, C. (2009). Hsp70 translocates to the nuclei and nucleoli, binds to XRCC1 and PARP-1, and protects HeLa cells from single-strand DNA breaks. Cell Stress Chaperones *14*, 391–406.

Koutelou, E., Hirsch, C.L., and Dent, S.Y.R. (2010). Multiple faces of the SAGA complex. Curr. Opin. Cell Biol. *22*, 374–382.

Kraulis, P.J., Raine, A.R.C., Gadhavi, P.L., and Laue, E.D. (1992). Structure of the DNA-binding domain of zinc GAL4. Nature *356*, 448–450.

Krishnamurthy, S., Ghazy, M. A., Moore, C., and Hampsey, M. (2009). Functional interaction of the Ess1 prolyl isomerase with components of the RNA polymerase II initiation and termination machineries. Mol. Cell. Biol. *29*, 2925–2934.

Krogan, N.J., Dover, J., Wood, A., Schneider, J., Heidt, J., Boateng, M.A., Dean, K., Ryan, O.W., Golshani, A., Johnston, M., et al. (2003). The Paf1 complex is required for histone H3 methylation by COMPASS and Dot1p: Linking transcriptional elongation to histone methylation. Mol. Cell *11*, 721–729.

Krogan, N.J., Keogh, M.C., Datta, N., Sawa, C., Ryan, O.W., Ding, H., Haw, R.A., Pootoolal, J., Tong, A., Canadien, V., et al. (2003). A Snf2 Family ATPase Complex Required for Recruitment of the Histone H2A Variant Htz1. Mol. Cell *12*, 1565–1576.

Krogan, N.J., Kim, M., Tong, A., Golshani, A., Cagney, G., Canadien, V., Richards, D.P., Beattie, B.K., Emili, A., Boone, C., et al. (2003). Methylation of histone H3 by Set2 in *Saccharomyces cerevisiae* is linked to transcriptional elongation by RNA polymerase II. Mol. Cell. Biol. *23*, 4207–4218.

Kubik, S., Bruzzone, M.J., Jacquet, P., Falcone, J.L., Rougemont, J., and Shore, D. (2015). Nucleosome Stability Distinguishes Two Different Promoter Types at All Protein-Coding Genes in Yeast. Mol. Cell *60*, 422–434.

Kuehner, J.N., Pearson, E.L., and Moore, C. (2011). Unravelling the means to an end: RNA polymerase II transcription termination. Nat. Rev. Mol. Cell Biol. *12*, 283–294.

Kuhlman, T.C., Cho, H., Reinberg, D., and Hernandez, N. (1999). The General Transcription Factors IIA, IIB, IIF, and IIE Are Required for RNA Polymerase II Transcription from the Human U1 Small Nuclear RNA Promoter. Mol. Cell. Biol. *19*, 2130–2141.

Kulak, N.A., Pichler, G., Paron, I., Nagaraj, N., and Mann, M. (2014). Minimal, encapsulated proteomic-sample processing applied to copy-number estimation in eukaryotic cells. Nat. Methods *11*, 319–324.

Kuo, M.H., Brownell, J.E., Sobel, R.E., Ranalli, T.A., Cook, R.G., Edmondson, D.G., Roth, S.Y., and Allis, C.D. (1996). Transcription-linked acetylation by Gcn5p of histones H3 and H4 at specific lysines. Nature *383*, 269–272.

Kuras, L., and Struhl, K. (1999). Binding of TBP to promoters in vivo is stimulated by activators and requires Pol II holoenzyme. Nature *399*, 609–613.

Kurat, C.F., Recht, J., Radovani, E., Durbic, T., Andrews, B., and Fillingham, J. (2014). Regulation of histone gene transcription in yeast. Cell. Mol. Life Sci. *71*, 599–613.

Kurz, T., and Brunk, U.T. (2009). Autophagy of HSP70 and chelation of lysosomal iron in a non-redox-active form. Autophagy *5*, 93–95.

Lafon, A., Taranum, S., Pietrocola, F., Dingli, F., Loew, D., Brahma, S., Bartholomew, B., and Papamichos-Chronakis, M. (2015). INO80 Chromatin Remodeler Facilitates Release of RNA Polymerase II from Chromatin for Ubiquitin-Mediated Proteasomal Degradation. Mol. Cell *60*, 784–796.

Lakhotia, S.C., and Mutsuddi, M. (1996). Heat shock but not benzamide and colchicine response elements are present within the -844 bp upstream region of the hrsω gene of *Drosophila melanogaster*. J. Biosci. *21*, 235–246.

Lakhotia, S.C., and Ray, P. (1996). hsp 83 mutation is a dominant enhancer of lethality associated with absence of the non-protein coding hsrω locus in *Drosophila melanogaster*. J. Biosci. *21*, 207–219.

Lambert, J.P., Fillingham, J., Siahbazi, M., Greenblatt, J., Baetz, K., and Figeys, D. (2010). Defining the budding yeast chromatin-associated interactome. Mol. Syst. Biol. *6*, 1–16.

Langmead, B., Trapnell, C., Pop, M., and Salzberg, S.L. (2009). Ultrafast and memory-efficient alignment of short DNA sequences to the human genome. Genome Biol. *10*, R25.

Längst, G., and Becker, P.B. (2001). Nucleosome mobilization and positioning by ISWI-containing chromatin-remodeling factors. J. Cell Sci. *114*, 2561–2568.

Laskey, R.A., Honda, B.M., Mills, A.D., and Finch, J.T. (1978). Nucleosomes are assembled by an acidic protein which binds histones and transfers them to DNA. Nature *275*, 416–420.

Latchman, D.S. (1997). Transcription factors: An overview. Int. J. Biochem. Cell Biol. *29*, 1305–1312.LeBowitz, J.H., Zylicz, M., Georgopoulos, C., and McMacken, R. (1985). Initiation of DNA replication on single-stranded DNA templates catalyzed by purified replication proteins of bacteriophage lambda and *Escherichia coli*. Proc. Natl. Acad. Sci. U. S. A. *82*, 3988–3992.

Latchman, D. S. (1991). Eukaryotic transcription factors. Sci., Academic Press.

Lee, T.I., Rinaldi, N.J., Robert, F., Odom, D.T., Bar-Joseph, Z., Gerber, G.K., Hannet, N.M., Haribson, C.T., Thompson, C.M., Simon, I., et al. (2002). Transcriptional regulatory networks in *Saccharomyces cerevisiae*. Science *298*, 799–804.

Lee, T.I., Rinaldi, N.J., Robert, F., Odom, D.T., Bar-Joseph, Z., Gerber, G.K., Hannet, N.M., Haribson, C.T., Thompson, C.M., Simon, I., et al. (2002). Transcriptional regulatory networks in *Saccharomyces cerevisiae*. Science *298*, 799–804.

Lee, Y.C., Chang, W.W., Chen, Y.Y., Tsai, Y.H., Chou, Y.H., Tseng, H.C., Chen, H.L., Wu, C.C., Chang-Chien, J., Lee, H. Te, et al. (2017). Hsp90α mediates BMI1 expression in breast cancer stem/progenitor cells through facilitating nuclear translocation of c-Myc and EZH2. Int. J. Mol. Sci. *18*.

Lees-Miller, S.P., and Anderson, C.W. (1989). The human double-stranded DNA-activated protein kinase phosphorylates the 90-kDa heat-shock protein, hsp90α at two NH2-terminal threonine residues. J. Biol. Chem. *264*, 17275–17280.

Leuba, S.H., Yang, G., Robert, C., Samori, B., van Holde, K., Zlatanova, J., and Bustamante, C. (1994). Three-dimensional structure of extended chromatin fibers as revealed by tapping-mode scanning force microscopy. Proc. Natl. Acad. Sci. *91*, 11621–11625.

Lewis, E.B. (1950). The phenomenon of position effect. Adv. Genet. *3*, 73–115.Lewis, V.A., Hynes, G.M., Zheng, D., Saibil, H., and Willison, K. (1992). T-complex polypeptide-1 is a subunit of a heteromeric particle in the eukaryotic cytosol. Nature *358*, 249–252.

Li, B., Pattenden, S.G., Lee, D., Gutierrez, J., Chen, J., Seidel, C., Gerton, J., and Workman, J.L. (2005). Preferential occupancy of histone variant H2AZ at inactive promoters influences local histone modifications and chromatin remodeling. Proc. Natl. Acad. Sci. *102*, 18385–18390.

Li, B., Howe, L., Anderson, S., Yates, J.R., and Workman, J.L. (2003). The Set2 Histone Methyltransferase Functions through the Phosphorylated Carboxyl-terminal Domain of RNA Polymerase II. J. Biol. Chem. *278*, 8897–8903.

Li, H., Handsaker, B., Wysoker, A., Fennell, T., Ruan, J., Homer, N., Marth, G., Abecasis, G., and Durbin, R. (2009). The Sequence Alignment/Map format and SAMtools. Bioinformatics *25*, 2078–2079.

Li, J., Soroka, J., and Buchner, J. (2012). The Hsp90 chaperone machinery: Conformational dynamics and regulation by co-chaperones. Biochim. Biophys. Acta - Mol. Cell Res. *1823*, 624–635.

Li, S.H., and Li, X.J. (2004). Huntingtin-protein interactions and the pathogenesis of Huntington's disease. Trends Genet. *20*, 146–154.

Li, X. (2000). Distinct Classes of Yeast Promoters Revealed by Differential TAF Recruitment. Sci. Reports *288*, 1242–1244.

Liberek, K., Galitski, T.P., Zylicz, M., and Georgopoulos, C. (1992). The DnaK chaperone modulates the heat shock response of *Escherichia coli* by binding to the sigma 32 transcription factor. Proc. Natl. Acad. Sci. *89*, 3516–3520.

Liberek, K., Georgopoulos, C., and Zylicz, M. (1988). Role of the *Escherichia coli* DnaK and DnaJ heat shock proteins in the initiation of bacteriophage lambda DNA replication. Proc. Natl. Acad. Sci. U. S. A. *85*, 6632–6636.

Lieb, J.D., Liu, X., Botstein, D., and Brown, P.O. (2001). Promoter-specific binding of Rap1 revealed by genome-wide maps of protein-DNA association. Nat. Genet. *28*, 327–334.

Lindquist, S., and Craig, E.A. (1988). The Heat Shock Proteins. Annu. Rev. Genet *22*, 631–677.

Liu, J., and DeFranco, D.B. (1999). Chromatin recycling of glucocorticoid receptors: implications for multiple roles of heat shock protein 90. Mol Endocrinol *13*, 355–365.

Liu, J., and DeFranco, D.B. (1999). Chromatin recycling of glucocorticoid receptors: implications for multiple roles of heat shock protein 90. Mol Endocrinol *13*, 355–365.

Liu, J.S., Kuc, S.R., Makhov, A.M., Cyr, D.M., Griffith, J.D., Broker, T.R., and Chow, L.T. (1998). Human Hsp70 and Hsp40 chaperone proteins facilitate human papillomavirus-11 E1 protein binding to the origin and stimulate cell-free DNA replication. J. Biol. Chem. *273*, 30704–30712.

Liu, X., Bushnell, D.A., and Kornberg, R.D. (2013). RNA polymerase II transcription: Structure and mechanism. Biochim. Biophys. Acta - Gene Regul. Mech. *1829*, 2–8.

Loewen, C.J.R., Gaspar, M.L., Jesch, S. a, Delon, C., Ktistakis, N.T., Henry, S. a, and Levine, T.P. (2004). Phospholipid metabolism regulated by a transcription factor sensing phosphatidic acid. Science *304*, 1644–1647.

Logie, C., Tse, C., Hansen, J.C., and Peterson, C.L. (1999). The core histone N-terminal domains are required for multiple rounds of catalytic chromatin remodeling by the SWI/SNF and RSC complexes. Biochemistry *38*, 2514–2522.

Lopes, J.M., and Henry, S.A. (1991). Interaction of trans and cis regulatory elements in the INO1 promoter of Saccharomyces cerevisiae. Nucleic Acids Res. *19*, 3987–3994.

Lorch, Y., Cairns, B.R., Zhang, M., and Kornberg, R.D. (1998). Activated RSC-nucleosome complex and persistently altered form of the nucleosome. Cell *94*, 29–34.

Lorch, Y., Zhang, M., and Kornberg, R.D. (1999). Histone octamer transfer by a chromatin-remodeling complex. Cell *96*, 389–392.

Lowary, P.T., and Widom, J. (1998). New DNA sequence rules for high affinity binding to histone octamer and sequence-directed nucleosome positioning. J. Mol. Biol. *276*, 19–42.

Luger, K., Rechsteiner, T. J., Richmond, T. J. (1999). Expression and Purification of Recombinant Histones and Nucleosome Reconstitution. In: Becker P.B. (eds) Chromatin Protocols. Methods in Molecular Biology *119*, Humana Press.

Lyon, M.F., Zenthon, J., Evans, E.P., Burtenshaw, M.D., and Willison, K.R. (1988). Extent of the mouse t complex and its inversions shown by in situ hybridization. Immunogenetics *27*, 375–382.

Lyon, M.F. (1984). Transmission ratio distortion in mouse t-haplotypes is due to multiple distorter genes acting on a responder locus. Cell *37*, 621–628.

Lyon, M.F. (1986). Male sterility of the mouse t-complex is due to homozygosity of the distorter genes. Cell *44*, 357–363.

MacIsaac, K.D., Wang, T., Gordon, D.B., Gifford, D.K., Stormo, G.D., Fraenkel, E., Bell, G., Walker, K., Rolfe, P., Herbolsheimer, E., et al. (2006). Widespread remodeling of mid-coding sequence nucleosomes by Isw1. BMC Bioinformatics *7*, 113.

Malki, A., Hughes, P., and Kohiyama, M. (1991). In vitro roles of *Escherichia coli* DnaJ and DnaK heat shock proteins in the replication of oriC plasmids. Mol. Gen. Genet. *225*, 420–426.

Mallik, M., and Lakhotia, S.C. (2009). The developmentally active and stress-inducible noncoding hsromega gene is a novel regulator of apoptosis in *Drosophila*. Genetics *183*, 831–852.

Marino Gammazza, A., Caruso Bavisotto, C., Barone, R., Conway De Macario, E., and Macario, A.J.L. (2016). Alzheimer's Disease and Molecular Chaperones: Current Knowledge and the Future of Chaperonotherapy. Curr. Pharm. Des. *22*, 4040–4049.

Marquardt, S., Escalante-Chong, R., Pho, N., Wang, J., Churchman, L.S., Springer, M., and Buratowski, S. (2014). A chromatin-based mechanism for limiting divergent noncoding transcription. Cell *157*, 1712–1723.

Martin, C., and Zhang, Y. (2005). The diverse functions of histone lysine methylation. Nat. Rev. Mol. Cell Biol. *6*, 838–849.

Martin, J., Langer, T., Boteva, R., Schramel, A., Horwich, A.L., and Hartl, F.-U. (1991). Chaperonin-mediated protein folding at the surface of groEL through a 'molten globule'-like intermediate. Nature *352*, 36–42.

Mason, P.B., and Struhl, K. (2003). The FACT complex travels with elongating RNA polymerase II and is important for the fidelity of transcriptional initiation in vivo. Mol. Cell. Biol. *23*, 8323–8333.

Maston, G.A., Zhu, L.J., Chamberlain, L., Lin, L., Fang, M., and Green, M.R. (2012). Non-canonical TAF complexes regulate active promoters in human embryonic stem cells. Elife *2012*, 1–19.

Matsumoto, M., Hatakeyama, S., Oyamada, K., Oda, Y., Nishimura, T., and Nakayama, K.I. (2005). Large-scale analysis of the human ubiquitin-related proteome. Proteomics *5*, 4145–4151.

Maxon, M.E., Goodrich, J.A., and Tjian, R. (1994). Transcription factor IIE binds preferentially to RNA polymerase IIa and recruits TFIIH: A model for promoter clearance. Genes Dev. *8*, 515–524.

Mayer, M.P. (2010). Gymnastics of molecular chaperones. Mol. Cell *39*, 321–331.

McAlister, L., Strausberg, S., Kulaga, A., and Finkelstein, D.B. (1979). Altered patterns of protein synthesis induced by heat shock of yeast. Curr. Genet. *1*, 63–74.

McCallum, C.D., Do, H., Johnson, A.E., and Frydman, J. (2000). The interaction of the chaperonin tailless complex polypeptide 1 (TCP1) ring complex (TRiC) with ribosome-bound nascent chains examined using photo- cross-linking. J. Cell Biol. *149*, 591–601.

Mendez, F., Kozin, E., and Bases, R. (2003). Heat shock protein 70 stimulation of the deoxyribonucleic acid base excision repair enzyme polymerase beta. Cell Stress Chaperones *8*, 153–161.

Meneghini, M.D., Wu, M., and Madhani, H.D. (2003). Conserved histone variant H2A.Z protects euchromatin from the ectopic spread of silent heterochromatin. Cell *112*, 725–736.

Metuzals, J., Robitaille, Y., Houghton, S., Gauthier, S., and Leblanc, R. (1988). Paired helical filaments and the cytoplasmic-nuclear interface in Alzheimer's disease. J. Neurocytol. *17*, 827–833.

Mizuguchi, G., Shen, X., Landry, J., Wu, W.H., Sen, S., and Wu, C. (2004). ATP-Driven Exchange of Histone H2AZ Variant Catalyzed by SWR1 Chromatin Remodeling Complex. Science *303*, 343–348.

Mohler, J., and Pardue, M.L.O.U. (1984). Mutational analysis of the region surrounding the 93D heat shock locus of *Drosophila melanogaster*. Genetics *106*, 249–265.

Mohrmann, L., and Verrijzer, C.P. (2005). Composition and functional specificity of SWI2/SNF2 class chromatin remodeling complexes. Biochim. Biophys. Acta - Gene Struct. Expr. *1681*, 59–73.

Morcillo, G., Diez, J.L., Carbajal, M.E., and Tanguay, R.M. (1993). HSP90 associates with specific heat shock puffs (hsrω) in polytene chromosomes of *Drosophila* and *Chironomus*. Chromosoma *102*, 648–659.

Morimoto, R.I. (1993). Cells in tress: transcriptional activation of heat shock genes. Science *259*, 1409 1410.

Morris, S.A., Rao, B., Garcia, B.A., Hake, S.B., Diaz, R.L., Shabanowitz, J., Hunt, D.F., Allis, C.D., Lieb, J.D., and Strahl, B.D. (2007). Identification of histone H3 lysine 36 acetylation as a highly conserved histone modification. J. Biol. Chem. *282*, 7632–7640.

Morrison, A.J., and Shen, X. (2009). Chromatin remodelling beyond transcription: The INO80 and SWR1 complexes. Nat. Rev. Mol. Cell Biol. *10*, 373–384.

Morse, R.H. (2003). Getting into chromatin: how do transcription factors get past the histones? Biochem. Cell Biol. *81*, 101–112.

Mukherjee, K., Nagai, H., Shimamoto, N., and Chatterji, D. (1999). GroEL is involved in activation of *Escherichia coli* RNA polymerase devoid of the omega subunit in vivo. Eur. J. Biochem. *266*, 228–235.

Murawska, M., and Brehm, A. (2011). CHD chromatin remodelers and the transcription cycle. Transcription *2*, 244–253.

Myer, V.E., and Young, R.A. RNA polymerase II holoenzymes and subcomplexes. J. Biol. Chem. *273*, 27757–27760.

Nathan, D.F., and Lindquist, S. (1995). Mutational analysis of Hsp90 function: interactions with a steroid receptor and a protein kinase. Mol. Cell. Biol. *15*, 3917–3925.

Nathan, D.F., Vos, M.H., and Lindquist, S. (1997). In vivo functions of the *Saccharomyces cerevisiae* Hsp90 chaperone. Proc. Natl. Acad. Sci. U. S. A. *94*, 12949–12956.

Natsoulis, G., Winston, F., and Boeke, J.D. (1994). The SPT10 and SPT21 genes of *Saccharomyces cerevisiae*. Genetics *136*, 93–105.

Neil, H., Malabat, C., D'Aubenton-Carafa, Y., Xu, Z., Steinmetz, L.M., and Jacquier, A. (2009). Widespread bidirectional promoters are the major source of cryptic transcripts in yeast. Nature *457*, 1038–1042.

Nelson, R.J., Ziegelhoffer, T., Nicolet, C., Werner-Washburne, M., and Craig, E.A. (1992). The translation machinery and 70 kD heat shock protein cooperate in protein synthesis. Cell *71*, 97–105.

Nemoto, T., Ohara-Nemoto, Y., Ota, M., Takagi, T., and Yokoyama, K. (1995). Mechanism of Dimer Formation of the 90-kDa Heat-Shock Protein. Eur. J. Biochem. *233*, 1–8.

Ng, H.H., Ciccone, D.N., Morshead, K.B., Oettinger, M.A., and Struhl, K. (2003). Lysine-79 of histone H3 is hypomethylated at silenced loci in yeast and mammalian cells: A potential mechanism for position-effect variegation. Proc. Natl. Acad. Sci. *100*, 1820–1825.

Ng, H.H., Feng, Q., Wang, H., Erdjument-Bromage, H., Tempst, P., Zhang, Y., and Struhl, K. (2002). Lysine methylation within the globular domain of histone H3 by Dot1 is important for telomeric silencing and Sir protein association. Genes Dev. *16*, 1518–1527.

Ng, H.H., Robert, F., Young, R.A., and Struhl, K. (2002). Genome-wide location and regulated recruitment of the RSC nucleosome-remodeling complex. Genes Dev. *16*, 806–819.

Ng, H.H., Robert, F., Young, R.A., and Struhl, K. (2003). Targeted recruitment of Set1 histone methylase by elongating Pol II provides a localized mark and memory of recent transcriptional activity. Mol. Cell *11*, 709–719.

Nguyen, A.T., and Zhang, Y. (2011). The diverse functions of Dot1 and H3K79 methylation. Genes Dev. *3*, 1345–1358.

Noll, M. (1977). DNA folding in the nucleosome. J. Mol. Biol. *116*, 49–71.

Nollen, E.A.A., Garcia, S.M., van Haaften, G., Kim, S., Chavez, A., Morimoto, R.I., and Plasterk, R.H.A. (2004). Genome-wide RNA interference screen identifies previously undescribed regulators of polyglutamine aggregation. Proc. Natl. Acad. Sci. *101*, 6403–6408.

Noma, K.I., Allis, C.D., and Grewal, S.I.S. (2001). Transitions in distinct histone H3 methylation patterns at the heterochromatin domain boundaries. Science *293*, 1150–1155.

Norton, V.G., Imai, B.S., Yau, P., and Bradbury, E.M. (1989). Histone acetylation reduces nucleosome core particle linking number change. Cell *57*, 449–457.

Ohki, M., and Smith, C.L. (1989). Tracking bacterial DNA replication forks in vivo by pulsed field gel electrophoresis. Nucleic Acids Res. Acid Res. *17*, 3479–3490.

Olins, A.L., and Olins, D.E. (1974). Spheroid Chromatin Units (v bodies). Science *183*, 330–332.

Orphanides, G., LeRoy, G., Chang, C.H., Luse, D.S., and Reinberg, D. (1998). FACT, a factor that facilitates transcript elongation through nucleosomes. Cell *92*, 105–116.

Ossipow, V., Tassan, J.P., Nigg, E.A., and Schibler, U. (1995). A mammalian RNA polymerase II holoenzyme containing all components required for promoter-specific transcription initiation. Cell *83*, 137–146.

Ouspenski, I.I., Elledge, S.J., and Brinkley, B.R. (1999). New yeast genes important for chromosome integrity and segregation identified by dosage effects on genome stability. Nucleic Acids Res. *27*, 3001–3008.

Pabo, C.O., and Sauer, R.T. (1992). Transcription Factors: Structural Families and Principles of DNA Recognition. Annu. Rev. Biochem. *61*, 1053–1095.

Paek, K.H., and Walker, G.C. (1987). *Escherichia coli dnaK* null mutants are inviable at high temperature. J. Bacteriol. *169*, 283–290.

Papamichos-Chronakis, M., Watanabe, S., Rando, O.J., and Peterson, C.L. (2011). Global regulation of H2A.Z localization by the INO80 chromatin-remodeling enzyme is essential for genome integrity. Cell *144*, 200–213.

Parnell, T.J., Schlichter, A., Wilson, B.G., and Cairns, B.R. (2015). The chromatin remodelers RSC and ISW1 display functional and chromatin-based promoter antagonism. Elife *2015*, 1–21.

Pedersen, S., Bloch, P., Reeh, S., and Neidhardt, F. (1978). Patterns of protein synthesis in E. coli: a catalog of the amount of 140 individual proteins at different growth rates. Cell *14*, 179–190.

Pelham, H.R.B. (1984). Hsp70 accelerates the recovery of nucleolar morphology after heat shock. EMBO J. *3*, 3095–3100.

Pelham, H.R.B. (1986). Speculations on the functions of the major heat shock and glucose-regulated proteins. Cell *46*, 959–961.

Pelling, G. (1959). Chromosomal sythesis of ribonucleic acid as shown by incorporation of uridine labelled with tritium. Nature *184*, 655–656.

Pesavento, J.J., Mizzen, C.A., and Kelleher, N.L. (2006). Quantitative analysis of modified proteins and their positional isomers by tandem mass spectrometry: Human histone H4. Anal. Chem. *78*, 4271–4280.

Peterson, C.L., and Laniel, M.-A. (2004). Histones and histone modifications. Curr. Biol. *14*, R546–R551.

Petit, M.A., Bedale, W., Osipiuk, J., Lu, C., Rajagopalant, M., McInerney, P., Goodman, M.F., and Echols, H. (1994). Sequential folding of UmuC by the Hsp70 and Hsp60 chaperone complexes of *Escherichia coli*. J. Biol. Chem. *269*, 23824–23829.

Phatnani, H.P., and Greenleaf, a L. (2006). Phosphorylation and functions of the RNA polymerase II CTD. Genes Dev. *20*, 2922–2936.

Picard, D., Khursheed, B., Garabedian, M.J., Fortin, M.G., Lindquist, S., and Yamamoto, K.R. (1990). Reduced levels of hsp90 compromise steroid receptor action in vivo. Nature *348*, 166–168.

Pienta, K.J., and Coffey, D.S. (1984). A structural analysis of the role of the nuclear matrix and DNA loops in the organization of the nucleus and chromosome. J. Cell Sci. *1*, 123–135.

Piper, J., Elze, M.C., Cauchy, P., Cockerill, P.N., Bonifer, C., and Ott, S. (2013). Wellington: A novel method for the accurate identification of digital genomic footprints from DNase-seq data. Nucleic Acids Res. *41*.

Pokholok, D.K., Harbison, C.T., Levine, S., Cole, M., Hannett, N.M., Tong, I.L., Bell, G.W., Walker, K., Rolfe, P.A., Herbolsheimer, E., et al. (2005). Genome-wide map of nucleosome acetylation and methylation in yeast. Cell *122*, 517–527.

Prasanth, K. V, Rajendra, T.K., Lal, A.K., and Lakhotia, S.C. (2000). Omega speckles - a novel class of nuclear speckles containing hnRNPs associated with noncoding hsr-omega RNA in *Drosophila*. J. Cell Sci. *113*, 3485–3497.

Pratt, W.B., and Toft, D.O. (1997). Steroid receptor interactions with heat shock protein and immunophilin chaperones. Endocr. Rev. *18*, 306–360.

Pratt, W.B. (1997). The role of the Hsp90-based chaperone system in signal transduction by nuclear receptors and receptors signaling via map kinase. Annu. Rev. Pharmacol. Toxicol. *37*, 297–326.

Prodromou, C., Panaretou, B., Chohan, S., Siligardi, G., O'Brien, R., Ladbury, J.E., Roe, S.M., Piper, P.W., and Pearl, L.H. (2000). The ATPase cycle of Hsp90 drives a molecular "clamp" via transient dimerization of the N-terminal domains. EMBO J. *19*, 4383–4392.

Prodromou, C., Roe, S.M., O'Brien, R., Ladbury, J.E., Piper, P.W., and Pearl, L.H. (1997). Identification and structural characterization of the ATP/ADP-binding site in the Hsp90 molecular chaperone. Cell *90*, 65–75.

Puri, R.K., Grandics, P., Dougherty, J.J., and Toft, D.O. (1982). Purification of "Nontransformed" Avian Progesterone Receptor and Preliminary Characterization. J. Biol. Chem. *257*, 10831–10837.

Qiu, H., Hu, C., Wong, C.-M., and Hinnebusch, A.G. (2006). The Spt4p subunit of yeast DSIF stimulates association of the Paf1 complex with elongating RNA polymerase II. Mol. Cell. Biol. *26*, 3135–3148.

Quan, T.K., and Hartzog, G.A. (2010). Histone H3K4 and K36 methylation, Chd1 and Rpd3S oppose the functions of *Saccharomyces cerevisiae* Spt4-Spt5 in transcription. Genetics *184*, 321–334.

Quanz, M., Herbette, A., Sayarath, M., De Koning, L., Dubois, T., Sun, J.S., and Dutreix, M. (2012). Heat shock protein 90α (Hsp90α) is phosphorylated in response to DNA damage and accumulates in repair foci. J. Biol. Chem. *287*, 8803–8815.

Queitsch, C., Sangster, T.A., and Lindquist, S. (2002). Hsp90 as a capacitor for genetic variation. Nature *417*, 618–624.

Quinlan, A.R., and Hall, I.M. (2010). BEDTools: A flexible suite of utilities for comparing genomic features. Bioinformatics *26*, 841–842.

Rappold, G.A., Stubbs, L., Labeit, S., Crkvenjakov, R.B., and Lehrach, H. (1987). Identification of a testis-specific gene from the mouse t-complex next to a CpG-rich island. EMBO J. *6*, 1975–1980.

Ray, P., and Lakhotia, S.C. (1998). Interaction of the non-protein-coding developmental and stress-inducible hsrω gene with Ras genes of *Drosophila melanogaster*. J. Biosci. *23*, 377–386.

Reid, J.L., Iyer, V.R., Brown, P.O., and Struhl, K. (2000). Coordinate regulation of yeast ribosomal protein genes is associated with targeted recruitment of Esa1 histone acetylase. Mol. Cell *6*, 1297–1307.

Reis, S.D., Pinho, B.R., and Oliveira, J.M.A. (2017). Modulation of Molecular Chaperones in Huntington's Disease and Other Polyglutamine Disorders. Mol. Neurobiol. *54*, 5829–5854.

Reissmann, S., Parnot, C., Booth, C.R., Chiu, W., and Frydman, J. (2007). Essential function of the built-in lid in the allosteric regulation of eukaryotic and archaeal chaperonins. Nat. Struct. Mol. Biol. *14*, 432–440.

Renoir, J. -M, Yang, C. -R, Formstecher, P., Lustenberger, P., Wolfson, A., Redeulich, G., Mester, J., Richard-Foy, H., and Baulieu, E. -E (1982). Progesterone Receptor from Chick Oviduct: Purification of Molybdate-Stabilized Form and Preliminary Characterization. Eur. J. Biochem. *127*, 71–80.

Reznikoff, W.S. (1972). The operon revisited. Annu. Rev. Genet. *6*, 133–156.

kimRhee, H.S., and Pugh, B.F. (2012). Genome-wide structure and organization of eukaryotic pre-initiation complexes. Nature *483*, 295–301.

Richards, E.J., and Elgin, S.C.R. (2002). Epigenetic codes for heterochromatin formation and silencing: Rounding up the usual suspects. Cell *108*, 489–500.

Richter, K., and Buchner, J. (2006). Hsp90: Twist and Fold. Cell *127*, 251–253.

Richter, K., Moser, S., Hagn, F., Friedrich, R., Hainzl, O., Heller, M., Schlee, S., Kessler, H., Reinstein, J., and Buchner, J. (2006). Intrinsic inhibition of the Hsp90 ATPase activity. J. Biol. Chem. *281*, 11301–11311.

Rill, R., and Van Holde, K.E. (1973). Properties of nuclease-resistant fragments of calf thymus chromatin. J. Biol. Chem. *248*, 1080–1083.

Ris, H., and Kubai, D.F. (1970). Chromosome Structure. Annu. Rev. Genet. *4*, 263–294.

Ritossa, F. (1962). A new puffing pattern induced by temperature shock and DNP in *Drosophila*. Experientia *18*, 571–573.

Robert, F., Pokholok, D.K., Hannett, N.M., Rinaldi, N.J., Chandy, M., Rolfe, A., Workman, J.L., Gifford, D.K., and Young, R.A. (2004). Global position and recruitment of HATs and HDACs in the yeast genome. Mol. Cell *16*, 199–209.

Roberts, S., and Szego, C.M. (1946). The nature of circulating estrogen: Lipoprotein-bound estrogen in human plasma. Endocrinology *39*, 183–187.

Robyr, D., Suka, Y., Xenarios, I., Kurdistani, S.K., Wang, A., Suka, N., and Grunstein, M. (2002). Microarray deacetylation maps determine genome-wide functions for yeast histone deacetylases. Cell *109*, 437–446.

Rodriguez, C.R., Cho, E.-J., Keogh, M.-C., Moore, C.L., Greenleaf, A.L., and Buratowski, S. (2000). Kin28, the TFIIH-Associated Carboxy-Terminal Domain Kinase, Facilitates the Recruitment of mRNA Processing Machinery to RNA Polymerase II. Mol. Cell. Biol. *20*, 104–112.

Roeder, R.G., Reeder, R.H., and Brown, D.D. (1970). Multiple Forms of RNA Polymerase in Xenopus Laevis: Their Relationship to RNA Synthesis *in Vivo* and Their Fidelity of Transcription *in Vitro*. Cold Spring Harb. Symp. Quant. Biol. *35*, 727–735.

Roeder, R.G., and Rutter, W.J. (1969). Multiple forms of DNA-dependent RNA polymerase in eukaryotic organisms. Nature *224*, 234–237.

Roh, T.Y., Ngau, W.C., Cui, K., Landsman, D., and Zhao, K. (2004). High-resolution genome-wide mapping of histone modifications. Nat. Biotechnol. *22*, 1013–1016.

Rommelaere, H., Van Troys, M., Gao, Y., Melki, R., Cowan, N.J., Vandekerckhove, J., and Ampe, C. (1993). Eukaryotic cytosolic chaperonin contains t-complex polypeptide 1 and seven related subunits. Proc. Natl. Acad. Sci. U. S. A. *90*, 11975–11979.

Roobol, A., and Carden, M.J. (1999). Subunits of the eukaryotic cytosolic chaperonin CCT do not always behave as components of a uniform hetero-oligomeric particle. Eur. J. Cell Biol. *78*, 21–32.

Roskams, J., and Rodgers, L. (2002). Lab Ref. Cold Spring Harbor Laboratory Press.

Rufiange, A., Jacques, P.É., Bhat, W., Robert, F., and Nourani, A. (2007). Genome-Wide Replication-Independent Histone H3 Exchange Occurs Predominantly at Promoters and Implicates H3 K56 Acetylation and Asf1. Mol. Cell *27*, 393–405.

Russell, J.S., Burgan, W., Oswald, K.A., Camphausen, K., and Tofilon, P.J. (2003). Enhanced Cell Killing Induced by the Combination of Radiation and the Heat Shock Protein 90 Inhibitor 17-Allylamino-17- Demethoxygeldanamycin: A Multitarget Approach to Radiosensitization. Clin. Cancer Res. *9*, 3749–3755.

Rutherford, S.L., and Lindquist, S. (1998). Hsp90 as a capacitor for morphologival evolution. Nature *396*, 336–342.

Sabbah, M., Radanyi, C., Redeuilh, G., and Baulieu, E.E. (1996). The 90 kDa heat-shock protein (hsp90) modulates the binding of the oestrogen receptor to its cognate DNA. Biochem. J. *314*, 205–213.

Sahasrabuddhe, C.G., and Van Holde, K.E. (1974). The Effect of Trypsin on Nuclease-resistant Chromatin Fragments. J. Biol. Chem. *249*, 152–156.

Saito, H., and Uchida, H. (1978). Organization and Expression of DnaJ and DnaK Genes of *Escherichia coli* K12. Mol. Gen. Genet. *164*, 1–8.

Sakakibara, Y. (1988). The dnaK gene of *Escherichia coli* functions in initiation of chromosome replication. J. Bacteriol. *170*, 972–979.

Sanchez, E.R., Toft, D.O., Schlesinger, M.J., and Pratt, W.B. (1985). Evidence that the 90-kDa phosphoprotein associated with the untransformed L-cell glucocorticoid receptor is a murine heat shock protein. J. Biol. Chem. *260*, 12398–12401.

Sandelin, A. (2004). JASPAR: an open-access database for eukaryotic transcription factor binding profiles. Nucleic Acids Res. *32*, 91D–94.

Sanders, S.L., Jennings, J., Canutescu, A., Link, A.J., and Weil, P.A. (2002). Proteomics of the Eukaryotic Transcription Machinery: Identification of Proteins Associated with Components of Yeast TFIID by Multidimensional Mass Spectrometry. Mol. Cell. Biol. *22*, 4723–4738.

Santisteban, M.S., Hang, M., and Smith, M.M. (2011). Histone Variant H2A.Z and RNA Polymerase II Transcription Elongation. Mol. Cell. Biol. *31*, 1848–1860.

Santisteban, M.S., Arents, G., Moudrianakis, E.N., and Smith, M.M. (1997). Histone octamer function in vivo: Mutations in the dimer-tetramer interfaces disrupt both gene activation and repression. EMBO J. *16*, 2493–2506.

Santos-Rosa, H., Schneider, R., Bannister, A.J., Sherriff, J., Bernstein, B.E., EMre, N.C.T., Schreiber, S.L., Mellor, J., and Kouzarides, T. (2002). Active genes are tri-methylated at K4 of histone H3. Nature *419*, 407–411.

Sawarkar, R., Sievers, C., and Paro, R. (2012). Hsp90 globally targets paused RNA polymerase to regulate gene expression in response to environmental stimuli. Cell *149*, 807–818.

Schaeffer, L., Roy, R., Humbert, S., Moncollin, V., Vermeulen, W., Hoeijmakers, J.H.J., Chambon, P., and Egly, J. (1993). Repair helicase: A component of BTF2 (TFIIH) basic transcrition factor. Science *260*, 58–63.

Schaft, D., Roguev, A., Shevchenko, A., Tekotte, H., Wilm, M., Rigaut, G., Aasland, R., and Stewart, a F. (2001). S. cerevisiae. Genes Dev. *1*, 2991–3004.

Schimenti, J., Cebra-Thomas, J.A., Decker, C.L., Islam, S.D., Pilder, S.H., and Silver, L.M. (1988). A candidate gene family for the mouse t complex responder (Tcr) locus responsible for haploid effects on sperm function. Cell *55*, 71–78.

Schübeler, D., MacAlpine, D.M., Scalzo, D., Wirbelauer, C., Kooperberg, C., Van Leeuwen, F., Gottschling, D.E., O'Neill, L.P., Turner, B.M., Delrow, J., et al. (2004). The histone modification pattern of active genes revealed through genome-wide chromatin analysis of a higher eukaryote. Genes Dev. *18*, 1263–1271.

Schuh, S., Yonemoto, W., Brugge, J., Bauer, V.J., Riehl, R.M., Sullivan, W.P., and Toft, D.O. (1985). A 90,000-dalton binding protein common to both steroid receptors and the Rous sarcoma virus transforming protein, pp60(v-src). J. Biol. Chem. *260*, 14292–14296.

Schwabish, M.A., and Struhl, K. (2004). Evidence for Eviction and Rapid Deposition of Histones upon Transcriptional Elongation by RNA Polymerase II Evidence for Eviction and Rapid Deposition of Histones upon Transcriptional Elongation by RNA Polymerase II. Mol. Cell. Biol. *24*, 10111–10117.

Schwarzacher, H.G., Bielek, E., and Ruzicka, F. (1977). Neue Befunde zur Struktur der Chromosomen. Hum. Genet. *135*, 125–135.

Seila, A.C., Calabrese, J.M., Levine, S.S., Yeo, G.W., Rahl, P.B., Flynn, R.A., Young, R.A., and Sharp, P.A. (2008). Divergent transcription from active promoters. Science *322*, 1849–1851.

Sengupta, S.M., VanKanegan, M., Persinger, J., Logie, C., Cairns, B.R., Peterson, C.L., and Bartholomew, B. (2001). The Interactions of Yeast SWI/SNF and RSC with the Nucleosome before and after Chromatin Remodeling. J. Biol. Chem. *276*, 12636–12644.

Shaknovich, R., Shue, G., and Kohtz, D.S. (1992). Conformational activation of a basic helix-loop-helix protein (MyoD1) by the C-terminal region of murine HSP90 (HSP84). Mol. Cell. Biol. *12*, 5059–5068.

Sharma, S.K., De Los Rios, P., Christen, P., Lustig, A., and Goloubinoff, P. (2010). The kinetic parameters and energy cost of the Hsp70 chaperone as a polypeptide unfoldase. Nat. Chem. Biol. *6*, 914–920.

Sharp, S.J., Schaack, J., Cooley, L., Burke, D.J., and Soil, D. (1985). Structure and transcription of eukaryotic tRNA gene. Crit. Rev. Biochem. Mol. Biol. *19*, 107–144.

Shen, W.-C., Bhaumik, S.R., Causton, H.C., Simon, I., Zhu, X., Jennings, E.G., Wang, T.-H., Young, R.A., and Green, M.R. (2003). Systematic Analysis of Essential TAFs in Genome-Wide Transcription and Preinitiation Complex Assembly. Embo J, *22*, 3395–3402.

Sherrie L. Herendeen, Ruth A. VanBogelen, F.C.N. (1979). Levels of major proteins of *Escherichia coli* during growth at different temperatures. J. Bacteriol. *139*, 185–194.

Shevchenko, A., Roguev, A., Schaft, D., Buchanan, L., Habermann, B., Sakalar, C., Thomas, H., Krogan, N.J., Shevchenko, A., and Stewart, A.F. (2008). Chromatin Central: Towards the comparative proteome by accurate mapping of the yeast proteomic environment. Genome Biol. *9*.

Shevchenko, A., Schaft, D., Roguev, A., Pijnappel, W.W.M.P., Stewart, A.F., and Shevchenko, A. (2002). Deciphering Protein Complexes and Protein Interaction Networks by Tandem Affinity Purification and Mass Spectrometry. Mol. Cell. Proteomics *1*, 204–212.

Shia, W., Li, B., and Workman, J.L. (2006). SAS-mediated acetylation of histone H4 Lys 16 is required for H2A.Z incorporation at subtelomeric regions in *Saccharomyces cerevisiae*. Genes Dev. *20*, 2507–2512.

Sidera, K., and Patsavoudi, E. (2014). HSP90 inhibitors: current development and potential in cancer therapy. Recent Pat. Anticancer. Drug Discov. *9*, 1–20.

Silver, L.M. (1981). A structural gene (Tcp-1) within the mouse t complex is separable from effects on tail length and lethality but may be associated with effects on spermatogenesis. Genet. Res. *38*, 115–123.

Silver, L.M., Artzt, K., and Bennett, D. (1979). A major testicular cell protein specified by a mouse T/t complex gene. Cell *17*, 275–284.

Silver, L.M., Kleene, K.C., Distel, R.J., and Hecht, N.B. (1987). Synthesis of mouse t complex proteins during haploid stages of spermatogenesis. Dev. Biol. *119*, 605–608.

Singh, N., Ma, Z., Gemmill, T., Wu, X., DeFiglio, H., Rossettini, A., Rabeler, C., Beane, O., Morse, R.H., Palumbo, M.J., et al. (2009). The Ess1 Prolyl Isomerase Is Required for Transcription Termination of Small Noncoding RNAs via the Nrd1 Pathway. Mol. Cell *36*, 255–266.

Singleton, M.R., Dillingham, M.S., and Wigley, D.B. (2007). Structure and Mechanism of Helicases and Nucleic Acid Translocases. Annu. Rev. Biochem. *76*, 23–50.

Skelly, S., Fu, C.F., Dalie, B., Redfield, B., Coleman, T., Brot, N., and Weissbach, H. (1988). Antibody to sigma32 cross-reacts with DnaK: association of DnaK protein with *Escherichia coli* RNA polymerase. Proc. Natl. Acad. Sci. U. S. A. *85*, 5497–5500.

Skowyra, D., Georgopoulos, C., and Zylicz, M. (1990). The E. coli dnaK gene product, the hsp70 homolog, can reactivate heat-inactivated RNA polymerase in an ATP hydrolysis-dependent manner. Cell *62*, 939–944.

Smith, C.M., Gafken, P.R., Zhang, Z., Gottschling, D.E., Smith, J.B., and Smith, D.L. (2003). Mass spectrometric quantification of acetylation at specific lysines within the amino-terminal tail of histone H4. Anal. Biochem. *316*, 23–33.

Smith, D.F. (2000). Chaperones in progesterone receptor complexes. Semin. Cell Dev. Biol. *11*, 45–52.

Smith, D.F. (1993). Dynamics of heat shock protein 90-progesterone receptor binding and the disactivation loop model for steroid receptor complexes. Mol. Endocrinol. *7*, 1418–1429.

Smith, D.F., Faber, L.E., and Toft, D.O. (1990). Purification of unactivated progesterone receptor and identification of novel receptor-associated proteins. J. Biol. Chem. *265*, 3996–4003.

Smith, E.R., Eisen, A., Gu, W., Sattah, M., Pannuti, A., Zhou, J., Cook, R.G., Lucchesi, J.C., and Allis, C.D. (1998). ESA1 is a histone acetyltransferase that is essential for growth in yeast. Proc. Natl. Acad. Sci. U. S. A. 95, 3561–3565.

Solis, E.J., Pandey, J.P., Zheng, X., Jin, D.X., Gupta, P.B., Airoldi, E.M., Pincus, D., and Denic, V. (2016). Defining the Essential Function of Yeast Hsf1 Reveals a Compact Transcriptional Program for Maintaining Eukaryotic Proteostasis. Mol. Cell 63, 60–71.

Sollars, V., Lu, X., Xiao, L., Wang, X., Garfinkel, M.D., and Ruden, D.M. (2003). Evidence for an epigenetic mechanism by which Hsp90 acts as a capacitor for morphological evolution. Nat. Genet. *33*, 70–74.

Sonenberg, N. (1993). Remarks on the mechanism of ribosome binding to eukaryotic mRNAs. Gene Expr. *3*, 317–323.

Souès, S., Kann, M.L., Fouquet, J.P., and Melki, R. (2003). The cytosolic chaperonin CCT associates to cytoplasmic microtubular structures during mammalian spermiogenesis and to heterochromatin in germline and somatic cells. Exp. Cell Res. *288*, 363–373.

Spain, M.M., Ansari, S.A., Pathak, R., Palumbo, M.J., Morse, R.H., and Govind, C.K. (2014). The RSC Complex Localizes to Coding Sequences to Regulate Pol II and Histone Occupancy. Mol. Cell *56*, 653–666.

Specchia, V., Piacentini, L., Tritto, P., Fanti, L., Dalessandro, R., Palumbo, G., Pimpinelli, S., and Bozzetti, M.P. (2010). Hsp90 prevents phenotypic variation by suppressing the mutagenic activity of transposons. Nature *463*, 662–665.

Spellman, P., Sherlock, G., Zhang, M., Iyer, V., Anders, K., Eisen, M., Brown, P., Botstein, D., and Futcher, B. (1998). Comprehensive identification of cell cycle-regulated genes of the yeast *Saccharomyces cerevisiae* by microarray hybridization. Mol. Biol. Cell *9*, 3273–3297.

Spiess, C., Meyer, A.S., Reissmann, S., and Frydman, J. (2004). Mechanism of the eukaryotic chaperonin: Protein folding in the chamber of secrets. Trends Cell Biol. *14*, 598–604.

Spradling, A., Pardue, M. Lou, and Penman, S. (1977). Messenger RNA in heat-shocked *Drosophila* cells. J. Mol. Biol. *109*, 559–587.

Srikakulam, R., and Winkelmann, D.A. (1999). Myosin II folding is mediated by a molecular chaperonin. J. Biol. Chem. *274*, 27265–27273.

Stedman, E. (1951). The Basic Proteins of Cell Nuclei. Philos. Trans. R. Soc. B Biol. Sci. *235*, 565–595.

Steinmetz, E.J., Conrad, N.K., Brow, D.A., and Corden, J.L. (2001). RNA-binding protein Nrd1 directs poly(A)-independent 3'-end formation of RNA polymerase II transcripts. Nature *413*, 327–331.

Stemmann, O., Neidig, A., Köcher, T., Wilm, M., and Lechner, J. (2002). Hsp90 enables Ctf13p/Skp1p to nucleate the budding yeast kinetochore. PNAS *99*, 8585–8590.

Sternberg, N. (1973). Properties of a mutant of *Escherichia coli* defective in bacteriophage lambda head formation (groE). II. The propagation of phage lambda. J. Mol. Biol. *76*, 25–44.

Sterner, D.E., Grant, P.A., Roberts, S.M., Duggan, L.J., Belotserkovskaya, R., Pacella, L.A., Winston, F., Workman, J.L., and Berger, S.L. (1999). Functional Organization of the Yeast SAGA Complex: Distinct Components Involved in Structural Integrity, Nucleosome Acetylation, and TATA-Binding Protein Interaction. Mol. Cell. Biol. *19*, 86–98.

Strahl, B.D., and Allis, C.D. (2000). The language of covalent histone modifications. Nature *403*, 41.

Strahl, B.D., Grant, P.A., Briggs, S.D., Bone, J.R., Caldwell, J.A., Mollah, S., Cook, R.G., Shabanowitz, J., Hunt, D.F., Allis, C.D., et al. (2002). Set2 Is a Nucleosomal Histone H3-Selective Methyltransferase That Mediates Transcriptional Repression. Mol. Cell. Biol. *22*, 1298–1306.

Straube, K., Blackwell, J.S., and Pemberton, L.F. (2010). Nap1 and Chz1 have separate Htz1 nuclear import and assembly functions. Traffic *11*, 185–197.

Straus, D., Walter, W., and Gross, C. a. (1990). DnaK, DnaJ, and GrpE heat shock proteins negatively regulate heat shock gene expression by controlling the synthesis and stability of σ32. Genes Dev. *4*, 2202–2209.

Shue, G., and Kohtz, D.S. (1994). Structural and functional aspects of basic helix-loop-helix protein folding by heat-shock protein 90. J. Biol. Chem. *269*, 2707–2711.

Suka, N., Suka, Y., Carmen, A.A., Wu, J., and Grunstein, M. (2001). Highly specific antibodies determine histone acetylation site usage in yeast heterochromatin and euchromatin. Mol. Cell *8*, 473–479.

Sullivan, W.P., Owen, B.A.L., and Toft, D.O. (2002). The influence of ATP and p23 on the conformation of hsp90. J. Biol. Chem. *277*, 45942–45948.

Sung, M.H., Guertin, M.J., Baek, S., and Hager, G.L. (2014). DNase footprint signatures are dictated by factor dynamics and DNA sequence. Mol. Cell *56*, 275–285.

Szego, C.M., and Roberts, S. (1946). The Nature of Circulating Estrogen. 161–164.

Takeda, Y., and Hirota, Y. (1982). Suppressor genes of a dnaA temperature sensitive mutation in *Escherichia coli*. Mol. Gen. Genet. *187*, 67–71.

Tam, S., Spiess, C., Auyeung, W., Joachimiak, L., Chen, B., Poirier, M.A., and Frydman, J. (2009). The chaperonin TRiC blocks a huntingtin sequence element that promotes the conformational switch to aggregation. Nat. Struct. Mol. Biol. *16*, 1279–1285.

Tang, L., Nogales, E., and Ciferri, C. (2010). Structure and function of SWI/SNF chromatin remodeling complexes and mechanistic implications for transcription. Prog. Biophys. Mol. Biol. *102*, 122–128.

Tariq, M., Nussbaumer, U., Chen, Y., Beisel, C., and Paro, R. (2009). Trithorax requires Hsp90 for maintenance of active chromatin at sites of gene expression. Proc. Natl. Acad. Sci. *106*, 1157–1162.

Taxis, C., Hitt, R., Park, S.H., Deak, P.M., Kostova, Z., and Wolf, D.H. (2003). Use of modular substrates demonstrates mechanistic diversity and reveals differences in chaperone requirement of ERAD. J. Biol. Chem. *278*, 35903–35913.

Terzi, N., Churchman, L.S., Vasiljeva, L., Weissman, J., and Buratowski, S. (2011). H3K4 Trimethylation by Set1 Promotes Efficient Termination by the Nrd1-Nab3-Sen1 Pathway. Mol. Cell. Biol. *31*, 3569–3583.

Thulasiraman, V., Yang, C.F., and Frydman, J. (1999). In vivo newly translated polypeptides are sequestered in a protected folding environment. EMBO J. *18*, 85–95.

Thulasiraman, V., Yang, C.F., and Frydman, J. (1999). In vivo newly translated polypeptides are sequestered in a protected folding environment. EMBO J. *18*, 85–95.

Tilly, K., Murialdo, H., and Georgopoulos, C. (1981). Identification of a second *Escherichia coli* groE gene whose product is necessary for bacteriophage morphogenesis. Proc. Natl. Acad. Sci. *78*, 1629–1633.

Tilly, K., McKittrick, N., Zylicz, M., and Georgopoulos, C. (1983). The dnaK protein modulates the heat-shock response of *Escherichia coli*. Cell *34*, 641–646.

Tirosh, I., Sigal, N., and Barkai, N. (2010). Widespread remodeling of mid-coding sequence nucleosomes by Isw1. Genome Biol. *11*, R49.

Tissiéres, A., Mitchell, H.K., and Tracy, U.M. (1974). Protein synthesis in salivary glands of *Drosophila melanogaster*: Relation to chromosome puffs. J. Mol. Biol. *84*, 389–398.

Toft, D., and Gorski, J. (1966). A receptor molecule for estrogens: isolation from the rat uterus and preliminary characterization. Proc. Natl. Acad. Sci. *55*, 1574–1581.

Toogun, O.A., DeZwaan, D.C., and Freeman, B.C. (2008). The Hsp90 Molecular Chaperone Modulates Multiple Telomerase Activities. Mol. Cell. Biol. *28*, 457–467.

Toogun, O.A., Zeiger, W., and Freeman, B.C. (2007). The p23 molecular chaperone promotes functional telomerase complexes through DNA dissociation. Proc. Natl. Acad. Sci. *104*, 5765–5770.

Tramantano, M., Sun, L., Au, C., Labuz, D., Liu, Z., Chou, M., Shen, C., and Luk, E. (2016). Constitutive turnover of histone H2A.Z at yeast promoters requires the preinitiation complex. Elife *5*, 1–30.

Tse, C., Georgieva, E.I., Ruiz-García, A.B., Sendra, R., and Hansen, J.C. (1998). Gcn5p, a transcription-related histone acetyltransferase, acetylates nucleosomes and folded nucleosomal arrays in the absence of other protein subunits. J. Biol. Chem. *273*, 32388–32392.

Tsubota, T., Berndsen, C.E., Erkmann, J.A., Smith, C.L., Yang, L., Freitas, M.A., Denu, J.M., and Kaufman, P.D. (2007). Histone H3-K56 Acetylation Is Catalyzed by Histone Chaperone-Dependent Complexes. Mol. Cell *25*, 703–712.

Tsukiyama, T., Palmer, J., Landel, C.C., Shiloach, J., and Wu, C. (1999). Characterization of the imitation switch subfamily of ATP-dependent chromatin-remodeling factors in *Saccharomyces cerevisiae*. Genes Dev. *13*, 686–697.

Turner, B.M., Birley, A.J., and Lavender, J. (1992). Histone H4 isoforms acetylated at specific lysine residues define individual chromosomes and chromatin domains in *Drosophila* polytene nuclei. Cell *69*, 375–384.

Turowski, T.W., and Tollervey, D. (2016). Transcription by RNA polymerase III: insights into mechanism and regulation. Biochem. Soc. Trans. *44*, 1367–1375.

Ursic, D., Sedbrook, J.C., Himmel, K.L., and Culbertson, M.R. (1994). The essential yeast Tcp1 protein affects actin and microtubules. Mol. Biol. Cell *5*, 1065–1080.

Ursic, D., and Ganetzky, B. (1988). A *Drosophila melanogaster* gene encodes a protein homologous to the mouse t complex polypeptide 1. Gene *68*, 267–274.

Ursic, D., and Culbertson , M.R. (1991). The Yeast Homolog to Mouse Tcp-1 Affects Microtubule-Mediated Processest. Mol. Cell. Biol. *11*, 2629–2640.

Vakoc, C.R., Sachdeva, M.M., Wang, H., and Blobel, G.A. (2006). Profile of Histone Lysine Methylation across Transcribed Mammalian Chromatin. Mol. Cell. Biol. *26*, 9185–9195.

Van Attikum, H., and Gasser, S.M. (2005). The histone code at DNA breaks: A guide to repair? Nat. Rev. Mol. Cell Biol. *6*, 757–765.

van Helden, J. (2003). Regulatory Sequence Analysis Tools. Nucleic Acids Res. *31*, 3593–3596.

Van Holde, K.E., Sahasrabuddhe, C.G., Shaw, B.R., van Bruggen, E.F.J., and Arnberg, A.C. (1974). Electron microscopy of chromatin subunit particles. Biochem. Biophys. Res. Commun. *60*, 1365–1370.

Van Hoof, A., Lennertz, P., and Parker, R. (2000). Yeast exosome mutants accumulate 3'-extended polyadenylated forms of U4 small nuclear RNA and small nucleolar RNAs. Mol. Cell. Biol. *20*, 441–452.

Van Leeuwen, F., Gafken, P.R., and Gottschling, D.E. (2002). Dot1p modulates silencing in yeast by methylation of the nucleosome core. Cell *109*, 745–756.

Vannini, A., and Cramer, P. (2012). Conservation between the RNA Polymerase I, II, and III Transcription Initiation Machineries. Mol. Cell *45*, 439–446.

Varshavsky, A.J., and Georgiev, G.P. (1975). Studies on chromatin. Mol. Biol. Rep. *2*, 255–262.

Vasiljeva, L., and Buratowski, S. (2006). Nrd1 interacts with the nuclear exosome for 3′ processing of RNA polymerase II transcripts. Mol. Cell *21*, 239–248.

Vázquez-Nin, G.H., Echeverría, O.M., Carbajal, M.E., Tanguay, R.M., Diez, J.L., and Fakan, S. (1992). Immunoelectron microscope localization of Mr 90000 heat shock protein and Mr 70000 heat shock cognate protein in the salivary glands of Chironomus thummi. Chromosoma *102*, 50–59.

Velazquez, J.M., and Lindquist, S. (1984). Hsp70: nuclear concentration during environmental stress and cytoplasmic storage during recovery. Cell *36*, 655–662.

Vogelauer, M., Wu, J., Suka, N., and Grunstein, M. (2000). Global histone acetylation and deacetylation in yeast. Nature *408*, 495–498.

Vonsattel, J.P.G., and DiFigilia, M. (1988). Huntington Disease. J. Neuropathol. Exp. Neurol. *57*, 369–384.

Voong, L.N., Xi, L., Wang, J.P., and Wang, X. (2017). Genome-wide Mapping of the Nucleosome Landscape by Micrococcal Nuclease and Chemical Mapping. Trends Genet. *33*, 495–507.

Wada, M., and Itikawa, H. (1984). Participation of *Escherichia coli* K-12 groE gene products in the synthesis of cellular DNA and RNA. J. Bacteriol. *157*, 694–696.

Walker, A.I., Hunt, T., Jackson, R.J., and Anderson, C.W. (1985). Double-stranded DNA induces the phosphorylation of several proteins including the 90 000 mol. wt. heat-shock protein in animal cell extracts. EMBO J. *4*, 139–145.

Wang, A., Kurdistani, S.K., and Grunstein, M. (2002). Requirement of Hos2 histone deacetylase for gene activity in yeast. Science *298*, 1412–1414.

Wang, K.L., and Warner, J.R. (1998). Positive and negative autoregulation of REB1 transcription in *Saccharomyces cerevisiae*. Mol. Cell. Biol. *18*, 4368–4376.

Weake, V.M., and Workman, J.L. (2008). Histone Ubiquitination: Triggering Gene Activity. Mol. Cell *29*, 653–663.

Weaver, A.J., Sullivan, W.P., Felts, S.J., Owen, B.A.L., and Toft, D.O. (2000). Crystal structure and activity of human p23, a heat shock protein 90 co-chaperone. J. Biol. Chem. *275*, 23045–23052.

Wegele, H., Muller, L., and Buchner, J. (2004). Hsp70 and Hsp90 - a relay team for protein folding. Rev. Physiol. Biochem. Pharmacol. *151*, 1–44.

Weikl, T., Abelmann, K., and Buchner, J. (1999). An unstructured C-terminal region of the Hsp90 co-chaperone p23 is important for its chaperone function. J. Mol. Biol. *293*, 685–691.

Weiler, K., and Wakimoto, B. (1995). Heterochromatin and gene expression in *Drosophila*. Annu. Rev. Genet. *29*, 577–605.

Welch, W.J., and Feramisco, J.R. (1984). Nuclear and nucleolar localization of the 72,000-dalton heat shock protein in heat shocked mammalian cells. J. Biol. Chem. *259*, 4501–4513.

Whitehouse, I., Rando, O.J., Delrow, J., and Tsukiyama, T. (2007). Chromatin remodelling at promoters suppresses antisense transcription. Nature *450*, 1031–1035.

Wilcox, C.B., Rossettini, A., and Hanes, S.D. (2004). Genetic interactions with C-terminal domain (CTD) kinases and the CTD of RNA pol II suggest a role for ESS1 in transcription initiation and elongation in *Saccharomyces cerevisiae*. Genetics *167*, 93–105.

Wilhelmsson, A., Cuthill, S., Denis, M., Wikström, A.C., Gustafsson, J.A., and Poellinger, L. (1990). The specific DNA binding activity of the dioxin receptor is modulated by the 90 kd heat shock protein. EMBO J. *9*, 69–76.

Willison, K.R., Dudley, K., and Potter, J. (1986). Molecular cloning and sequence analysis of a haploid expressed gene encoding t complex polypeptide 1. Cell *44*, 727–738.

Willison, K., Kelly, A., Dudley, K., Goodfellow, P., Spurr, N., Groves, V., Gorman, P., Sheer, D., and Trowsdale, J. (1987). The human homologue of the mouse t-complex gene, TCPI, is located on chromosome 6 but is not near the HLA region. EMBO J. *6*, 1967–1974.

Willison, K., Lewis, V., Zuckerman, K.S., Cordell, J., Dean, C., Miller, K., Lyon, M.F., and Marsh, M. (1989). The t complex polypeptide 1 (TCP-1) is associated with the cytoplasmic aspect of Golgi membranes. Cell *57*, 621–632.

Wilson, B., Erdjument-Bromage, H., Tempst, P., and Cairns, B.R. (2006). The RSC chromatin remodeling complex bears an essential fungal-specific protein module with broad functional roles. Genetics *172*, 795–809.

Wippo, C.J., Israel, L., Watanabe, S., Hochheimer, A., Peterson, C.L., and Korber, P. (2011). The RSC chromatin remodelling enzyme has a unique role in directing the accurate positioning of nucleosomes. EMBO J. *30*, 1277–1288.

Wood, A., Krogan, N.J., Dover, J., Schneider, J., Heidt, J., Boateng, M.A., Dean, K., Golshani, A., Zhang, Y., Greenblatt, J.F., et al. (2003). Bre1, an E3 ubiquitin ligase required for recruitment and substrate selection of Rad6 at a promoter. Mol. Cell *11*, 267–274.

Wood, K., Tellier, M., and Murphy, S. (2018). DOT1L and H3K79 methylation in transcription and genomic stability. Biomolecules *8*, 1–16.

Worcel, A., and Benyajati, C. (1977). Higher Order Coiling of DNA in Chromatin. Cell *12*, 83–100.

Workman, J.L., and Kingston, R.E. (1992). Nucleosome core displacement in vitro via a metastable transcription factor-nucleosome complex. Science *258*, 1780–1784.

Workman, J.L. (2006). Nucleosome displacement in transcription. Genes Dev. *20*, 2009–2017.

Wu, J., Suka, N., Carlson, M., Grunstein, M., Allard, S., Utley, R.T., Savard, J., Clarke, A., Grant, P., Brandl, C.J., et al. (2001). TUP1 utilizes histone H3/H2B-specific HDA1 deacetylase to repress gene activity in yeast. Mol. Cell *7*, 117–126.

Wu, P.-Y.J., and Winston, F. (2002). Analysis of Spt7 function in the *Saccharomyces cerevisiae* SAGA coactivator complex. Mol. Cell. Biol. *22*, 5367–5379.

Wu, W.S., and Li, W.H. (2008). Identifying gene regulatory modules of heat shock response in yeast. BMC Genomics *9*, 1–15.

Wu, X., Rossettini, A., and Hanes, S.D. (2003). The ESS1 Prolyl Isomerase and Its Suppressor BYE1 Interact with RNA Pol II to Inhibit Transcription Elongation in *Saccharomyces cerevisiae*. Genetics *165*, 1687–1702.

Wu, X., Wilcox, C.B., Devasahayam, G., Hackett, R.L., Arévalo-Rodríguez, M., Cardenas, M.E., Heitman, J., and Hanes, S.D. (2000). The Ess1 prolyl isomerase is linked to chromatin remodeling complexes and the general transcription machinery. EMBO J. *19*, 3727–3738.

Xu, F., Zhang, K., and Grunstein, M. (2005). Acetylation in histone H3 globular domain regulates gene expression in yeast. Cell *121*, 375–385.

Xu, Z., Horwich, A.L., and Sigler, P.B. (1997). The crystal structure of the asymmetric GroEL-GroES-(ADP)7 chaperonin complex. Nature *388*, 741–750.

Xu, Z., Wei, W., Gagneur, J., Perocchi, F., Clauder-Münster, S., Camblong, J., Guffanti, E., Stutz, F., Huber, W., and Steinmetz, L.M. (2009). Bidirectional promoters generate pervasive transcription in yeast. Nature *457*, 1033–1037.

Xue, Y., Pradhan, S.K., Sun, F., Chronis, C., Tran, N., Su, T., Van, C., Vashisht, A., Wohlschlegel, J., Peterson, C.L., et al. (2017). Mot1, Ino80C, and NC2 Function Coordinately to Regulate Pervasive Transcription in Yeast and Mammals. Mol. Cell *67*, 594–607.

Xue, Y., Van, C., Pradhan, S.K., Su, T., Gehrke, J., Kuryan, B.G., Kitada, T., Vashisht, A., Tran, N., Wohlschlege, J., et al. (2015). The INO80 complex prevents invasion of euchromatin into silent chromatin. Genes Dev. *29*, 350–355.

Yaffe, M.B., Farr, G.W., Miklos, D., Horwich, A.L., Sternlicht, M.L., and Sternlicht, H. (1992). TCP1 complex is a molecular chaperone in tubulin biogenesis. Nature *358*, 245–248.

Yamamoto, K.R. (1985). Steroid receptor regulated transcription of specific genes and gene networks. Annu. Rev. Genet. *19*, 209–252.

Yarragudi, A., Miyake, T., Li, R., and Morse, R.H. (2004). Comparison of ABF1 and RAP1 in Chromatin Opening and Transactivator Potentiation in the Budding Yeast *Saccharomyces cerevisiae*. Mol. Cell. Biol. *24*, 9152–9164.

Yarragudi, A., Parfrey, L.W., and Morse, R.H. (2007). Genome-wide analysis of transcriptional dependence and probable target sites for Abf1 and Rap1 in *Saccharomyces cerevisiae*. Nucleic Acids Res. *35*, 193–202.

Yochem, J., Uchida, H., Sunshine, M., Saito, H., Georgopoulos, C., and Feiss, M. (1978). Genetic Analysis of Two Genes, dnaJ and dnaK, Necessary for *Escherichia coil* and Bacteriophage Lambda DNA Replication. Mol. Gen. Genet. *164*, 9–14.

Yost, H.J., and Lindquist, S. (1986). RNA splicing is interrupted by heat shock and is rescued by heat shock protein synthesis. Cell *45*, 185–193.

Young, J.C., Moarefi, I., and Ulrich Hartl, F. (2001). Hsp90: A specialized but essential protein-folding tool. J. Cell Biol. *154*, 267–273.

Young, R.A. (1991). RNA polymerase II. Annu. Rev. Biochem. *60*, 689–715.

Zawel, L., and Reinberg, D. (1993). Initiation of Transcription by RNA Polymerase II: A Multi-step Process. Prog. Nucleic Acid Res. Mol. Biol. *44*, 67–108.

Zelin, E., Zhang, Y., Toogun, O.A., Zhong, S., and Freeman, B.C. (2012). The p23 Molecular Chaperone and GCN5 Acetylase Jointly Modulate Protein-DNA Dynamics and Open Chromatin Status. Mol. Cell *48*, 459–470.

Zhang, H., Roberts, D.N., and Cairns, B.R. (2005). Genome-wide dynamics of Htz1, a histone H2A variant that poises repressed/basal promoters for activation through histone loss. Cell *123*, 219–231.

Zhao, R., Davey, M., Hsu, Y.C., Kaplanek, P., Tong, A., Parsons, A.B., Krogan, N., Cagney, G., Mai, D., Greenblatt, J., et al. (2005). Navigating the chaperone network: An integrative map of physical and genetic interactions mediated by the Hsp90 chaperone. Cell *120*, 715–727.

Zhou, B.O., Wang, S.S., Xu, L.X., Meng, F.L., Xuan, Y.J., Duan, Y.M., Wang, J.Y., Hu, H., Dong, X., Ding, J., et al. (2010). SWR1 Complex Poises Heterochromatin Boundaries for Antisilencing Activity Propagation. Mol. Cell. Biol. 30, 2391–2400.

Zhu, X., Zhao, X., Burkholder, W.F., Gragov, A., Ogata, C.M., Gottesman, M.E., and Hendrickson, W.A. (1996). Structural analysis of substrate binding by the molecular chaperone DnaK. Sci *272*, 1616–1614.

Ziemienowicz, A., Skowyra, D., Zeilstra-ryallsqli, J., Fayet, O., Georgopoulos, C., and Zylicz, M. (1993). Both the *Escherichia coli* Chaperone Systems , GroEL/GroES and DnaK/DnaJ/GrpE , Can Reactivate Heat-treated RNA Polymerase. J Biol. Chem. *268*, 25425–25431.

Zlatanova, J., and Thakar, A. (2008). H2A.Z: View from the Top. Cell *16*, 166–179.

Zou, Y., Crowley, D.J., and Houten, B. Van (1998). Involvement of Molecular Chaperonins in Nucleotide Excision Repair. J. Biol. Chem. *273*, 12887–12892.

Zweig, M., and Cummings, D.J. (1973). Cleavage of head and tail proteins during bacteriophage T5 assembly: Selective host involvement in the cleavage of a tail protein. J. Mol. Biol. *80*, 505–518.

Zylicz, M., Yamamoto, T., McKittrick, N., Sell, S., and Georgopoulos, C. (1985). Purification and properties of the dnaJ replication protein of *Escherichia coli*. J. Biol. Chem. *260*, 7591–7598.

9. Publications

F.J. Echtenkamp*, **Z. Gvozdenov***, N.L. Adkins, Y. Zhang, M.A. Day-Lynch, S. Watanabe, C.L. Peterson and B.C. Freeman. Hsp90 and p23 Molecular Chaperones Control Chromatin Architecture by Maintaining the Functional Pool of the RSC Chromatin Remodeler. 2016. Mol. Cell *64*, 888-899.

*co-first author

> **Cover photo** idea, initial sketch and interpretation for Molecular Cell, Volume 64, Issue 5, 2016.

In preparation

Zlata Gvozdenov and Brian C. Freeman. The TRiC/CCT Chaperonin Globally Controls Aberrant Transcription.

In preparation

Zlata Gvozdenov and Brian C. Freeman. Hsp90 Actively Stabilizes Transcription Factors.

In preparation

Zlata Gvozdenov and Brian C. Freeman. Historical overview of Molecular Chaperones in the Nucleus.

10. Acknowledgements

To Brian, for bringing me to the University of Illinois and for supporting me all these years. For introducing me to hard-core science, for teaching me all subtleties ranging from small lab tricks over to NIH modular vs. non-modular grants. For his patience. For not giving up when I did. Perhaps the most important – for teaching me not to publish just to publish, but how to publish to change the textbooks. For listening to what I had to say. For taking my results seriously, which speeded up our progress. For writing such a great letter of recommendation that placed me in one of the best labs in the world. While I have never seen that letter, I saw the reflections – doors of world-renowned scientists opened for me. For making a scientist out of me. To my lab mates, Brian, Anqi and Janhavi, for being deeply empathic about my final hectic year. To the head of our CDB department at the University of Illinois, Dr. Chen for her incredible moral support. To many other friends, professors and coworkers from our CDB department – for sharing knowledge and materials, for giving feedback, for helping privately.

To Prof. Buchner for acceptance to the Master program at Technische Universität München (TUM). For the outstanding academic opportunities. For trusting and allowing me to come to the States for my entire Ph.D., and for being supportive throughout. To Prof. Bausch at TUM Physics Department and to Prof. Buch at University of Zurich for all the research opportunities, their insightfulness, and their very valuable moral support even after my work in their labs was completed. To Prof. Sieber, Prof. Eppinger and Dr. Haslbeck. To Frau Hilber for flawless bureaucracy. To my German mom, Bibianne and her husband, peace upon him, for the happy home in the best neighborhood in Munich. Đura iz Veča – „пријатељ, друг, брат" – for immense help whenever I needed it. It was enough to call him and formidable obstacles were gone. To my friend Mina, who convinced me to come to the States, while we were swimming in the Saudi Arabian Red Sea.

To Prof. Breitenbach-Koller. To my colleagues at Naturwissenschaftliche Fakultät in Salzburg for accepting me. They never made me feel different, even though I was the only foreigner – non-native German speaker amongst the Molecular Biosciences students. To the Mladenović family in Salzburg, especially Ivana and Jelena, who helped me so many times when I needed a roof over my head. To the Hadžić family and their help. To teta Granica for accommodating me in Vienna on numerous occasions due to awkward flight times. To čika Brana who equally provided so much help during my transitions.

To my middle school teacher Gordana who directed me towards the best school in the country and for her efforts to prepare me to get in. I would also like to thank other JS Popović middle school teachers in Vršac who believed in me and promoted me to represent our generation, without me being aware at the time that I deserved it. I would

11. Declaration

I declare that this thesis was composed by myself and that the work contained herein is my own except where explicitly stated otherwise in the text. All experiments were performed by myself, with exception of the experiments in the Figures 4.2.3 and 4.3.5 that were done by our collaborators in Dr. Crag Peterson's laboratory, as well as select generated bioinformatics figures for which data sources from the published works, as cited. The Code in Appendices 7.9. was written by Zeno-Dan Barcutean. Parts of this work have been published as stated in the chapter Publications. This work has not been submitted for any degree or other examination board.

Ich erkläre, dass ich die vorliegende Dissertation selbstständig verfasst habe und die Arbeit von mir ausgeführt wurde, sofern es nicht ausdrücklich im Text angegeben wurde. Alle Experimente wurden von mir durchgeführt. Ausnahmen sind dabei die Abbildungen 4.2.3 and 4.3.5, die von unseren Kooperationspartner in Dr. Crag Peterson's Labor ausgeführt wurden, sowie einige bioinformatisch generierte Abbildungen, für die Daten aus den veröffentlichten und zitierten Arbeiten stammen. Der Code in den Anhängen 7.9. wurde von Zeno-Dan Barcutean verfasst. Wie im Kapitel Publikationen beschrieben, wurden Teile dieser Arbeit veröffentlicht,. Diese Arbeit hat nicht als Vorlage für einen anderen Abschluss gedient und wurde auch nicht bei einem anderen Prüfungsausschuss eingereicht.

Zlata Gvozdenov
Urbana, Illinois, USA, 2018